Summer 8-15-2019

Polarization Division Multiplexing for Optical Data Communications

Darko Ivanovich
Washington University in St. Louis

WASHINGTON UNIVERSITY IN ST.LOUIS

School of Engineering & Applied Science
Department of Computer Science and Engineering

Dissertation Examination Committee:
Roger D. Chamberlain, Chair
Shantanu Chakrabartty
Viktor Gruev
Ulugbek Kamilov
Richard Livingston
Xuan 'Silvia' Zhang

Polarization Division Multiplexing for Optical Data Communications

by
Darko Ivanovich

A dissertation presented to
The Graduate School
of Washington University in
partial fulfillment of the
requirements for the degree
of Doctor of Philosophy

August 2019
St. Louis, Missouri

Table of Contents

List of Figures

List of Tables

Acknowledgments

I am very pleased to thank those great people who made this thesis possible and also those wonderful people who have supported me along the way. I am especially grateful to my PhD research advisor Dr. Roger Chamberlain who has provided me with guidance, advise and help during my years of PhD research studies.

Dr. Chamberlain has been very good to me throughout the years since I have known him. In the last 20+ years since I have known him, Dr. Chamberlain has been my undergraduate and graduate professor and PhD adviser and mentor. He has been my boss at one of my jobs and he has been my friend all these years. He provided lots of help, encouragement and patience through the years.

Also, I am very grateful to all help and advices from my co-advisor Dr. Viktor Gruev who especially helped me with his knowledge and guidance in CMOS circuit design, Cadence software tools and simulations and chip design.

Thanks to all members of Dr. Gruev's research group that I have worked at Washington University in St. Louis and at University of Illinois at Urbana-Champaign. These members are Nun Cui, Samuel Powell and Amit Deliwala. Nan Cui helped me a lot with receiver chip design and layout and with printed circuit board for the receiver chip. Samuel Powell helped me with optical signal polarization analysis and Amit Deliwala helped me with some

experiments with Polarization filters and light processing through them and light data analysis at the receiver output. Thank you guys so much!

Thanks to all the members of my PhD dissertation defense committee for agreeing to serve on the committee and for their valuable input and questions about different portions of my research.

My PhD research years have been long and busy years but I have enjoyed tremendously the entire ride! Thanks again to everybody!

Darko Ivanovich

Washington University in Saint Louis

August 2019

Dedicated to my parents Branka and Slobodan Ivanovich and academic and work mentor Dr. Roger Chamberlain.

There are three people in my life who made a big impact in my choice to pursue an engineering carrier. My mother Branka Ivanovich has spent countless hours with me trying to encourage me to chose science as my carrier path. My father Slobodan Ivanovich has helped me to understand basic principles of mathematics and physics which helped me later in my engineering studies and engineering carrier path. I am very thankful to both of my parents for their help and support throughout the years. Also I am very thankful to my PhD advisor and mentor Dr. Roger Chamberlain for his encouragement, help and support to pursue my Ph.D.

ABSTRACT OF THE DISSERTATION

Polarization Division Multiplexing

for Optical Data Communications

by

Darko Ivanovich

Doctor of Philosophy in Computer Engineering

Washington University in St. Louis, 2019

Professor Roger D. Chamberlain

Multiple parallel channels are ubiquitous in optical communications, with spatial division multiplexing (separate physical paths) and wavelength division multiplexing (separate optical wavelengths) being the most common forms. In this research work, we investigate the viability of polarization division multiplexing, the separation of distinct parallel optical communication channels through the polarization properties of light. We investigate polarization division multiplexing based optical communication systems in five distinct parts.

In the first part of the work, we define a simulation model of two or more linearly polarized optical signals (at different polarization angles) that are transmitted through a common medium (e.g., air), filtered using aluminum nanowire optical filters fabricated on-chip, and received using individual silicon photodetectors (one per channel). The filter model is based upon an input optical signal formed as the sum of the Stokes vectors for each individual channel, transformed by the Mueller matrix that models the filter proper, resulting in an output optical signal that impinges on each photodiode. The simulation results show that two and three channel systems can operate with a fixed-threshold comparator in the receiver circuit, but four channel systems (and larger) will require channel coding of some form. The

entire simulation model is designed in Cadence tools and the receiver (including optics) is compatible with standard CMOS fabrication processes.

In the second part of the work, we design and manufacture a two channel chip that is used as the light receiver to confirm the simulation results from the first part of the research. Since logistics for the receiver's chip testing were not favorable we constrained our testing to single channel operation, which we demonstrated functionality using both electrical and optical inputs. In addition, we used data from a pair of optical imagers (one linear and the second with a logarithmic response) to investigate the noise properties of both the optical and electrical signals within the system.

In the third part of the work, we provide examples of channel coding that enable the four channel system to operate with positive noise margins.

In the fourth part of the work, we define an end-to-end simulation model of two, three or four channel systems that utilize air, fiber, and a pair of mirrors in the optical path from transmitter to receiver. Each of these systems is shown to have positive noise margins (albeit using channel coding on the four channel editions); however, there are many circumstances where the noise margins are quite small.

In the final part of the work, we examine the trade-offs between number of channels, signal power, and noise margins, including the use of pulse amplitude modulation within the two channel system.

Chapter 1

Introduction

Multiple parallel channels are ubiquitous in optical communications, with spatial division multiplexing (separate physical paths) and wavelength division multiplexing (separate optical wavelengths) being the most common forms. These two forms of multiplexing are used in modern high-speed data communications systems that operate on both short and long distances. Our definition of the phrases short distance and long distance means distances ranging from chip to chip on a circuit board all the way to city-to-city distances.

Wavelength division multiplexing has been a backbone of modern high-speed bidirectional fiber-optic digital data communications for a long time, basically since the late 1970s [29]. It is a technology which uses multiplexing of a number of optical carrier signals onto a single optical fiber by using different wavelengths (or colors) of laser light [8, 12, 24, 29].

A typical wavelength division multiplexing bidirectional optical transmission system is shown in Figure 1.1 [29]. Modern wavelength division multiplexing systems can handle 160 signals each with different wavelength and carrying a 100 Gbit/s digital data rate. This means that a single fiber pair can carry over 16 Tbit/s data rates. Modern wavelength division

multiplexing systems dominate high-speed digital data communications for long distances (e.g., multi-kilometer lengths).

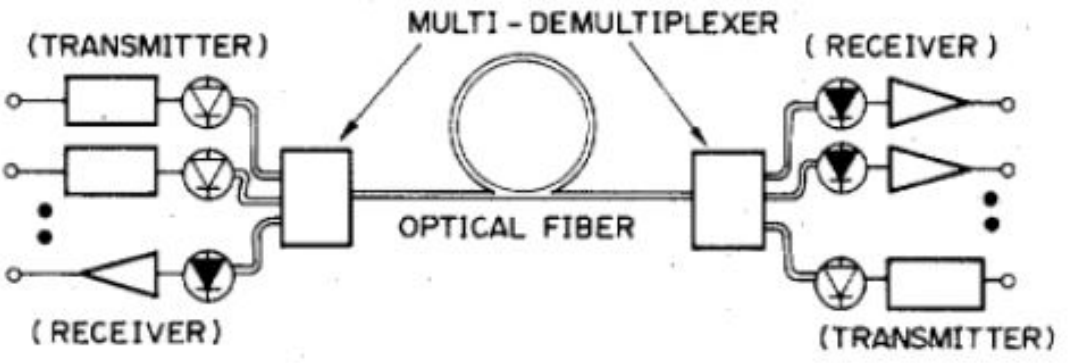

Figure 1.1: Wavelength division multiplexing optical transmission system [29].

Spatial division multiplexing is a technology which uses separate physical paths for communications [50, 56, 57, 68]. Spatial division multiplexing systems perform data transmission based on multiple parallel fibers, each with a separate cladding comprising one or more cores, without coupling between the fibers.

In order for spatial division multiplexing to be considered for future high-speed fiber-optic communications systems this technology needs to be compatible with existing systems and also it has to outperform existing systems in terms of data rates, costs and power consumption [24]. Figure 1.2 shows an example of a modern spatial division multiplexing optical transmission system [44].

There have also been systems that use both techniques. For example, Lemoff et al. [37] demonstrated a system designed for short-distance (between processor and memory) communications using four distinct wavelengths and 12 parallel fibers. The performance implications of using optics in the processor-to-memory data path were investigated (in simulation) by

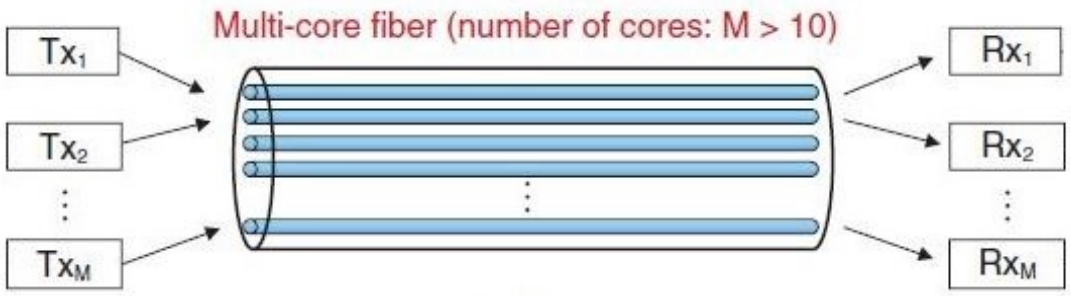

Figure 1.2: Spatial division multiplexing optical transmission system [44]

Fritts and Chamberlain [14] as an approach to address the performance limitations of the memory wall [69].

In this research, we investigate the viability of polarization division multiplexing (PDM), the separation of distinct parallel optical communication channels through the polarization properties of light [5, 22, 25, 63, 73]. Two or more linearly polarized optical signals (at different polarization angles) are transmitted through a common medium, filtered using aluminum nanowire optical filters fabricated on-chip, and received using individual silicon photodetectors (one per channel).

We desire the entire transmitter and receiver to be compatible with standard CMOS fabrication processes. Our interest is in both the practical aspects (e.g., the degree to which manufacturing variability effects the operation of the system) and the theoretical limits (e.g., the fundamental trade-offs among optical power, noise margin and number of channels).

The motivation for this work is primarily short distance (on-chip, chip-to-chip on board, and box-to-box within a machine room). As such, an important consideration is the cost of implementation (especially relative to the fairly expensive end-point designs that can be economically justified for long-haul, or city-to-city, distances).

According to a recent article by Levi [38], there have been many attempts in the last 20 years to integrate optical communications for electronic applications at short distances, such as chip-to-chip communications, board-to-board, box-to-box within equipment racks, and rack-to-rack within a room or a building.

These efforts have not yielded extensive usage of optical communication systems for short distance applications, and in that realm traditional electrical wire communications are still dominant. According to [38], the main reason for this is that the cost penalty for using optical wavelength division multiplexing systems is too high for commercial companies to adopt the approach. Expensive wavelength division multiplexing receiver filtering designs are not practical to be placed on processor chips and that is the main reason why the much faster and higher bandwidth optical communication systems that are used for long distances are not used for short distance applications.

We propose an optical communication system based on polarization division multiplexing. Even though the channel count for PDM in a given transmission media is modest (3 to 4 channels) compared with over 100 data channels for long-haul WDM systems, it represents a significant improvement over traditional electrical communication systems.

As part of this work, an end-to-end polarization division multiplexing system is modeled (both mathematically and using the Cadence simulation tools) to investigate this concept. The system simulation starts from an array of input signals that are multiplexed into one light signal travelling through several media as transmission paths (free space, an optical fiber, and free space with a pair of mirrors).

The light signal is represented as the sum of Stokes vectors for each individual data channel, and the media is modeled via its Mueller matrix [10, 21, 33]. This light signal hits the filters that are mounted on the receiver CMOS integrated chip. The filter model is based upon

this input optical signal transformed by the Mueller matrix that models the filter proper, resulting in an output optical signal that impinges on each photodiode. An illustration of a polarization division multiplexing optical transmission system is shown in Figure 1.3.

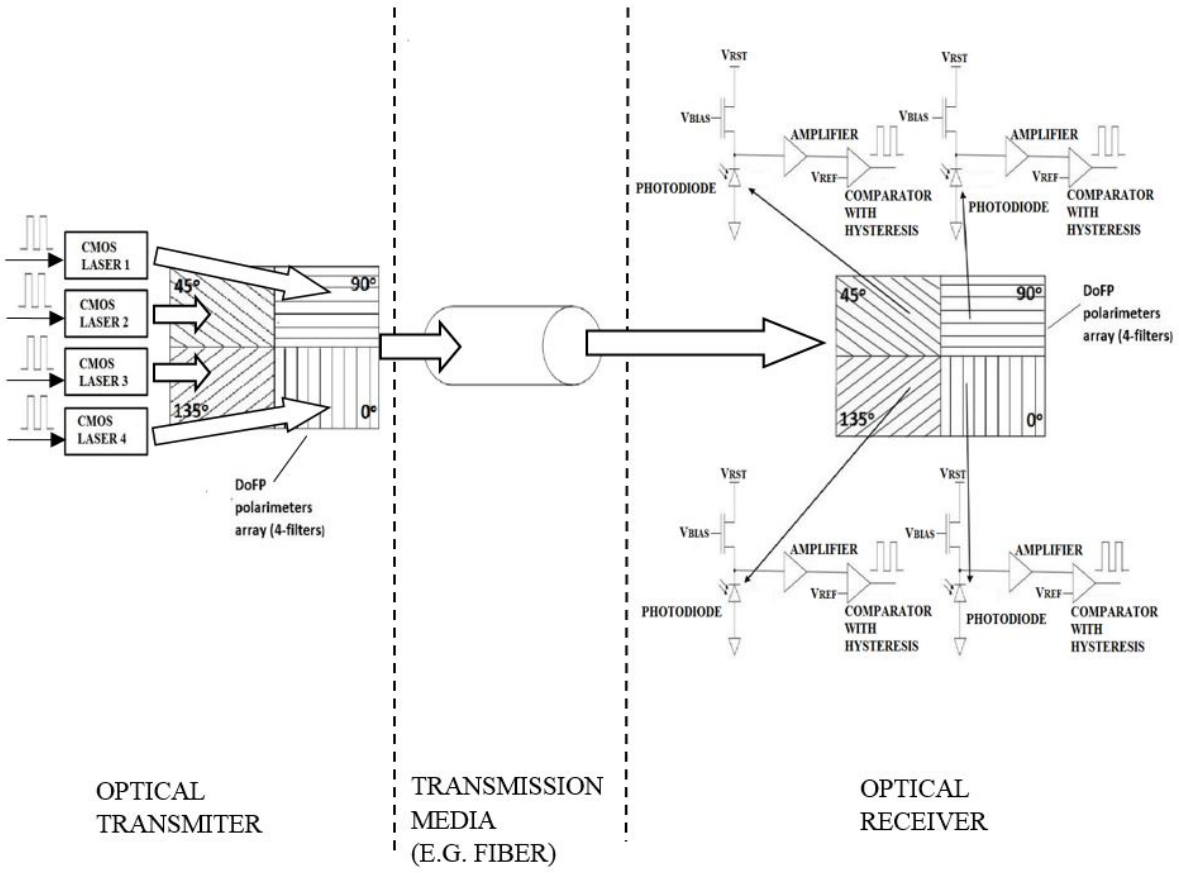

Figure 1.3: Polarization division multiplexing optical transmission system.

The results show that two and three channel systems can operate with a fixed-threshold comparator in the receiver circuit, but four-channel systems (and larger) will require channel coding of some form. For example, in the four-channel system, 10 of 16 distinct bit patterns are separable by the receiver without using channel coding. The model also supports investigation of the range of variability tolerable in the fabrication of the on-chip polarization filters. The

system model is supported by the development and testing of a custom receiver CMOS integrated chip.

To overcome the signal level limitations of the four channel system, simple channel coding techniques are introduced that support four channel operation. The resulting noise margins, however, are quite limited.

Two, three, and four channel systems are investigated using a variety of transmission media, including air, fiber optics, and mirrored reflections. Also, the general relationships between input optical power, number of channels, and noise margins in the receiver decoders are shown.

1.1 Contributions

In this dissertation the following contributions are made. Citations are included for the already published work.

- Design of 2, 3 and 4 channel Visible Light Communication (VLC) Polarization Division Multiplexing (PDM) systems for usage in short distance communications such as chip-to-chip, board-to-board, box-to-box within equipment racks, and rack-to-rack within a room or a building.
- Design of 2, 3 and 4 channel VLC PDM systems with transmission media such as air, fiber optic cables and air with mirror reflections. The media are represented by their respective Mueller matrices [30].
- Usage of DoFP polarimeters bonded on a receiver chip for separation of polarized light communication channels [31].

- Cadence simulation of the full 2, 3 and 4 channel VLC PDM systems with air transmission media [31].
  - Design of VerilogA models for optical parts of the system from transmitter input lasers, through transmitter's DoFP polarimeters, via transmission media to receiver's DoFP polarimeters.
  - Design of VerilogA models for photodiodes.
  - Design of receiver channel amplifier circuit.
  - Design of receiver channel comparator with hysteresis circuit.
  - Design of receiver channel 2-to-1 multiplexer.
- Noise analysis of the entire 2, 3 and 4 channel VLC PDM systems with transmission media such as air, fiber optic cables, and air with mirror reflections [30].
  - Noise analysis of optical part of the system
  - Noise analysis of electrical part of the system
- Development of coding techniques to overcome noise problems caused by system optical and electrical noise models.
- Design, layout, and fabrication of a prototype test receiver chip to demonstrate system concept.
- Design, layout, and fabrication of a printed circuit board (PCB) for testing the prototype receiver chip.
- Experimental results for characterizations of components of the VLC PDM system [30].

1.2 Outline of the Dissertation

The outline of the dissertation is as follows. Chapter 2 provides relevant background information about VLC PDM systems, input lasers, DoFP polarimeters, fiber optic cables, high-speed photodiodes, and Transimpendance Amplifiers (TIA) circuits used for high speed data processing within receiver chip. Chapter 3 describes the conversion of combined polarized light data channels for 2, 3 and 4 channels VLC PDM systems into individual electrical signals (one per channel). Chapter 4 describes the design, layout and fabrication of the custom receiver chip and its testing. This chapter also describes some optical bench testing of DoFP polarimeters in air. Chapter 5 describes the channel coding which is used to overcome noise problems that are an intrinsic part of the optical and electrical portions of the system. Chapter 6 describes different 2, 3 and 4 channel VLC PDM system models with transmission media such as air, fiber optic cables, and air with mirror reflections. This chapter describes all these models analytically and using Cadence simulation. Chapter 7 describes noise properties of the system and end-to-end comparison of the system. Finally Chapter 8 presents conclusions and future work.

Chapter 2

Background and Related Work

Light has three basic properties: intensity, wavelength, and polarization as shown in Figure 2.1 [71]. The first two properties, intensity and wavelength, are the basis of modern high-speed optical communication systems based on fiber optics. Fiber optic communication systems frequently use Wavelength Division Multiplexing (WDM) for separation of multiple optical channels. Modulated input optical signals that carry many data channels encoded by different wavelengths are separated on the receiver side using well-known WDM techniques [24].

Our focus is on the exploitation of polarization, which can be efficiently represented using Stokes parameters [42, 43]. Using Stokes vectors we characterize the polarized light signals coming from modulated CMOS-based optical lasers which are used as the transmitters in our PDM optical transmission system. These polarized light signals are sent through some transmission media (e.g. fiber cable) and then they are received by CMOS-based receiver with Division of Focal Plane (DoFP) polarimeter filter array bonded on the receiver chip surface.

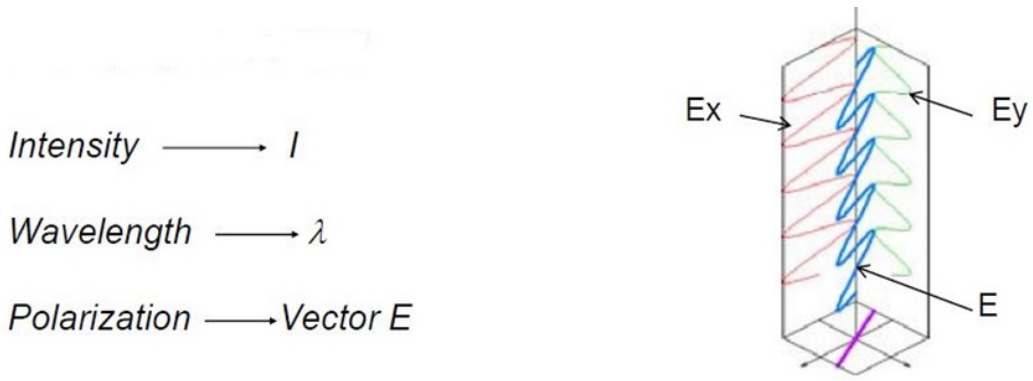

Figure 2.1: Properties of light [71].

Both transmission media and DoFP polarimeter filter array are represented by Mueller matrices [48]. Following approach of Herad and Lacourt the models for various transmission media can be derived and used for simulation of high-speed optical data communications systems [23]. The DoFP polarimeter filter array on the CMOS receiver separates optical signals with different polarization angles. Each optical signal is then converted to electrical signal using high-speed photodiode and it is conditioned into digital data stream for each channel on the CMOS receiver [31].

There have been reported a number of research projects of PDM system designs built on an optical bench. Wang et al., Hsu et al., Morant et al. and Kwon et al. showed that visible light communication systems based on polarization division multiplexing can be used for gigabit data transfers [26, 35, 45, 67]. These demonstrations were all on an optical bench, and therefore not well suited for CMOS integration.

They showed effective signal separation with two optical channels arranged 90° apart. Also, there has been some previous work where three optical signals with different polarization angles were sent thru a single-mode fiber cable (without polarization preservation) and these signals were recovered on receiver side of the experiment [23]. This experiment was also

performed on an optical bench. Further, Chen et al. showed a similar optical bench PDM system for four independent channels [7].

Goossens et al. proposed a PDM system based on nonlinear Fourier transforms and their simulation results show feasibility for PDM communication systems over single-mode fiber [18]. Yao at el. also showed two-channel PDM system on an optical bench [70]. Dou et al. reported two channel PDM system of chaotic laser secure communications on an optical bench [11]. Olsson et al. showed a two channel PDM system over 200 km long optical fiber [46]. Evangelides et al. showed that polarization division multiplexing with solitons can be using for optical data transfer over very long distance equal to 10000 km [13].

Recent work using Division of focal plane (DoFP) polarimeters integrated with CMOS technology enables compact, real-time polarization imaging systems [17, 20, 47, 48]. The DoFP polarimeters are manufactured from aluminum nanowire materials and mounted on custom CMOS ICs. This system contains an entire image processing pipeline that operates at frame rates of 40 frames per second or higher and thus enables real-time extraction of the polarization properties from the imaged environment.

Recently, Thangaraj et al. described the design and successful integration of high speed photodiodes on CMOS ICs for a fully operational CMOS-compatible optical digital clock distribution and electrical recovery system in a 0.35 nm CMOS process [1, 36, 49, 62]. This work demonstrates the viability of inexpensive optical-electrical signal transformations at GHz speeds in CMOS technology.

There are reported designs of high-speed CMOS based optical laser drivers that can be used as the transmitters of high-speed digital data [27, 28, 32, 55].

We will build upon these designs to show the viability of an entire high-speed PDM optical transmission system where both the transmitter and the receiver are CMOS-based and where the transmission media might be any of the following: free space, waveguides, fiber optic cable with preservation of polarization, and fiber optic cable without preservation of polarization. There are available literature resources and experimental data that model all these different types of transmission media [9, 41, 51, 52, 53, 65, 66].

In this research work for the receiver chip channel design we use slower circuit design that has amplifier and comparator with hysteresis that operate in the MHz frequency range. For future VLC PDM high-speed system design in the multiple GHz range we will use transimpedance amplifier (TIA) designs which are well described in the literature [2, 6, 39, 40, 58, 59, 61].

2.1 Stokes Vector Representation of Light

The Stokes parameters are a set of values that describe the polarization state of a traveling light beam. The Stokes parameters are usually combined into a vector, known as the Stokes vector which can be defined as

$$S_\Theta = \begin{bmatrix} S_0 \\ S_1 \\ S_2 \\ S_3 \end{bmatrix}. \tag{2.1}$$

Here Θ is polarization angle and S_0 is the intensity of the light beam and it is defined as

$$S_0 = I \tag{2.2}$$

where I is the total intensity of the light beam.

(S_1,S_2,S_3) are the Cartesian coordinates of the three-dimensional vector of position in space of the light beam. These Cartesian coordinates S_1, S_2 and S_3 can be transformed into the spherical coordinates Ip, 2ψ and 2χ as is shown in Figure 2.2 and Figure 2.3.

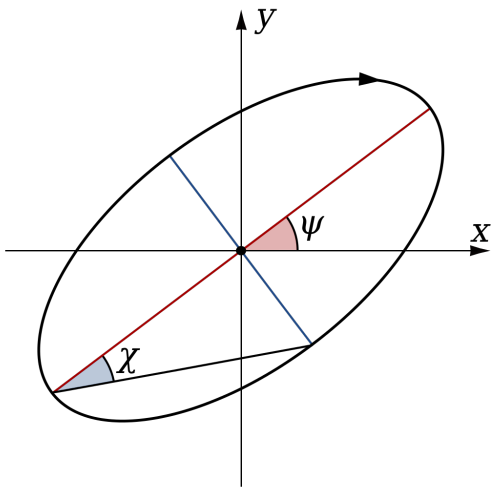

Figure 2.2: Polarization ellipse, showing the relationship to the Poincaré sphere parameters ψ and χ [60].

Here p is the degree of polarization which is defined as $0 \leq p \leq 1$. The factor of two before ψ represents the fact that any polarization ellipse is indistinguishable from one rotated by 180°. Also, the factor of two before χ indicates that an ellipse is indistinguishable from one with the semi-axis lengths swapped accompanied by a 90° rotation. Note that the phase information of the polarized light is not recorded in the Stokes parameters.

The Cartesian coordinates S_1, S_2 and S_3 are defined as:

$$S_1 = Ip\cos 2\psi \cos 2\chi \tag{2.3}$$

$$S_2 = Ip\sin 2\psi \cos 2\chi \tag{2.4}$$

$$S_3 = Ip\sin 2\chi \tag{2.5}$$

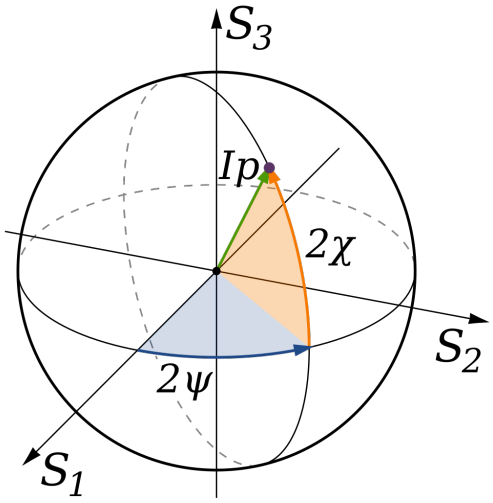

Figure 2.3: The Poincaré sphere is the parametrisation of the last three Stokes parameters in spherical coordinates [60].

If we have defined the Stokes parameters S_0, S_1, S_2 and S_3 we can calculate the spherical coordinates as

$$I = S_0 \tag{2.6}$$

$$p = \frac{\sqrt{S_1^2 + S_2^2 + S_3^2}}{S_0} \tag{2.7}$$

$$2\psi = \arctan \frac{S_2}{S_1} \tag{2.8}$$

$$2\chi = \arctan \frac{S_3}{\sqrt{S_1^2 + S_2^2}} \tag{2.9}$$

Here are some examples of the Stokes vectors that we will extensively use in this research:

1. The Stokes vector for unpolarized light is defined as

$$S_{unpolarized} = \begin{bmatrix} 1 \\ 0 \\ 0 \\ 0 \end{bmatrix}. \tag{2.10}$$

This makes sense because in this case the spherical coordinates are

$$I = 1; \qquad p = 0; \qquad 2\psi = 0^{\circ}; \qquad 2\chi = 0^{\circ}; \tag{2.11}$$

2. The Stokes vector for 0^{o} linearly polarized light is defined as

$$S_{0^{\circ}} = \begin{bmatrix} 1 \\ 1 \\ 0 \\ 0 \end{bmatrix}. \tag{2.12}$$

Which also makes sense because in this case the spherical coordinates are

$$I = 1; \qquad p = 1; \qquad 2\psi = 0^{\circ}; \qquad 2\chi = 0^{\circ}; \tag{2.13}$$

3. The Stokes vector for 45^{o} linearly polarized light is defined as

$$S_{45^{\circ}} = \begin{bmatrix} 1 \\ 0 \\ 1 \\ 0 \end{bmatrix}. \tag{2.14}$$

In this case the spherical coordinates are

$$I = 1; \qquad p = 1; \qquad 2\psi = 90^{\circ}; \qquad 2\chi = 0^{\circ}; \tag{2.15}$$

4. The Stokes vector for 90° linearly polarized light is defined as

$$S_{90^\circ} = \begin{bmatrix} 1 \\ -1 \\ 0 \\ 0 \end{bmatrix}. \tag{2.16}$$

In this case the spherical coordinates are

$$I = 1; \qquad p = 1; \qquad 2\psi = 180^\circ; \qquad 2\chi = 0^\circ; \tag{2.17}$$

5. The Stokes vector for 135° linearly polarized light is defined as

$$S_{135^\circ} = \begin{bmatrix} 1 \\ 0 \\ -1 \\ 0 \end{bmatrix}. \tag{2.18}$$

In this case the spherical coordinates are

$$I = 1; \qquad p = 1; \qquad 2\psi = 270^\circ; \qquad 2\chi = 0^\circ; \tag{2.19}$$

6. The Stokes vector for 60° linearly polarized light is defined as

$$S_{60^\circ} = \begin{bmatrix} 1 \\ \frac{-1}{2} \\ \frac{\sqrt{3}}{2} \\ 0 \end{bmatrix}. \tag{2.20}$$

In this case the spherical coordinates are

$$I = 1; \qquad p = 1; \qquad 2\psi = 120^{\circ}; \qquad 2\chi = 0^{\circ}; \tag{2.21}$$

7. The Stokes vector for 120º linearly polarized light is defined as

$$S_{120^{\circ}} = \begin{bmatrix} 1 \\ \frac{-1}{2} \\ \frac{-\sqrt{3}}{2} \\ 0 \end{bmatrix}. \tag{2.22}$$

In this case the spherical coordinates are

$$I = 1; \qquad p = 1; \qquad 2\psi = 240^{\circ}; \qquad 2\chi = 0^{\circ}; \tag{2.23}$$

When exploiting multiple distinct polarization angles for separate channels, we follow the theoretical guidance of Tyo [64] and evenly space the channels around the circle.

2.2 Mueller Matrix Representation of Aluminum Mirror with Oxide Layer

In Chapter 6 we will model a chip-to-chip path that includes mirrors. What follows is the derivation of a Mueller matrix model that represents an aluminum mirror with oxide layer, from van Harten et al. [21].

We can recall that as light travels through the space it is defined with two electromagnetic waves which are perpendicular to each other and they can be defined as p-polarized light or

horizontal axis directed electromagnetic wave and s-polarized light or vertical axis directed electromagnetic wave. (Here, we are adopting the notation of van Harten et al., which is equivalent to the notions of 0° and 90° polarization described above.)

The Mueller matrix of the aluminum mirror with oxide layer (Al_2O_3) M_{R} is shown below [21] and it is defined with the reflection coefficients of p-polarized light r_{P} and the reflection coefficients of s-polarized light r_{S}.

$$M_R = \begin{bmatrix} 1 & \frac{-R_P+R_S}{R_P+R_S} & 0 & 0 \\ \frac{-R_P+R_S}{R_P+R_S} & 1 & 0 & 0 \\ 0 & 0 & \frac{-2\sqrt{R_P R_S}\cos(E_P-E_S)}{R_P+R_S} & \frac{-2sqrtR_P R_S \sin(E_P-E_S)}{R_P+R_S} \\ 0 & 0 & \frac{2\sqrt{R_P R_S}\sin(E_P-E_S)}{R_P+R_S} & \frac{-2\sqrt{R_P R_S}\cos(E_P-E_S)}{R_P+R_S} \end{bmatrix} \tag{2.24}$$

Since both r_{P} and r_{S} are complex numbers, we define the elements from the Muller matrix for the aluminum mirror as

$$R_P = |r_P|^2 \tag{2.25}$$

$$R_S = |r_S|^2 \tag{2.26}$$

$$E_P = \arg(r_P) \tag{2.27}$$

$$E_S = \arg(r_S) \tag{2.28}$$

The reflection coefficient of p-polarized light r_P is defined as

$$r_P = \frac{\eta_m E_m - H_m}{\eta_m E_m + H_m} \tag{2.29}$$

where

$$E_m = \cos\delta_f + i\frac{\eta_b}{\eta_f}\sin\delta_f \tag{2.30}$$

$$H_m = \eta_b \cos\delta_f + i\eta_f \sin\delta_f \tag{2.31}$$

with

$$\delta_f = \frac{2\pi}{\lambda} n_f(\lambda) d_f \cos\Theta_f \tag{2.32}$$

$$\eta_b = n_b(\lambda)\cos\Theta_b \tag{2.33}$$

$$\eta_f = n_f(\lambda)\cos\Theta_f \tag{2.34}$$

and

$$\eta_m = n_m(\lambda)\cos\Theta_o \tag{2.35}$$

Also the angles Θ_b and Θ_f are calculated using Snell's law [21],

$$n_m(\lambda)\sin\Theta_o = n_f(\lambda)\sin\Theta_f \tag{2.36}$$

$$n_b(\lambda)\sin\Theta_b = n_f(\lambda)\sin\Theta_f \tag{2.37}$$

If we make calculations for wavelength $\lambda = 500$ nm, we can calculate the reflection coefficient of p-polarized light r_P as it is shown below. The index of refraction of air is

$$n_m(\lambda) = 1. \tag{2.38}$$

The angle of incidence when the polarized multiple channel light beam reflects of the aluminum mirror is

$$\Theta_o = 45^\circ. \tag{2.39}$$

From $n_m(\lambda)$ and Θ_o we obtain η_m using equation (2.35)

$$\eta_m = 0.7071. \tag{2.40}$$

Index of refraction of the aluminum mirror is [21]

$$n_f(\lambda) = 1.61. \tag{2.41}$$

Also thickness of aluminum oxide layer on the mirror is [21]

$$d_f = 4.12 \text{ nm}. \tag{2.42}$$

Using Snell's law equation (2.36) we can obtain

$$\Theta_f = 26.0526^\circ. \tag{2.43}$$

Index of refraction of bulk metal is [21]

$$n_b(\lambda) = 0.769 - i5.88. \tag{2.44}$$

Using Snell's law equation (2.37) we obtain Θ_b. Note that in equation (2.37) we only used the real part of $n_b(\lambda)$

$$\Theta_b = 66.855^\circ. \tag{2.45}$$

Using equation (2.33) we obtain η_b. Note that in equation (2.33) we only used the real part of $n_b(\lambda)$

$$\eta_b = 0.3023. \tag{2.46}$$

Using equation (2.32) we obtain δ_f

$$\delta_f = 4.2906^\circ. \tag{2.47}$$

From equation (2.34) we get η_f

$$\eta_f = 1.4464. \tag{2.48}$$

Using equations (2.30) and (2.31) we obtain E_m and H_m

$$E_m = 0.9972 + i0.0156 \tag{2.49}$$

$$H_m = 0.3015 + i0.1082. \tag{2.50}$$

Finally, using equation (2.29) we obtain the reflection coefficient of p-polarized light r_P

$$r_P = 0.3841 + i0.142. \tag{2.51}$$

Using equations (2.25) and (2.27) we obtain

$$R_P = 0.1677 \tag{2.52}$$

and

$$E_P = -20.2891^\circ. \tag{2.53}$$

The reflection coefficient of s-polarized light r_S is also defined as

$$r_S = \frac{\eta_m E_m - H_m}{\eta_m E_m + H_m} \tag{2.54}$$

where

$$E_m = \cos\delta_f + i\frac{\eta_b}{\eta_f}\sin\delta_f \tag{2.55}$$

$$H_m = \eta_b \cos\delta_f + i\eta_f \sin\delta_f \tag{2.56}$$

with

$$\delta_f = \frac{2\pi}{\lambda} n_f(\lambda) d_f \cos\Theta_f \tag{2.57}$$

$$\eta_b = \frac{n_b(\lambda)}{\cos\Theta_b} \tag{2.58}$$

$$\eta_f = \frac{n_f(\lambda)}{\cos\Theta_f} \tag{2.59}$$

and

$$\eta_m = \frac{n_m(\lambda)}{\cos\Theta_o} \tag{2.60}$$

Also the angles Θ_b and Θ_f are calculated using Snell's law [21],

$$n_m(\lambda)\sin\Theta_o = n_f(\lambda)\sin\Theta_f \tag{2.61}$$

$$n_b(\lambda)\sin\Theta_b = n_f(\lambda)\sin\Theta_f \tag{2.62}$$

Again if we make calculations for wavelength $\lambda = 500$ nm, we can calculate the reflection coefficient of s-polarized light r_S as it is shown below. The index of refraction of air is

$$n_m(\lambda) = 1. \tag{2.63}$$

The angle of incidence when the polarized multiple channel light beam reflects of the aluminum mirror is

$$\Theta_o = 45^\circ. \tag{2.64}$$

From $n_m(\lambda)$ and Θ_o we obtain η_m using equation (2.60)

$$\eta_m = 1.4142. \tag{2.65}$$

Again, index of refraction of the aluminum mirror is [21]

$$n_f(\lambda) = 1.61. \tag{2.66}$$

Also thickness of aluminum oxide layer on the mirror is [21]

$$d_f = 4.12 \text{ nm}. \tag{2.67}$$

Using Snell's law equation (2.61) we obtain

$$\Theta_f = 26.0526^\circ. \tag{2.68}$$

Index of refraction of bulk metal is [21]

$$n_b(\lambda) = 0.769 - i5.88. \tag{2.69}$$

Using Snell's law equation (2.62) we obtain Θ_b. Note that in equation (2.62) we only used the real part of $n_b(\lambda)$

$$\Theta_b = 66.855^\circ. \tag{2.70}$$

Using equation (2.58) we obtain η_b. Note that in equation (2.58) we only used the real part of $n_b(\lambda)$

$$\eta_b = 1.9564. \tag{2.71}$$

Using equation (2.57) we obtain δ_f

$$\delta_f = 4.2906^\circ. \tag{2.72}$$

From equation (2.59) we get η_f

$$\eta_f = 1.7921. \tag{2.73}$$

Using equations (2.55) and (2.56) we obtain E_m and H_m

$$E_m = 0.9972 + i0.0817 \tag{2.74}$$

$$H_m = 1.9509 + i0.1341. \tag{2.75}$$

Finally, using equation (2.54) we obtain the reflection coefficient of s-polarized light r_S

$$r_S = -0.1604 + i0.0064. \tag{2.76}$$

Using equations (2.26) and (2.28) we obtain

$$R_S = 0.0258 \tag{2.77}$$

and

$$E_S = 177.7151^\circ. \tag{2.78}$$

Finally, the Mueller matrix of the aluminum mirror is defined as

$$M_R = \begin{bmatrix} 1 & -0.734 & 0 & 0 \\ -0.734 & 1 & 0 & 0 \\ 0 & 0 & 0.6463 & -0.21 \\ 0 & 0 & 0.21 & 0.6463 \end{bmatrix} \tag{2.79}$$

Chapter 3

Polarization-sensitive Receiver

A light signal is defined by its intensity, wavelength and polarization. In the present system, we use intensity to encode the information to be delivered, and polarization to separate multiple channels. Each input light signal at a different polarization angle is modulated to represent one digital data channel. All these input light signals are combined at the source into one incident light signal traveling in free space. This incident light signal will form the input to our receiver.

Each data channel has a unique angle of polarization. If it is a dual data channel system then data channel angles of polarization are 0^o and 90^o. If it is a three channel system then data channel angles of polarization are 0^o, 60^o and 120^o. And if it is a four channel system then data channel angles of polarization are 0^o, 45^o, 90^o and 135^o.

This aggregate input light signal is received at a DoFP polarimeter array that may have two, three or four filters depending if we have a two, three or four channel design. Each filter from the array will have its own polarization angle that will match a polarization angle of

one channel of input light. The operation of the polarimeter array is modeled via its Mueller matrix, which has been parameterized using measurements from fabricated devices [48].

In the remainder of this chapter, we will define the appropriate mathematical models behind PDM for two, three, or four channel receiver designs.

3.1 Two Channel DoFP Polarization Filter Array

For a two channel DoFP polarization filter array the two input data channels have angles of polarization of 0º and 90º, respectively. Each input data channel is represented by a Stokes vector S_Θ [48]. The Stokes vectors for incident input light channels with polarization angles of 0º and 90° and intensity i are:

$$S_\Theta = \begin{bmatrix} S_0 \\ S_1 \\ S_2 \\ S_3 \end{bmatrix}, \qquad S_{0^\circ} = \begin{bmatrix} i \\ i \\ 0 \\ 0 \end{bmatrix}, \qquad S_{90^\circ} = \begin{bmatrix} i \\ -i \\ 0 \\ 0 \end{bmatrix}$$

The incident light that includes both data channels' signals has the total Stokes vector S_{INPUT} at any moment of time defined as

$$S_{\text{INPUT}} = b_0 S_{0^\circ} + b_{90} S_{90^\circ} \tag{3.1}$$

where b_0 and b_{90} represent the modulating bits (each valued at either 0 or 1).

If we modulate an incident input light signal (of intensity $i = 1$) with the binary sequence for two data channels, then the total Stokes vector S_{INPUT} for incident input light at any moment is illustrated in Figure 3.1.

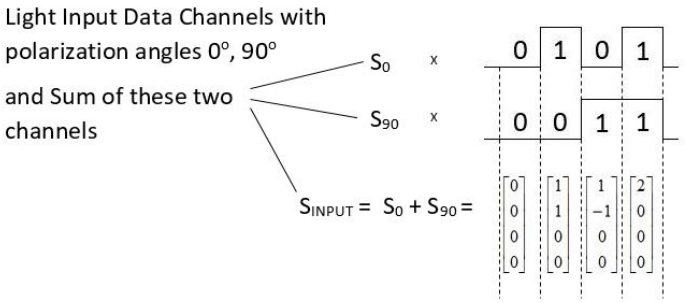

Figure 3.1: Input light signal modulated as binary sequence for two data channels with polarization angles of 0° and 90°.

The incident light signal S_{INPUT} reaches the DoFP polarization filter array, which separates the two channels. Each polarization filter is represented by the filter's Mueller matrix M_Θ [48].

$$M_\Theta = \frac{1}{2}\begin{bmatrix} (p_x^2+p_y^2) & (p_x^2-p_y^2)\mathrm{c}_{2\Theta} & (p_x^2-p_y^2)\mathrm{s}_{2\Theta} & 0 \\ (p_x^2-p_y^2)\mathrm{c}_{2\Theta} & (p_x^2+p_y^2)(\mathrm{c}_{2\Theta})^2+2p_xp_y(\mathrm{s}_{2\Theta})^2 & \frac{1}{2}(p_x-p_y)^2\mathrm{s}_{4\Theta} & 0 \\ (p_x^2-p_y^2)\mathrm{s}_{2\Theta} & \frac{1}{2}(p_x-p_y)^2\mathrm{s}_{4\Theta} & 2p_xp_y(\mathrm{c}_{2\Theta})^2+(p_x^2+p_y^2)(\mathrm{s}_{2\Theta})^2 & 0 \\ 0 & 0 & 0 & p_xp_y \end{bmatrix} \tag{3.2}$$

where $\mathrm{c}_{2\Theta}$ is $\cos 2\Theta$, $\mathrm{s}_{2\Theta}$ is $\sin 2\Theta$, and $\mathrm{s}_{4\Theta}$ is $\sin 4\Theta$. In the Mueller matrix M_Θ, Θ is the angle of polarization and p_x and p_y are the transmission coefficients in the x and y axes (they characterize the properties, including imperfections, of the aluminum nanowire filters). Figure 3.2 illustrates the input light signal S_{INPUT} that reaches the DoFP polarization filter array and the output light signals from the filters I_{0° and I_{90°.

The output of each filter from the DoFP polarization filter array is [48]:

$$I_\Theta = g\begin{bmatrix} 1 & 0 & 0 & 0 \end{bmatrix} M_\Theta S_{\text{INPUT}} + d \tag{3.3}$$

In the equation above I_Θ represents the light intensity of each filter from the DoFP polarization filter array. Variables g and d are the internal gain and dark offset of each filter. We will

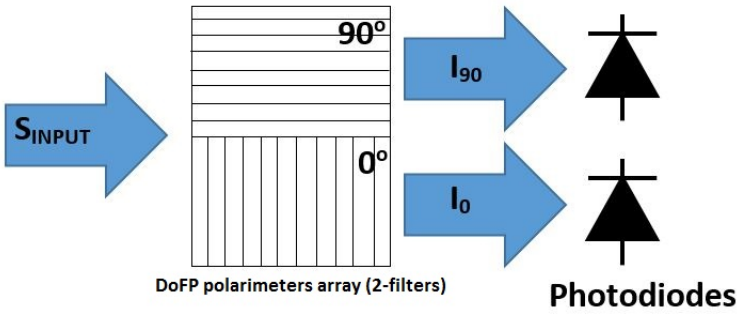

Figure 3.2: The input light signal for two data channels with polarization angles of 0° and 90° incident upon the DoFP polarization filter array generates the output light signals from the filters I_0 and I_{90}.

assume that gain is equal to 1. Also for our application we can ignore the dark offset because this current is measured in fA and a single channel's photodiode current is between fA when there is no light and a few µA when there is light so the dark offset current is negligible. Therefore,

$$I_\Theta = \begin{bmatrix} 1 & 0 & 0 & 0 \end{bmatrix} M_\Theta S_{\text{INPUT}} \tag{3.4}$$

This yields the following model for the filter output:

$$I_\Theta = \begin{bmatrix} \frac{1}{2} \\ 0 \\ 0 \\ 0 \end{bmatrix}^T \begin{bmatrix} (p_x^2+p_y^2) & (p_x^2-p_y^2)\mathrm{c}_{2\Theta} & (p_x^2-p_y^2)\mathrm{s}_{2\Theta} & 0 \\ (p_x^2-p_y^2)\mathrm{c}_{2\Theta} & (p_x^2+p_y^2)(\mathrm{c}_{2\Theta})^2+2p_xp_y(\mathrm{s}_{2\Theta})^2 & \frac{1}{2}(p_x-p_y)^2\mathrm{s}_{4\Theta} & 0 \\ (p_x^2-p_y^2)\mathrm{s}_{2\Theta} & \frac{1}{2}(p_x-p_y)^2\mathrm{s}_{4\Theta} & 2p_xp_y(\mathrm{c}_{2\Theta})^2+(p_x^2+p_y^2)(\mathrm{s}_{2\Theta})^2 & 0 \\ 0 & 0 & 0 & p_xp_y \end{bmatrix} \begin{bmatrix} S_0 \\ S_1 \\ S_2 \\ S_3 \end{bmatrix} \tag{3.5}$$

where again $\mathrm{c}_{2\Theta}$ is $\cos 2\Theta$, $\mathrm{s}_{2\Theta}$ is $\sin 2\Theta$, and $\mathrm{s}_{4\Theta}$ is $\sin 4\Theta$. Assuming that the intensity in the Stokes vectors for S_{0° and S_{90° is 2, this will yield the the following Stokes vectors for incident input light with polarization angles of 0° and 90° (we allow for un-normalized expression of

Stokes vectors):

$$S_{0^\circ} = \begin{bmatrix} 2 \\ 2 \\ 0 \\ 0 \end{bmatrix}, \qquad S_{90^\circ} = \begin{bmatrix} 2 \\ -2 \\ 0 \\ 0 \end{bmatrix} \tag{3.6}$$

Each filter output I_Θ is defined as

$$I_\Theta = \frac{1}{2}[S_0(p_x^2 + p_y^2) + S_1(p_x^2 - p_y^2)\cos(2\Theta) + S_2(p_x^2 - p_y^2)\sin(2\Theta)] \tag{3.7}$$

We use the following approximations to calculate the filter's outputs I_Θ [48]:

$$T = (p_x^2 + p_y^2) = \frac{1}{2} \tag{3.8}$$

$$D = \frac{(p_x^2 - p_y^2)}{(p_x^2 + p_y^2)} = 0.99 \tag{3.9}$$

These represent the physical properties of the fabricated filters themselves. The above leads to filter output I_Θ represented by

$$I_\Theta = \frac{1}{4}S_0 + \frac{0.99}{4}S_1\cos(2\Theta) + \frac{0.99}{4}S_2\sin(2\Theta) \tag{3.10}$$

so for the filter with polarization angle of 0^o the output light signal is calculated as:

$$\begin{aligned} I_0 &= \frac{1}{4}S_0 + \frac{0.99}{4}S_1\cos(0^o) + \frac{0.99}{4}S_2\sin(0^o) \\ &= \frac{1}{4}S_0 + \frac{0.99}{4}S_1 \end{aligned} \tag{3.11}$$

and for the filter with polarization angle of 90° the output light signal is calculated as:

$$\begin{aligned} I_{90} &= \frac{1}{4}S_0 + \frac{0.99}{4}S_1\cos(180^o) + \frac{0.99}{4}S_2\sin(180^o) \\ &= \frac{1}{4}S_0 - \frac{0.99}{4}S_1 \end{aligned} \tag{3.12}$$

If we examine a binary truth table for this two channel DoFP polarization filter array we can see that we can have the correct binary outputs given we use a reasonable comparison point for light intensity (anywhere near 0.5 will be sufficient). This is shown in Table 3.1.

Table 3.1: Binary truth table for two channel DoFP polarization filter array.

b_{90}	b_0	S_{INPUT}	I_{90}	I_0
0	0	$[0 \quad 0 \quad 0 \quad 0]^T$	0	0
0	1	$[2 \quad 2 \quad 0 \quad 0]^T$	0.005	0.995
1	0	$[2 \quad -2 \quad 0 \quad 0]^T$	0.995	0.005
1	1	$[4 \quad 0 \quad 0 \quad 0]^T$	1	1

3.2 Three Channel DoFP Polarization Filter Array

For a three channel DoFP polarization filter array the three input data channels have angles of polarization of 0°, 60° and 120°, respectively. The Stokes vectors for incident input light (of intensity i) with polarization angles of 0°, 60°, and 120° are:

$$S_{0^\circ} = \begin{bmatrix} i \\ i \\ 0 \\ 0 \end{bmatrix}, \qquad S_{60^\circ} = \begin{bmatrix} i \\ -\frac{1}{2}i \\ \frac{\sqrt{3}}{2}i \\ 0 \end{bmatrix}, \qquad S_{120^\circ} = \begin{bmatrix} i \\ -\frac{1}{2}i \\ -\frac{\sqrt{3}}{2}i \\ 0 \end{bmatrix} \tag{3.13}$$

The incident input light signal that includes all of the channels' signals has the total Stokes vector S_{INPUT} at any moment of time defined as

$$S_{\text{INPUT}} = b_0 S_{0^\circ} + b_{60} S_{60^\circ} + b_{120} S_{120^\circ} \tag{3.14}$$

If we modulate an intensity $i = 1$ light signal with the binary sequence for three data channels, then the total Stokes vector S_{INPUT} for incident input light at any moment is illustrated in Figure 3.3. Figure 3.4 shows the filter system.

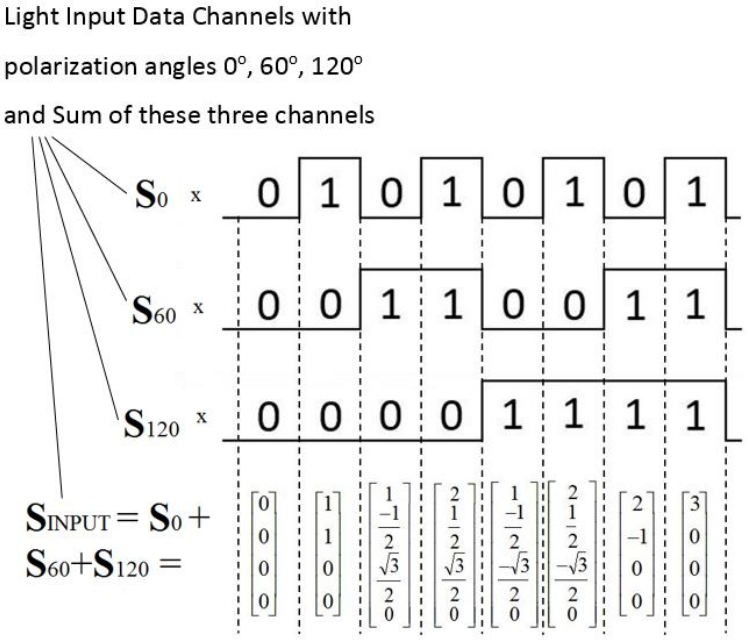

Figure 3.3: The light signal modulated as binary sequence for three data channels with polarization angles of 0°, 60°, and 120°.

Again each DoFP polarization filter is represented by the filter's Mueller matrix M_Θ from equation (3.2), and the output of each filter is:

$$I_\Theta = \begin{bmatrix} 1 & 0 & 0 & 0 \end{bmatrix} M_\Theta S_{\text{INPUT}} \tag{3.15}$$

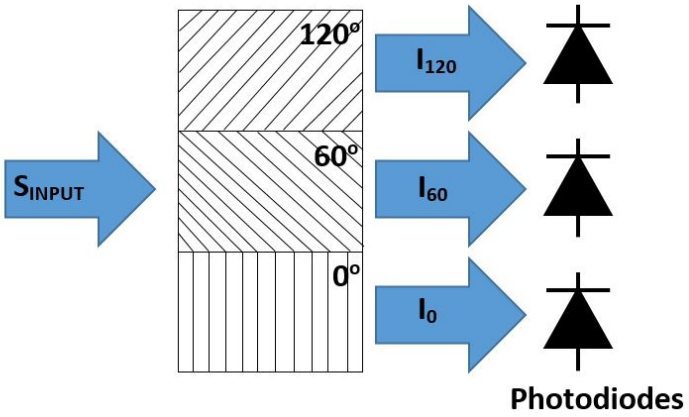

Figure 3.4: The incident input light signal for three data channels with polarization angles of 0°, 60° and 120° reaches the DoFP polarization filter array and generates the output light signals from the filters I_0, I_{60}, and I_{120}.

If we assume that intensity i in the Stokes vectors for S_{0°, S_{60° and S_{120° is 2, this will yield

$$S_{0^\circ} = \begin{bmatrix} 2 \\ 2 \\ 0 \\ 0 \end{bmatrix}, \qquad S_{60^\circ} = \begin{bmatrix} 2 \\ -1 \\ \sqrt{3} \\ 0 \end{bmatrix}, \qquad S_{120^\circ} = \begin{bmatrix} 2 \\ -1 \\ -\sqrt{3} \\ 0 \end{bmatrix} \tag{3.16}$$

Each filter output I_Θ is again defined as

$$I_\Theta = \frac{1}{2}[S_0(p_x^2 + p_y^2) + S_1(p_x^2 - p_y^2)\cos(2\Theta) + S_2(p_x^2 - p_y^2)\sin(2\Theta)] \tag{3.17}$$

Using equations (3.8), (3.9) and (3.10) gives filter output I_Θ. For the filter with polarization angle of 0° the output light signal is:

$$\begin{aligned} I_0 &= \frac{1}{4}S_0 + \frac{0.99}{4}S_1\cos(0^o) + \frac{0.99}{4}S_2\sin(0^o) \\ &= \frac{1}{4}S_0 + \frac{0.99}{4}S_1 \end{aligned} \tag{3.18}$$

for the filter with polarization angle of 60° the output light signal is:

$$\begin{aligned} I_{60} &= \frac{1}{4}S_0 + \frac{0.99}{4}S_1\cos(120^o) + \frac{0.99}{4}S_2\sin(120^o) \\ &= \frac{1}{4}S_0 - \frac{0.99}{8}S_1 + \frac{0.99}{8}\sqrt{3}S_2 \end{aligned} \tag{3.19}$$

and for the filter with polarization angle of 120° the output light signal is:

$$\begin{aligned} I_{120} &= \frac{1}{4}S_0 + \frac{0.99}{4}S_1\cos(240^o) + \frac{0.99}{4}S_2\sin(240^o) \\ &= \frac{1}{4}S_0 - \frac{0.99}{8}S_1 - \frac{0.99}{8}\sqrt{3}S_2 \end{aligned} \tag{3.20}$$

If we examine the binary truth table for this three channel DoFP polarization filter array (see Table 3.2) we can see that we can still have the correct output binary values with an appropriately chosen threshold; all input 0s have output intensity ≤ 0.505 and all input 1s have output intensity ≥ 0.995. However, the available noise margin is significantly reduced due to crosstalk between the channels.

Table 3.2: Binary truth table for three channel DoFP polarization filter array.

b_{120}	b_{60}	b_0	S_{INPUT}	I_{120}	I_{60}	I_0
0	0	0	$[0 \quad 0 \quad 0 \quad 0]^T$	0	0	0
0	0	1	$[2 \quad 2 \quad 0 \quad 0]^T$	0.253	0.253	0.995
0	1	0	$[2 \quad -1 \quad \sqrt{3} \quad 0]^T$	0.253	0.995	0.253
0	1	1	$[4 \quad 1 \quad \sqrt{3} \quad 0]^T$	0.505	1.248	1.248
1	0	0	$[2 \quad -1 \quad -\sqrt{3} \quad 0]^T$	0.995	0.253	0.253
1	0	1	$[4 \quad 1 \quad -\sqrt{3} \quad 0]^T$	1.248	0.505	1.248
1	1	0	$[4 \quad -2 \quad 0 \quad 0]^T$	1.248	1.248	0.505
1	1	1	$[6 \quad 0 \quad 0 \quad 0]^T$	1.5	1.5	1.5

3.3 Four Channel DoFP Polarization Filter Array

In a four channel DoFP Polarization filter array four input data channels have angles of polarization of 0º, 45º, 90º and 135º, respectively. The Stokes vectors for incident input light with polarization angles of 0º, 45°, 90°, and 135° and intensity i are:

$$S_{0^\circ} = \begin{bmatrix} i \\ i \\ 0 \\ 0 \end{bmatrix}, \qquad S_{45^\circ} = \begin{bmatrix} i \\ 0 \\ i \\ 0 \end{bmatrix}, \qquad S_{90^\circ} = \begin{bmatrix} i \\ -i \\ 0 \\ 0 \end{bmatrix}, \qquad S_{135^\circ} = \begin{bmatrix} i \\ 0 \\ -i \\ 0 \end{bmatrix} \tag{3.21}$$

The incident input light signal that includes all data channels has the total Stokes vector S_{INPUT} defined as

$$S_{\text{INPUT}} = b_0 S_{0^\circ} + b_{45} S_{45^\circ} + b_{90} S_{90^\circ} + b_{135} S_{135^\circ} \tag{3.22}$$

Once again, each filter is represented by the filter's Mueller matrix M_Θ from equation (3.2), and the output of each filter is:

$$I_\Theta = \begin{bmatrix} 1 & 0 & 0 & 0 \end{bmatrix} M_\Theta S_{\text{INPUT}} \tag{3.23}$$

If we assume that the intensity parameter i in the Stokes vectors S_{0°, S_{45°, S_{90° and S_{135° is 2, this will yield

$$S_{0^\circ} = \begin{bmatrix} 2 \\ 2 \\ 0 \\ 0 \end{bmatrix}, \qquad S_{45^\circ} = \begin{bmatrix} 2 \\ 0 \\ 2 \\ 0 \end{bmatrix}, \qquad S_{90^\circ} = \begin{bmatrix} 2 \\ -2 \\ 0 \\ 0 \end{bmatrix}, \qquad S_{135^\circ} = \begin{bmatrix} 2 \\ 0 \\ -2 \\ 0 \end{bmatrix} \tag{3.24}$$

Figure 3.5 shows the input light S_{INPUT} that reaches the DoFP polarization filter array and the output light signals from the filters I_0, I_{45}, I_{90} and I_{135}.

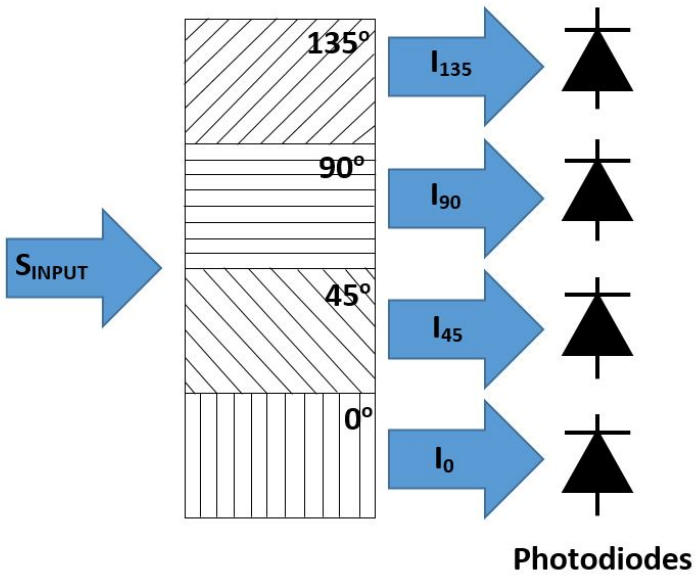

Figure 3.5: The input light signal for four data channels with polarization angles of 0°, 45°, 90° and 135° reaches the DoFP polarization filter array and generates the output light signals from the filters I_0, I_{45}, I_{90} and I_{135}.

Each filter output I_Θ is

$$I_\Theta = \frac{1}{2}[S_0(p_x^2 + p_y^2) + S_1(p_x^2 - p_y^2)\cos(2\Theta) + S_2(p_x^2 - p_y^2)\sin(2\Theta)] \tag{3.25}$$

Using equations (3.8), (3.9) and (3.25) gives filter output I_Θ. For the filter with polarization angle of 0^o the output light signal is calculated as:

$$\begin{aligned} I_0 &= \frac{1}{4}S_0 + \frac{0.99}{4}S_1\cos(0^o) + \frac{0.99}{4}S_2\sin(0^o) \\ &= \frac{1}{4}S_0 + \frac{0.99}{4}S_1 \end{aligned} \tag{3.26}$$

for the filter with polarization angle of 45^o the output light signal is calculated as:

$$\begin{aligned} I_{45} &= \frac{1}{4}S_0 + \frac{0.99}{4}S_1\cos(90^o) + \frac{0.99}{4}S_2\sin(90^o) \\ &= \frac{1}{4}S_0 + \frac{0.99}{4}S_2 \end{aligned} \tag{3.27}$$

for the filter with polarization angle of 90^o the output light signal is calculated as:

$$\begin{aligned} I_{90} &= \frac{1}{4}S_0 + \frac{0.99}{4}S_1\cos(180^o) + \frac{0.99}{4}S_2\sin(180^o) \\ &= \frac{1}{4}S_0 - \frac{0.99}{4}S_1 \end{aligned} \tag{3.28}$$

and for the filter with polarization angle of 135^o the output light signal is calculated as:

$$\begin{aligned} I_{135} &= \frac{1}{4}S_0 + \frac{0.99}{4}S_1\cos(270^o) + \frac{0.99}{4}S_2\sin(270^o) \\ &= \frac{1}{4}S_0 - \frac{0.99}{4}S_2 \end{aligned} \tag{3.29}$$

When we examine the binary truth table for the four channel DoFP polarization filter array we see that we cannot have the correct output for each input combination (see Table 3.3). At the very least, the input combination 0101 will be indistinguishable from input combination 1010.

Table 3.3: Binary truth table for four channel DoFP polarization filter array.

b_{135}	b_{90}	b_{45}	b_0	S_{INPUT}	I_{135}	I_{90}	I_{45}	I_0
0	0	0	0	$[0 \quad 0 \quad 0 \quad 0]^T$	0	0	0	0
0	0	0	1	$[2 \quad 2 \quad 0 \quad 0]^T$	0.5	0.005	0.5	0.995
0	0	1	0	$[2 \quad 0 \quad 2 \quad 0]^T$	0.005	0.5	0.995	0.5
0	0	1	1	$[4 \quad 2 \quad 2 \quad 0]^T$	0.505	0.505	1.495	1.495
0	1	0	0	$[2 \quad -2 \quad 0 \quad 0]^T$	0.5	0.995	0.5	0.005
0	1	0	1	$[4 \quad 0 \quad 0 \quad 0]^T$	1	1	1	1
0	1	1	0	$[4 \quad -2 \quad 2 \quad 0]^T$	0.505	1.495	1.495	0.505
0	1	1	1	$[6 \quad 0 \quad 2 \quad 0]^T$	1.005	1.5	1.995	1.5
1	0	0	0	$[2 \quad 0 \quad -2 \quad 0]^T$	0.995	0.5	0.005	0.5
1	0	0	1	$[4 \quad 2 \quad -2 \quad 0]^T$	1.495	0.505	0.505	1.495
1	0	1	0	$[4 \quad 0 \quad 0 \quad 0]^T$	1	1	1	1
1	0	1	1	$[6 \quad 2 \quad 0 \quad 0]^T$	1.5	1.005	1.5	1.995
1	1	0	0	$[4 \quad -2 \quad -2 \quad 0]^T$	1.495	1.495	0.505	0.505
1	1	0	1	$[6 \quad 0 \quad -2 \quad 0]^T$	1.995	1.5	1.005	1.5
1	1	1	0	$[6 \quad -2 \quad 0 \quad 0]^T$	1.5	1.995	1.5	1.005
1	1	1	1	$[8 \quad 0 \quad 0 \quad 0]^T$	2	2	2	2

For example, if we posit a threshold of 0.7 for each of four filter outputs I_0, I_{45}, I_{90} and I_{135} in Table 3.3 we can see that:

1. I_{135} will not result in 0 for two input sequences 0101 and 0111.

2. I_{90} will not result in 0 for two input sequences 1010 and 1011.

3. I_{45} will not result in 0 for two input sequences 0101 and 1101.

4. I_0 will not result in 0 for two input sequences 1010 and 1110.

The crosstalk between neighboring channels is sufficiently large that only 10 of the 16 input combinations give unique output combinations. We defer until Chapter 6 to determine coding techniques that can improve upon this.

We have developed VerilogA models for DoFP polarization filter arrays of two, three and four channels. In the next section, we will describe a simulation model of the complete receiver system, including both the optical and electronic subsystems.

3.4 Simulation Model

Figure 3.6 shows the entire four data channel receiver of the VLC PDM system. Simulation models have been constructed for two, three, and four data channel receiver subsystems using Cadence software tools.

Transmitter laser input signals are simulated with square wave voltage sources with proper amplitudes that represent input laser signal power. These transmitter laser input signals are are connected to DoFP filter arrays for two, three and four channel VLC PDM designs.

The VLC PDM system receiver's DoFP filter arrays are modeled using VerilogA. They are connected to the photodiode in each data communication channel. Each photodiode is also modeled using VerilogA.

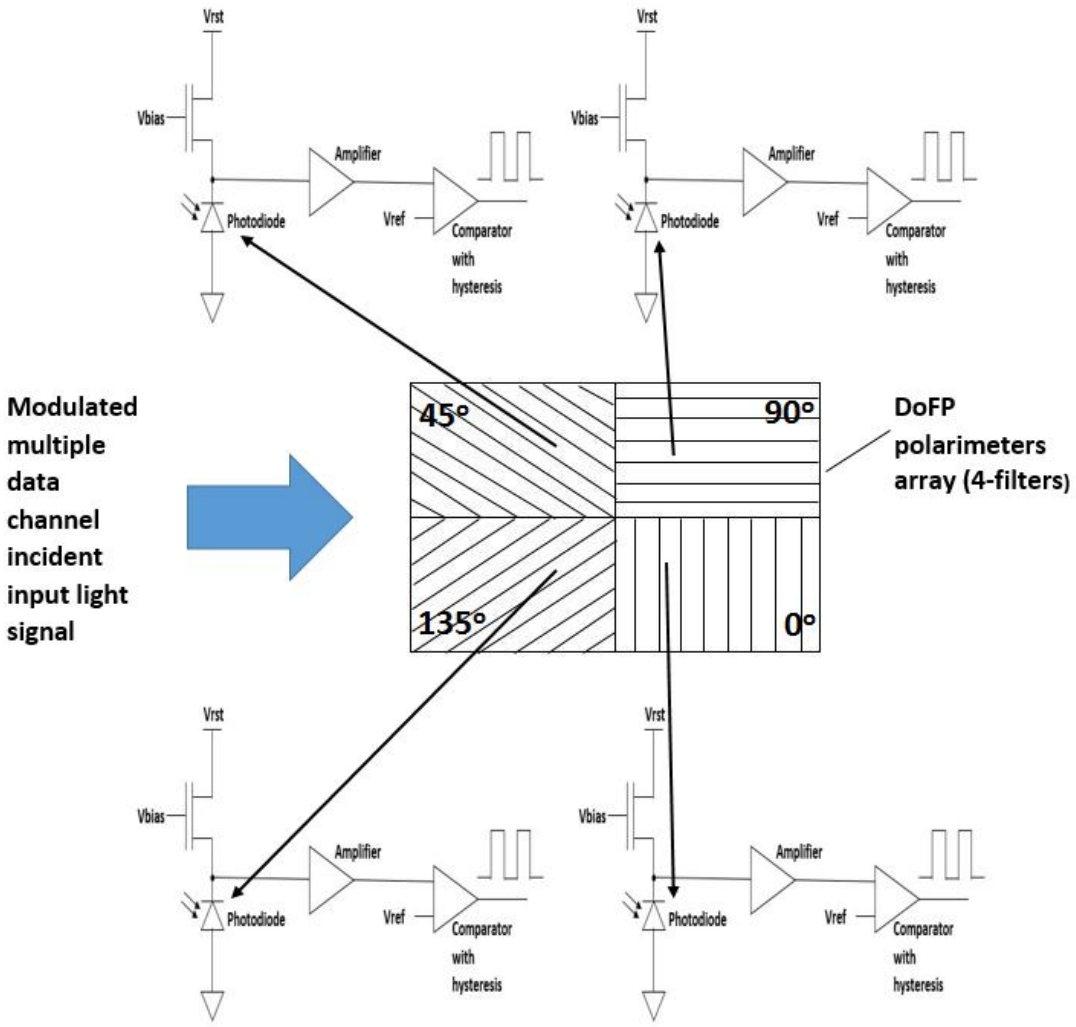

Figure 3.6: Four channel VLC system.

The rest of the simulation model was designed using Cadence 180 nm node design software. This part of each receiver channel has the amplifier circuit followed by the comparator with hysteresis circuit. The electronic subsystem for each data channel is designed as shown in Figure 3.7.

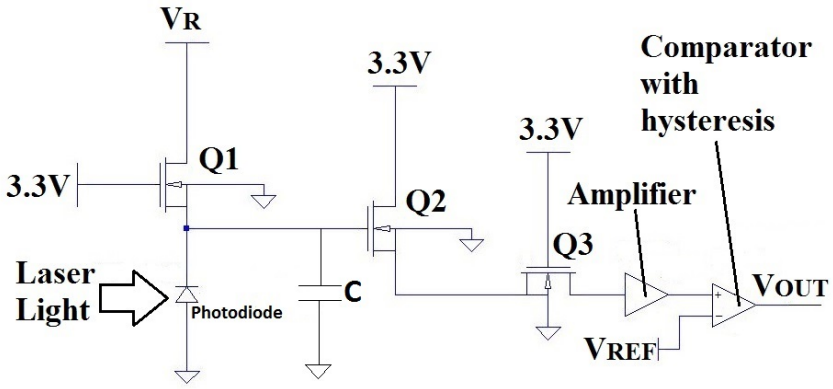

Figure 3.7: One data channel of VLC system.

3.4.1 Photodiode

Photodiodes used in the VLC system have to be fast switching diodes and they should have low capacitance. Fast switching photodiodes have been used for optical high speed digital clocking in various silicon chips. [1, 36, 49] The photodiode model was designed using VerilogA. Examples of complex photodiode model designs created in VerilogA exist in the literature [4]. For the VLC system we will use a simpler photodiode model. The photodiode circuit is shown in Figure 3.8.

The photodiode is reverse biased by $V_R = 2.25$ V, a voltage source connected through the active CMOS transistor Q1. The transistor Q1 is biased with $V_{\text{bias}} = 3.3$ V, and a parallel capacitance (20 fF) simulates the photodiode's internal capacitance. In the VerilogA model, the photodiode current is calculated using the following expression [3]:

$$I_{photodiode} = I_{forward} - I_{optical} = qA(\frac{D_p}{L_p}p_n + \frac{D_n}{L_n}n_p)(e^{V_R/V_T} - 1) - qAg_{op}(L_p + L_n + W) \tag{3.30}$$

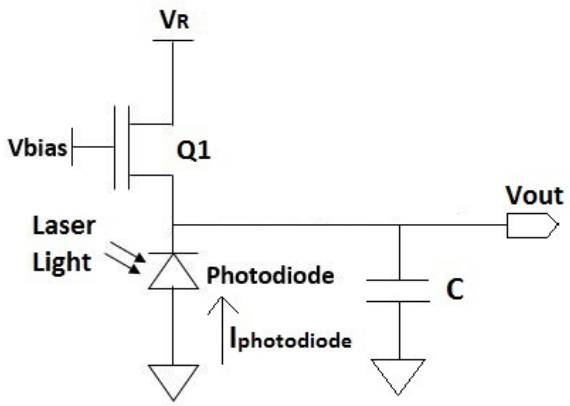

Figure 3.8: Photodiode circuit of one data channel of VLC system.

The photodiode forward current I_{forward} is a dark current approximation that represents current flowing from anode to cathode when reverse bias voltage V_{R} is applied and no light shines on the photodiode.

$$I_{forward} = qA(\frac{D_p}{L_p}p_n + \frac{D_n}{L_n}n_p)(e^{V_R/V_T} - 1) \tag{3.31}$$

This current is in the order of few fA, which is negligible current for this application. The photodiode optical current I_{optical} is a reverse current created by shining light on the photodiode. This current is in the order of few µA.

$$I_{optical} = qAg_{op}(L_p + L_n + W) \tag{3.32}$$

The model parameters for the above expressions are given in Table 3.4.

Table 3.4: Photodiode model parameters [3, 72].

Parameter	Symbol	Value
Basic electric charge	q	1.6×10^{-19} C
Area of Si-pn junction	A	0.0001 cm^2
Temperature	T	300 K
Boltzmann constant	K	1.38×10^{-23} $\frac{\text{m}^2\text{kg}}{\text{s}^2 K}$
Thermal voltage	V_T	$\frac{KT}{q} = 0.025875$ V
Intrinsic electron and hole concentration for Si at 25°C	n_i	1.5×10^{-10} cm^{-3}
Dielectric constant of vacuum	ε_o	8.85×10^{-14} F/cm
Relative dielectric constant of Si	ε_r	11.8
Acceptor concentration of photodiode N-junction	N_d	10^{15} cm^{-3}
Carrier recombination lifetime of N-junction	τ_p	0.00001 s
Electron mobility of photodiode N-junction	μ_n	1300 $\frac{\text{cm}^2}{\text{Vs}}$
Hole mobility of photodiode N-junction	μ_p	450 $\frac{\text{cm}^2}{\text{Vs}}$
Acceptor concentration of photodiode P-junction	N_a	10^{17} cm^{-3}
Carrier Recombination lifetime of P-junction	τ_n	0.0000001 s
Electron mobility of photodiode P-junction	μ_n	700 $\frac{\text{cm}^2}{\text{Vs}}$
Hole mobility of photodiode P-junction	μ_p	200 $\frac{\text{cm}^2}{\text{Vs}}$
Optical generation rate	g_{op}	$\frac{\alpha P_O}{E_{PH} q} = 8.68056 \times 10^{19}$
Absorption coefficient of Si	α	500 cm^{-1}
Uniform illumination of red light	E_{PH}	1.8 eV
Laser optical power	P_O	0.05 $\frac{W}{\text{cm}^2}$
Diffusion coefficient on photodiode N-junction	D_p	$V_T \mu_p$
Diffusion coefficient on photodiode P-junction	D_n	$V_T \mu_n$
Diffusion length for holes	L_p	$\sqrt{D_p \tau_p}$
Diffusion length for electrons	L_n	$\sqrt{D_n \tau_n}$
Minority concentration of electrons in P-junction	p_n	$\frac{n_i^2}{N_d}$
Minority concentration of holes in N-junction	n_p	$\frac{n_i^2}{N_a}$
Contact potential	V_o	$V_T \ln(\frac{N_a N_d}{n_i^2})$
Depletion region width	W	$\sqrt{\frac{2\varepsilon_o \varepsilon_r}{q}(V_o - V_R)(\frac{1}{N_a} + \frac{1}{N_d})}$

3.4.2 Amplifier

The amplifier circuit shown in Figure 3.9 is used to boost the input voltage signal range to an appropriate level for the comparator. It is a common-source stage amplifier with a diode-connected PMOS device used as an active load [54].

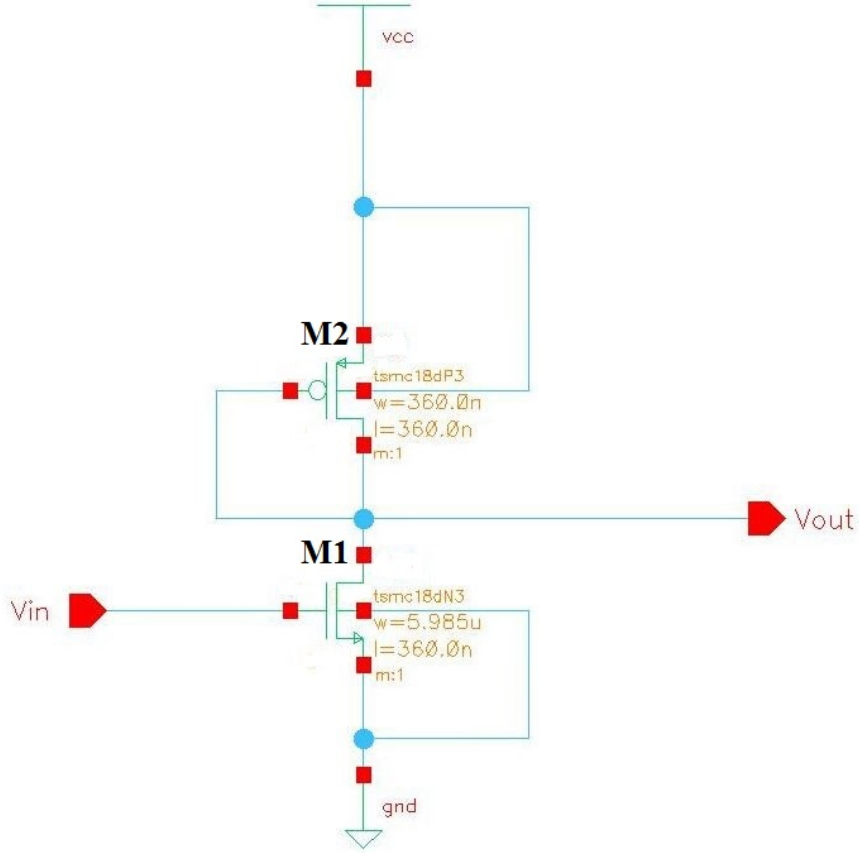

Figure 3.9: Amplifier circuit of one data channel of VLC system.

The relationship between V_{IN} and V_{OUT} is shown in Figure 3.10. V_{IN} is the voltage coming out of the photodiode circuit stage and it is in the range 600 mV to 850 mV. Using a common-source stage amplifier with diode-connected PMOS device this voltage range is changed to the inverted V_{OUT} signal in range 1.5 V to 2.5 V. This is much larger voltage

range and it is easier for the comparator with hysteresis to detect between voltage low (binary "0") and voltage high (binary "1") with proper threshold voltage.

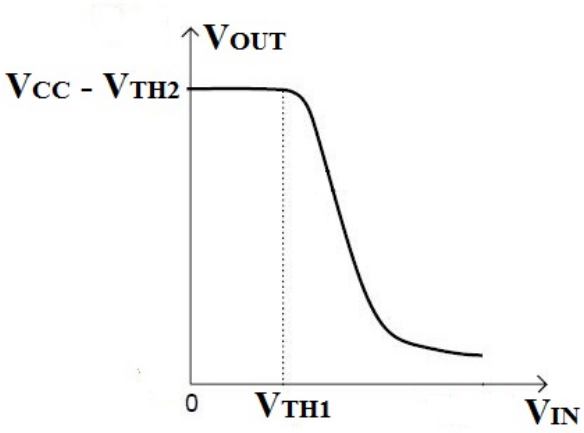

Figure 3.10: Input-output characteristics of common-stage amplifier with diode-connected PMOS device as load [54].

3.4.3 Comparator

A comparator with settable hysteresis band is used to differentiate between a high voltage or binary 1 and a low voltage or binary 0 in each data channel. In the simulated design each channel uses a three-stage comparator with internal hysteresis, which is shown in Figure 3.11.

Figure 3.12 shows a high-level block diagram. The comparator consists of five blocks. [15, 34] The first block is a differential stage which uses internal bias and internal hysteresis blocks to detect a voltage high or voltage low. The Common Source amplifier block is used to increase the gain. Finally the last block stage is an inverter stage, it is used to increase the gain and to improve the slew-rate of the output voltage. The inverter stage consists of nine inverters for the VLC system design.

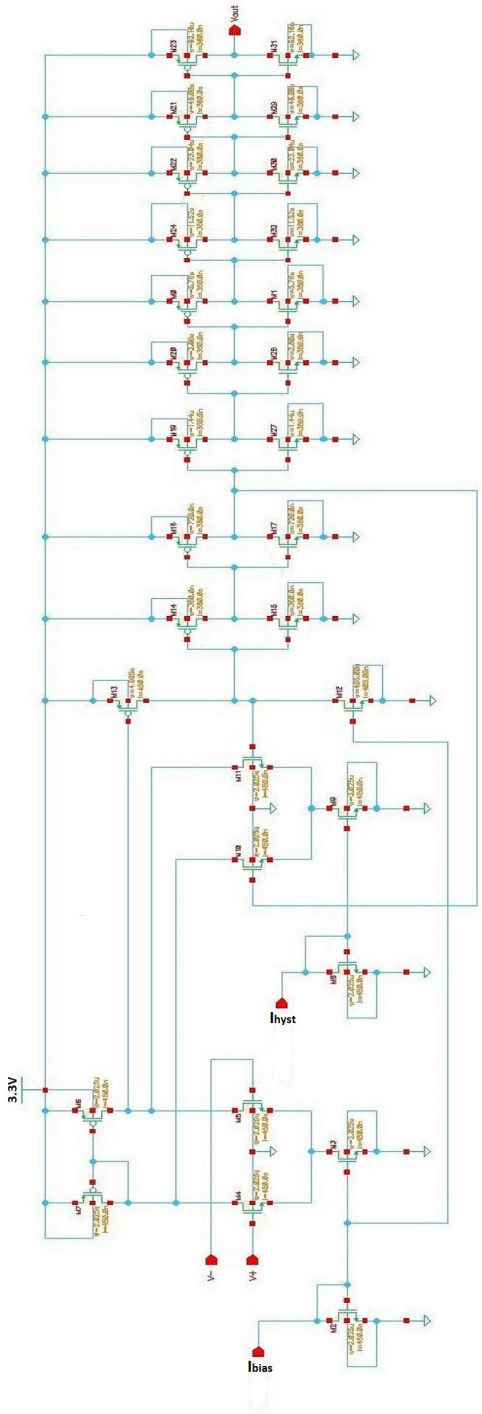

Figure 3.11: The three-stage comparator with internal hysteresis.

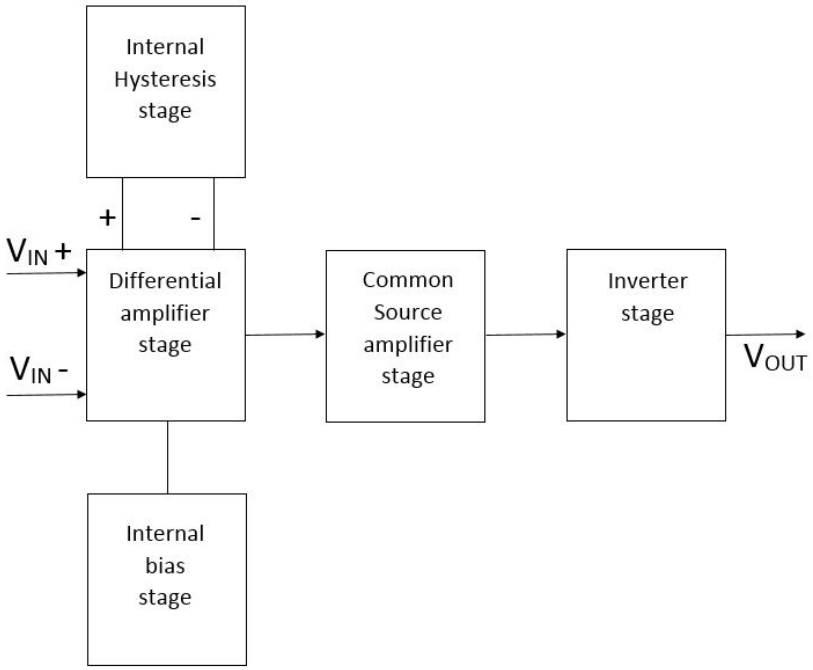

Figure 3.12: Block diagram of the 3-stage comparator with internal hysteresis.

The $V_{\text{IN}}+$ input of the comparator is connected to the output voltage of the amplifier stage of the VLC system. The V_{IN}- input is connected to a reference voltage which is used to compare to the input voltage $V_{\text{IN}}+$.

3.5 Simulation Results

The results that follow, we will illustrate the correct operation of the two channel and three channel systems, show the resilience of the three channel system to variations in the fabrication of the filters, and demonstrate how the four channel system is capable of reliably delivering 10 of 16 possible bit patterns.

For the two channel system, we will show a number of internal signals, indicating the internal operation of each channel. For the three channel system we will highlight the internal signals that vary as the fabricated instances can vary.

3.5.1 Two Channel System

The two channel VLC system consists of 0° and 90° polarization angle data channels. The schematic diagram for the two channel VLC system is shown in Figure 3.13. Two laser input sources are in the lower left-hand corner of the schematic. They are simulated using square wave voltage sources each with amplitudes of 50 mV and with frequency of 1MHz. One square wave voltage source represents the laser input source with 0° polarization angle and other square wave voltage source represents the laser input source with 90° polarization angle. In the VerilogA model, we use a 50 mV amplitude voltage signal to represent light power of 50 mW. These two square wave voltage sources are inputs to two channel DoFP filter array.

Two channel DoFP filter array, immediately to the right of the light sources is based on the Muller matrix computation described in Section 3.1. Two channel DoFP filter array was designed in VerilogA and it is defined as custom part of the VLC system that is simulated in Cadence.

Each DoFP filter array output is connected to a photodiode from Section 4.1 (shown at the top of the schematic). The photodiode was also modeled in VerilogA and it is defined as a custom part of the VLC system. The photodiode output is connected to the common-source amplifier with diode-connected PMOS device described in Section 4.2. The output of the common-source stage amplifier is connected to the comparator with internal hysteresis described in Section 4.3.

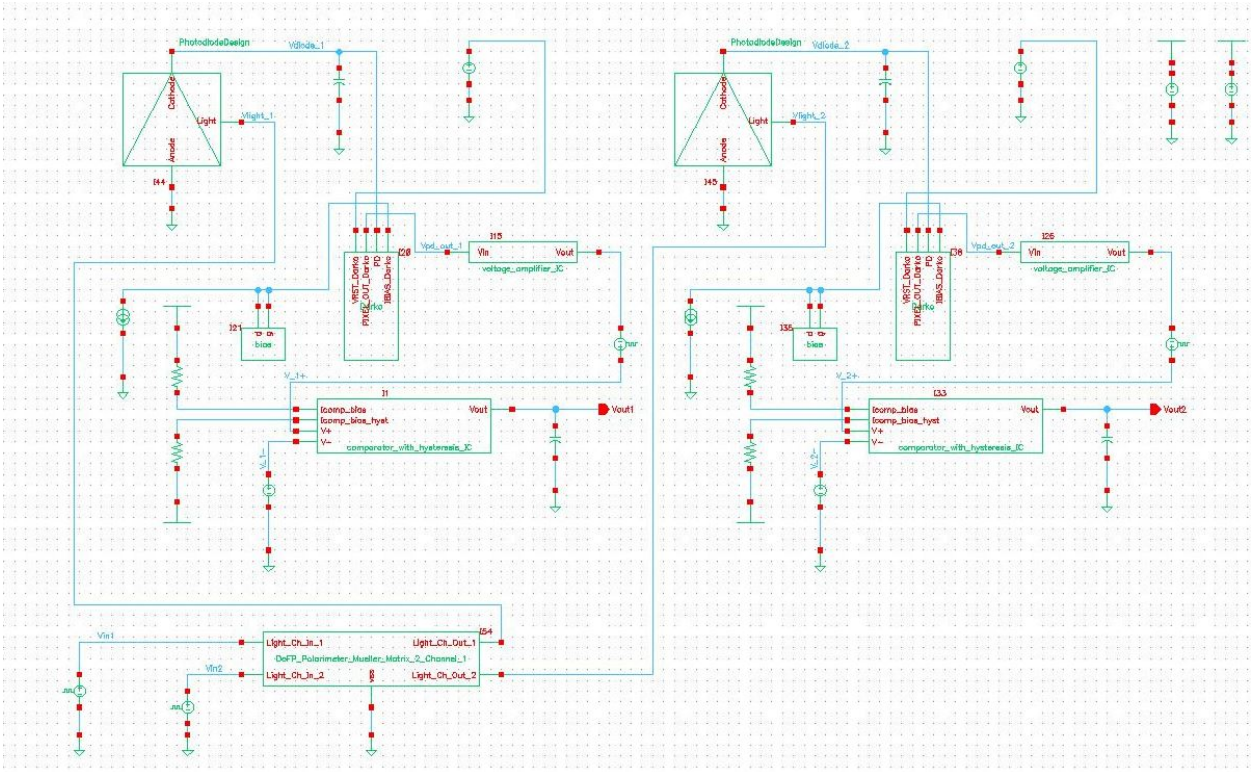

Figure 3.13: Two channel system with 0° and 90° polarization angles.

Figure 3.14 shows two modulated laser sources as input signals V_{in1} with 0° polarization angle and V_{in2} with 90° polarization angle. $V_{\text{light\_1}}$ and $V_{\text{light\_2}}$ represent the light signals from the filter array, $V_{\text{diode\_1}}$ and $V_{\text{diode\_2}}$ represent the signals from the photodiodes, $V_{\text{pd\_out\_1}}$ and $V_{\text{pd\_out\_2}}$ represent the output of the bias circuit (input to the amplifier),

and V_{1+} and V_{2+} are the non-inverting inputs to the comparator. The input light signals are completely recovered at each data channel output of the VLC system, V_{out1} and V_{out2}.

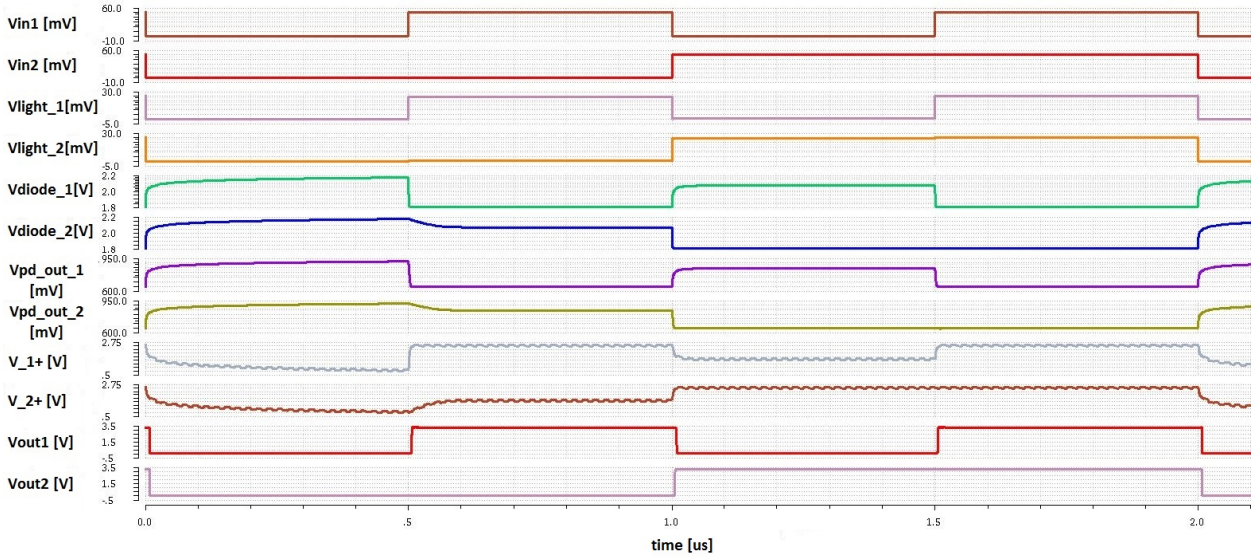

Figure 3.14: Two channels with 0° and 90° polarization angles.

3.5.2 Three Channel System

The three channel VLC system consists of 0°, 60° and 120° polarization angles data channels and is shown in Figure 3.15. Three laser sources are simulated with square wave voltage sources each 100 mW (100 mV) that are input to a three channel DoFP filter array. The rest of the three channel VLC system is exactly the same as the two channel VLC system. Again, the light sources and filter are in the lower left-hand corner of the schematic and the photodiodes are across the top.

Figure 3.16 shows that three modulated laser sources input signals are completely recovered at each data channel output of the VLC system.

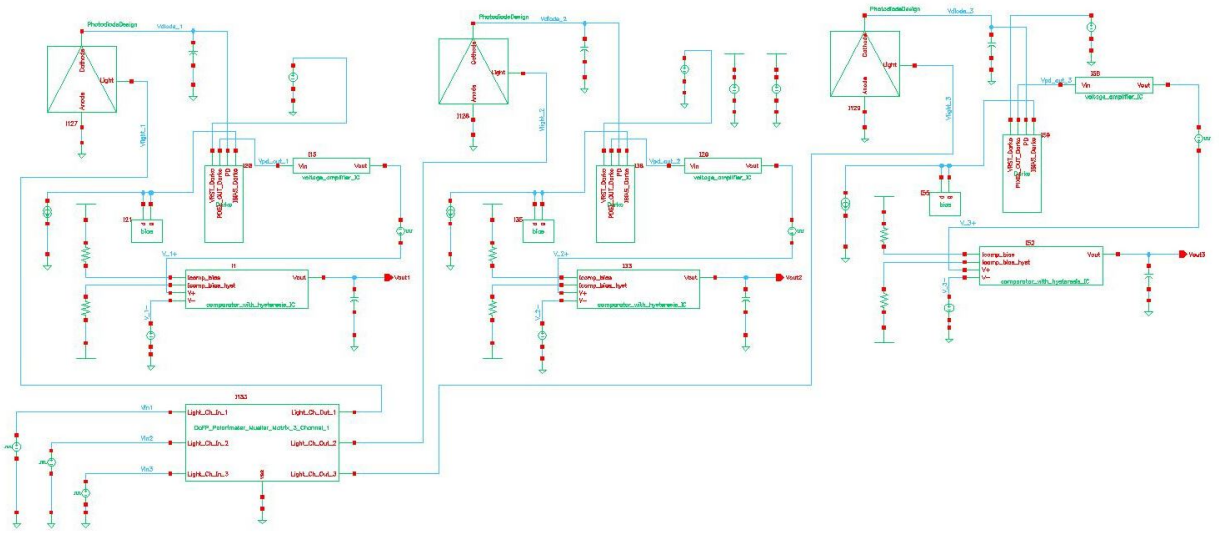

Figure 3.15: Three channel system with 0º, 60º and 120º polarization angles.

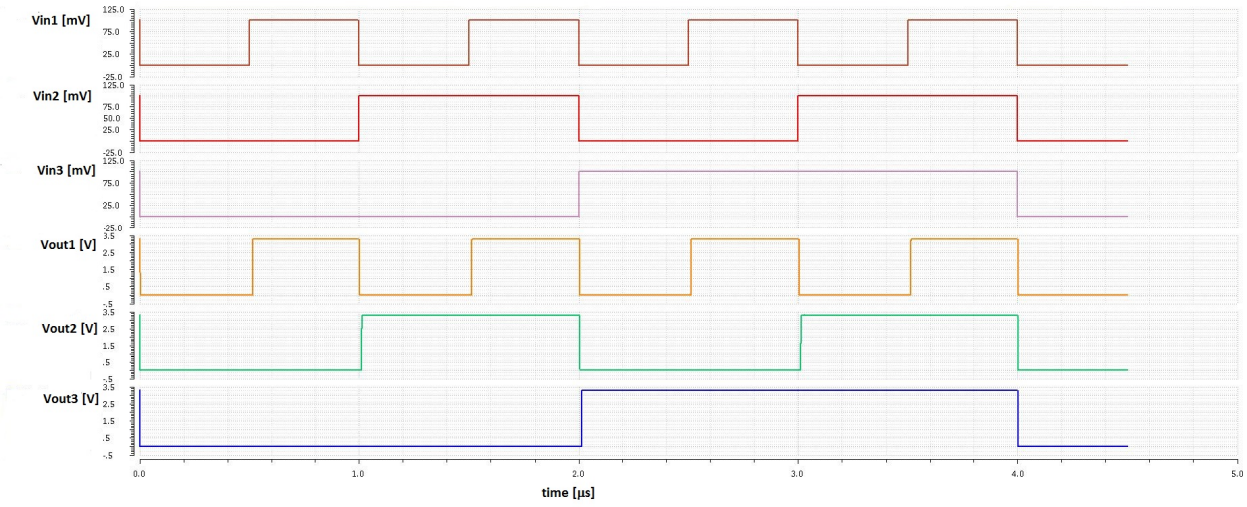

Figure 3.16: Three channel system input and output signals.

A (simulation-based) characterization of the properties of the optical communications channels under realistic variation in the fabrication of the filters is performed on the three channel VLC system. Due to fabrication imperfections, DoFP filter array polarization angles can have errors of 5°. [48] Figure 3.17 shows internal signals of the three Channel VLC system when DoFP filter array polarization angles are 0°, 60° and 120°, while Figure 3.18 shows the same internal signals when DoFP filter array polarization angles are 5°, 55° and 125° which is the worst case of fabrication imperfections. Only DoFP filter array output signals $V_{\text{light\_1}}$, $V_{\text{light\_2}}$ and $V_{\text{light\_3}}$ have different signal levels and all other following internal signals of the VLC system are almost identical between the two simulations. As a result, the performance of the three channel VLC system is not impacted by the fabrication imperfection of the filters.

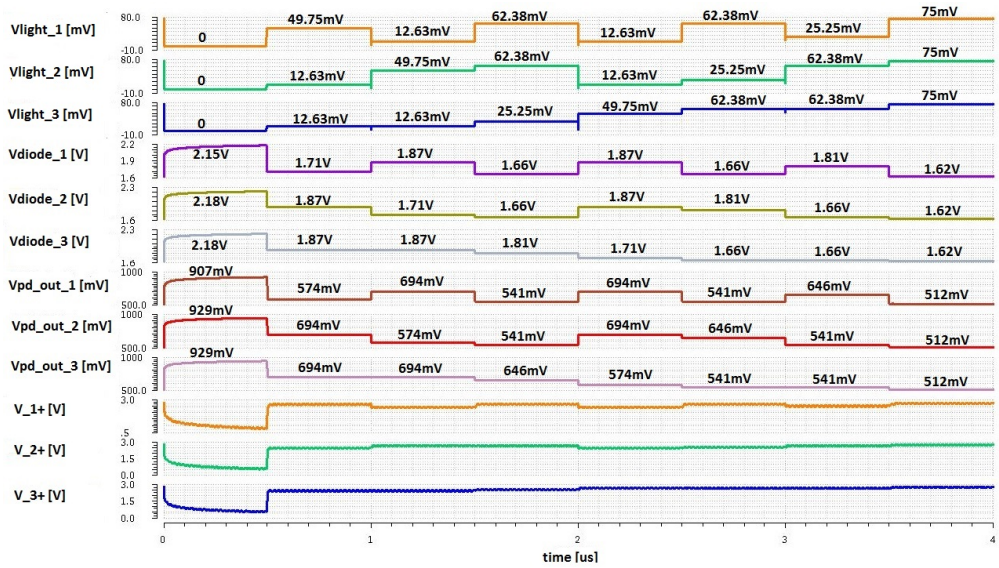

Figure 3.17: 3 channel 0°, 60° and 120° polarization angles internal signals.

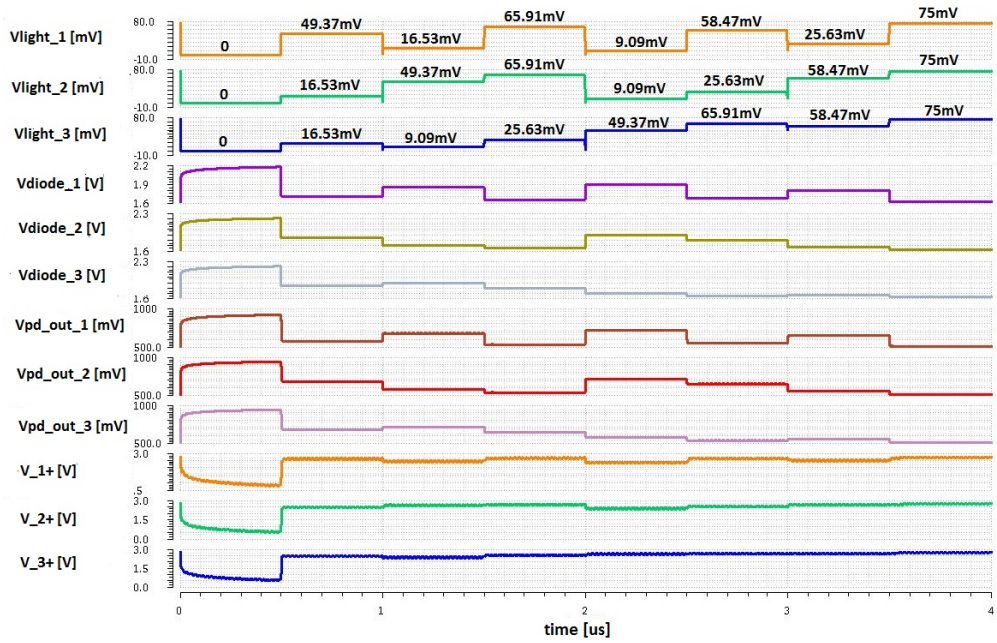

Figure 3.18: 3 channel 5°, 55° and 125° polarization angles internal signals.

3.5.3 Four Channel System

The four channel VLC system consists of 0°, 45°, 90° and 135° polarization angles data channels and is shown in Figure 3.19. Four laser sources are simulated with square wave voltage sources each 100 mW (100 mV) that are input to a four channel DoFP filter array. The rest of the four channel VLC system is the same as the two or three channel VLC systems.

Figure 3.20 shows that four modulated laser input signals are not completely recovered at each data channel output of the VLC system. Crosstalk between the channels on the input of the VLC system and DoFP filters supports the recovery of 10 out of 16 distinct symbols at the outputs of the VLC system. We will return to this issue in Chapter 5.

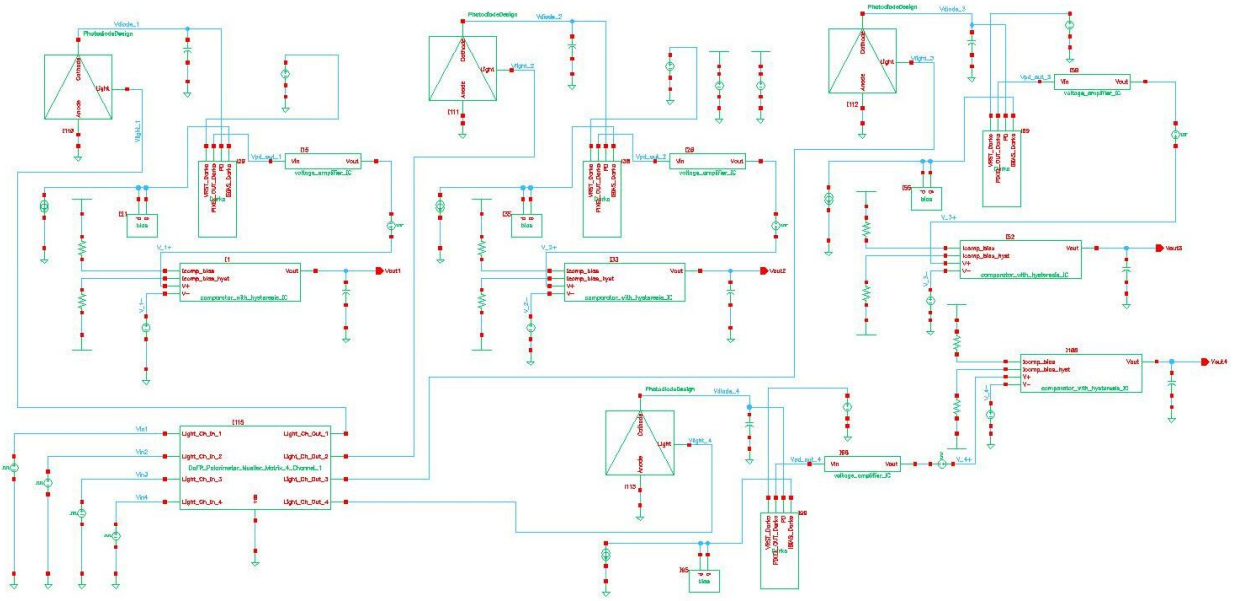

Figure 3.19: 4 channel 0°, 45°, 90° and 135° polarization angles.

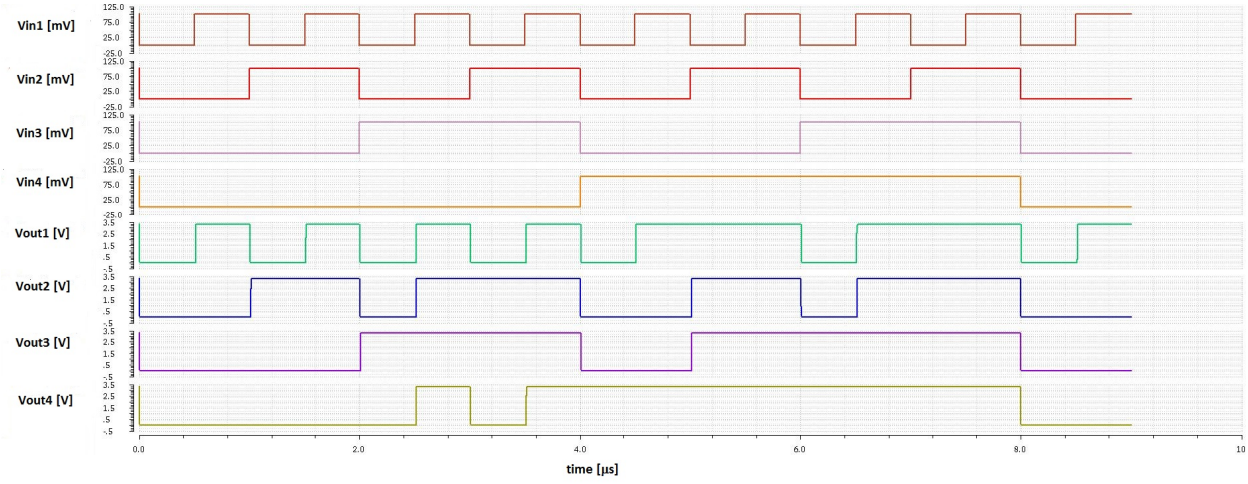

Figure 3.20: Four channel system input and output signals.

Chapter 4

Experimental Evaluation

4.1 Receiver Chip Design and Testing

A receiver integrated chip (IC) looks as shown in Figure 4.1. The IC is custom CMOS IC designed in 180 nm CMOS node technology. DoFP optical filters are designed to be mounted on the surface of the IC to create the optical receiver. The DoFP optical filters are made of aluminum nanowire and they have various incident angles of light polarization which is used to design independent digital communications channels.

Figure 4.2 [20] shows image of 45° oriented aluminum nanowire and side view of aluminum nanowire. Each filter is connected to high-speed photodiode that converts optical signal to electrical signal before the electrical signal is sent through digital data channel that is shown in Figure 3.7. Since our IC design has two channels we will use 0° and 90° optical filters to observe various properties of this design.

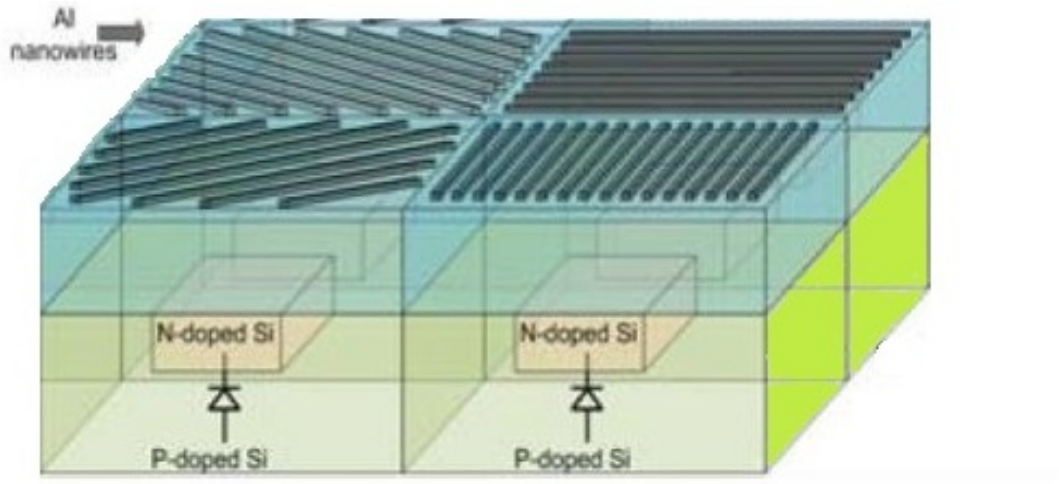

Figure 4.1: Custom IC with DoFP filters mounted on the surface of the IC.

The approach is for two optical modulated input signals with different polarization angles to be sent to the IC and then observe output signals from both channels on the IC. Figure 4.3 shows two channel system conversion of optical to electrical signal.

A custom two channel CMOS chip was designed using Cadence software chip layout 180 nm node technology. Figure 3.7 shows the design of one channel of this chip. The photodiode circuit is input stage of a receiver's channel. It is followed by common-source stage amplifier with a diode-connected PMOS device which is used as an active load which is used as middle stage of the receiver's channel. The receiver's channel also has a comparator with externally adjustable hysteresis and inverter chain as output stage.

Figure 4.4 shows the top layout view of the chip. The circled area is our portion of the chip because the chip design also has another research design project on it at the same time.

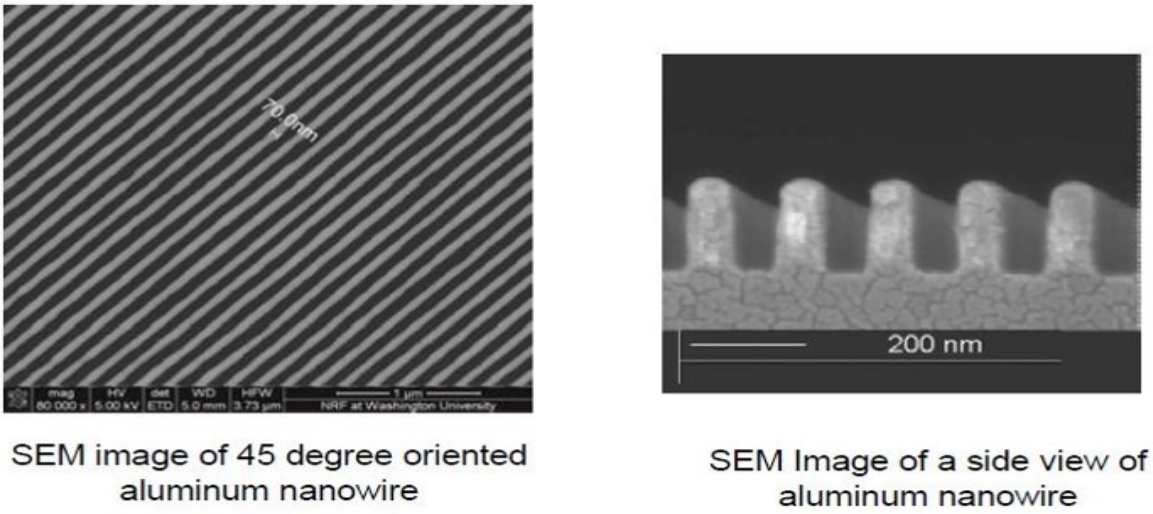

Figure 4.2: 45° oriented aluminum nanowire filter [20].

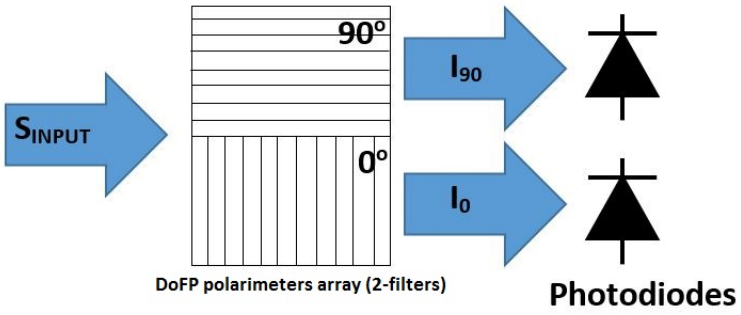

Figure 4.3: Two channel optical to electrical conversion.

The photodiodes are laid out so that they cover as much surface area as possible, so that DoFP filters can be bonded easier over the each channel photodiode. This is also so that they can absorb as much light as possible. In that way we are trying to reduce input light power requirements as much as possible.

Figure 4.5 shows bottom view of printed wiring board (PWB) that was designed together with the custom chip for testing purposes. The chip is placed in socket that is soldered on the PWB. The PWB is providing various functions for the custom chip. The PWB provides

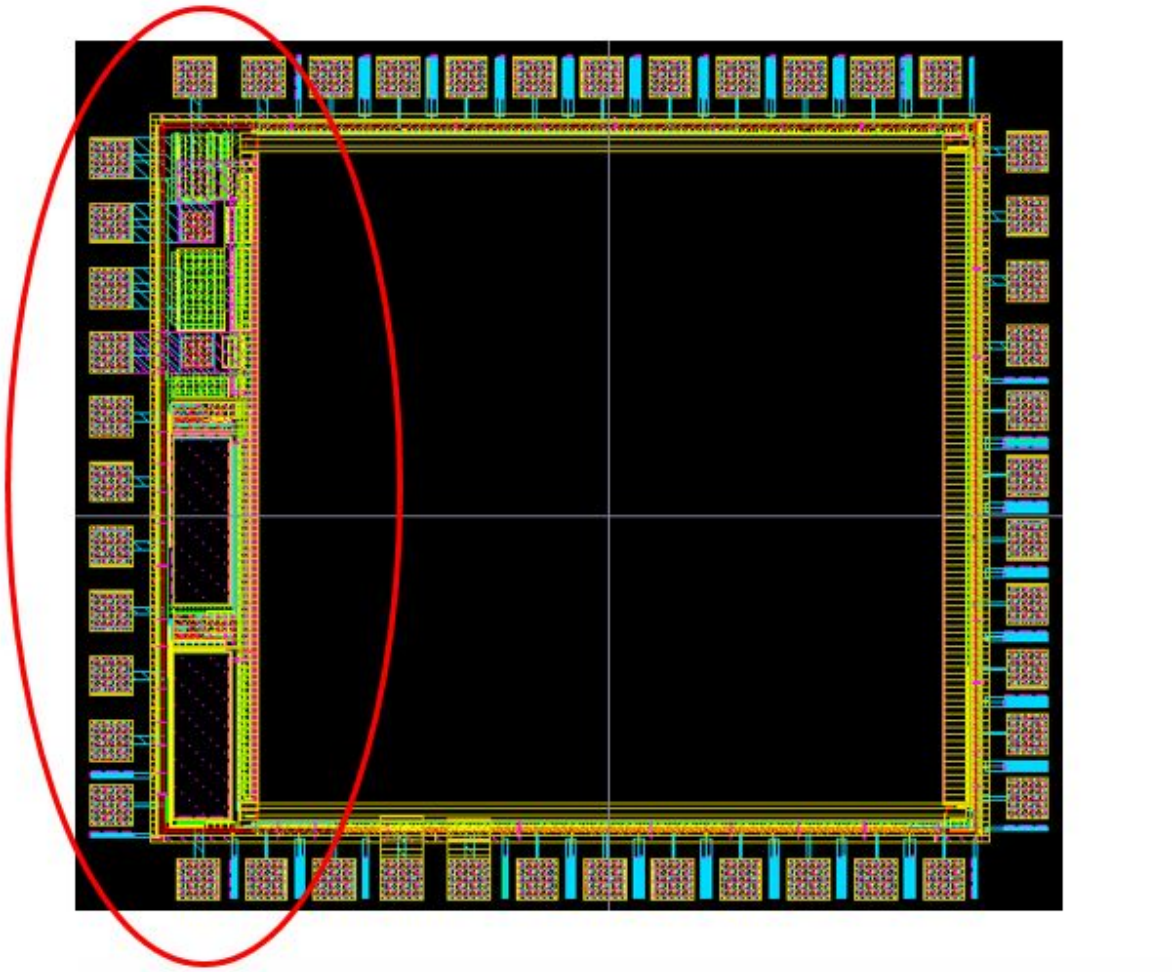

Figure 4.4: Top view of IC 2 channel layout designed in Cadence 180 nm node.

3.3V rail voltage to the chip and surrounding circuitry. It also provides external resistors that are used to adjust threshold voltages and hysteresis for each channel's comparator. The PWB is also connected with external connector to a FPGA board for some possible future development.

Once fabricated, the CMOS chip was placed into the socket on the PWB. First test we applied was to power up the board and make sure that everything is connected properly. This test was successful and we then performed a chip functionality test.

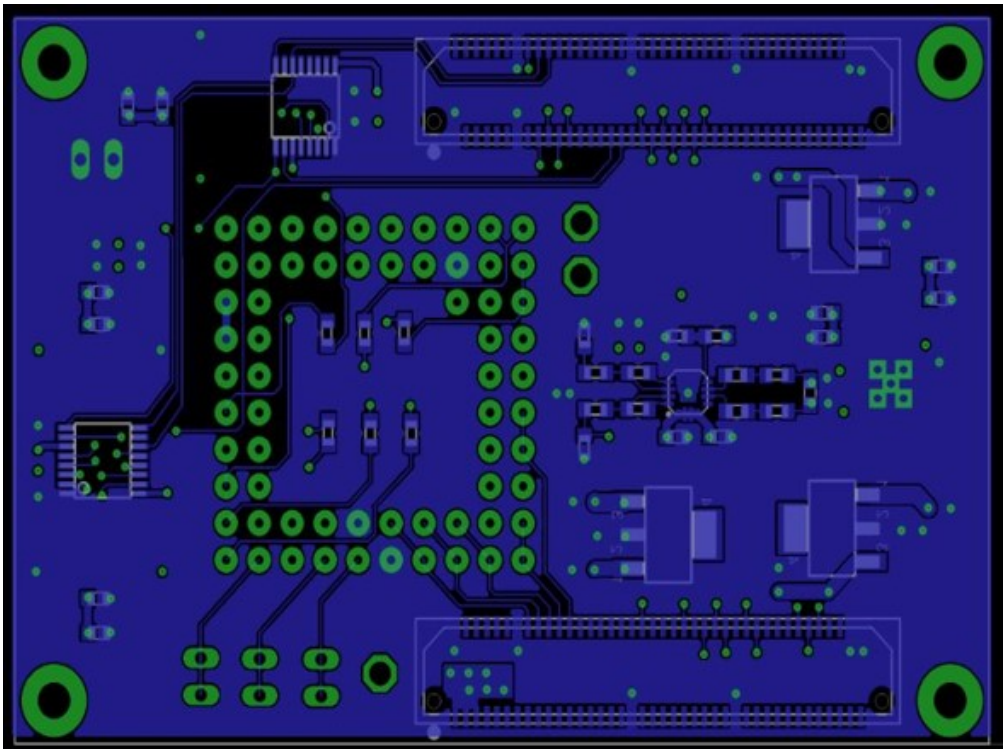

Figure 4.5: Bottom view of PWB that is used for testing of the IC.

This test shows that the custom chip is functioning properly. In this test we ignore the photodiode and we apply a square wave voltage with amplitude of 3.3V and with frequency of 1 MHz at V_{R} input shown in Figure 4.6. If everything works properly we should see the same square wave voltage at the channel's output.

Using a digital oscilloscope we observed the input square wave voltage signal and voltage output signal of the channel tested in this experiment. As we can see on Figure 4.7, the input square wave voltage signal is oscilloscope channel A1 and the output signal is oscilloscope channel A2. We can see that the output voltage signal is also 3.3V, 1 MHz square wave which shows that the chip internal circuitry is working properly.

In the second chip test we apply a regular red LED diode as input optical signal transmitter device. The red LED was connected to signal generator square wave 1V, 5 Hz output and

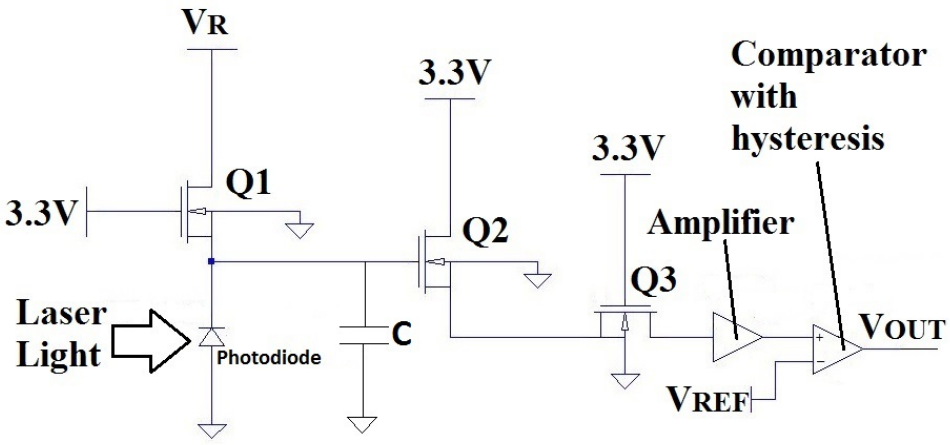

Figure 4.6: One data channel of VLC system.

the LED was pointed to one custom chip channel and we observed the channel output, which is shown in Figure 4.8.

As we can see from this test, the photodiode responds properly to LED diode light input signal and the receiver's channel output looks like desired 3.3V, 5 Hz square wave. Noise on the bottom of the output signal shown in Figure 4.8 can be filtered by adjusting comparator hysteresis. Due to filter bonding problems we did not perform more chip testing.

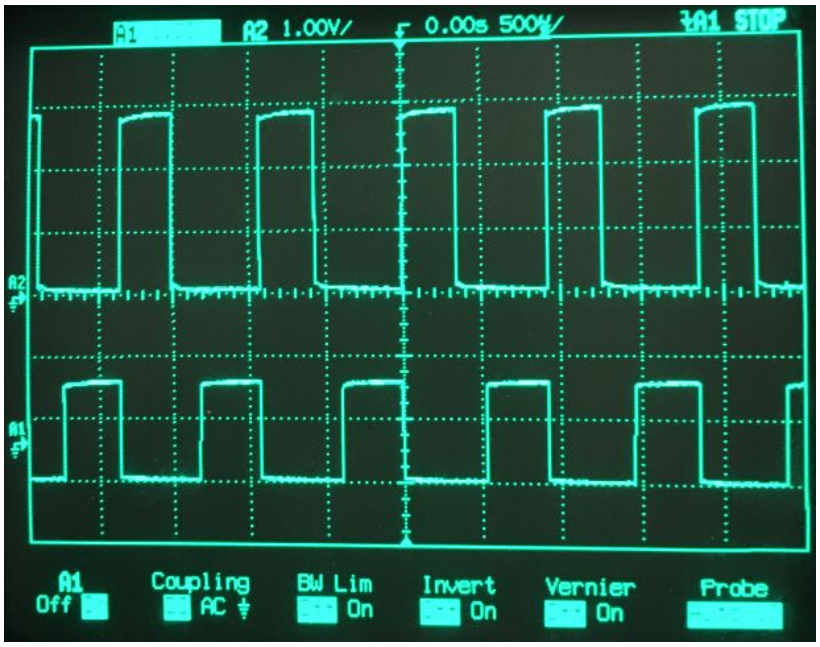

Figure 4.7: Experiment 1 of the chip where photodiode was neglected.

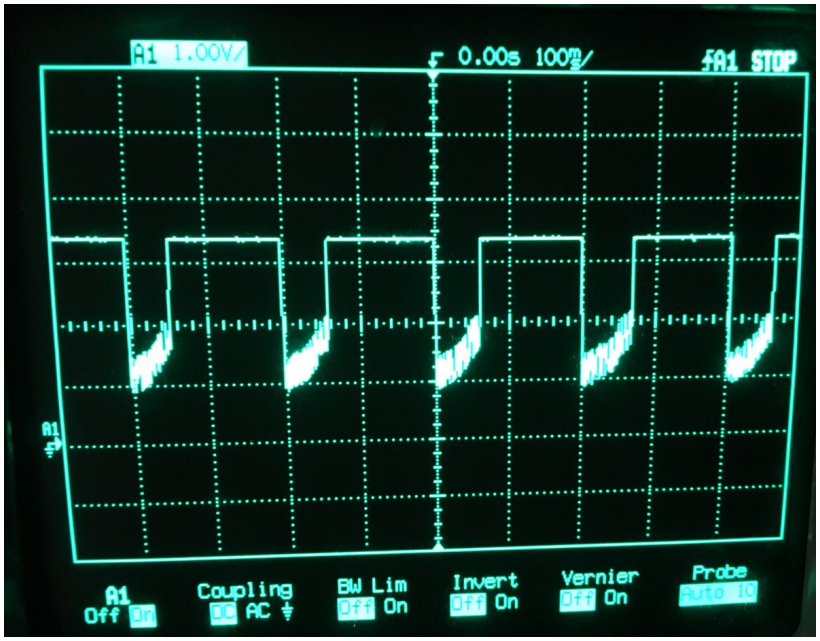

Figure 4.8: Experiment 2 of the chip using photodiode.

4.2 Linear CMOS Sensor Testing

The research described in this and the following section is reported in [30], and we would like to thank our co-authors for their contributions, specifically Amit Deliwala for the collection of data presented here.

Since we were unable to perform the optical experiments with the fabricated chip, we instead used a commercial image sensor [19]. The experiment was performed on the optical bench shown in Figure 4.9, and is intended to investigate two features of our system:

1. how will multiple polarized light signals interact in the air that is used as the transmission media, and
2. how does the electrical noise in the receiver compare with the optical interference we model between channels.

From Figure 4.9 we can see that a 530 nm uniform green LED light source illuminates light that travels to an integrating sphere where the light signal is diffused and then an aperture is used to create a narrow light beam. After this process a collimating lens is used to create a straight, uniform beam.

This beam is polarized with a fixed linear polarizer (manufactured by Newport) located inside the tube that is adjacent to the integrating sphere. The polarized light travels through the air and passes through a rotation stage with linear polarizer also made by Newport that is manually rotated from 0° to 180° in steps of 2 degrees. The light is then passed to the linear low-noise monochrome CMOS sensor [19] and the data is recorded.

The image received by the CMOS sensor is limited to a 100x100 pixel square array to ensure uniformity of illumination.

The measured data is a 4D array structure with 91 angles from 0° to 180°, every two degrees, 100 pixels in the x-axis direction, 100 pixels in the y-axis direction, with 64 frames of data for each angle.

Internal to the CMOS sensor, the light signal is digitized using a 12-bit analog-to-digital converter (ADC) with a 3.5 V reference voltage range.

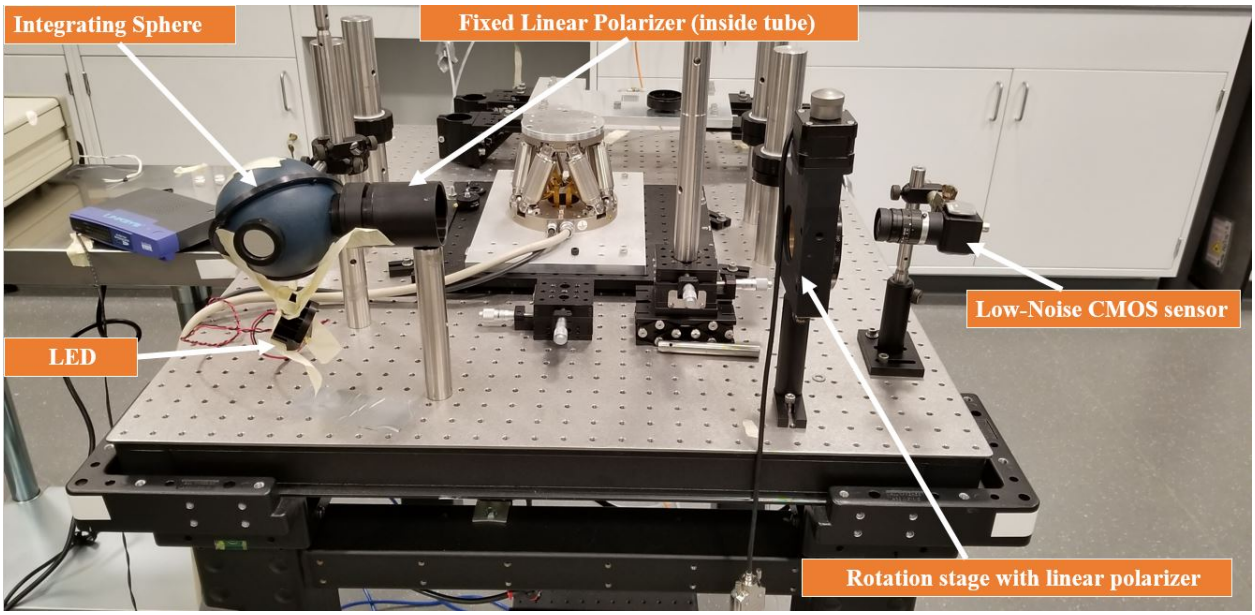

Figure 4.9: Optical bench experiment.

For each angle, the mean sensor value was calculated from the 100 pixel by 100 pixel array each with 64 frames (samples). Figure 4.10 shows these results, plotting mean and std. dev. of the signal value for each angle. The data is, as expected, showing Malus's law distribution with noise approximately equivalent to that predicted by shot noise.

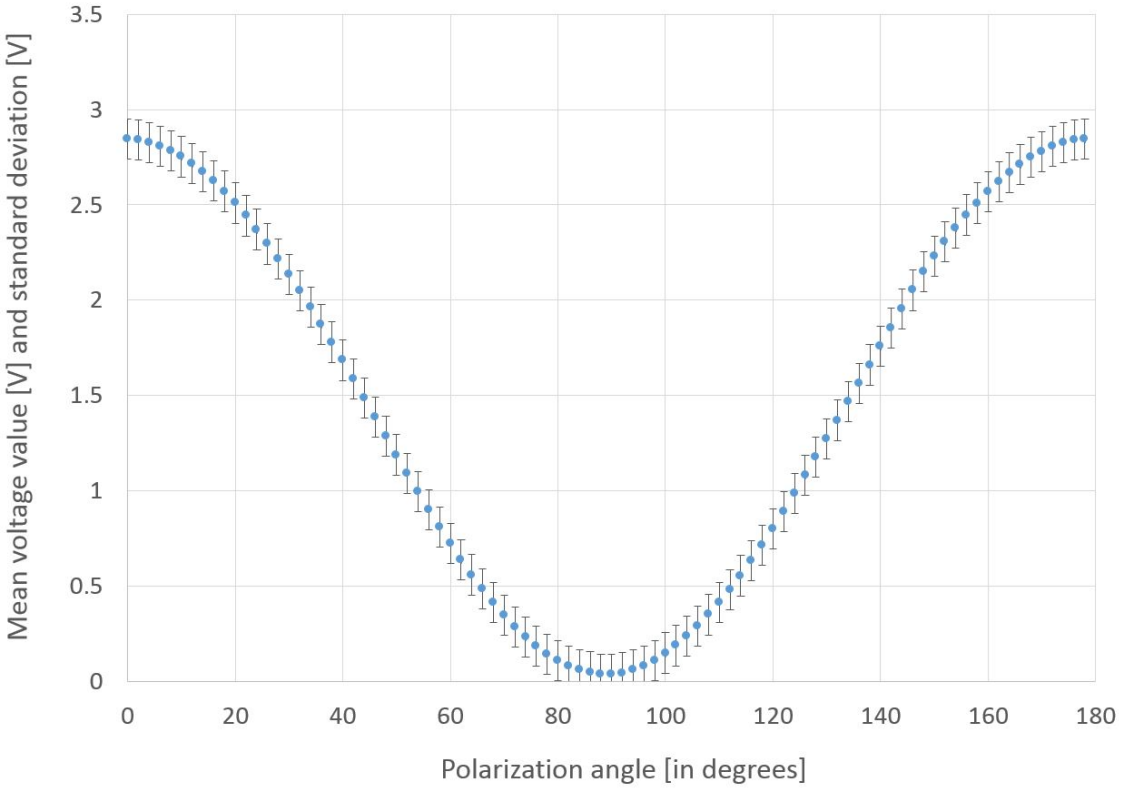

Figure 4.10: Experimental results for the linear CMOS sensor.

When the angles of the two polarizers match (0° in the plot), the sensor reading is at a maximum. Also, when the two angles are 90° apart the sensor voltage reading is at its minimum.

Figure 4.11 shows the relationship between the standard deviation and received signal for the linear CMOS sensor. A least mean squared error curve fit to this data yields the expression

$$y = 0.0107x + 0.0036 \tag{4.1}$$

where y is the std. dev. of the sensor reading and x is the mean reading for a fixed angle.

Figure 4.11 shows the noise data distribution for the entire set of pixels. If we only use noise data for one pixel (or photodiode) of the linear image sensor as it is shown in Figure 4.12 we can see that photodiode shot noise follows Poisson noise distribution which is expected.

In what follows, we will use the relationship from the Equation (4.1) as a calibration (i.e., a proxy) for the electrical noise in linear receiver circuits, although clearly for practical applications it will be necessary to use the noise properties of the actual receiver electronics in use.

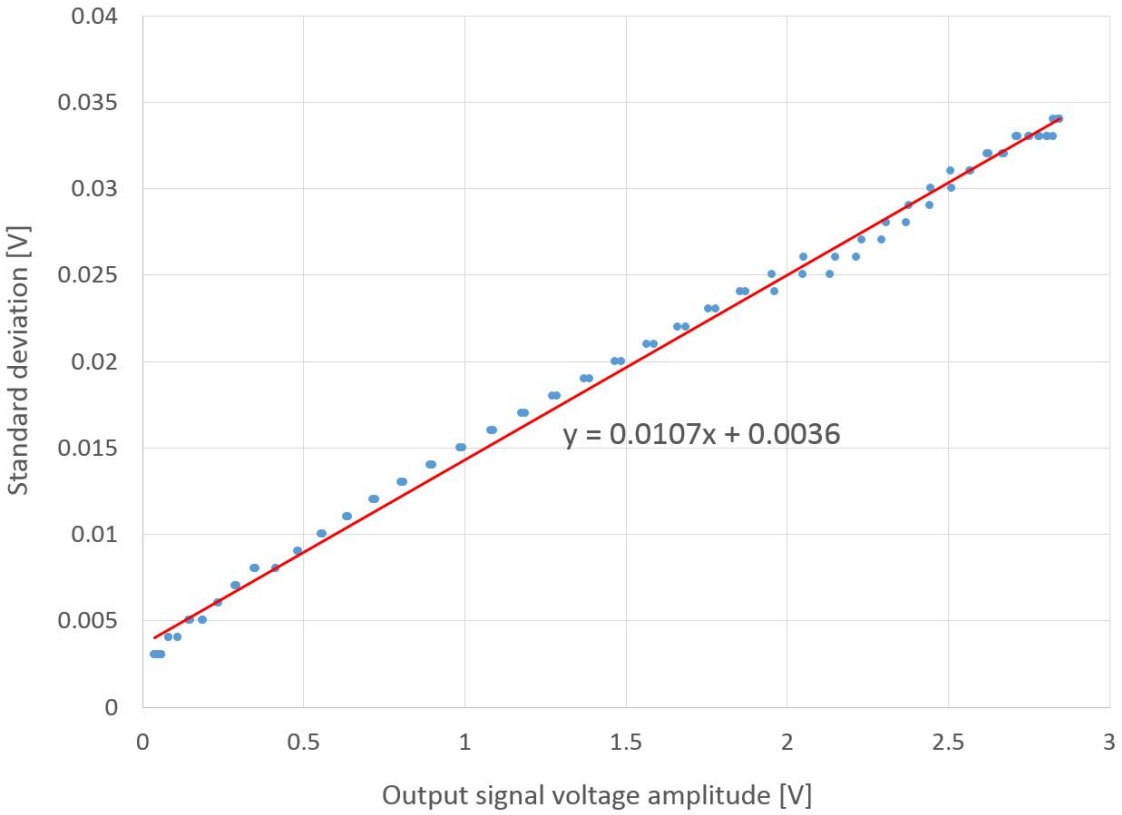

Figure 4.11: Standard deviation versus mean signal for the linear CMOS sensor.

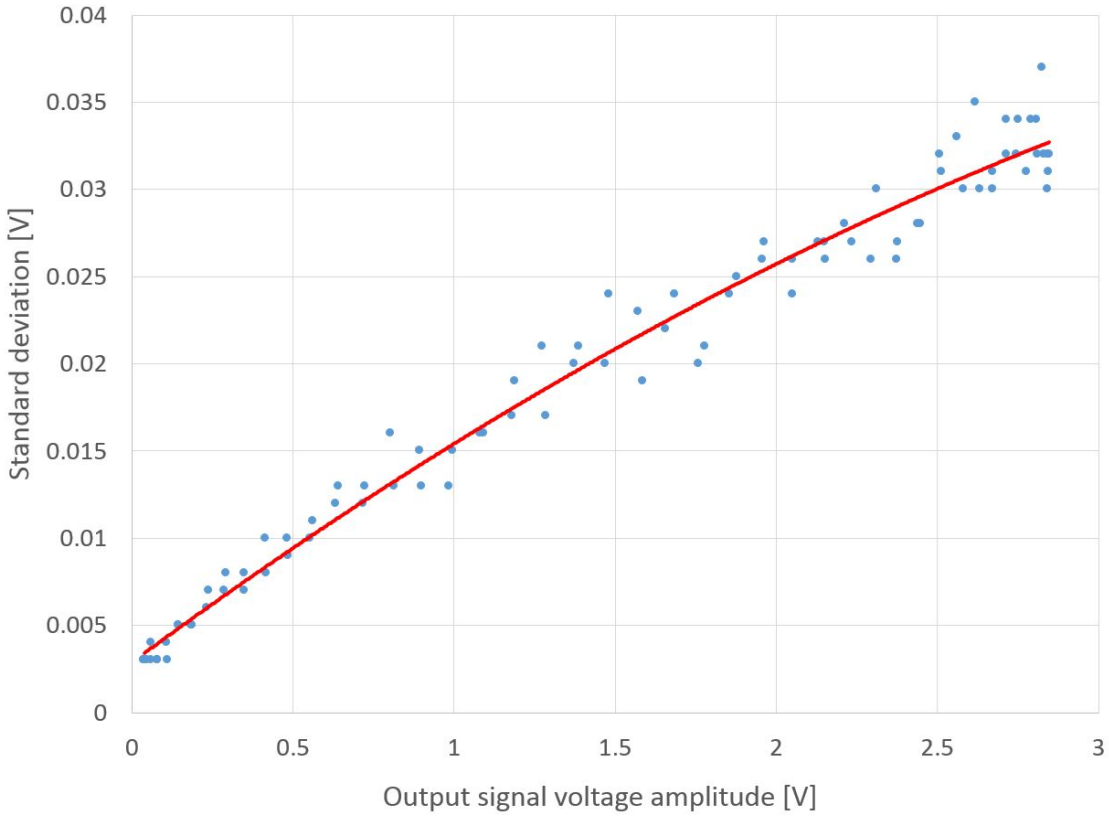

Figure 4.12: Linear CMOS Sensor pixel (photodiode) has Poisson noise distribution.

4.2.1 Implications for Two Channel System

In this experiment the angle where two polarizer angles match is 0º and the voltage reading for this angle is ADC value 3330 or $\frac{3330}{4096}(3.5\text{ V}) = 0.81304(3.5\text{ V}) = 2.846\text{ V}$. Similarly, for 90° the voltage reading is ADC value 45 or $\frac{45}{4096}(3.5\text{ V}) = 0.010904(3.5\text{ V}) = 0.038\text{ V}$.

Extrapolating these single-signal values back to the optical input signals of the two channel system described in Chapter 3, Table 4.1 shows the receiver's both channels photodiodes light inputs for all four data combinations of binary input values.

If we compare data from Table 4.1 with theoretical data from Table 3.1 from Chapter 3 we can see that they match reasonably well.

Table 4.1: Two channel linear low-noise CMOS sensor VLC PDM system.

b_{90°	b_{0°	I_{90}	I_0
0	0	0	0
0	1	0.011	0.813
1	0	0.813	0.011
1	1	0.824	0.824

4.2.2 Implications for Three Channel System

For the three-channel VLC system defined in Chapter 3, we will use three values from the experimental data. The first value is the 0° angle reading of the rotation stage which is already defined as ADC reading of 3330, or 0.81304 value referenced to 1.

The second reading is at 60° and it is an ADC reading of 847 or 0.206863 value referenced to 1. The third value is at 120° with an ADC reading of 938 or 0.229017 value referenced to 1.

Table 4.2 shows each channel 0°, 60°, and 120° photodiode outputs based on three experimental data points. Again the assumption is that max value is 1 (or 4096) and values are scaled to this reference value. As we can see from Table 4.2, the three channel VLC PDM system design will work well within adequate noise margins.

Threshold between binary value 0 and binary value 1 is 0.6 for this case. The noise margin went down comparing to the two channel VLC PDM system but it is still well within limits of constant proper operation.

Again, if we compare data from Table 4.2 with theoretical data from Table 3.2 from Chapter 3 we can see that they match reasonably well.

Table 4.2: Three channel linear low-noise CMOS sensor VLC PDM system.

b_{120°	b_{60°	b_{0°	I_{120}	I_{60}	I_0
0	0	0	0	0	0
0	0	1	0.229	0.207	0.813
0	1	0	0.207	0.813	0.207
0	1	1	0.436	1	1
1	0	0	0.813	0.207	0.229
1	0	1	1	0.414	1
1	1	0	1	1	0.436
1	1	1	1	1	1

4.3 Logarithmic CMOS Sensor Testing

In this experiment the light is detected using a logarithmic CMOS sensor [16] (in which the photodiode is operated in the forward bias region) and the data is recorded. The image received by the logarithmic CMOS sensor is limited to a 151x151 pixel square array to ensure uniformity of illumination.

The measured data is a 4D array structure with 180 angles from 0º to 179º, every degree, 151 pixels in the x-axis direction, 151 pixels in the y-axis direction, with 91 frames of data for each angle.

Again just like for the linear CMOS sensor, internal to the logarithmic CMOS sensor, the light signal is digitized using a 12-bit analog-to-digital converter (ADC) with a 3.5 V reference voltage range.

For each angle, the mean sensor value was calculated from the 151 pixel by 151 pixel array each with 91 frames (samples). Figure 4.13 shows these results, plotting mean and std. dev. of the signal value for selected angles.

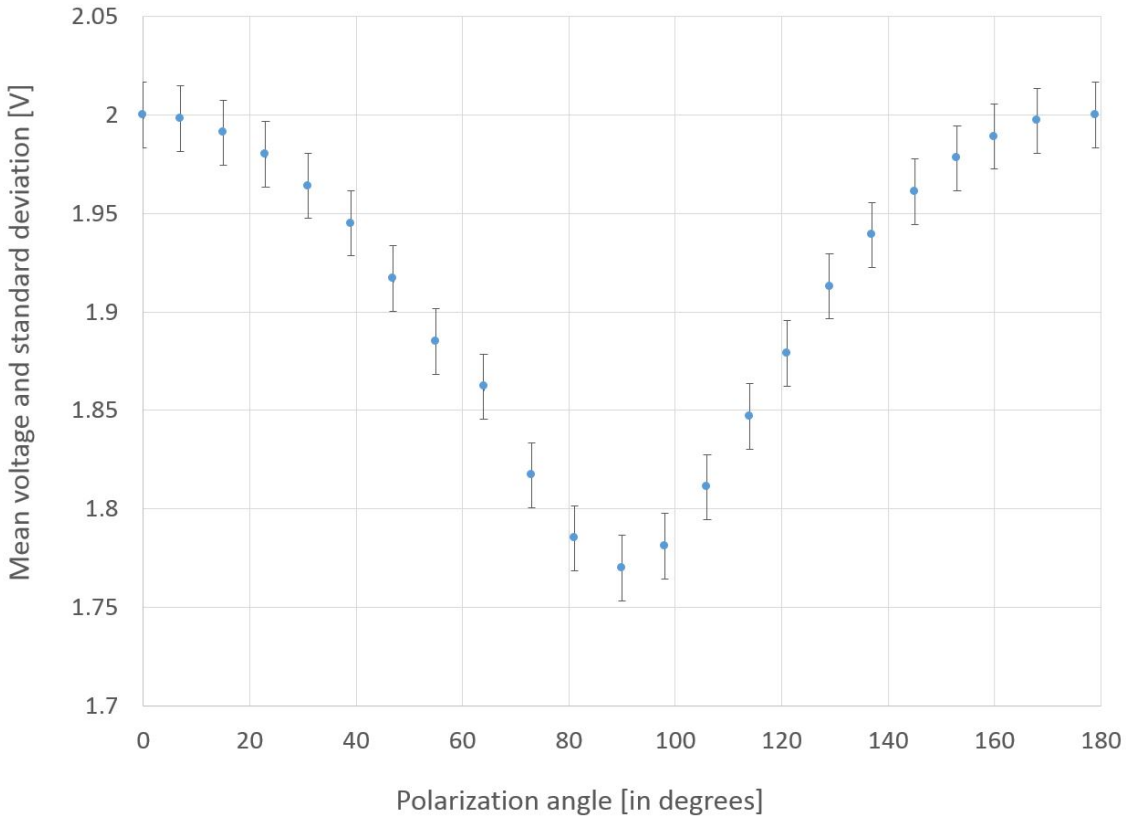

Figure 4.13: Experimental results for the logarithmic CMOS sensor.

Just like for the linear CMOS sensor, when the angles of the two polarizers match (0° in the plot), the logarithmic CMOS sensor reading is at a maximum. Also, when the two angles are 90° apart the sensor voltage reading is at its minimum.

Figure 4.14 shows the relationship between the standard deviation and received signal for the logarithmic CMOS sensor. We can see from the figure that the relationship between the standard deviation and received signal increases for low light intensities and then is fairly flat for higher light intensities. This style of detector provides interesting opportunities for the construction of systems that are limited by high shot noise at high signal amplitudes.

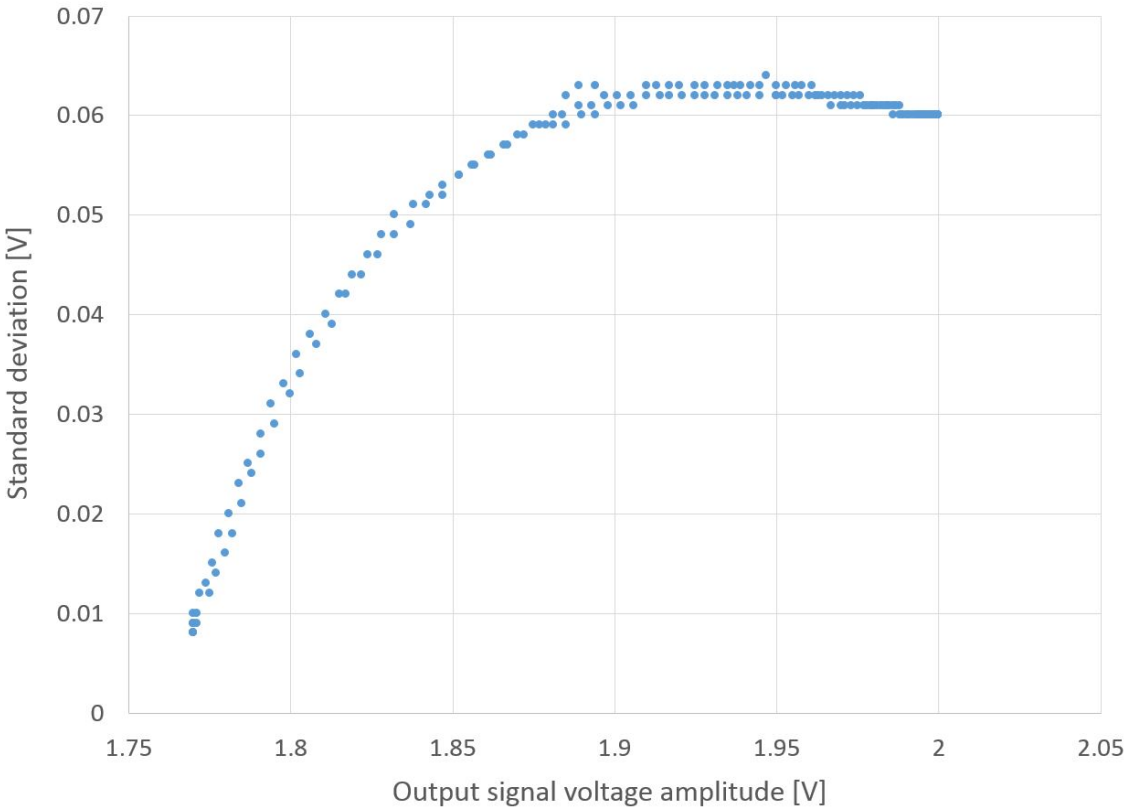

Figure 4.14: Standard deviation versus mean signal for the logarithmic CMOS sensor.

Chapter 5

Coding

In Chapter 3 we showed how 2 and 3 channel PDM systems work with a linear CMOS sensor. As we can see from that analysis the 2 and 3 channel systems have wide enough noise margins that the receiver's channel outputs can easily recover the transmitter's input binary sequences.

For the four channel system as we observed that the noise margins are not wide enough so that 4 receivers' output channels are error free. In order to have an error free 4 channel system we need to introduce some simple channel coding techniques on the input transmitter's side and the output receiver's side. Note that in this chapter we refer to the techniques that we are proposing as channel coding. In the literature, it is occasionally referred to as line coding; however, we will consistently refer to it as channel coding.

5.1 Channel Coding Techniques at the Transmitter

Channel coding techniques on the input transmitter side of the system are based on applying different amplitudes for different input data channel's lasers. Each input data channel's laser is emitting a visible light beam with a defined light power. These visible light beams represent binary sequences.

Each data channel's light beam is not polarized and it is represented with the Stokes vector $S_{\text{IN}} = [I_T \quad 0 \quad 0 \quad 0]^T$ where I_T is the amplitude of the light signal. In order to perform channel coding on the transmitter side, we apply different values of I_T to different input channels.

So if an input data channel's laser is sending binary value of '1' then the Stokes vector is $S_{\text{IN1}} = [G_1 I_T \quad 0 \quad 0 \quad 0]^T$ and when the laser is sending binary value of '0' then the Stokes vector is ideally close to $S_{\text{IN2}} = [0 \quad 0 \quad 0 \quad 0]^T$. Note that G_1 is the channel's gain factor for a binary '1' and its value can be less than 1 or greater than 1.

The above approach allows the light amplitude for a binary '1' to vary from channel to channel (i.e., the gain G_1 is channel specific). Occasionally it is also desirable to have a non-zero light amplitude when transmitting a binary '0'. In this case, the transmitter sends light with a Stokes vector $S_{\text{IN2}} = [G_0 I_T \quad 0 \quad 0 \quad 0]^T$. As above, G_0 is channel specific. In each of the cases we illustrate below, $G_0 < 1$.

5.2 Channel Decoding Techniques at the Receiver

Our general approach to channel decoding at the receiver is enabling multiple comparator threshold levels to be operational based on the input symbols received on other channels.

This is accomplished by employing multiple comparators in parallel and selecting which comparator output is relevant based on the received value from another channel or channels.

Specifically, on the receiver side of the 4 channel system we have one of the following three cases:

- Regular receiver channel with one comparator
- Receiver channel with 2 comparators with different thresholds and 2-to-1 multiplexer
- Receiver channel with 3 comparators with different thresholds and 3-to-1 multiplexer

In the sections below, we describe all three channel decoding techniques used on the receiver's side of the 4 channel system.

5.2.1 Regular Receiver Channel with One Comparator

Figure 5.1 shows a regular receiver channel with one comparator.

In this case the light signal is converted into an electrical current and then into an electrical voltage and then amplified before it reaches the comparator with hysteresis. The amplified electrical voltage signal is compared with the comparator threshold voltage to output either Vdd or binary '1' or 0 or binary '0'. This receiver is the one we have been exclusively using up to this point in the research.

5.2.2 Receiver Channel with Two Comparators

The general approach to a multiple-threshold decoding is to have different thresholds separating the two output states that are dependent upon the decoded output from a different

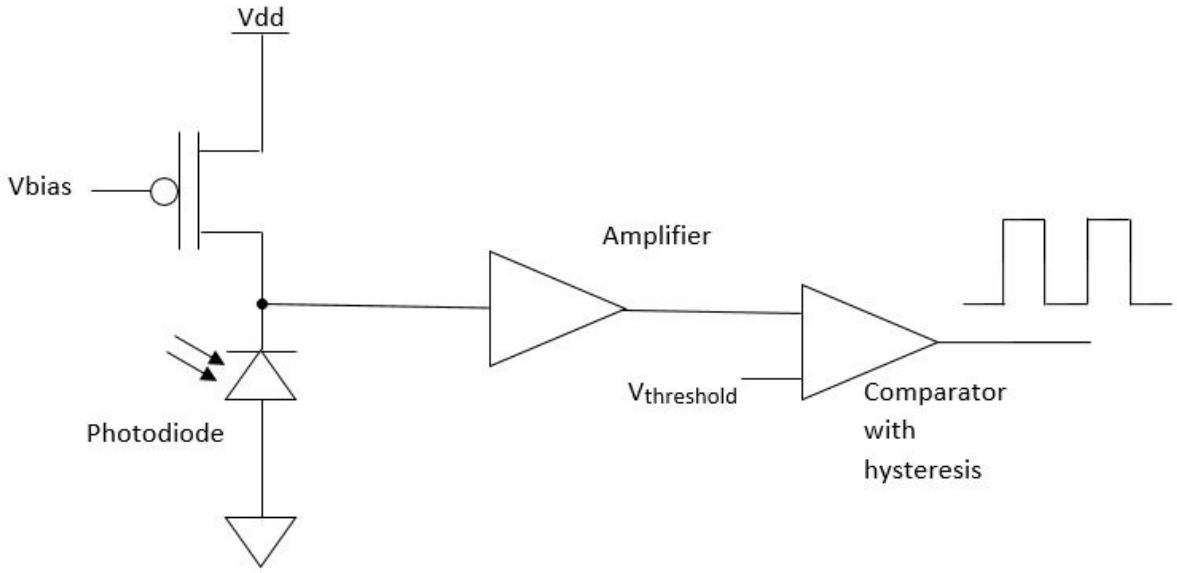

Figure 5.1: Regular receiver channel with one comparator.

channel. Figure 5.2 shows a receiver channel decoder with 2 comparators with different thresholds and 2-to-1 multiplexer.

In this case the channel's light signal is converted into an electrical current and then into an electrical voltage. The electrical voltage signal is then amplified before it is delivered, in parallel, to two comparators with hysteresis. The amplified electrical voltage signal is compared with each comparator's threshold voltage.

Depending on the value of the control signal $Output_X$ as shown in Figure 5.2 one of the two comparator outputs represents the receiver data channel's output $Output_Y$. Note that the control signal $Output_X$ is an output of different receiver data channel in the same system.

5.2.3 Receiver Channel with Three Comparators

The notion just described can easily be extended to more than just 2 thresholds. Figure 5.3 shows a receiver channel with 3 comparators with different thresholds and a 3-to-1 multiplexer.

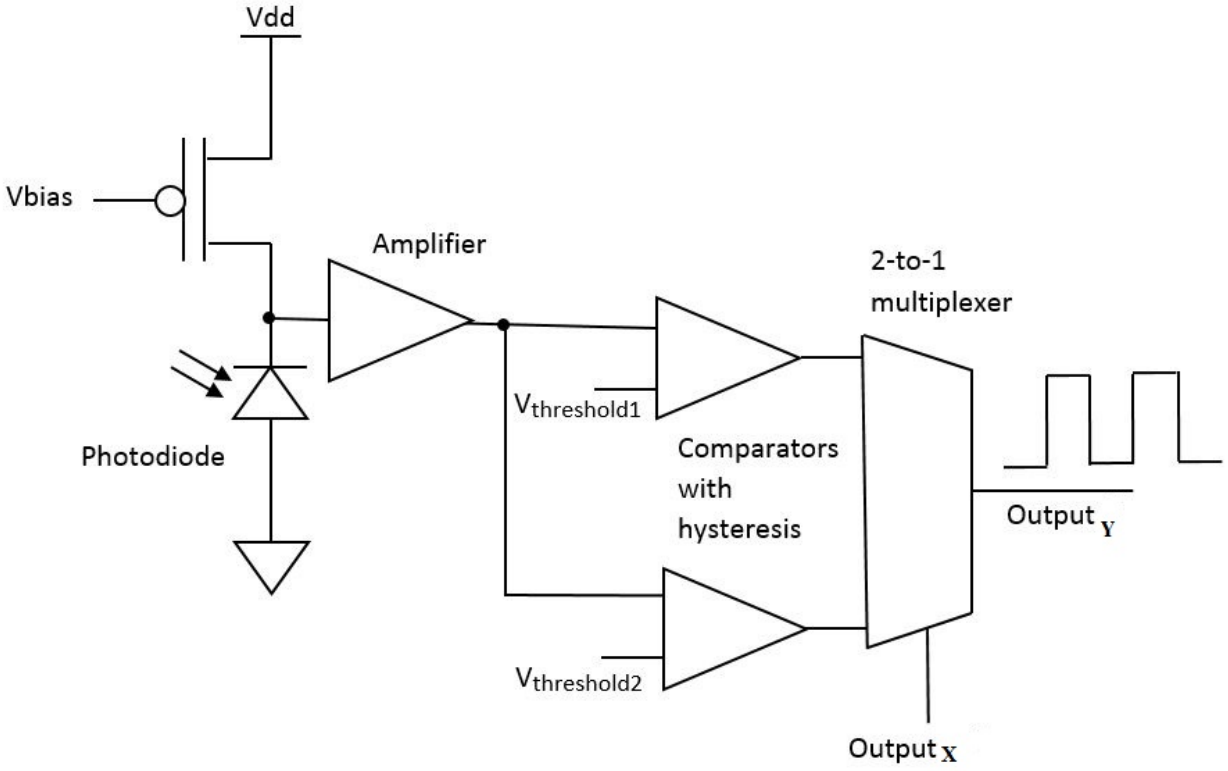

Figure 5.2: Receiver channel with 2 comparators with different thresholds and 2-to-1 multiplexer.

In this case the light signal is converted into an electrical current and then an electrical electrical voltage. This volatge signal is then amplified before it reaches three comparators with hysteresis.

The amplified electrical voltage signal is compared with each comparator's different threshold voltage, and the three outputs are input to a 3-to-1 multiplexer. Depending on the values of the control signals $Output_X$ and $Output_Y$ one of the three comparator output signals represents the channel's output $Output_Z$. Note that the control signals $Output_X$ and $Output_Y$ are outputs of different receiver data channels in the same system.

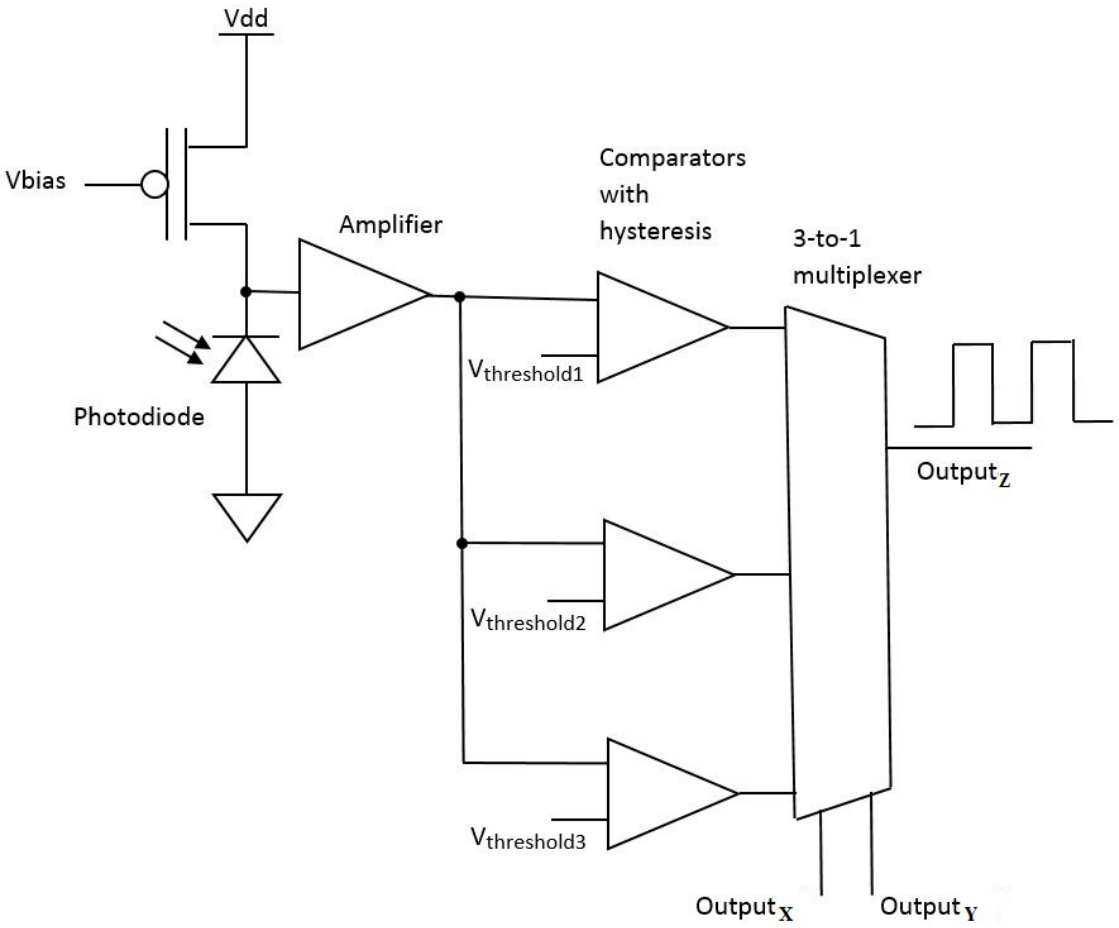

Figure 5.3: Receiver channel with 3 comparators with different thresholds and 3-to-1 multiplexer.

5.3 Channel Coding for a Four Channel System

In this section, we will describe a sufficient channel coding design that enables the four channel system of Chapter 3 to successfully decode all 16 combinations of binary input symbols. To make the example more concrete, we will exploit the measured data from Chapter 4 to quantify the operation of the system.

For the four channel system, we will use four values from the experimental data, at 0°, 45°, 90°, and 135°. These data are repeated in Table 5.1, with the signal level normalized to 1 (so as to ease comparisons with the analysis of Chapter 3).

Table 5.1: 4 channel system experimental data

Angle	ADC value	Signal level
0°	3330	0.81304
45°	1623	0.396315
90°	53	0.012956
135°	1944	0.0474507

Table 5.2 shows the 0º input laser data channel that represents binary stream b'0101010101010101'. For S_{0° if the light signal is sent, the Stokes vector is defined as $S_{0^\circ} = 0.81304[1 \quad 1 \quad 0 \quad 0]^T = [0.81304 \quad 0.81304 \quad 0 \quad 0]^T$, and if the light signal is not sent the Stokes vector is defined as $S_{0^\circ} = [0 \quad 0 \quad 0 \quad 0]^T$.

Table 5.2: 0º channel polarized light laser input.

Binary input	0	1	2	3	4	5	6	7	8	9	10	11	12	13	14	15
Stokes vector	0	0.813	0	0.813	0	0.813	0	0.813	0	0.813	0	0.813	0	0.813	0	0.813
	0	0.813	0	0.813	0	0.813	0	0.813	0	0.813	0	0.813	0	0.813	0	0.813
	0	0	0	0	0	0	0	0	0	0	0	0	0	0	0	0
	0	0	0	0	0	0	0	0	0	0	0	0	0	0	0	0

Table 5.3 shows 45º input laser data channel that represents binary stream b'0011001100110011'. For S_{45° if the light signal is sent $S_{45^\circ} = 0.59596[1 \quad 0 \quad 1 \quad 0]^T = [0.59596 \quad 0 \quad 0.59596 \quad 0]^T$ and if the light signal is not sent $S_{45^\circ} = [0 \quad 0 \quad 0 \quad 0]^T$. Notice that 45º input laser data channel has 0.733 amplitude of the 0º input laser data channel.

Table 5.4 shows 90º input laser data channel that represents binary stream b'0000111100001111'. For S_{90° if the light signal is sent, $S_{90^\circ} = 0.91874[1 \quad -1 \quad 0 \quad 0]^T = [0.91874 \quad -0.91874 \quad 0 \quad 0]^T$

Table 5.3: 45° channel polarized light laser input.

Binary input	0	1	2	3	4	5	6	7	8	9	10	11	12	13	14	15
Stokes vector	0	0	0.596	0.596	0	0	0.596	0.596	0	0	0.596	0.596	0	0	0.596	0.596
	0	0	0	0	0	0	0	0	0	0	0	0	0	0	0	0
	0	0	0.596	0.596	0	0	0.596	0.596	0	0	0.596	0.596	0	0	0.596	0.596
	0	0	0	0	0	0	0	0	0	0	0	0	0	0	0	0

and if the light signal is not sent (i.e., the system wishes to transmit a binary '0'), $S_{90^\circ} = 0.59596\ [1 \quad -1 \quad 0 \quad 0]^T = [0.59596 \quad -0.59596 \quad 0 \quad 0]^T$. Here, notice that the 90° input laser data channel has 0.733 amplitude of the 0° input laser data channel when it is sending data value '0' and 1.13 amplitude of the 0° input laser data channel when it is sending data value '1'.

Table 5.4: 90° channel polarized light laser input.

Binary input	0	1	2	3	4	5	6	7	8	9	10	11	12	13	14	15
Stokes vector	0.596	0.596	0.596	0.596	0.919	0.919	0.919	0.919	0.596	0.596	0.596	0.596	0.919	0.919	0.919	0.919
	-0.6	-0.6	-0.6	-0.6	-0.92	-0.92	-0.92	-0.92	-0.6	-0.6	-0.6	-0.6	-0.92	-0.92	-0.92	-0.92
	0	0	0	0	0	0	0	0	0	0	0	0	0	0	0	0
	0	0	0	0	0	0	0	0	0	0	0	0	0	0	0	0

Table 5.5 shows 135° input laser data channel that represents binary stream b'0000000011111111'. For S_{135° if the light signal is sent from transmitter laser and polarized $S_{135^\circ} = 0.97565[1 \quad 0 \quad -1 \quad 0]^T = [0.97565 \quad 0 \quad -0.97565 \quad 0]^T$ and if the light signal is not sent $S_{135^\circ} = [0 \quad 0 \quad 0 \quad 0]^T$. Notice that 135° input laser data channel has 1.2 amplitude of the 0° input laser data channel when it is sending data.

Table 5.5: 135° channel polarized light laser input.

Binary input	0	1	2	3	4	5	6	7	8	9	10	11	12	13	14	15
Stokes vector	0	0	0	0	0	0	0	0	0.976	0.976	0.976	0.976	0.976	0.976	0.976	0.976
	0	0	0	0	0	0	0	0	0	0	0	0	0	0	0	0
	0	0	0	0	0	0	0	0	-0.98	-0.98	-0.98	-0.98	-0.98	-0.98	-0.98	-0.98
	0	0	0	0	0	0	0	0	0	0	0	0	0	0	0	0

All 4 input LED data channels are added together

$$S_{IN} = S_{0^\circ} + S_{45^\circ} + S_{90^\circ} + S_{135^\circ} \tag{5.1}$$

after the transmitter input polarization filter array and they travel through the air used as the transmission media in this example, until they reach the receiver polarization filter array. Table 5.6 shows all 4 channels' combined optical signal as it travels through the air between input and output polarization filter arrays.

Table 5.6: All 4 polarized channels' light signals combined.

Input	0	1	2	3	4	5	6	7	8	9	10	11	12	13	14	15
S_{AIR}	0.596	1.409	1.192	2.005	0.919	1.732	1.515	2.328	1.572	2.385	2.168	2.981	1.894	2.707	2.49	3.303
	-0.6	0.217	-0.6	0.217	-0.92	-0.11	-0.92	-0.11	-0.6	0.217	-0.6	0.217	-0.92	-0.11	-0.92	-0.11
	0	0	0.596	0.596	0	0	0.596	0.596	-0.98	-0.98	-0.38	-0.38	-0.98	-0.98	-0.38	-0.38
	0	0	0	0	0	0	0	0	0	0	0	0	0	0	0	0

The receiver defined in Chapter 3 will yield 4 distinct channel outputs as shown in Table 5.7. Receiver outputs I_{0°, I_{45°, I_{90° and I_{135° are shown in the Table 5.7 and they are calculated using the same approach as in Chapter 3.

Table 5.7: All 4 receiver channels' output signals.

Input	0	1	2	3	4	5	6	7	8	9	10	11	12	13	14	15
I_{0°	0.001	0.406	0.15	0.555	0.002	0.407	0.151	0.556	0.245	0.65	0.394	0.799	0.246	0.651	0.395	0.8
I_{45°	0.149	0.352	0.445	0.649	0.23	0.433	0.526	0.729	0.151	0.355	0.448	0.651	0.232	0.435	0.529	0.732
I_{90°	0.296	0.299	0.445	0.448	0.457	0.459	0.606	0.608	0.54	0.542	0.689	0.691	0.701	0.703	0.85	0.852
I_{135°	0.149	0.352	0.15	0.354	0.23	0.433	0.231	0.434	0.634	0.838	0.636	0.839	0.715	0.918	0.717	0.92

Receiver output I_{0° for the 0^o polarization data channel is obtained by applying comparator with threshold of 0.4 on data points from Table 5.7. From that data processing Table 5.8 is obtained which shows I_{0° or 0^o polarization data channel output binary stream is b'0101010101010101' as is expected.

Table 5.8: 0° polarization data receiver channel output signals.

Input	0	1	2	3	4	5	6	7	8	9	10	11	12	13	14	15
I_0	0	1	0	1	0	1	0	1	0	1	0	1	0	1	0	1

Receiver output I_{45° for the 45° polarization data channel is obtained by applying comparator with threshold 0.44 on data points from Table 5.7. From that comparator data processing Table 5.9 is obtained and this table shows I_{45° or 45° polarization data channel output binary stream is b'0011001100110011' as is expected.

Table 5.9: 45° polarization data receiver channel output signals.

Input	0	1	2	3	4	5	6	7	8	9	10	11	12	13	14	15
I_{45}	0	0	1	1	0	0	1	1	0	0	1	1	0	0	1	1

Receiver output I_{135° for the 135° polarization data channel is obtained by applying comparator with threshold of 0.445 on data points from the Table 5.7. From that comparator data processing Table 5.10 is obtained and this table shows I_{135° or 135° polarization data channel output binary stream is b'0000000011111111' as is expected.

Table 5.10: 135° polarization data receiver channel output signals.

Input	0	1	2	3	4	5	6	7	8	9	10	11	12	13	14	15
I_{135}	0	0	0	0	0	0	0	0	1	1	1	1	1	1	1	1

Finally, receiver output I_{90° for the 90° polarization data channel is obtained by applying two comparators with thresholds 0.45 and 0.695 on data points from the Table 5.7. From those two comparators' data processing Table 5.11 is obtained.

The data from Table 5.11 shows two comparator outputs for 90° polarization data receiver channel I_{90° for threshold 0.45 and I_{90° for threshold 0.695. Both of these 90° polarization

Table 5.11: 90° polarization data receiver channel two comparators outputs.

Input	0	1	2	3	4	5	6	7	8	9	10	11	12	13	14	15
$I_{90} > 0.45$	0	0	0	0	1	1	1	1	1	1	1	1	1	1	1	1
$I_{90} > 0.695$	0	0	0	0	0	0	0	0	0	0	0	0	1	1	1	1

data receiver channel's comparator outputs are inputs to 2-to-1 multiplexer controlled by the output from the 135° polarization data channel.

Figure 5.4 shows the 90° data channel circuit block diagram on the receiver with two comparators and 2-to-1 multiplexer used for simple channel coding to recover proper channel data.

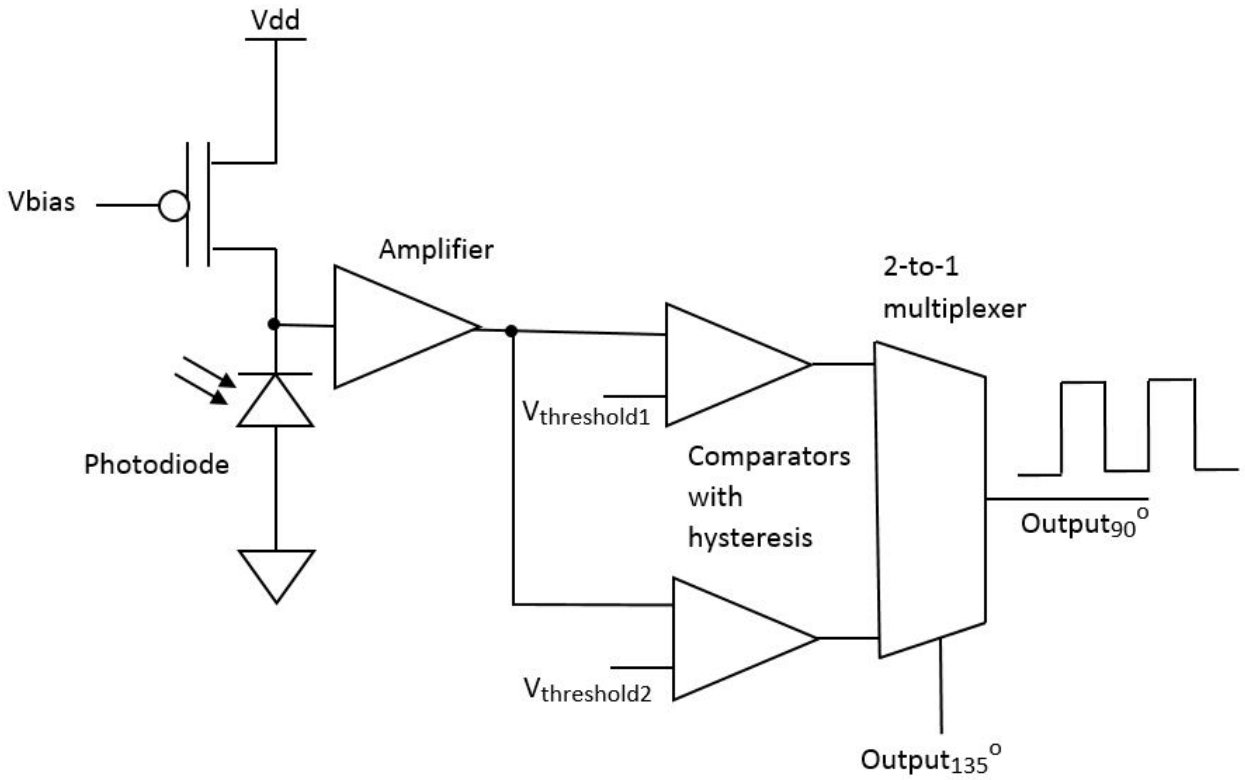

Figure 5.4: 90° data channel circuit with 2 comparators and 2-to-1 multiplexer.

If I_{135° output is equal to b'0', then I_{90° polarization data with comparator threshold of 0.45 is 90^o polarization data channel output and if I_{135° is equal to b'1', then I_{90° polarization data with comparator threshold of 0.695 is 90^o polarization data channel output.

In this way we apply simple channel coding hardware based routine on the receiver's output side that creates proper binary data stream on the 90^o polarization data channel output without any errors. This is shown in Table 5.12 which indicates that the 90^o polarization data channel output binary stream is b'0000111100001111' is as expected.

Table 5.12: 90^o polarization data receiver channel output signal.

Input	0	1	2	3	4	5	6	7	8	9	10	11	12	13	14	15
I_{90}	0	0	0	0	1	1	1	1	0	0	0	0	1	1	1	1

Chapter 6

Channel Models

In Chapter 3 we analyzed and simulated the receiver side of the 2, 3, and 4 channel VLC PDM systems assuming air as the transmission media. We now extend that work to include more of the optical path. Specifically, in this chapter we include in the analysis the polarization filters at the light source.

In addition, we will extend the transmission media investigations to include two more light paths. The first is a fiber-optic cable and the second is the a free-space path that includes a pair of mirrors. For each of these channel models, we will analyze a 2, 3, and 4 channel system, and for the 4 channel systems will include channel coding as described in Chapter 5.

6.1 VLC PDM Systems with Air Transmission Media

6.1.1 Two Channel System

A diagram of the 2 channel VLC PDM system with air used as transmission media is shown in Figure 6.1. The transmitter side of the system has two lasers that illuminate two light beams in two distinct and different binary patterns creating all four possible binary combinations.

For example, laser 1 light beam is polarized by the 0° DoFP polarization filter and laser 2 is polarized by the 90° DoFP polarization filter. These 0° and 90° polarized light beams are combined into one light beam and they travel through the air that is used as the transmission media. They are again separated by the DoFP polarization filter array bonded on the receiver chip.

Analysis of this two channel system can be done similarly as we have done the receiver analysis in Chapter 3. Figure 6.2 shows transmitter laser 1 that illuminates light in binary sequence b'0101'. Note that the light beam is non-polarized until it reaches the transmitter's DoFP filter array and is represented with the Stokes vector $S_{\text{IN}} = [1 \quad 0 \quad 0 \quad 0]^T$.

When the non-polarized light beam from the transmitter laser 1 reaches DoFP filter array it gets polarized. This light beam is polarized with 0° DoFP polarization filter that has Mueller matrix representation M_{Θ} as shown in Chapter 3, equation (3.2).

The output of the 0° DoFP polarization filter is the light beam that still represents the binary sequence b'0101' and its Stokes vector representation is defined as S_{0° which represents the

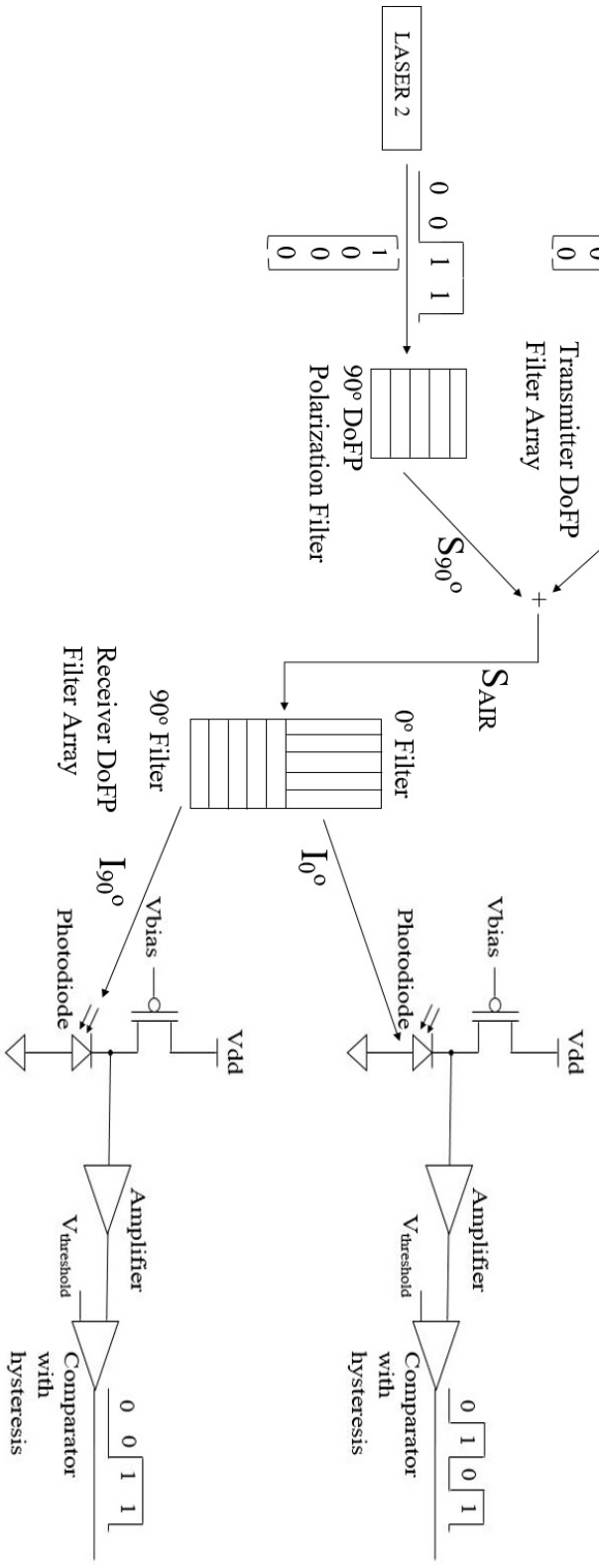

Figure 6.1: Two channel system with air used as transmission media.

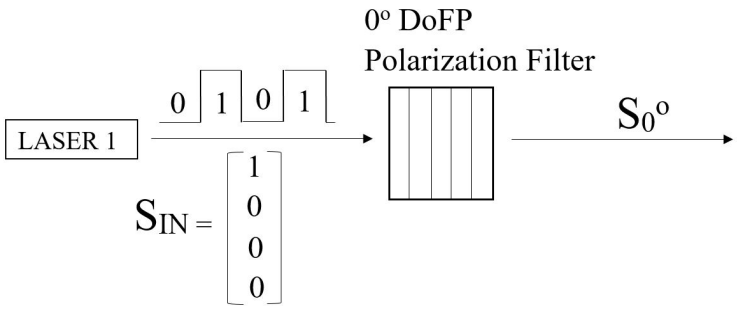

Figure 6.2: Transmitter 1 illuminates light in binary sequence b'0101'.

Stokes vector for 0° polarized light. The Stokes vector S_{0° is shown below.

$$S_{0^\circ} = M_{0^\circ} S_{\text{IN}} = \frac{1}{2} \begin{bmatrix} (p_x^2 + p_y^2) \\ (p_x^2 - p_y^2)\cos(2\Theta) \\ (p_x^2 - p_y^2)\sin(2\Theta) \\ 0 \end{bmatrix} \tag{6.1}$$

We can use the measured parameters for Aluminum nanowire filters as we did in Chapter 3.

$$T = (p_x^2 + p_y^2) = \frac{1}{2} \tag{6.2}$$

$$D = \frac{(p_x^2 - p_y^2)}{(p_x^2 + p_y^2)} = 0.99 \tag{6.3}$$

Also since the polarization angle $\theta = 0^\circ$ we can see that S_{0° can be expressed as

$$S_{0^\circ} = \frac{1}{2} \begin{bmatrix} T \\ TD\cos(0^\circ) \\ TD\sin(0^\circ) \\ 0 \end{bmatrix} = \frac{1}{2} \begin{bmatrix} \frac{1}{2} \\ \frac{0.99}{2} \\ 0 \\ 0 \end{bmatrix} = \begin{bmatrix} 0.25 \\ 0.2475 \\ 0 \\ 0 \end{bmatrix} \tag{6.4}$$

Figure 6.3 shows transmitter chip laser 2 that illuminates with binary sequence b'0011'. The light source is also represented with Stokes vector $S_{\text{IN}} = [1 \quad 0 \quad 0 \quad 0]^T$. This light beam is

polarized with a 90° DoFP polarization filter that has the same Mueller matrix representation M_Θ as the 0° DoFP polarization filter but with an angle of 90°.

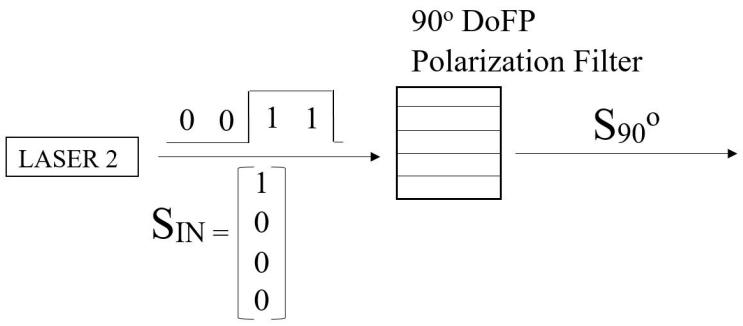

Figure 6.3: Transmitter 2 illuminates light in binary sequence b'0011'.

The output of the 90° DoFP polarization filter is the light beam that represents the binary sequence b'0011' and its Stokes vector representation is defined as S_{90° which represents the Stokes vector for 90° polarized light. The Stokes vector S_{90° is shown below.

$$S_{90^\circ} = M_{90^\circ} S_{\text{IN}} = \frac{1}{2} \begin{bmatrix} (p_x^2 + p_y^2) \\ (p_x^2 - p_y^2)\cos(2\Theta) \\ (p_x^2 - p_y^2)\sin(2\Theta) \\ 0 \end{bmatrix} \tag{6.5}$$

We use again the measured values for parameters T and D. Also since the polarization angle $\theta = 90^\circ$ we can see that S_{90° can be expressed as

$$S_{90^\circ} = \frac{1}{2} \begin{bmatrix} T \\ TD\cos(180^\circ) \\ TD\sin(180^\circ) \\ 0 \end{bmatrix} = \frac{1}{2} \begin{bmatrix} \frac{1}{2} \\ \frac{-0.99}{2} \\ 0 \\ 0 \end{bmatrix} = \begin{bmatrix} 0.25 \\ -0.2475 \\ 0 \\ 0 \end{bmatrix} \tag{6.6}$$

Two polarized light beams are combined in the air as shown in Figure 6.4. The combined light beam is defined as

$$S_{\text{AIR}} = b_O S_{0^\circ} + b_{90} S_{90^\circ} \tag{6.7}$$

where b_0 and b_{90} are binary 0 or 1 representing the data to be transmitted.

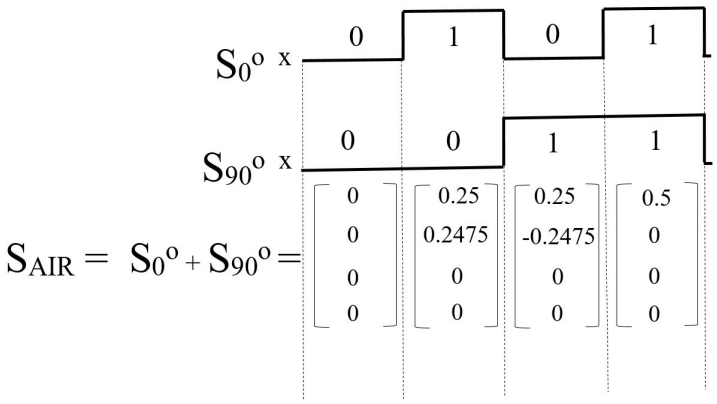

Figure 6.4: Two combined light signals.

The combined light beam S_{AIR} will be filtered through each of the 0° and 90° filters on the receiver and light input to the photodiodes is represented by I_{0° and I_{90°, which are

$$I_{0^\circ} = [1 \quad 0 \quad 0 \quad 0] M_{0^\circ} S_{\text{AIR}} \tag{6.8}$$

$$= [1 \quad 0 \quad 0 \quad 0] M_{0^\circ} [S_0 \quad S_1 \quad S_2 \quad S_3]^T \tag{6.9}$$

$$= \frac{1}{2}(\frac{1}{2} S_0 + \frac{0.99}{2} S_1) \tag{6.10}$$

$$I_{90^\circ} = [1 \quad 0 \quad 0 \quad 0] M_{90^\circ} S_{\text{AIR}} \tag{6.11}$$

$$= [1 \quad 0 \quad 0 \quad 0] M_{90^\circ} [S_0 \quad S_1 \quad S_2 \quad S_3]^T \tag{6.12}$$

$$= \frac{1}{2}(\frac{1}{2}S_0 - \frac{0.99}{2}S_1) \tag{6.13}$$

We can now calculate all four possible values for each channel and we obtain Table 6.1. The table shows each channel (0º and 90º) photodiode light signal I_{0° and I_{90°. These signals are converted to an electrical signal, amplified, and compared to a threshold.

Table 6.1: Outputs from air 2 channel system.

I_{90°	I_{0°	$Output_{90^\circ}$	$Output_{0^\circ}$
0	0	0	0
0.001244	0.123756	0	1
0.123756	0.001244	1	0
0.125	0.125	1	1

With a threshold that corresponds to 0.06, the binary outputs that are intended are correctly recovered.

6.1.2 Three Channel System

A diagram of the three channel VLC PDM system with air used as transmission media is shown in Figure 6.5. The transmitter side of the system has three lasers that illuminate three light beams using three distinct and different binary patterns creating all eight possible binary combinations.

Laser 1 illuminates the light beam in binary pattern b'01010101', laser 2 illuminates the light beam in binary pattern b'00110011' and laser 3 illuminates the light beam in binary pattern

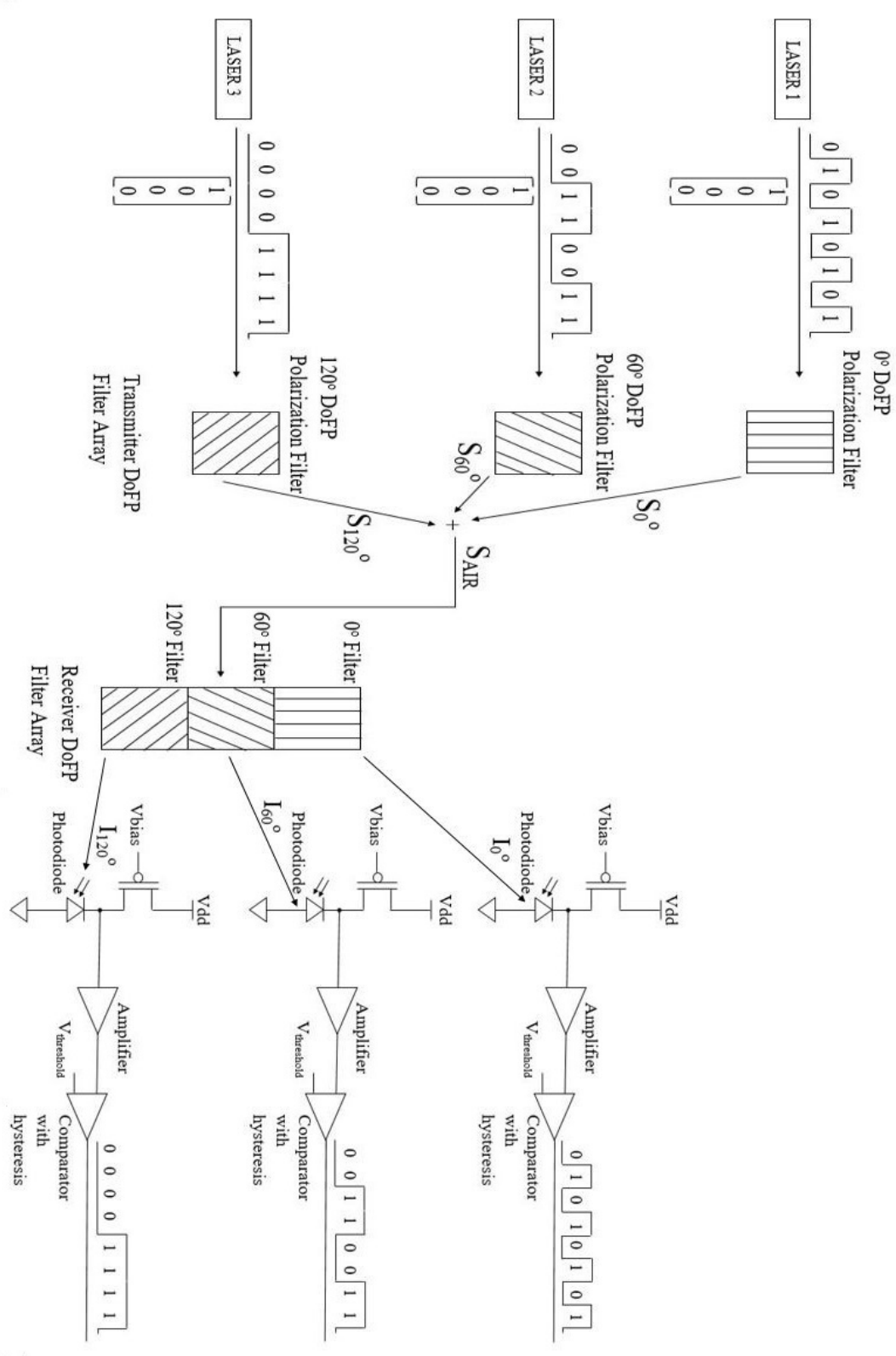

Figure 6.5: Three channel system with air used as transmission media.

b'00001111'. All three light beams are not polarized when they are initially transmitted from the lasers and before they reach the filter array at the transmitter.

After the transmitter filter array, the 0°, 60° and 120° polarized light beams are combined into one light beam as they travel through the air that is used as transmission media and they are again separated by 0°, 60° and 120° DoFP polarization filters that are bonded on the surface of the receiver chip.

Analysis of the three channel system with air used as transmission media is performed as above. Figure 6.6 shows transmitter chip's laser 1 that illuminates light using binary sequence b'01010101'.

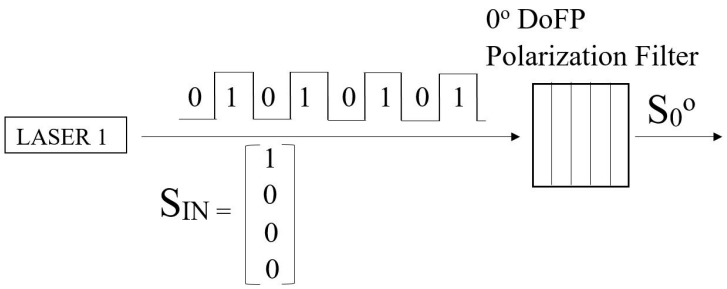

Figure 6.6: Transmitter 1 illuminates light in binary sequence b'01010101'.

The output of the 0° DoFP polarization filter is the light beam that represents the binary sequence b'01010101' and its Stokes vector representation is defined as S_{0° which represents the Stokes vector for 0° polarized light. The Stokes vector S_{0° is shown below.

$$S_{0^\circ} = M_{0^\circ} S_{\text{IN}} = \frac{1}{2} \begin{bmatrix} (p_x^2 + p_y^2) \\ (p_x^2 - p_y^2)\cos(2\Theta) \\ (p_x^2 - p_y^2)\sin(2\Theta) \\ 0 \end{bmatrix} \tag{6.14}$$

Again, we can use the measured values for parameters T and D. Since the polarization angle $\theta = 0^\circ$ we can see that S_{0° can be represented as

$$S_{0^\circ} = \frac{1}{2}\begin{bmatrix} T \\ TD\cos(0^\circ) \\ TD\sin(0^\circ) \\ 0 \end{bmatrix} = \frac{1}{2}\begin{bmatrix} \frac{1}{2} \\ \frac{0.99}{2} \\ 0 \\ 0 \end{bmatrix} = \begin{bmatrix} 0.25 \\ 0.2475 \\ 0 \\ 0 \end{bmatrix} \tag{6.15}$$

Figure 6.7 shows transmitter chip's laser 2 that illuminates light using binary sequence b'00110011'. That light source is also represented with Stokes vector $S_{\text{IN}} = [1 \quad 0 \quad 0 \quad 0]^T$. This light beam is polarized with 60° DoFP polarization filter that has the same Mueller matrix representation M_Θ as the 0° DoFP polarization filter has but evaluated with 60° polarization angle.

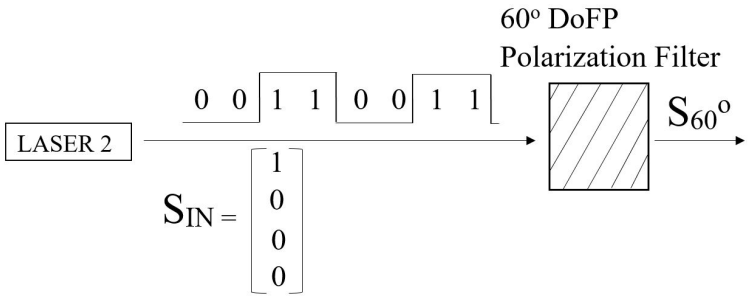

Figure 6.7: Transmitter 2 illuminates light in binary sequence b'00110011'.

The output of the 60° DoFP polarization filter is S_{60° which is shown below.

$$S_{60^\circ} = M_{60^\circ}S_{\text{IN}} = \frac{1}{2}\begin{bmatrix} (p_x^2 + p_y^2) \\ (p_x^2 - p_y^2)\cos(2\Theta) \\ (p_x^2 - p_y^2)\sin(2\Theta) \\ 0 \end{bmatrix} \tag{6.16}$$

Again, we can use the measured values for T and D. Since the polarization angle $\theta = 60°$ we can see that $S_{60°}$ can be represented as

$$S_{60°} = \frac{1}{2}\begin{bmatrix} T \\ TD\cos(120°) \\ TD\sin(120°) \\ 0 \end{bmatrix} = \frac{1}{2}\begin{bmatrix} \frac{1}{2} \\ \frac{-0.99}{2}\frac{1}{2} \\ 0.99\frac{\sqrt{3}}{2}\frac{1}{2} \\ 0 \end{bmatrix} = \begin{bmatrix} 0.25 \\ -0.124 \\ 0.2145 \\ 0 \end{bmatrix} \tag{6.17}$$

Figure 6.8 shows transmitter chip laser 3 that illuminates light using binary sequence b'00001111'. This light beam is polarized with 120° DoFP polarization filter that has the same Mueller matrix representation M_Θ as the 0° DoFP polarization filter has but evaluated for 120° polarization angle.

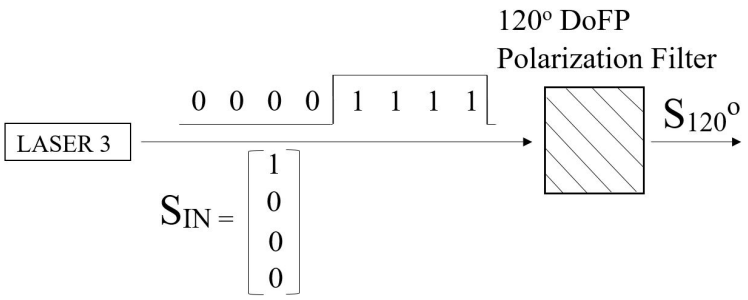

Figure 6.8: Transmitter 3 illuminates light in binary sequence b'00001111'.

The Stokes vector $S_{120°}$ is shown below.

$$S_{120°} = M_{120°}S_{\text{IN}} = \frac{1}{2}\begin{bmatrix} (p_x^2 + p_y^2) \\ (p_x^2 - p_y^2)\cos(2\Theta) \\ (p_x^2 - p_y^2)\sin(2\Theta) \\ 0 \end{bmatrix} \tag{6.18}$$

Since the polarization angle $\theta = 120°$ we can see that $S_{120°}$ can be represented as

$$S_{120°} = \frac{1}{2}\begin{bmatrix} T \\ TD\cos(240°) \\ TD\sin(240°) \\ 0 \end{bmatrix} = \frac{1}{2}\begin{bmatrix} \frac{1}{2} \\ \frac{-0.99}{2}\frac{1}{2} \\ -0.99\frac{1}{2}\frac{\sqrt{3}}{2} \\ 0 \end{bmatrix} = \begin{bmatrix} 0.25 \\ -0.124 \\ -0.2145 \\ 0 \end{bmatrix} \tag{6.19}$$

Three polarized light beams are added together in the air as shown in Figure 6.9. The combined light beam is defined as

$$S_{\text{AIR}} = b_0 S_{0°} + b_{60} S_{60°} + b_{120} S_{120°} \tag{6.20}$$

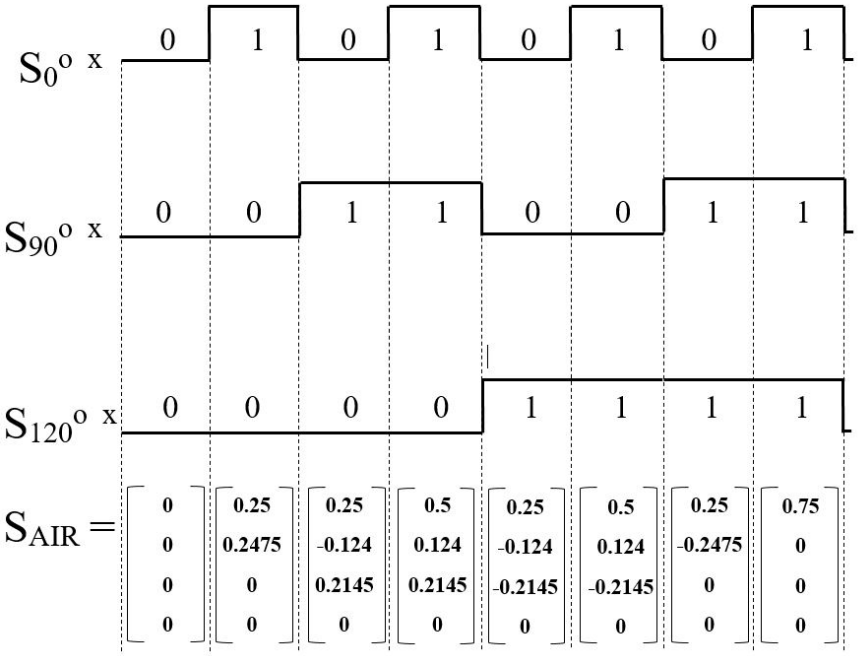

Figure 6.9: Three combined light signals.

The combined light beam S_{AIR} is filtered through each of the three 0°, 60° and 120° DoFP polarization filters on the receiver and from here the light inputs to receiver's output channels photodoides I_{0°, I_{60° and I_{120° are defined as

$$I_{0^\circ} = [1 \quad 0 \quad 0 \quad 0] M_{0^\circ} S_{\text{AIR}} \tag{6.21}$$

$$= [1 \quad 0 \quad 0 \quad 0] M_{0^\circ} [S_0 \quad S_1 \quad S_2 \quad S_3]^T \tag{6.22}$$

$$= \frac{1}{4} S_0 + \frac{0.99}{4} S_1 \tag{6.23}$$

$$I_{60^\circ} = [1 \quad 0 \quad 0 \quad 0] M_{60^\circ} S_{\text{AIR}} \tag{6.24}$$

$$= [1 \quad 0 \quad 0 \quad 0] M_{60^\circ} [S_0 \quad S_1 \quad S_2 \quad S_3]^T \tag{6.25}$$

$$= \frac{1}{4} S_0 - \frac{0.99}{8} S_1 + 0.99 \frac{\sqrt{3}}{8} S_2 \tag{6.26}$$

$$I_{120^\circ} = [1 \quad 0 \quad 0 \quad 0] M_{120^\circ} S_{\text{AIR}} \tag{6.27}$$

$$= [1 \quad 0 \quad 0 \quad 0] M_{90^\circ} [S_0 \quad S_1 \quad S_2 \quad S_3]^T \tag{6.28}$$

$$= \frac{1}{4} S_0 - \frac{0.99}{8} S_1 - 0.99 \frac{\sqrt{3}}{8} S_2 \tag{6.29}$$

Now we can calculate all eight values for each of three channels to obtain Table 6.2. The table shows each of the three channels' photodiode light inputs (I_{0°, I_{60° and I_{120°). Using a threshold of 0.1, it is possible to resolve all eight input combinations. As we can see noise margins for three channel system are wide enough so that all three input binary sequence are recovered at the receiver's outputs.

Table 6.2: Outputs from air 3 channel system.

I_{120°	I_{60°	I_{0°	$Output_{120^\circ}$	$Output_{60^\circ}$	$Output_{0^\circ}$
0	0	0	0	0	0
0.031872	0.031872	0.123756	0	0	1
0.031869	0.123821	0.03181	0	1	0
0.063679	0.155631	0.15569	0	1	1
0.123821	0.031869	0.03181	1	0	0
0.155631	0.063679	0.15569	1	0	1
0.15569	0.15569	0.06362	1	1	0
0.1875	0.1875	0.1875	1	1	1

6.1.3 Four Channel System

The four channel system with air as the transmission media is shown in Figure 6.10.

The laser 1 light beam is polarized by the 0° DoFP polarization filter, the laser 2 beam is polarized by the 45° DoFP polarization filter, the laser 3 beam is polarized by the 90° DoFP polarization filter and the laser 4 beam is polarized by 135° DoFP polarization filter.

Figure 6.11 shows the transmitter chip's laser 1 that illuminates light using binary sequence b'0101010101010101'.

The Stokes vector S_{0° is shown below

$$S_{0^\circ} = M_{0^\circ} S_{\text{IN}} = \frac{1}{2} \begin{bmatrix} (p_x^2 + p_y^2) \\ (p_x^2 - p_y^2)\cos(2\Theta) \\ (p_x^2 - p_y^2)\sin(2\Theta) \\ 0 \end{bmatrix} \tag{6.30}$$

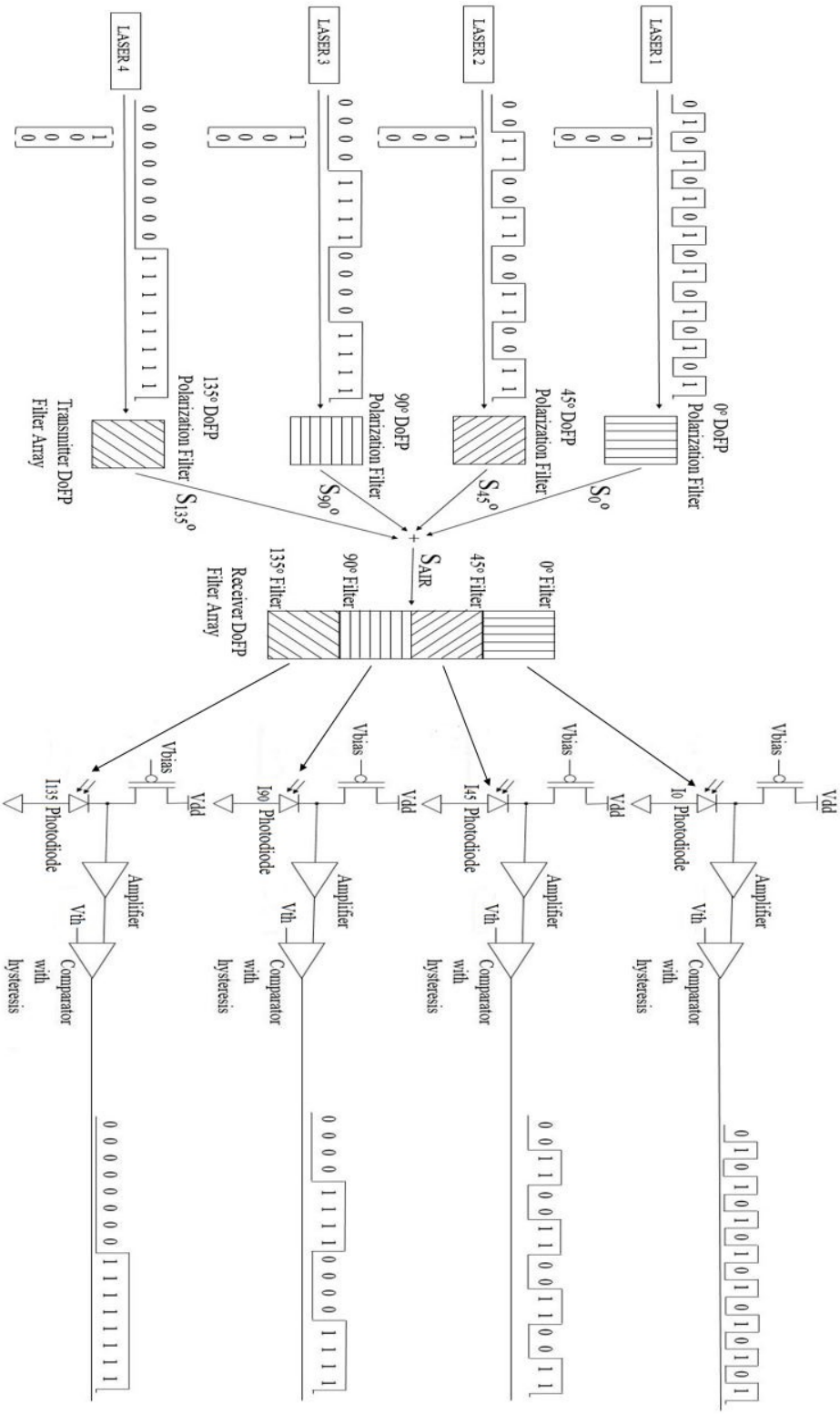

Figure 6.10: Four channel system with air used as transmission media.

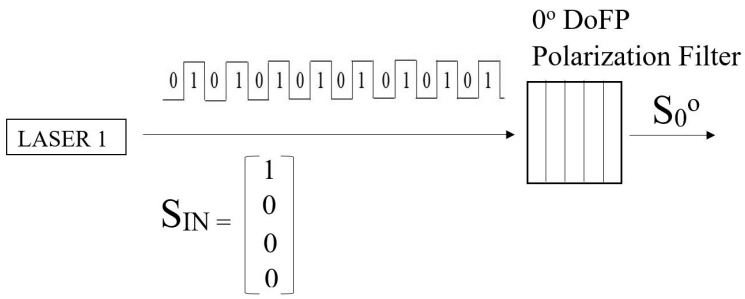

Figure 6.11: Transmitter 1 sends sequence b'0101010101010101'.

and

$$S_{0^\circ} = \frac{1}{2}\begin{bmatrix} T \\ TD\cos(0^\circ) \\ TD\sin(0^\circ) \\ 0 \end{bmatrix} = \frac{1}{2}\begin{bmatrix} \frac{1}{2} \\ \frac{0.99}{2} \\ 0 \\ 0 \end{bmatrix} = \begin{bmatrix} 0.25 \\ 0.2475 \\ 0 \\ 0 \end{bmatrix} \tag{6.31}$$

Figure 6.12 shows the transmitter chip's laser 2 that illuminates light in binary sequence b'0011001100110011'.

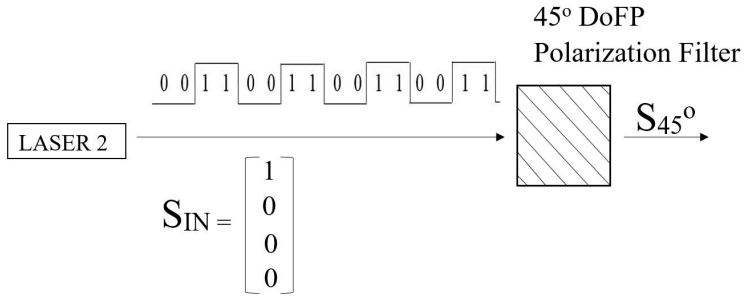

Figure 6.12: Transmitter 2 sends sequence b'0011001100110011'.

The Stokes vector S_{45° is shown below

$$S_{45^\circ} = M_{45^\circ} S_{\text{IN}} = \frac{1}{2} \begin{bmatrix} (p_x^2 + p_y^2) \\ (p_x^2 - p_y^2)\cos(2\Theta) \\ (p_x^2 - p_y^2)\sin(2\Theta) \\ 0 \end{bmatrix} \tag{6.32}$$

and

$$S_{45^\circ} = \frac{1}{2} \begin{bmatrix} T \\ TD\cos(90^\circ) \\ TD\sin(90^\circ) \\ 0 \end{bmatrix} = \frac{1}{2} \begin{bmatrix} \frac{1}{2} \\ 0 \\ \frac{0.99}{2} \\ 0 \end{bmatrix} = \begin{bmatrix} 0.25 \\ 0 \\ 0.2475 \\ 0 \end{bmatrix} \tag{6.33}$$

Figure 6.13 shows the transmitter chip's laser 3 that illuminates light using binary sequence b'0000111100001111'.

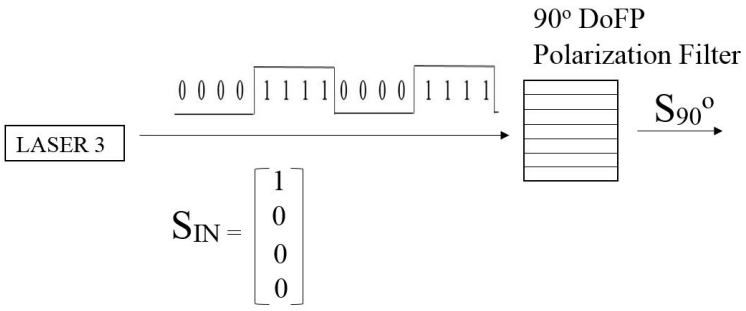

Figure 6.13: Transmitter 3 sends sequence b'0000111100001111'.

The Stokes vector S_{90° is shown below

$$S_{90^\circ} = M_{90^\circ} S_{\text{IN}} = \frac{1}{2} \begin{bmatrix} (p_x^2 + p_y^2) \\ (p_x^2 - p_y^2)\cos(2\Theta) \\ (p_x^2 - p_y^2)\sin(2\Theta) \\ 0 \end{bmatrix} \tag{6.34}$$

and

$$S_{90^\circ} = \frac{1}{2} \begin{bmatrix} T \\ TD\cos(180^\circ) \\ TD\sin(180^\circ) \\ 0 \end{bmatrix} = \frac{1}{2} \begin{bmatrix} \frac{1}{2} \\ \frac{-0.99}{2} \\ 0 \\ 0 \end{bmatrix} = \begin{bmatrix} 0.25 \\ -0.2475 \\ 0 \\ 0 \end{bmatrix} \tag{6.35}$$

Figure 6.14 shows the transmitter chip's laser 4 that illuminates light using binary sequence b'0000000011111111'.

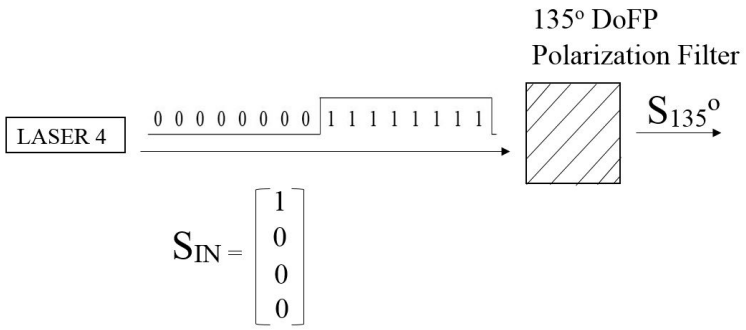

Figure 6.14: Transmitter 4 sends sequence b'0000000011111111'.

The Stokes vector S_{135° is shown below.

$$S_{135^\circ} = M_{135^\circ} S_{\text{IN}} = \frac{1}{2} \begin{bmatrix} (p_x^2 + p_y^2) \\ (p_x^2 - p_y^2)\cos(2\Theta) \\ (p_x^2 - p_y^2)\sin(2\Theta) \\ 0 \end{bmatrix} \tag{6.36}$$

and

$$S_{135^\circ} = \frac{1}{2} \begin{bmatrix} T \\ TD\cos(270^\circ) \\ TD\sin(270^\circ) \\ 0 \end{bmatrix} = \frac{1}{2} \begin{bmatrix} \frac{1}{2} \\ 0 \\ \frac{-0.99}{2} \\ 0 \end{bmatrix} = \begin{bmatrix} 0.25 \\ 0 \\ -0.2475 \\ 0 \end{bmatrix} \tag{6.37}$$

Four polarized light beams are combined in the air as shown in Figure 6.15. The combined light beam is defined as

$$S_{\text{AIR}} = b_0 S_{0^\circ} + b_{45} S_{45^\circ} + b_{90} S_{90^\circ} + b_{135} S_{135^\circ} \tag{6.38}$$

The combined light beam S_{AIR} will be filtered through each of the 0°, 45°, 90° and 135° filters on the receiver. These channels' photodiode inputs I_{0°, I_{45°, I_{90° and I_{135° are

$$I_{0^\circ} = [1 \quad 0 \quad 0 \quad 0] M_{0^\circ} S_{\text{AIR}} \tag{6.39}$$

$$= [1 \quad 0 \quad 0 \quad 0] M_{0^\circ} [S_0 \quad S_1 \quad S_2 \quad S_3]^T \tag{6.40}$$

$$= \frac{1}{4} S_0 + \frac{0.99}{4} S_1 \tag{6.41}$$

Figure 6.15: Four polarized light beams combined in the air.

$$I_{45^\circ} = [1 \quad 0 \quad 0 \quad 0] M_{45^\circ} S_{\text{AIR}} \tag{6.42}$$

$$= [1 \quad 0 \quad 0 \quad 0] M_{45^\circ} [S_0 \quad S_1 \quad S_2 \quad S_3]^T \tag{6.43}$$

$$= \frac{1}{4} S_0 + \frac{0.99}{4} S_2 \tag{6.44}$$

$$I_{90^\circ} = [1 \quad 0 \quad 0 \quad 0] M_{90^\circ} S_{\text{AIR}} \tag{6.45}$$

$$= [1 \quad 0 \quad 0 \quad 0] M_{90^\circ} [S_0 \quad S_1 \quad S_2 \quad S_3]^T \tag{6.46}$$

$$= \frac{1}{4} S_0 - \frac{0.99}{4} S_1 \tag{6.47}$$

$$I_{135^\circ} = [1 \quad 0 \quad 0 \quad 0] M_{135^\circ} S_{\text{AIR}} \tag{6.48}$$

$$= [1 \quad 0 \quad 0 \quad 0] M_{135^\circ} [S_0 \quad S_1 \quad S_2 \quad S_3]^T \tag{6.49}$$

$$= \frac{1}{4} S_0 - \frac{0.99}{4} S_2 \tag{6.50}$$

If we calculate all sixteen values for each of the four channels we will see that it is impossible to reconstruct all 16 values with a positive noise margin. This can be seen fairly readily in Figure 6.15, in which the Stokes vector S_{AIR} is the same, $[0.5 \quad 0 \quad 0 \quad 0]^T$, for both input symbols 0101 and 1010. If S_{AIR} is the same for that pair of input symbols, we cannot separate them in the receiver. In order to address this issue we introduce simple channel coding techniques on both the input transmitter side and output receiver side of the system to get correct binary sequences for all channels.

The techniques are all variations of the approach introduced in Chapter 5. On the input side we introduce different amplitudes for transmitters' lasers for each channel. On the output side at the receivers' end we introduce multi-threshold decoders to obtain the correct binary sequences for each of four channels.

For the four channel system we have four input laser sources that represent four distinct input data channels for polarization angles of 0°, 45°, 90° and 135°. Each binary value is represented by the Stokes vector $S_\Theta = [S_0 \quad S_1 \quad S_2 \quad S_3]^T$.

For S_{0° we use matrix (6.31) as the starting point to apply channel coding on the transmitter's input side. For S_{0° if the light signal is sent from the laser and then polarized with 0° DoFP filter which is defined with the Mueller Matrix representation M_Θ evaluated at polarization angle of 0°, the Stokes vector is defined as $S_{0^\circ} = 0.833[0.25 \quad 0.2475 \quad 0 \quad 0]^T = [0.20825 \quad 0.20617 \quad 0 \quad 0]^T$, and if the light signal is not sent the Stokes vector is defined as $S_{0^\circ} = [0 \quad 0 \quad 0 \quad 0]T$.

Note that amplitude of light signal is set up to 0.833 of the amplitude of 0.25 which represents channel coding on the input channel 1 side of the four channel VLC with PDM system. Table 6.3 shows 0° input laser data channel that represents binary stream b'0101010101010101' after the polarization filter at the source.

Table 6.3: 0° channel laser polarized light.

Binary input	0	1
Stokes vector	0	0.280
	0	0.206
	0	0
	0	0

Table 6.4 shows the 45° polarized laser data channel representing b'0011001100110011' binary stream. For S_{45° we use matrix (6.33) as the starting point to apply channel coding on the transmitter's input side. For S_{45° if the light signal is sent from the laser and then polarized with 45° DoFP filter that is defined with the Mueller Matrix representation M_Θ evaluated at polarization angle of 45°, it can be defined as $S_{45^\circ} = 0.611[0.25 \quad 0 \quad 0.2475 \quad 0]^T = [0.15275 \quad 0 \quad 0.15122 \quad 0]^T$.

If the light signal is off (binary 0) then $S_{45^\circ} = [0 \quad 0 \quad 0 \quad 0]^T$.

Table 6.4: 45° channel laser polarized light.

Binary input	0	1
Stokes vector	0	0.153
	0	0
	0	0.151
	0	0

Table 6.5 shows 90° input laser data channel that represents binary stream b'0000111100001111'. For S_{90° we use matrix (6.35) as the starting point to apply channel coding on the transmitter's input side. For S_{90° if the light signal is sent from the laser and then polarized with 90° DoFP filter that is defined with the Mueller Matrix representation M_{90°, then $S_{90^\circ} = 0.944[0.25 \quad 0.2475 \quad 0 \quad 0]^T = [0.236 \quad -0.234 \quad 0 \quad 0]^T$ and if the light signal is a binary 0 then $S_{90^\circ} = 0.611[0.25, -0.2475, 0, 0]^T = [0.15275, -0.15122, 0, 0]^T$.

Table 6.5: 90° channel Laser polarized light.

Binary input	0	1
Stokes vector	0.153	0.236
	-0.15	-0.23
	0	0
	0	0

Table 6.6 shows 135° input laser data channel that represents binary stream b'0000000011111111'. For S_{135° we use matrix (6.37) as the starting point to apply channel coding on the transmitter's input side. For S_{135° if the light signal is sent and then polarized with 135° filter that is defined with the Mueller Matrix representation M_{135°, $S_{135^\circ} = [0.25 \quad 0.2475 \quad 0 \quad 0]^T$ and if the light signal is not sent with this laser $S_{135^\circ} = [0 \quad 0 \quad 0 \quad 0]^T$.

Table 6.6: 135° channel laser polarized light.

Binary input	0	1
Stokes vector	0	0.25
	0	0
	0	-0.248
	0	0

Table 6.7 shows all 4 channels combined optical signals into one one optical signal as it travels thru the air between the transmitter's input and the receiver's output polarization filter arrays.

Table 6.7: All 4 polarized channels' light signals combined.

Input	0	1	2	3	4	5	6	7	8	9	10	11	12	13	14	15
S_{AIR}	0.153	0.361	0.306	0.514	0.236	0.444	0.389	0.597	0.403	0.611	0.556	0.764	0.486	0.694	0.639	0.847
	-0.15	0.055	-0.15	0.055	-0.23	-0.03	-0.23	-0.03	-0.15	0.055	-0.15	0.055	-0.23	-0.03	-0.23	-0.03
	0	0	0.151	0.151	0	0	0.151	0.151	-0.25	-0.25	-0.1	-0.1	-0.25	-0.25	-0.1	-0.1
	0	0	0	0	0	0	0	0	0	0	0	0	0	0	0	0

The receiver's polarized light inputs for each channel photodoide I_{0°, I_{45°, I_{90° and I_{135° are shown in Table 6.8.

Table 6.8: All 4 receiver channels' photodiode input light signals.

Input	0	1	2	3	4	5	6	7	8	9	10	11	12	13	14	15
I_{0°	0.001	0.104	0.039	0.142	0.001	0.104	0.039	0.142	0.063	0.166	0.101	0.205	0.064	0.167	0.102	0.205
I_{45°	0.038	0.09	0.114	0.166	0.059	0.111	0.135	0.187	0.039	0.091	0.115	0.167	0.06	0.112	0.136	0.188
I_{90°	0.076	0.077	0.114	0.115	0.117	0.118	0.155	0.156	0.138	0.139	0.176	0.177	0.179	0.18	0.218	0.219
I_{135°	0.038	0.09	0.039	0.091	0.059	0.111	0.06	0.112	0.162	0.214	0.163	0.215	0.183	0.235	0.184	0.234

Using a threshold of 0.103, Table 6.9 shows the receiver's 0° polarization data channel output binary stream is b'0101010101010101' as is expected.

Table 6.9: 0º polarization data receiver output signals.

Input	0	1	2	3	4	5	6	7	8	9	10	11	12	13	14	15
0° output	0	1	0	1	0	1	0	1	0	1	0	1	0	1	0	1

Receiver output I_{45° for 45º polarization data channel is obtained by applying comparator threshold 0.113 on the data from Table 6.8. Table 6.10 shows the receiver's 45º polarization data channel output binary stream is b'0011001100110011' as is expected.

Table 6.10: 45º polarization data receiver output signals.

Input	0	1	2	3	4	5	6	7	8	9	10	11	12	13	14	15
45° output	0	0	1	1	0	0	1	1	0	0	1	1	0	0	1	1

The receiver I_{135° for the 135º polarization data channel is obtained by applying comparator threshold 0.115 on the data from Table 6.8. Table 6.11 shows the 135º polarization data channel output binary stream is b'0000000011111111' as is expected.

Table 6.11: 135º polarization data receiver output signals.

Input	0	1	2	3	4	5	6	7	8	9	10	11	12	13	14	15
135° output	0	0	0	0	0	0	0	0	1	1	1	1	1	1	1	1

Finally, the receiver output for the 90º polarization data channel is obtained by applying two comparators with thresholds 0.115 and 0.178 on data from the Table 6.8. The outputs from both comparators is shown in Table 6.12.

Using the circuit of Figure 5.4, the output value of the 135° channel is used to select between the two comparator outputs.

Table 6.12: 90° polarization data receiver two comparator outputs.

Input	0	1	2	3	4	5	6	7	8	9	10	11	12	13	14	15
$I_{90^\circ} > 0.115$	0	0	0	0	1	1	1	1	1	1	1	1	1	1	1	1
$I_{90^\circ} > 0.178$	0	0	0	0	0	0	0	0	0	0	0	0	1	1	1	1

If the 135° output is equal to b'0', then I_{90° data with comparator threshold of 0.115 is selected as the 90° channel output and if the 135° output is equal to b'1', then I_{90° data with comparator threshold of 0.178 is selected as the 90° channel output.

This multi-threshold decoding of the 90° data channel is shown in Table 6.13. As we can see from this table, the 90° data channel output binary stream is b'0000111100001111' as is expected.

Table 6.13: 90° polarization data receiver output signal.

Input	0	1	2	3	4	5	6	7	8	9	10	11	12	13	14	15
90° output	0	0	0	0	1	1	1	1	0	0	0	0	1	1	1	1

6.1.4 Simulation of Polarization Division Multiplexing Systems

We used the Cadence simulation tool set to model the 2, 3 and 4 channel VLC PDM systems described above with air used as the transmission media. A block diagram of this simulation is shown in Figure 6.16.

The simulation model is decomposed into the following parts:

1. Input Laser Array is used to simulate input light data from the lasers. These input lasers are simulated in Cadence as voltage sources with periodic square wave voltages. The square wave voltage represent light source optical power [mW/cm] of present (or

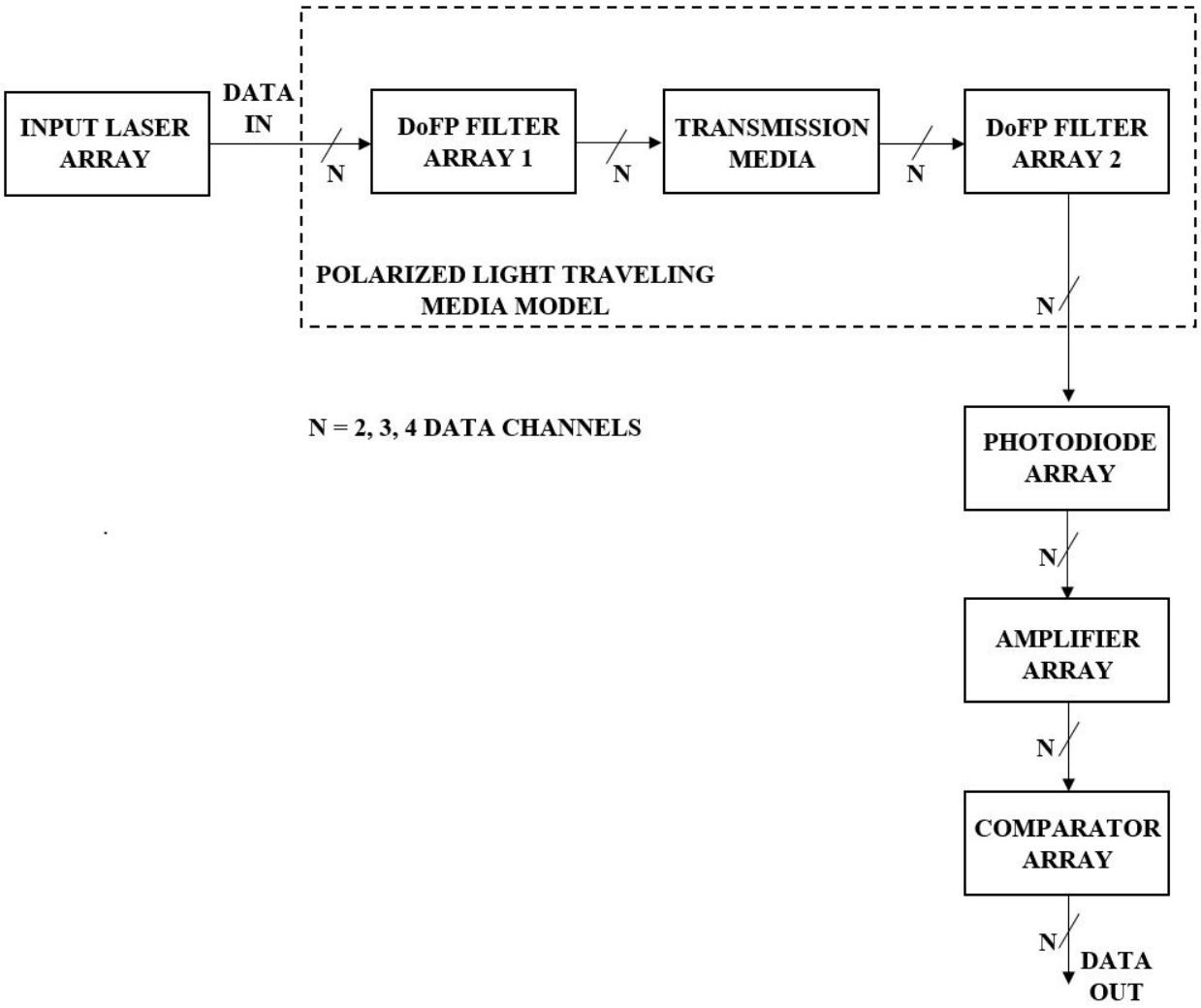

Figure 6.16: VLC PDM system Cadence simulation model block diagram.

binary b'1') or not present (or binary b'0') light signal that is transmitted out of the transmitter's input laser array. These input lasers optical signals (2, 3 or 4 signals) are travelling from the input lasers towards DoFP Filter Array 1.

2. DoFP Filter Array 1 or transmitters' DoFP filter array is used to simulate input laser data channels' polarization. This DoFP Filter Array 1 is represented with a Mueller matrix model which is designed using VerilogA. Each DoFP filter takes one voltage source from the Input Laser Array and polarizes it. Note that this DoFP Filter Array 1

is part of a single Cadence simulation part (Polarized Light Traveling Media Model) together with Transmission Media and DoFP Filter Array 2.

3. Transmission Media is either air, fiber optic cable or some other media (e.g., mirrors, waveguides) used for polarized light data channels to travel from the input laser array transmitter side to the photodiode receiver side of the VLC PDM system. In the transmission media all channels are combined and they travel together through it. If the transmission media is air there is no attenuation of the input light data signals. If the transmission media is fiber or waveguides then the media is represented by the Mueller matrix model appropriate to that media and it will attenuate the light signals. Transmission Media is also designed using VerilogA and it is part of the Cadence simulation part called Polarized Light Traveling Media Model.

4. DoFP Filter Array 2 or Receiver's DoFP Filter Array is used to model the polarized light data channels' separation at the receiver side of the VLC PDM system. The DOFP Filter Array 2 is also represented with a Mueller matrix model which is designed using VerilogA.

5. Photodiode Array is used to convert separated polarized light signals into electrical current signals. Each photodiode is designed VerilogA and implements the model described in Chapter 3. The input is a voltage signal that is indicative of the light intensity represented by a Stokes vector and the output is a current signal.

6. Amplifier Array is used to convert the data channel's electrical current signal into a voltage signal and then amplify it. This part of the system is a CMOS circuit designed to shape data channel electrical signal for the Comparator Array. It follows the design described in Chapter 3.

7. Comparator Array is used to decide weather the data channel output is binary value of '0' or binary value of '1'. This part of the system is also designed as a CMOS circuit. Chapter 3 also describes the details of this part of the system design.

Cadence simulation of two channel system

The Cadence simulation model of the two channel system with air used as the transmission media is shown in Figure 6.17. It directly follows the structure of Figure 6.16.

In Figure 6.17, the Input Laser Array is defined with two voltage sources V_{IN1} and V_{IN2}. The input voltage (light) signal V_{IN1} outputs a square wave of 1 MHz frequency with amplitude of 200 mV. This voltage source V_{IN1} is modeling an input laser source that generates binary sequence b'0101'.

The input voltage (light) signal V_{IN2} outputs a square wave of 0.5 MHz frequency with amplitude of 200 mV. This voltage source V_{IN2} is modeling an input laser source that generates binary sequence b'0011'.

In Figure 6.17, the Polarized Light Traveling Media Model is defined with VerilogA component DoFP_Polarimeter_Tx_Air_Rx_2_Ch_Full_System which is the Cadence component model for two DoFP filter arrays 1 and 2 and air as the transmission media, as it is shown in Figure 6.16.

Both DoFP Filter Arrays 1 and 2 are represented with 4-by-4 Mueller matrices and air is modeled as free space with no losses. In Figure 6.17, the two voltage (light) signals V_{IN1} and V_{IN2} are inputs to the VerilogA component and inside this component each light signal is represented with non-polarized Stokes vector $S_{IN} = [V_{IN} \quad 0 \quad 0 \quad 0]^T$.

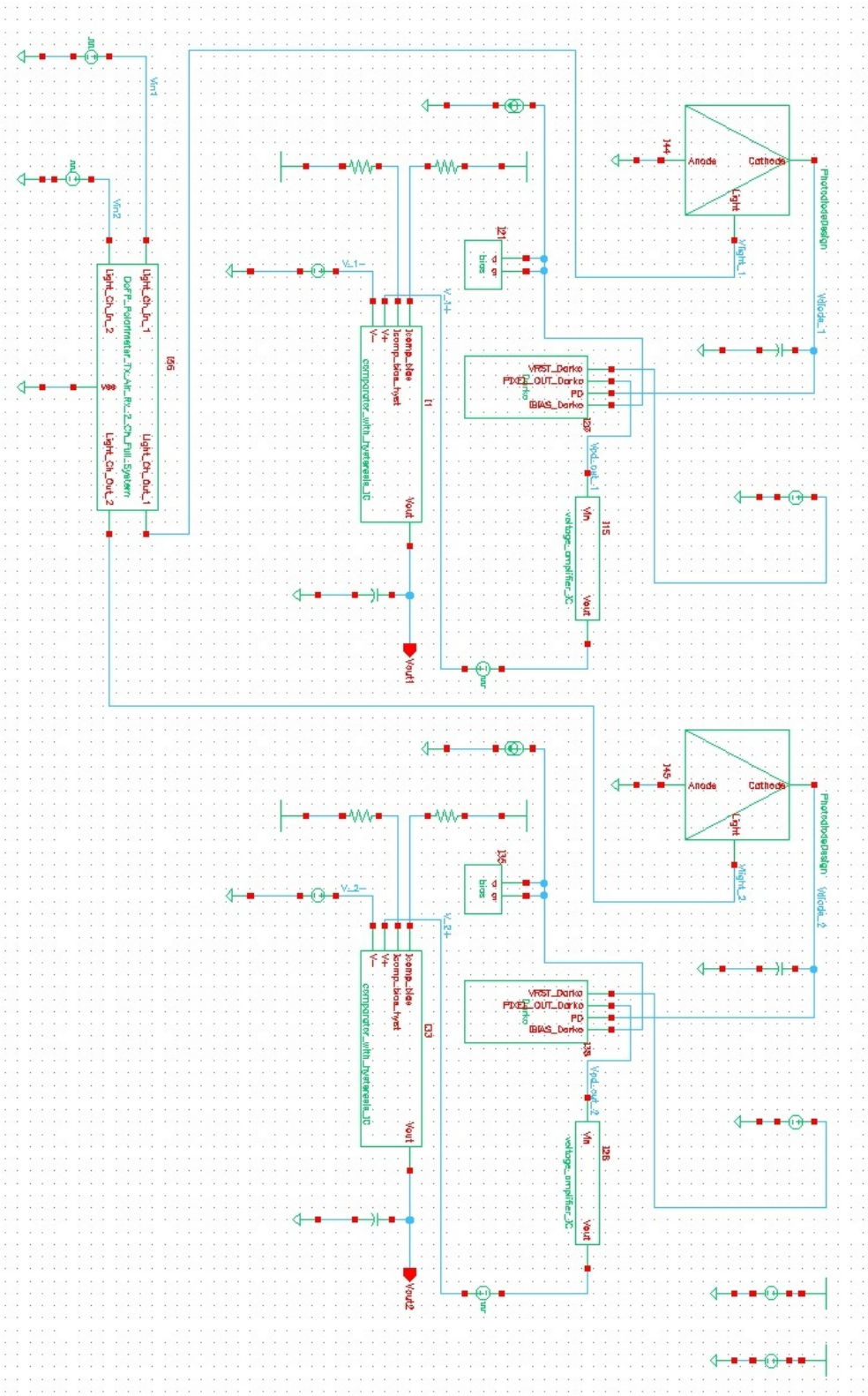

Figure 6.17: Cadence model of two channel system.

Figure 6.18 shows two non-polarized input voltage (light) signals V_{IN1} and V_{IN2} and two polarized voltage (light) signals V_{light1} and V_{light2} that are the outputs of the 2nd filter array. The signals shown in Figure 6.18 correspond with the predictions of Table 6.1. The only difference is that all values from the table have to be scaled by 200 mV amplitude in order to obtain the signal levels shown in the figure.

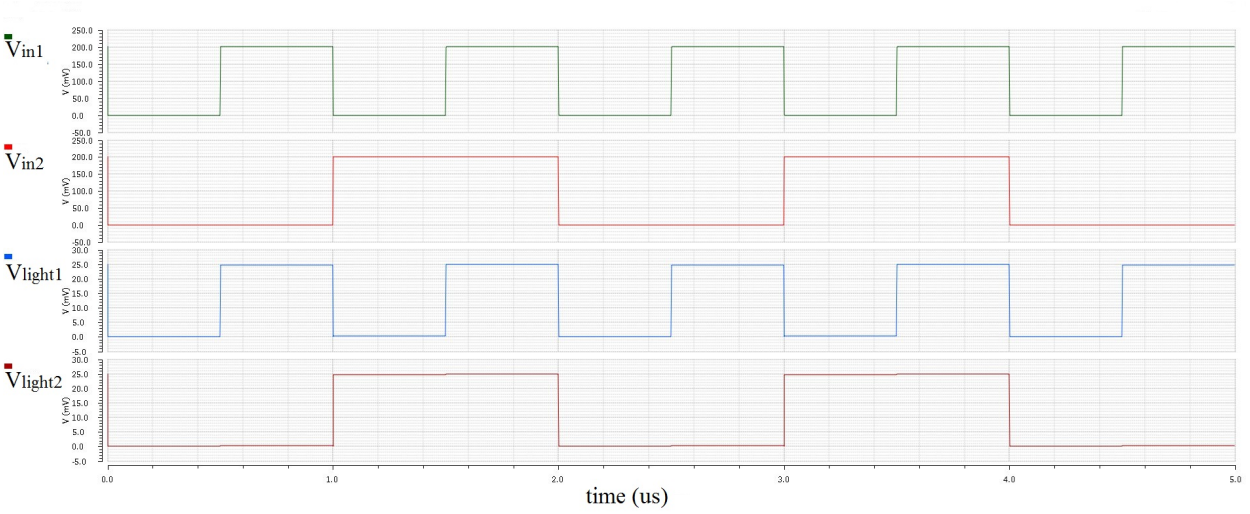

Figure 6.18: Input laser array light signals V_{IN1} and V_{IN2} and output light signals of the receiver DoFP filters V_{light1} and V_{light2} for the 2 channel system.

The light signals V_{light1} and V_{light2} signals are next input to two separate data channels where they are converted to electrical currents and then to electrical voltages and amplified to appropriate voltage levels for input to the channel's comparator. Before these voltage signals are processed through the comparator a noise voltage signal +/- 50 mV is added to the voltage signals to model noise sources in the receiver circuit.

Now, these voltage signals plus noise voltage signals are processed through the comparators with threshold voltage of 1.8 V. The outputs of both channels' comparators are 3.3V voltage signals that represent the 1 MHz square wave and 0.5 MHz square wave signals recovered

from the input. Figure 6.19 shows Cadence simulation results where two channels' system receiver's outputs match the system transmitter's input binary sequences.

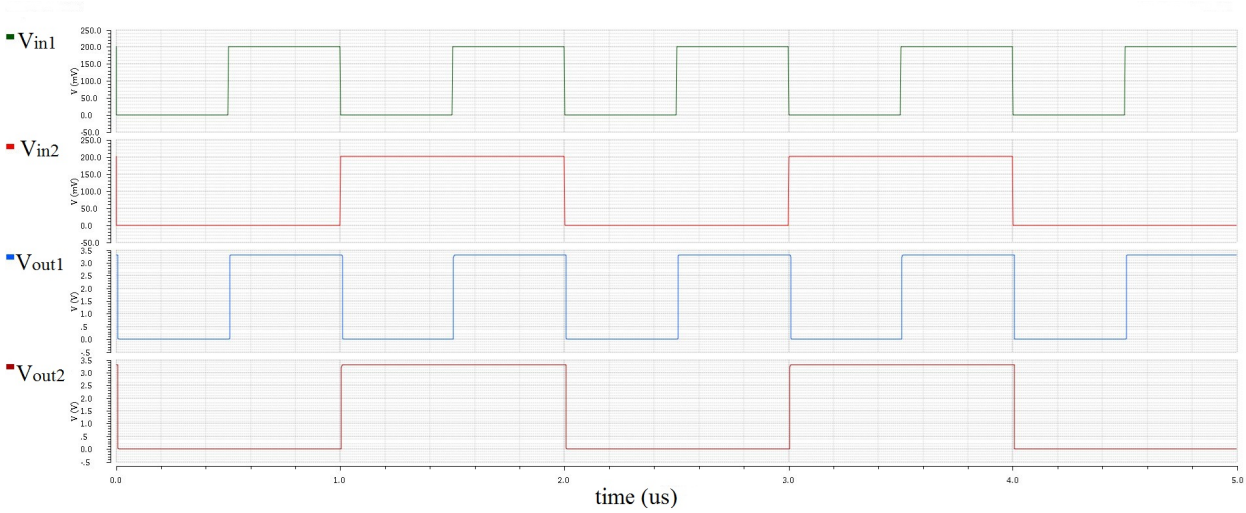

Figure 6.19: Input laser array light signals V_{IN1} and V_{IN2} and output voltage signals of the receiver data channels V_{OUT1} and V_{OUT2} for the two channel system.

Cadence simulation of three channel system

The Cadence simulation model of the three channel system with air used as the transmission media is shown in Figure 6.20.

The input laser array is defined with three voltage (light) sources V_{IN1}, V_{IN2} and V_{IN3}. The voltage (light) source V_{IN1} outputs a square wave of frequency 1 MHz with amplitude of 400 mV. The voltage (light) source V_{IN2} outputs a square wave of frequency 0.5 MHz with amplitude of 400 mV. Finally, the voltage (light) source V_{IN3} outputs a square wave of frequency 0.25 MHz with amplitude of 400 mV.

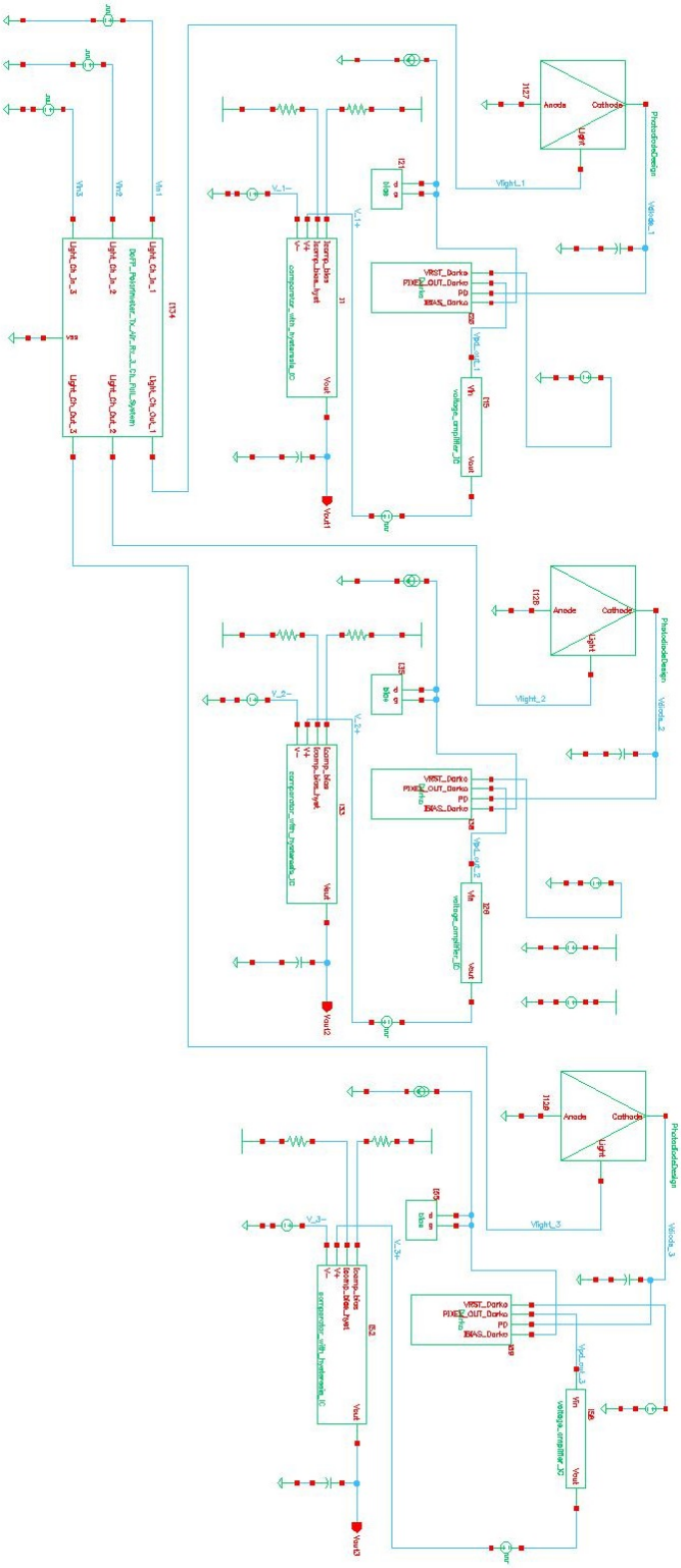

Figure 6.20: Cadence model of three channel system.

Figure 6.21 shows three non-polarized input voltage (light) signals V_{IN1}, V_{IN2} and V_{IN3} and three polarized voltage signals V_{light1}, V_{light2} and V_{light3} that represent three light data channels.

The signal levels of Figure 6.21 are a good match with the data of Table 6.2 The only difference is that all values from the table have to be multiplied by 400 mV amplitude in order to obtain the signal levels shown in Figure 6.21.

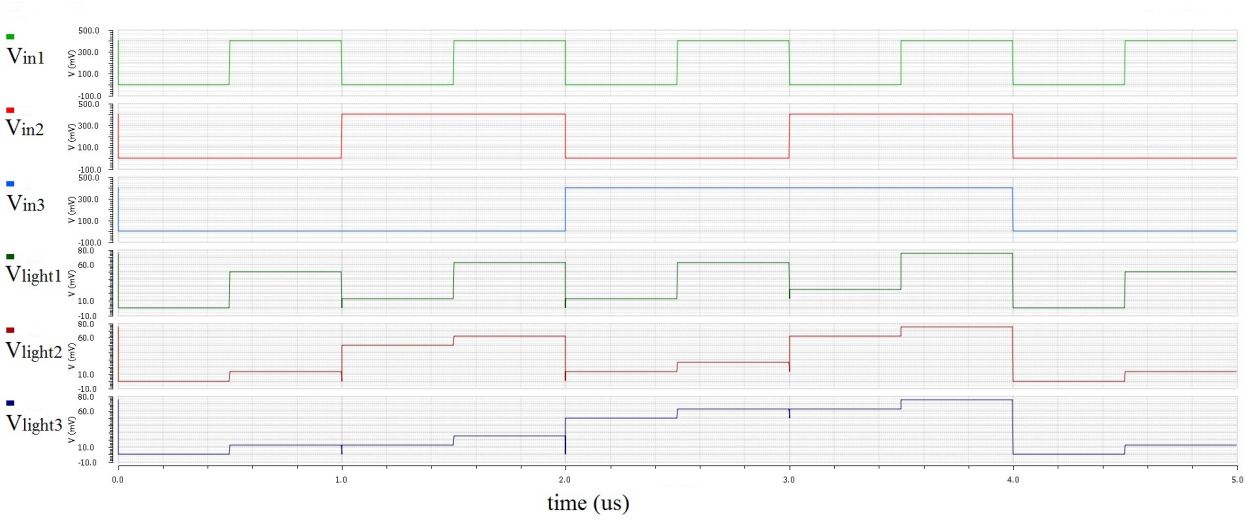

Figure 6.21: Input laser array light signals V_{IN1}, V_{IN2}, and V_{IN3} and output light signals of the receiver DoFP filters V_{light1}, V_{light2} and V_{light3} for the 3 channel system.

The light signals V_{light1}, V_{light2} and V_{light3} are now input to three separate data channels where they are converted to electrical currents and then to electrical voltages and amplified to appropriate voltage levels for input to comparators. Before these voltage signals are delivered to the comparators a noise voltage signal +/- 50 mV is added to the voltage signals to model noise sources.

Now, these voltage signals plus noise voltage signals are processed through the comparators with threshold voltages of 2.57 V. The outputs of all three channels' comparators are 3.3V

voltage signals that represent a 1 MHz square wave, a 0.5 MHz square wave and a 0.25 MHz square wave which are recovered from the source.

Figure 6.22 shows input laser array light signals V_{IN1}, V_{IN2} and V_{IN3} and output receiver array voltage signals V_{OUT1}, V_{OUT2} and V_{OUT3}. As we can from the figure, the Cadence three channel system is operating as expected.

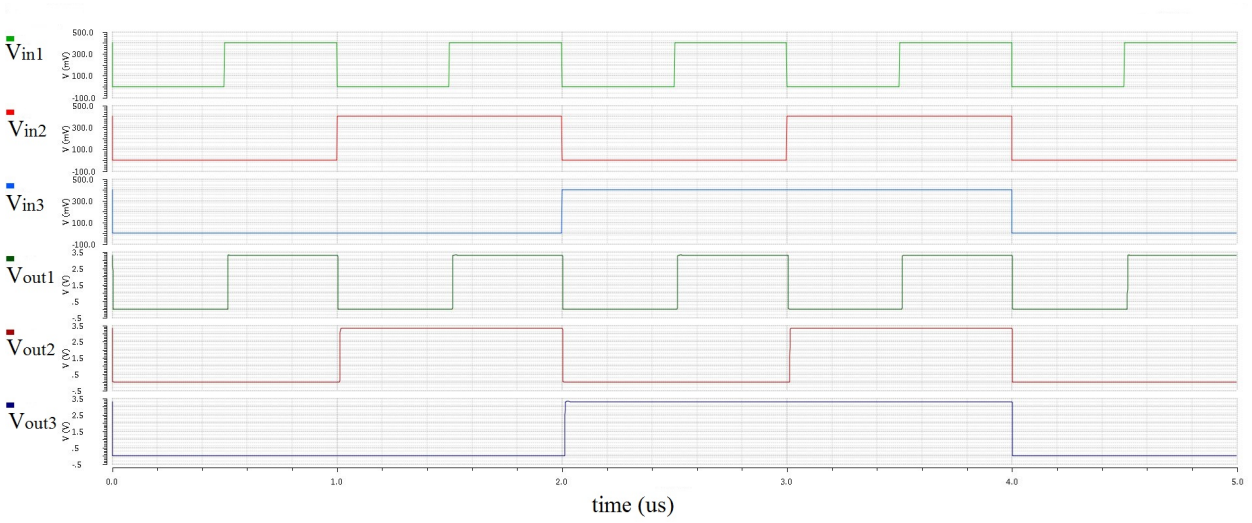

Figure 6.22: Input laser array light signals V_{IN1}, V_{IN2}, and V_{IN3} and output voltage signals of the receiver data channels V_{OUT1}, V_{OUT2}, and V_{OUT3} for the three channel system.

Cadence simulation of the four channel system

The Cadence simulation model of the four channel system with air used as the transmission media is shown in Figure 6.23.

In Figure 6.23, the input laser array is defined with four voltage (light) sources V_{IN1}, V_{IN2}, V_{IN3}, and V_{IN4}, outputting square waves with frequency 1 MHz (at amplitude 153 mV), 0.5 MHz (at amplitude 139 mV), 0.25 MHz (at amplitude 150 mV), and 0.125 MHz (at amplitude 140 mV) respectively.

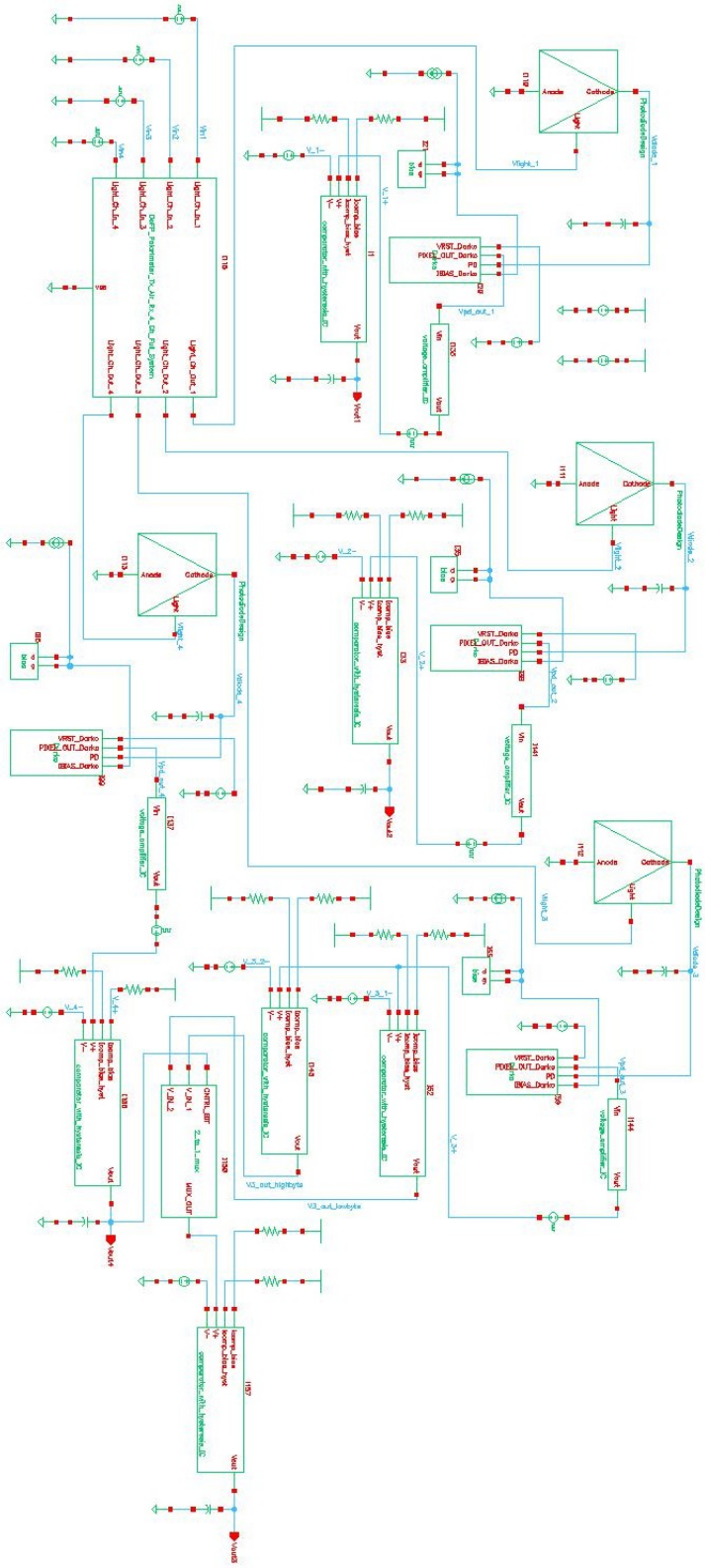

Figure 6.23: Cadence model of four channel system.

Channel coding on the input transmitter side means that all four input channels V_{IN1}, V_{IN2}, V_{IN3} and V_{IN4} have different amplitudes and in addition input channel V_{IN3} has two different amplitudes applied for binary '0' and binary '1'.

Figure 6.24 shows four non-polarized input voltage (light) signals V_{IN1}, V_{IN2}, V_{IN3}, and V_{IN4} and four polarized voltage signals V_{light1}, V_{light2}, V_{light3}, and V_{light4} that represent four light data channels. These results closely match the analytical results presented earlier in the chapter.

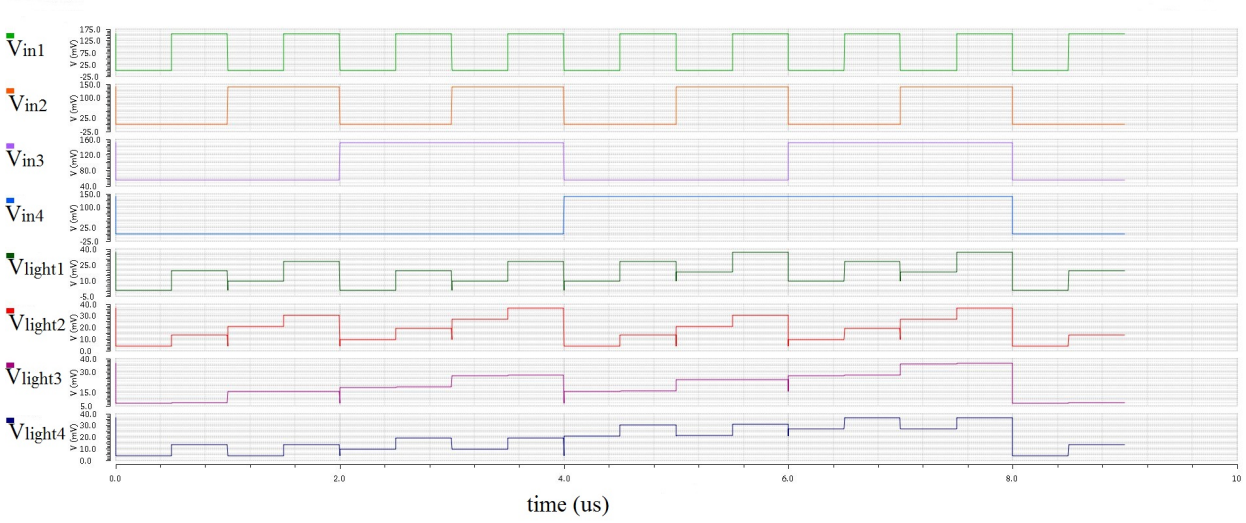

Figure 6.24: Input laser array light signals V_{IN1}, V_{IN2}, V_{IN3} and V_{IN4} and output light signals of the receiver DoFP filters V_{light1}, V_{light2}, V_{light3} and V_{light4} for the four channel system.

Figure 6.25 shows input laser array light signals V_{IN3} and V_{IN4}. It also shows two 90° data channel comparator outputs $V_{\text{OUT3\_lowbyte}}$ and $V_{\text{OUT3\_highbyte}}$ and 90° and 135° data channel outputs V_{OUT3} and V_{OUT4}. As we can from the figure, the simple channel coding applied on the 90° data channel helped out in the recovery of a proper output signal for that channel. We conclude that the four channel systems have tight noise margins and they are even worse if different transmission media is used to replace air (e.g., fiber optic cable).

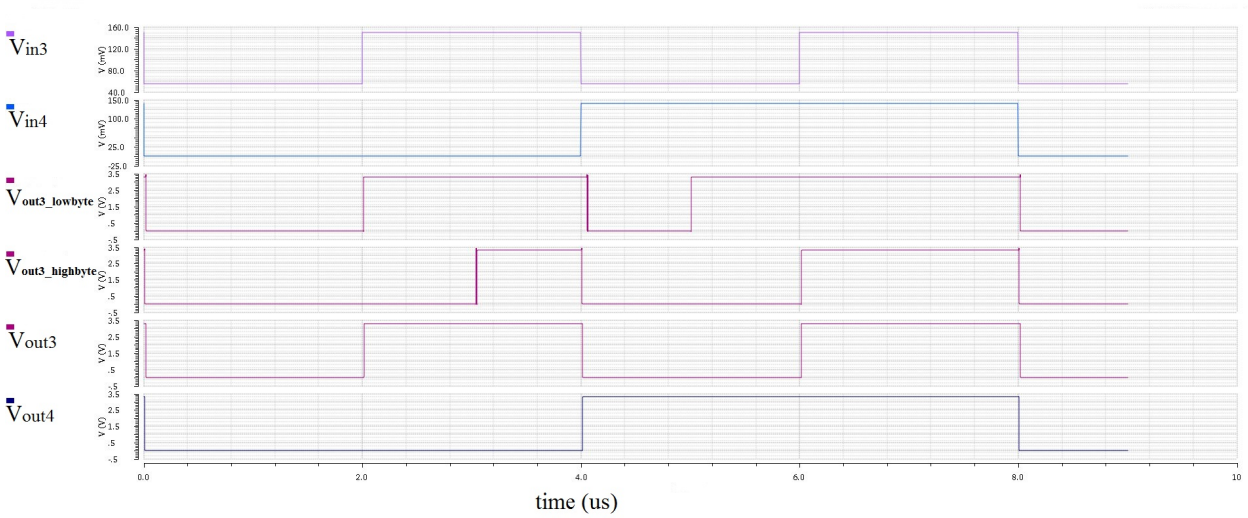

Figure 6.25: Input laser array light signals V_{IN3} and V_{IN4}, two 90° data channel comparators' outputs $V_{\mathrm{OUT3\_lowbyte}}$ and $V_{\mathrm{OUT3\_highbyte}}$ and 90° and 135° data channel outputs V_{OUT3} and V_{OUT4} for the 4 channel system.

Figure 6.26 shows all four input laser array light signals V_{IN1}, V_{IN2}, V_{IN3}, and V_{IN4} and all four receiver channel output voltage signals V_{OUT1}, V_{OUT2}, V_{OUT3}, and V_{OUT4}. We conclude that the four channel system with air used as the transmission media is working, however, within very tight noise margins.

Figure 6.27 shows 2-to-1 multiplexer design that is used for channel coding of 90° data channel.

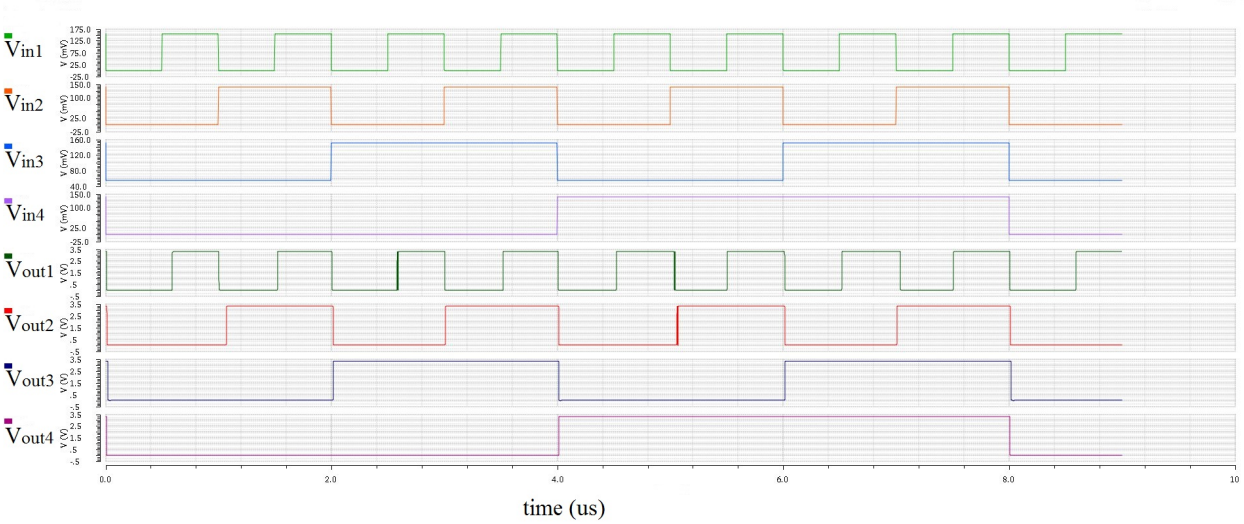

Figure 6.26: . Input laser array light signals V_{IN1}, V_{IN2}, V_{IN3}, and V_{IN4} and output voltage signals of the receiver data channels V_{OUT1}, V_{OUT2}, V_{OUT3}, and V_{OUT4} for the four channel system.

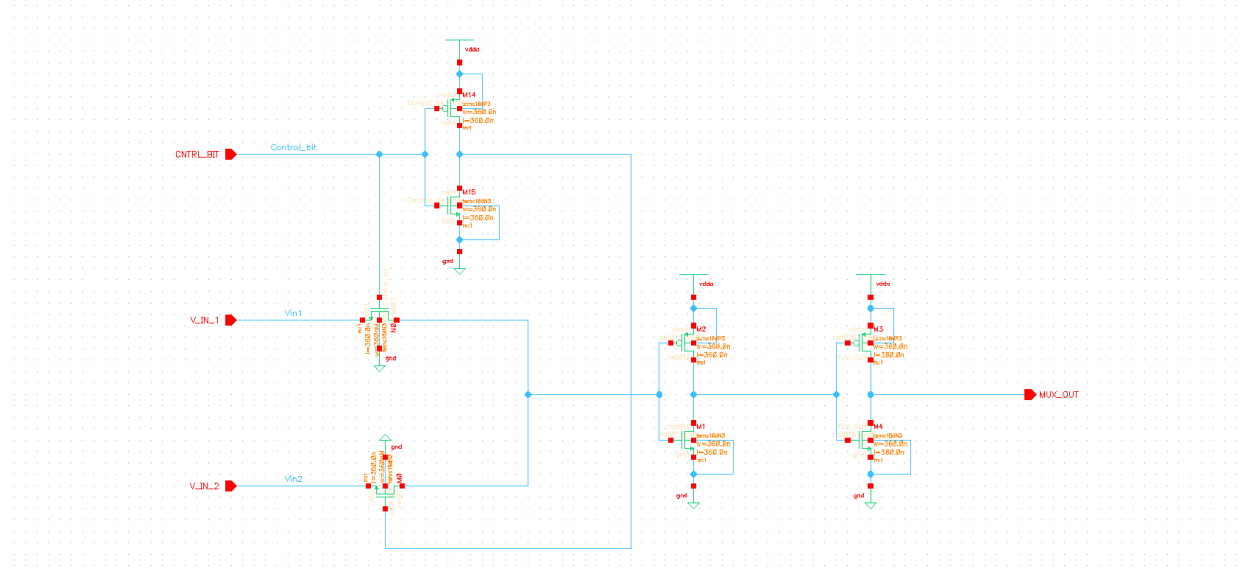

Figure 6.27: 2-to-1 multiplexer design for channel coding of 90° data channel.

6.2 Fiber Optic Cable Transmission Media

Just as we performed 2, 3 and 4 channel analysis of systems with air used as the transmission media we will perform analysis of 2, 3 and 4 channel systems with a fiber optic cable used as the transmission media. The analysis is the same as the analysis of the system with air as the transmission media with the only difference being that we need to introduce a Mueller matrix M_{FIBER} for the fiber optic cable.

6.2.1 Mueller Matrix for Fiber Optic Cable

The fiber optics cable is defined with Mueller matrix M_{FIBER}. The Mueller matrix M_{FIBER} used for fiber optic cable modeling is derived from the the work of Dong et al. [10]. In this paper, the Mueller matrix M_{FIBER} for a 10 km single-mode fiber (SMF) has been measured experimentally and defined analytically and both results match each other with less than 1.5% error. Figure 6.28 shows the experimental set up that was used to determine the Mueller matrix of the fiber.

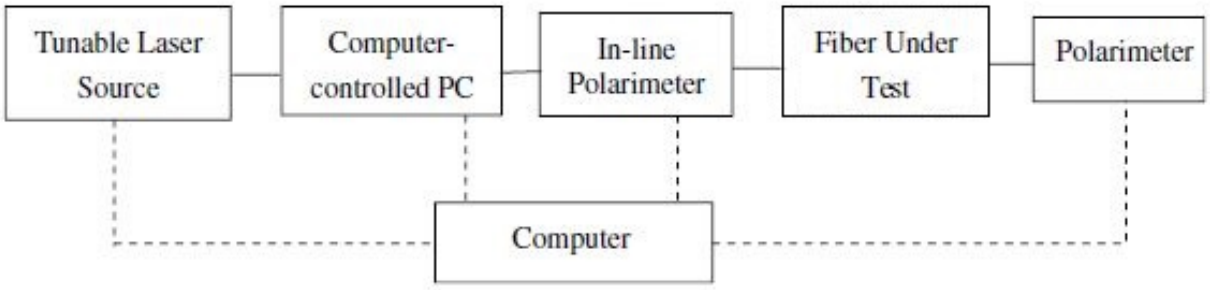

Figure 6.28: Experimental configuration for M_{FIBER} measurement [10].

In the first step, using the experimental setup shown in Figure 6.28 four pre-determined Stokes parameter inputs $I_0[1 \quad 1 \quad 0 \quad 0]^T$, $I_0[1 \quad -1 \quad 0 \quad 0]^T$, $I_0[1 \quad 0 \quad 1 \quad 0]^T$ and

$I_0[1 \quad 0 \quad 0 \quad 1]^T$ with $I_0 = 2$ mW are generated with the Computer, Tunable Laser Source, Computer-controlled Polarization Controller (PC) and in-line Polarimeter.

These Stokes parameter inputs are monitored and controlled using the Computer-controlled PC and in-line Polarimeter. The in-line Polarimter at the end is used to measure the output Stokes parameters.

In the second step three Stokes parameter inputs $I_0[1 \quad 1 \quad 0 \quad 0]^T$, $I_0[1 \quad -0.5 \quad 0.866 \quad 0]^T$ and $I_0[1 \quad -0.5 \quad -0.866 \quad 0]^T$ are generated one by one and their corresponding outputs are measured. Then the theoretical outputs corresponding to the first four pre-determined Stokes parameter inputs are calculated from the measured data of the three input-output pairs using the following Mueller matrix M_{FIBER} for the fiber.

$$M_{FIBER} = \begin{bmatrix} \frac{1}{2}(\frac{I_1}{I_0} + \frac{I_2}{I_0}) & \frac{1}{2}(\frac{I_1}{I_0} - \frac{I_2}{I_0}) & \frac{I_3}{I_0} - \frac{1}{2}(\frac{I_1}{I_0} + \frac{I_2}{I_0}) & \frac{I_4}{I_0} - \frac{1}{2}(\frac{I_1}{I_0} + \frac{I_2}{I_0}) \\ \frac{1}{2}(a_1\frac{I_1}{I_0} + b_1\frac{I_2}{I_0}) & \frac{1}{2}(a_1\frac{I_1}{I_0} - b_1\frac{I_2}{I_0}) & c_1\frac{I_3}{I_0} - \frac{1}{2}(a_1\frac{I_1}{I_0} + b_1\frac{I_2}{I_0}) & d_1\frac{I_4}{I_0} - \frac{1}{2}(a_1\frac{I_1}{I_0} + b_1\frac{I_2}{I_0}) \\ \frac{1}{2}(a_2\frac{I_1}{I_0} + b_2\frac{I_2}{I_0}) & \frac{1}{2}(a_2\frac{I_1}{I_0} - b_2\frac{I_2}{I_0}) & c_2\frac{I_3}{I_0} - \frac{1}{2}(a_2\frac{I_1}{I_0} + b_2\frac{I_2}{I_0}) & d_2\frac{I_4}{I_0} - \frac{1}{2}(a_2\frac{I_1}{I_0} + b_2\frac{I_2}{I_0}) \\ \frac{1}{2}(a_3\frac{I_1}{I_0} + b_3\frac{I_2}{I_0}) & \frac{1}{2}(a_3\frac{I_1}{I_0} - b_3\frac{I_2}{I_0}) & c_3\frac{I_3}{I_0} - \frac{1}{2}(a_3\frac{I_1}{I_0} + b_3\frac{I_2}{I_0}) & d_3\frac{I_4}{I_0} - \frac{1}{2}(a_3\frac{I_1}{I_0} + b_3\frac{I_2}{I_0}) \end{bmatrix} \tag{6.51}$$

In the final step the measured and calculated four output Stokes parameter vectors are compared in the wavelength range from 1540 nm to 1560 nm as shown in Figure 6.29.

We will use data extracted from this figure to determine the Mueller matrix M_{FIBER}. Chosing data for the 1546 nm wavelength we obtain the following four Stokes parameters vectors:

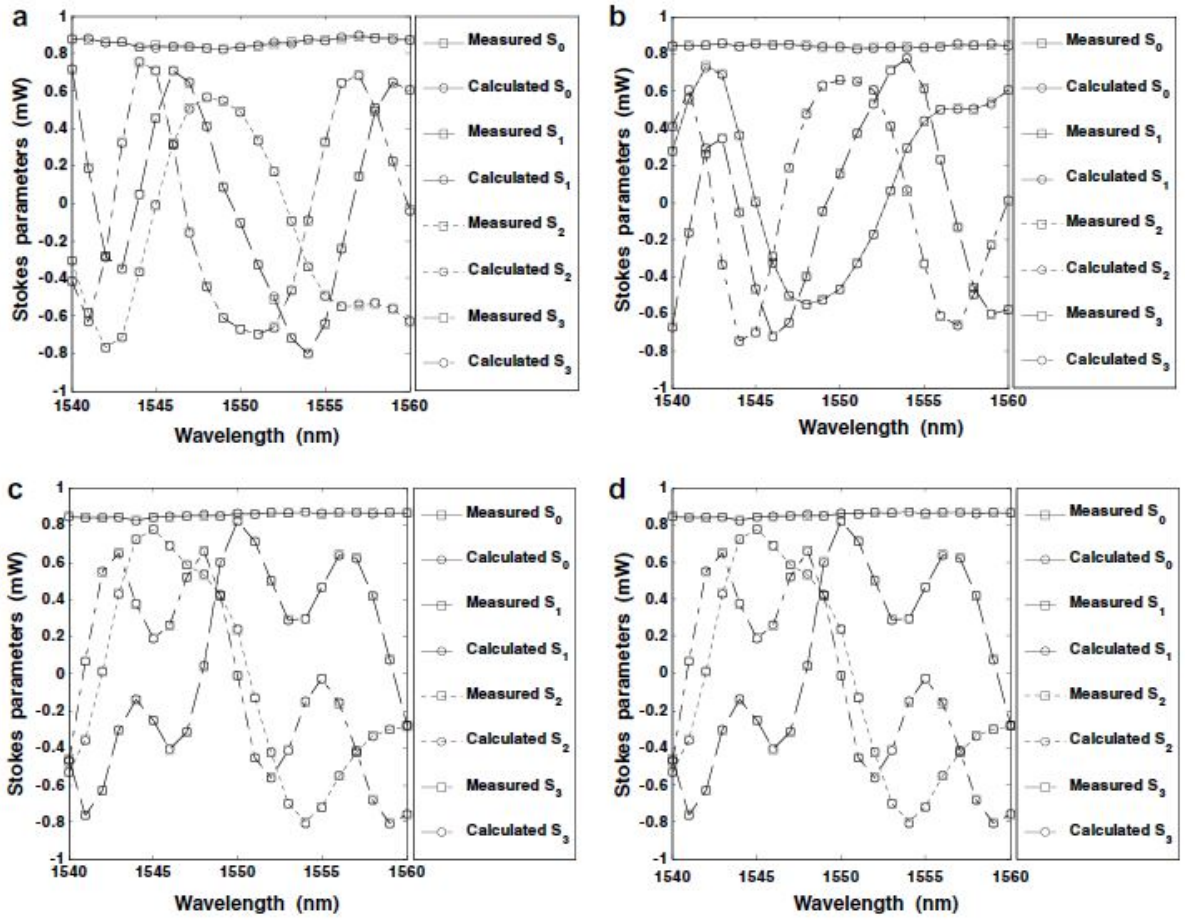

Figure 6.29: Measured and calculated output Stokes parameters corresponding to four predetermined inputs: (a) input polarization state $[1 \quad 1 \quad 0 \quad 0]^T$; (b) input polarization state $[1 \quad -1 \quad 0 \quad 0]^T$; (c) input polarization state $[1 \quad 0 \quad 1 \quad 0]^T$; (d) input polarization state $[1 \quad 0 \quad 0 \quad 1]^T$ [10].

1. The input Stokes parameters vector $[1 \quad 1 \quad 0 \quad 0]^T$ yields the output Stokes parameters vector $[0.83 \quad 0.75 \quad 0.3 \quad 0.3]^T = 0.83[1 \quad 0.9 \quad 0.36 \quad 0.36]^T = I_1[1 \quad a_1 \quad a_2 \quad a_3]^T$, where we have M_{FIBER} calculation parameters $I_1 = 0.83$, $a_1 = 0.9$, $a_2 = 0.36$, and $a_3 = 0.36$.

2. The input Stokes parameters vector $[1 \quad -1 \quad 0 \quad 0]^T$ yields the output Stokes parameters vector $[0.83 \quad -0.75 \quad -0.3 \quad -0.3]^T = 0.83[1 \quad -0.9 \quad -0.36 \quad -0.36]^T = I_2[1 \quad b_1 \quad b_2 \quad b_3]^T$, where we have M_{FIBER} calculation parameters $I_2 = 0.83$, $b_1 = -0.9$, $b_2 = -0.36$, and $b_3 = -0.36$.

3. The input Stokes parameters vector $[1 \quad 0 \quad 1 \quad 0]^T$ yields the output Stokes parameters vector $[0.83 \quad -0.4 \quad 0.75 \quad 0.25]^T = 0.83[1 \quad -0.48 \quad 0.9 \quad 0.3]^T = I_3[1 \quad c_1 \quad c_2 \quad c_3]^T$, where we have M_{FIBER} calculation parameters $I_3 = 0.83$, $c_1 = -0.48$, $c_2 = 0.9$, and $c_3 = 0.3$.

4. The input Stokes parameters vector $[1 \quad 0 \quad 0 \quad 1]^T$ yields the output Stokes parameters vector $[0.83 \quad -0.4 \quad 0.25 \quad 0.75]^T = 0.83[1 \quad -0.48 \quad 0.3 \quad 0.9]^T = I_4[1 \quad d_1 \quad d_2 \quad d_3]^T$, where we have M_{FIBER} calculation parameters $I_4 = 0.83$, $d_1 = -0.48$, $d_2 = 0.3$ and $d_3 = 0.9$.

If we use parameters I_1, I_2, I_3, I_4, and parameters $(a_1a_2a_3)$, $(b_1b_2b_3)$, $(c_1c_2c_3)$, $(d_1d_2d_3)$ and $I_0 = 1$ we can represent a 10 km fiber Mueller matrix M_{FIBER} as shown below:

$$M_{FIBER} = \begin{bmatrix} 0.83 & 0 & 0 & 0 \\ 0 & 0.747 & -0.3984 & -0.3984 \\ 0 & 0.2988 & 0.747 & 0.249 \\ 0 & 0.2988 & 0.249 & 0.747 \end{bmatrix} \tag{6.52}$$

Now we can use this Mueller matrix to model 2, 3 and 4 channel VLC PDM systems with a fiber optic cable used as the transmission media.

6.2.2 Two Channel System

A two channel system with fiber optic cable used as the transmission media can be represented the same as in Figure 6.1 with one difference. The difference is that the light path represented in the figure by S_{AIR} will be replaced with S_{FIBER}.

The transmitter (of Figures 6.2 and 6.3) is unchanged, resulting in the same Stokes vectors S_{0° and S_{90°.

$$S_{0^\circ} = \frac{1}{2}\begin{bmatrix} T \\ TD\cos(0^\circ) \\ TD\sin(0^\circ) \\ 0 \end{bmatrix} = \frac{1}{2}\begin{bmatrix} \frac{1}{2} \\ \frac{0.99}{2} \\ 0 \\ 0 \end{bmatrix} = \begin{bmatrix} 0.25 \\ 0.2475 \\ 0 \\ 0 \end{bmatrix} \tag{6.53}$$

$$S_{90^\circ} = \frac{1}{2}\begin{bmatrix} T \\ TD\cos(180^\circ) \\ TD\sin(180^\circ) \\ 0 \end{bmatrix} = \frac{1}{2}\begin{bmatrix} \frac{1}{2} \\ \frac{-0.99}{2} \\ 0 \\ 0 \end{bmatrix} = \begin{bmatrix} 0.25 \\ -0.2475 \\ 0 \\ 0 \end{bmatrix} \tag{6.54}$$

Two polarized light beams are combined and launched into the fiber optic cable together. The combined light beam that exists the fiber is defined as

$$S_{FIBER} = M_{FIBER}(b_0 S_{0^\circ} + b_{90} S_{90^\circ}) \tag{6.55}$$

For the two channel system we can now calculate S_{FIBER} and Figure 6.30 shows this Stokes vector for all 2-bit binary combinations.

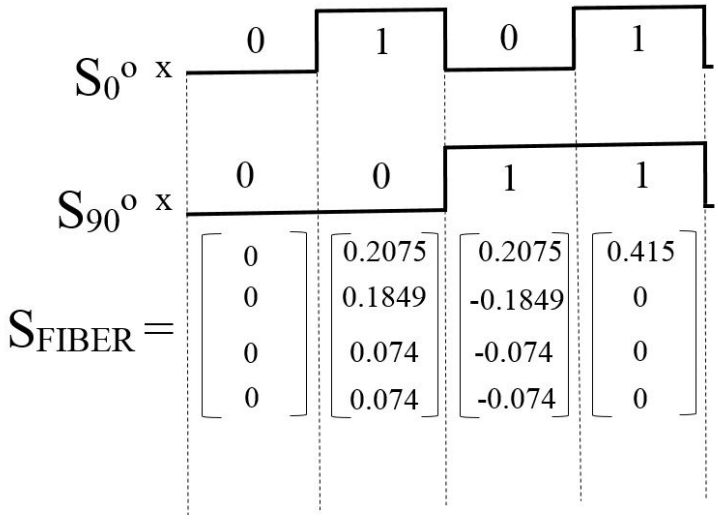

Figure 6.30: Two channel light signal exiting the fiber.

The combined light beam S_{FIBER} exits the fiber optic cable and illuminates the receiver chip's DoFP polarization filter array. The photodide light inputs I_{0° and I_{90° are evaluated as

$$I_{0^\circ} = [1 \quad 0 \quad 0 \quad 0] M_{0^\circ} S_{\text{FIBER}} \tag{6.56}$$

$$I_{90^\circ} = [1 \quad 0 \quad 0 \quad 0] M_{90^\circ} S_{\text{FIBER}} \tag{6.57}$$

We can now calculate all four values for each channel and we obtain Table 6.14. In this case if we assign threshold 0.02 for both 0^0 and 90^0 channels between binary value '0' and binary value '1' we can successfully decode the transmitted signals.

Table 6.14: Outputs from two channel system with fiber media.

I_{90°	I_{0°	$Output_{90^\circ}$	$Output_{0^\circ}$
0	0	0	0
0.006117	0.097633	0	1
0.097633	0.006117	1	0
0.10375	0.10375	1	1

6.2.3 Three Channel System

For a three channel system, we can refer to Figure 6.5 and again replace S_{AIR} with S_{FIBER}. The transmitter represented in Figures 6.6 to 6.8 is unchanged, resulting in the same Stokes vectors S_{0°, S_{60°, and S_{120°.

$$S_{0^\circ} = \frac{1}{2}\begin{bmatrix} T \\ TD\cos(0^\circ) \\ TD\sin(0^\circ) \\ 0 \end{bmatrix} = \frac{1}{2}\begin{bmatrix} \frac{1}{2} \\ \frac{0.99}{2} \\ 0 \\ 0 \end{bmatrix} = \begin{bmatrix} 0.25 \\ 0.2475 \\ 0 \\ 0 \end{bmatrix} \tag{6.58}$$

$$S_{60^\circ} = \frac{1}{2}\begin{bmatrix} T \\ TD\cos(120^\circ) \\ TD\sin(120^\circ) \\ 0 \end{bmatrix} = \frac{1}{2}\begin{bmatrix} \frac{1}{2} \\ \frac{-0.99}{2}\frac{1}{2} \\ 0.99\frac{\sqrt{3}}{2}\frac{1}{2} \\ 0 \end{bmatrix} = \begin{bmatrix} 0.25 \\ -0.124 \\ 0.2145 \\ 0 \end{bmatrix} \tag{6.59}$$

$$S_{120^\circ} = \frac{1}{2}\begin{bmatrix} T \\ TD\cos(240^\circ) \\ TD\sin(240^\circ) \\ 0 \end{bmatrix} = \frac{1}{2}\begin{bmatrix} \frac{1}{2} \\ \frac{-0.99}{2}\frac{1}{2} \\ -0.99\frac{\sqrt{3}}{2}\frac{1}{2} \\ 0 \end{bmatrix} = \begin{bmatrix} 0.25 \\ -0.124 \\ -0.2145 \\ 0 \end{bmatrix} \tag{6.60}$$

Three polarized light beams are combined and launched into the fiber optic cable and the combined light beam that exits the fiber is defined as

$$S_{FIBER} = M_{FIBER}(b_0 S_{0^\circ} + b_{60} S_{60^\circ} + b_{120} S_{120^\circ}) \tag{6.61}$$

where M_{FIBER} is defined as specified in (6.52). Figure 6.31 shows the signal as it exits the fiber.

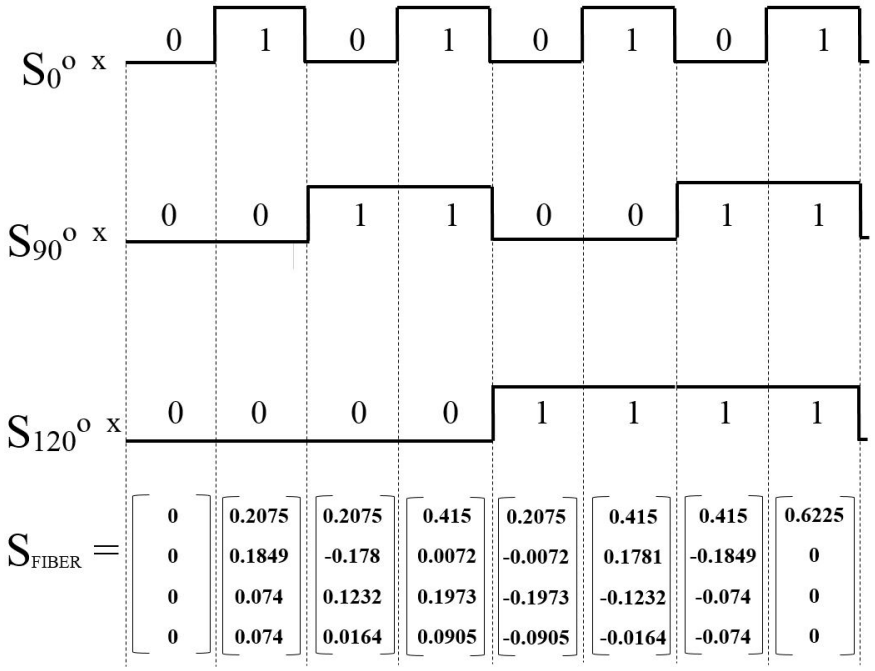

Figure 6.31: Three channel light signal exiting the fiber.

The combined light beam S_{FIBER} exits the fiber and illuminates the receiver chip's polarization filter array. The photodiode light inputs I_{0°, I_{60° and I_{120° are evaluated as

$$I_{0^\circ} = [1 \quad 0 \quad 0 \quad 0] M_{0^\circ} S_{\text{FIBER}} \tag{6.62}$$

$$I_{60^\circ} = [1 \quad 0 \quad 0 \quad 0] M_{60^\circ} S_{\text{FIBER}} \tag{6.63}$$

$$I_{120^\circ} = [1 \quad 0 \quad 0 \quad 0] M_{120^\circ} S_{\text{FIBER}} \tag{6.64}$$

Table 6.15 shows each of three channel 0^0, 60^0 and 120^0 photodiode light inputs I_{0°, I_{60° and I_{120° and the corresponding channel outputs when compared with a threshold value of 0.075.

Table 6.15: Outputs from three channel system with fiber media.

I_{120°	I_{60°	I_{0°	$Output_{120^\circ}$	$Output_{60^\circ}$	$Output_{0^\circ}$
0	0	0	0	0	0
0.013145	0.044847	0.097633	0	0	1
0.04751	0.100316	0.007799	0	1	0
0.060577	0.145148	0.105525	0	1	1
0.095048	0.010477	0.0501	1	0	0
0.108115	0.055309	0.147826	1	0	1
0.14248	0.110778	0.057992	1	1	0
0.155625	0.155625	0.155625	1	1	1

6.2.4 Four Channel System

For a four channel system, we refer to Figure 6.15 and replace S_{AIR} with S_{FIBER}.

In order to recover all four channels on the receiver outputs we will have to apply similar coding techniques as those described earlier for four channel systems. On the input side we will apply different amplitudes for each channel. On the output side we will use multiple

threshold detectors. Rather than a single channel requiring the multi-thresholding at the receiver, in this case it will be used on two of the channels.

Analysis of this four channel system with fiber will follow the path we have already established. The output of the 0º DoFP polarization filter is the light beam whose Stokes vector representation is S_{0°, defined as shown below.

$$S_{0^\circ} = 0.75 M_{0^\circ} S_{\text{IN}} = 0.75 \frac{1}{2} \begin{bmatrix} (p_x^2 + p_y^2) \\ (p_x^2 - p_y^2)\cos(2\Theta) \\ (p_x^2 - p_y^2)\sin(2\Theta) \\ 0 \end{bmatrix} \tag{6.65}$$

Note that for this channel we use 0.75 of its amplitude to apply channel coding on the input of the system. This yields

$$S_{0^\circ} = 0.75 \frac{1}{2} \begin{bmatrix} T \\ TD\cos(0^\circ) \\ TD\sin(0^\circ) \\ 0 \end{bmatrix} = 0.75 \frac{1}{2} \begin{bmatrix} \frac{1}{2} \\ \frac{0.99}{2} \\ 0 \\ 0 \end{bmatrix} = 0.75 \begin{bmatrix} 0.25 \\ 0.2457 \\ 0 \\ 0 \end{bmatrix} = \begin{bmatrix} 0.1875 \\ 0.185625 \\ 0 \\ 0 \end{bmatrix} \tag{6.66}$$

The Stokes vector S_{45° is defined as shown below.

$$S_{45^\circ} = 0.8 M_{45^\circ} S_{\text{IN}} = \begin{bmatrix} 0.2 \\ 0 \\ 0.198 \\ 0 \end{bmatrix} \tag{6.67}$$

Note that for this channel we use 0.8 of its amplitude to apply channel coding on the input of the system.

As an additional step in the coding, the 90° channel sends light for both binary levels. For binary '0' S_{90° is:

$$S_{90^\circ} = 0.611 M_{90^\circ} S_{\text{IN}} = \begin{bmatrix} 0.15275 \\ -0.15122 \\ 0 \\ 0 \end{bmatrix} \tag{6.68}$$

For binary '1' S_{90° is:

$$S_{90^\circ} = M_{90^\circ} S_{\text{IN}} = \begin{bmatrix} 0.25 \\ -0.2475 \\ 0 \\ 0 \end{bmatrix} \tag{6.69}$$

The Stokes vector S_{135° is defined as shown below. It uses an amplitude of 1.1.

$$S_{135^\circ} = 1.1 M_{135^\circ} S_{\text{IN}} = \begin{bmatrix} 0.275 \\ 0 \\ -0.27225 \\ 0 \end{bmatrix} \tag{6.70}$$

Four polarized light beams are added together in the fiber optics cable and the combined light beam is defined as

$$S_{FIBER} = M_{FIBER}(b_0 S_{0^\circ} + b_{45} S_{45^\circ} + b_{90} S_{90^\circ} + b_{135} S_{135^\circ}) \tag{6.71}$$

where M_{FIBER} is again defined as specified in (6.52).

Figure 6.32 shows all 4 channels' optical signal as it exits the fiber.

The photodiode light inputs I_{0°, I_{45°, I_{90°o and I_{135° are as follows. Their numerical values are given in Table 6.16.

$$I_{0^\circ} = [1 \quad 0 \quad 0 \quad 0] M_{0^\circ} S_{\text{FIBER}} \tag{6.72}$$

$$I_{45^\circ} = [1 \quad 0 \quad 0 \quad 0] M_{45^\circ} S_{\text{FIBER}} \tag{6.73}$$

$$I_{90^\circ} = [1 \quad 0 \quad 0 \quad 0] M_{90^\circ} S_{\text{FIBER}} \tag{6.74}$$

$$I_{135^\circ} = [1 \quad 0 \quad 0 \quad 0] M_{135^\circ} S_{\text{FIBER}} \tag{6.75}$$

Table 6.16: All 4 receiver channels' photodiode input light signals.

Input	0	1	2	3	4	5	6	7	8	9	10	11	12	13	14	15
I_{0°	0.004	0.077	0.026	0.099	0.006	0.079	0.028	0.101	0.088	0.161	0.11	0.183	0.09	0.163	0.112	0.185
I_{45°	0.021	0.073	0.099	0.151	0.034	0.086	0.112	0.164	0.027	0.08	0.105	0.158	0.04	0.093	0.118	0.171
I_{90°	0.06	0.064	0.121	0.125	0.098	0.102	0.159	0.163	0.09	0.094	0.151	0.155	0.128	0.132	0.189	0.193
I_{135°	0.043	0.068	0.048	0.073	0.07	0.095	0.075	0.1	0.15	0.175	0.155	0.18	0.178	0.203	0.182	0.207

The receiver output for the 45° polarization data channel is obtained by applying comparator threshold 0.097 on the data from Table 6.16. Similarly, receiver output for the 135° channel is

Figure 6.32: Four channel light signal exiting the fiber.

obtained by applying threshold 0.11. Tables 6.17 and 6.18 show the output for these channels, which are operating correctly.

Table 6.17: 45° polarization data receiver output signals.

Input	0	1	2	3	4	5	6	7	8	9	10	11	12	13	14	15
45° output	0	0	1	1	0	0	1	1	0	0	1	1	0	0	1	1

Table 6.18: 135° polarization data receiver output signals.

Input	0	1	2	3	4	5	6	7	8	9	10	11	12	13	14	15
135° output	0	0	0	0	0	0	0	0	1	1	1	1	1	1	1	1

The receiver output for the 0° polarization data channel is obtained by applying two comparators with thresholds of 0.04 and 0.115 on data from Table 6.16 as illustrated in Figure 6.33. The results out of these comparators are shown in Table 6.19

Table 6.19: 0° polarization data receiver 2 comparators' outputs.

Input	0	1	2	3	4	5	6	7	8	9	10	11	12	13	14	15
$I_{0^\circ} > 0.04$	0	1	0	1	0	1	0	1	1	1	1	1	1	1	1	1
$I_{0^\circ} > 0.115$	0	0	0	0	0	0	0	0	0	1	0	1	0	1	0	1

Controlling the multiplexer with the output of the 135° channel, the resulting channel output is shown in Table 6.20.

Table 6.20: 0° polarization data receiver output signal.

Input	0	1	2	3	4	5	6	7	8	9	10	11	12	13	14	15
0° output	0	1	0	1	0	1	0	1	0	1	0	1	0	1	0	1

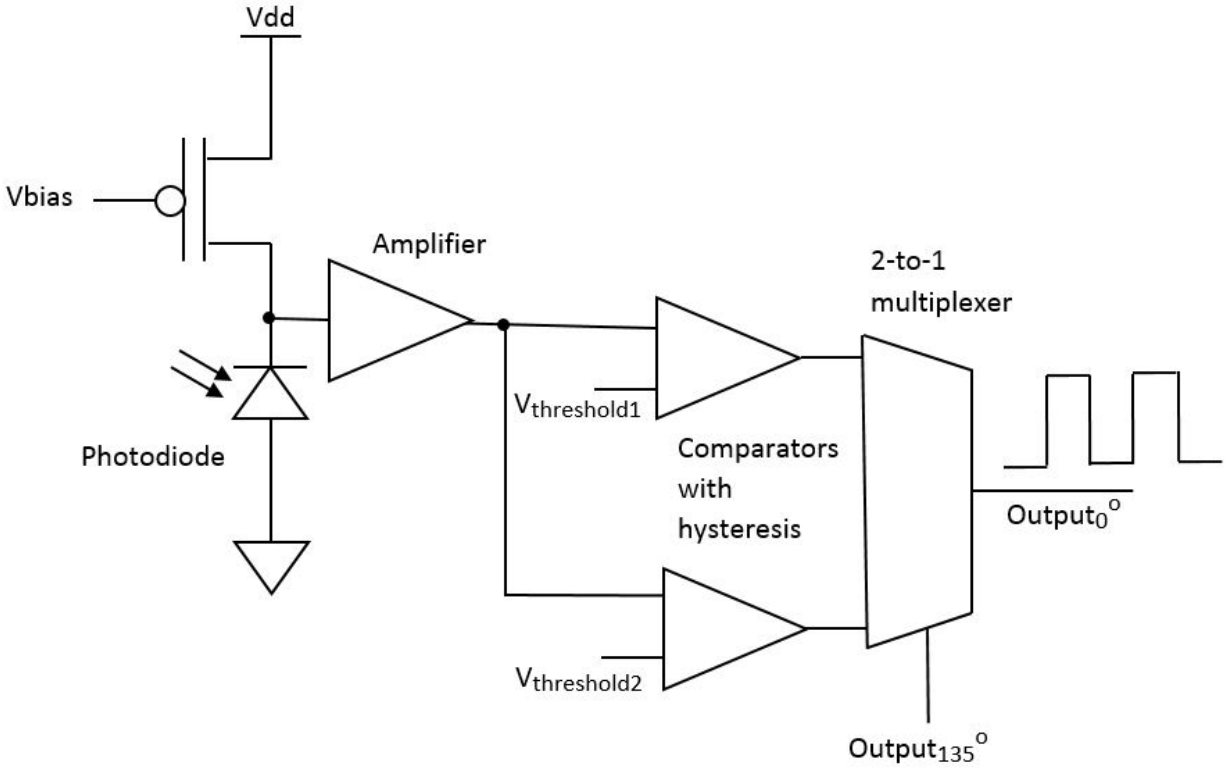

Figure 6.33: 0° data channel circuit with 2 comparators and 2-to-1 multiplexer.

Finally, the receiver output for the 90° polarization data channel is obtained by applying three comparators with thresholds 0.07, 0.126 and 0.17 on data from Table 6.16 as shown in Figure 6.34. This results in the comparator outputs of Table 6.21.

Table 6.21: 90° polarization data receiver 3 comparators' outputs.

Input	0	1	2	3	4	5	6	7	8	9	10	11	12	13	14	15
$I_{90°} > 0.07$	0	0	1	1	1	1	1	1	1	1	1	1	1	1	1	1
$I_{90°} > 0.126$	0	0	0	0	0	0	1	1	0	0	1	1	1	1	1	1
$I_{90°} > 0.17$	0	0	0	0	0	0	0	0	0	0	0	0	0	0	1	1

If the 135° and 45° output are both equal to b'0' then the 0.07 threshold is used to determine the 90° output. If the 135° and 45° output are both equal to b'1' then the 0.17 threshold is used to determine the 90° output. If the 135° and 45° outputs are not equal to each other

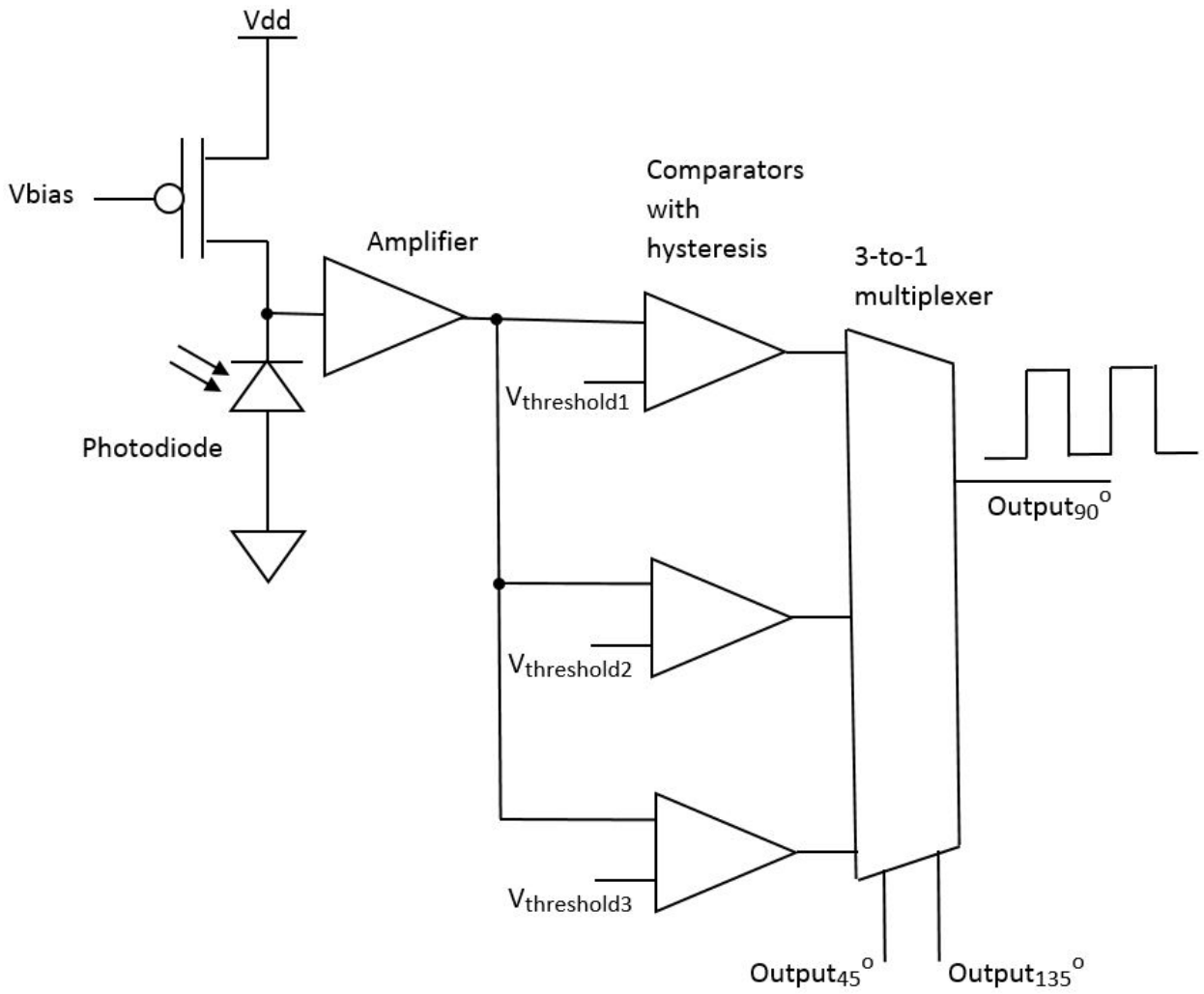

Figure 6.34: 90° data channel circuit with 3 comparators and 3-to-1 multiplexer.

then the 0.126 threshold is used to determine the 90° output. The results of these choices are shown in Table 6.22.

Table 6.22: 90° polarization data receiver output signal.

Input	0	1	2	3	4	5	6	7	8	9	10	11	12	13	14	15
90° output	0	0	0	0	1	1	1	1	0	0	0	0	1	1	1	1

6.3 Chip-to-chip VLC PDM System with Mirrors

An alternative system design that uses air as the transmission medium is illustrated in Figure 6.35. The intended use case here is communication between two chips that are on the same board (or other common substrate). In this design, vertical cavity lasers on the left chip launch the light signal up, it is reflected off a pair of mirrors, and is received on the right chip.

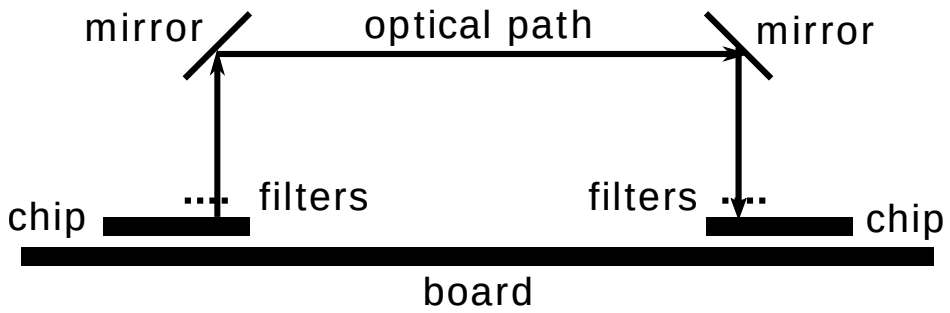

Figure 6.35: Chip-to-chip system with mirrors.

In the previous analysis of VLC PDM systems with air used as transmission media, we defined how multiple input laser light signals are polarized, how they travel combined through the air, and how they are detected at the receiver. We will use the same analysis techniques in this chip-to-chip system, adding the polarization implications of the two mirrors in the optical path.

We analyze 2, 3 and 4 channel chip-to-chip systems. The Mueller matrix for the mirrors, M_R, was derived in Chapter 2 and is due to van Harten et al. [21].

6.3.1 Two Channel Chip-to-chip System

A diagram of the two channel chip-to-chip mirror-based system is shown in Figure 6.36.

Both polarized light signals S_{0° and S_{90° are combined into signal S_{AIR} which travels from the transmitter to the first aluminum mirror. S_{AIR} is calculated as

$$S_{AIR} = b_0 S_{0^\circ} + b_{90} S_{90^\circ} \tag{6.76}$$

S_{AIR} for all four binary combinations of two channels system is shown in Figure 6.4. The light beam S_{AIR} reaches the first aluminum mirror by incident angle $\Theta_o = 45^\circ$ and reflects off this mirror by the same angle. The light beam that reflects of the first mirror is defined as $S_{reflected\_1}$ and it is calculated as

$$S_{reflected\_1} = M_R S_{AIR} \tag{6.77}$$

$S_{reflected\_1}$ for all four binary combinations of two channels system is shown in Figure 6.37.

This light signal $S_{reflected\_1}$ travels to the second aluminum mirror and it reaches the mirror with incident angle $\Theta_o = 45^\circ$ and reflects of this mirror by the same angle. The light beam that reflects of the second mirror is defined as $S_{reflected\_2}$ and it is calculated as

$$S_{reflected\_2} = M_R S_{reflected\_1} \tag{6.78}$$

and $S_{reflected\_2}$ for all four binary combinations of the two channel system is shown in Figure 6.38.

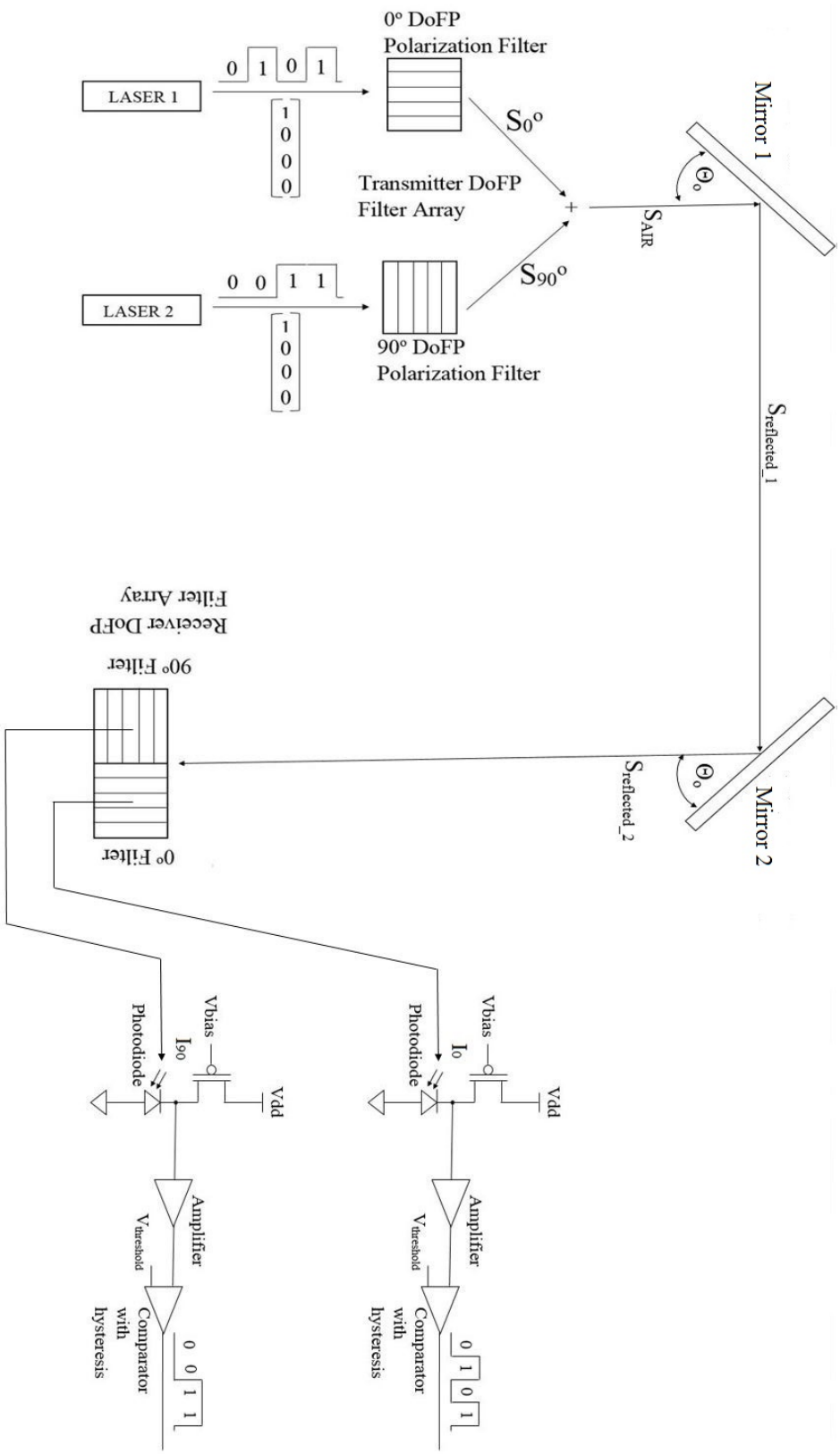

Figure 6.36: Two channel chip-to-chip system with mirrors.

$$
\begin{array}{cccc}
0 & 1 & 0 & 1 \\
0 & 0 & 1 & 1
\end{array}
$$

$$
S_{reflected\_1} = M_R S_{AIR} = \begin{bmatrix} 0 \\ 0 \\ 0 \\ 0 \end{bmatrix} \begin{bmatrix} 0.0683 \\ 0.064 \\ 0 \\ 0 \end{bmatrix} \begin{bmatrix} 0.4317 \\ -0.431 \\ 0 \\ 0 \end{bmatrix} \begin{bmatrix} 0.5 \\ -0.367 \\ 0 \\ 0 \end{bmatrix}
$$

Figure 6.37: $S_{reflected\_1}$ for two channel chip-to-chip system.

$$
\begin{array}{cccc}
0 & 1 & 0 & 1 \\
0 & 0 & 1 & 1
\end{array}
$$

$$
S_{reflected\_2} = M_R\, S_{reflected\_1} = \begin{bmatrix} 0 \\ 0 \\ 0 \\ 0 \end{bmatrix} \begin{bmatrix} 0.0214 \\ 0.0138 \\ 0 \\ 0 \end{bmatrix} \begin{bmatrix} 0.748 \\ -0.7478 \\ 0 \\ 0 \end{bmatrix} \begin{bmatrix} 0.7694 \\ -0.734 \\ 0 \\ 0 \end{bmatrix}
$$

Figure 6.38: $S_{reflected\_2}$ for two channel chip-to-chip system.

The light signal $S_{reflected\_2}$ travels to the receiver chip and illuminates the receiver's filter array. Each channel photodiode's input light signal can be calculated as

$$I_{0^\circ} = [1 \quad 0 \quad 0 \quad 0] M_{0^\circ} S_{\text{reflected\_2}} \tag{6.79}$$

$$I_{90^\circ} = [1 \quad 0 \quad 0 \quad 0] M_{90^\circ} S_{\text{reflected\_2}} \tag{6.80}$$

We can now calculate all four values for each channel and obtain Table 6.23 that shows photodiode light inputs I_{0° and I_{90° for each channel. A threshold comparison to 0.005 gives the expected binary outputs.

Table 6.23: Outputs from two channel chip-to-chip system.

I_{90°	I_{0°	$Output_{90^\circ}$	$Output_{0^\circ}$
0	0	0	0
0.001914	0.008766	0	1
0.372096	0.001914	1	0
0.37401	0.01068	1	1

6.3.2 Three Channel Chip-to-chip System

Figure 6.39 shows a three channel chip-to-chip mirror-based system.

Three polarized light signals are combined into signal S_{AIR} which travels from the transmitter to the first aluminum mirror. S_{AIR} for all binary combinations of three channels system is calculated using the following equation.

$$S_{AIR} = b_0 S_{0^\circ} + b_{60} S_{60^\circ} + b_{120} S_{120^\circ} \tag{6.81}$$

S_{AIR} for all eight binary combinations of three channels system is shown in Figure 6.9.

The light beam S_{AIR} reaches the first aluminum mirror by incident angle $\Theta_o = 45^\circ$ and reflects off this mirror by the same angle. The light beam that reflects off the first mirror is defined as $S_{reflected\_1}$ and it is calculated as

$$S_{reflected\_1} = M_R S_{AIR} \tag{6.82}$$

$S_{reflected\_1}$ for all eight binary combinations of three channels system is shown in Figure 6.40.

This light signal $S_{reflected\_1}$ travels to the second aluminum mirror and it reaches the mirror with incident angle $\Theta_o = 45^\circ$ and reflects off this mirror by the same angle. The light beam

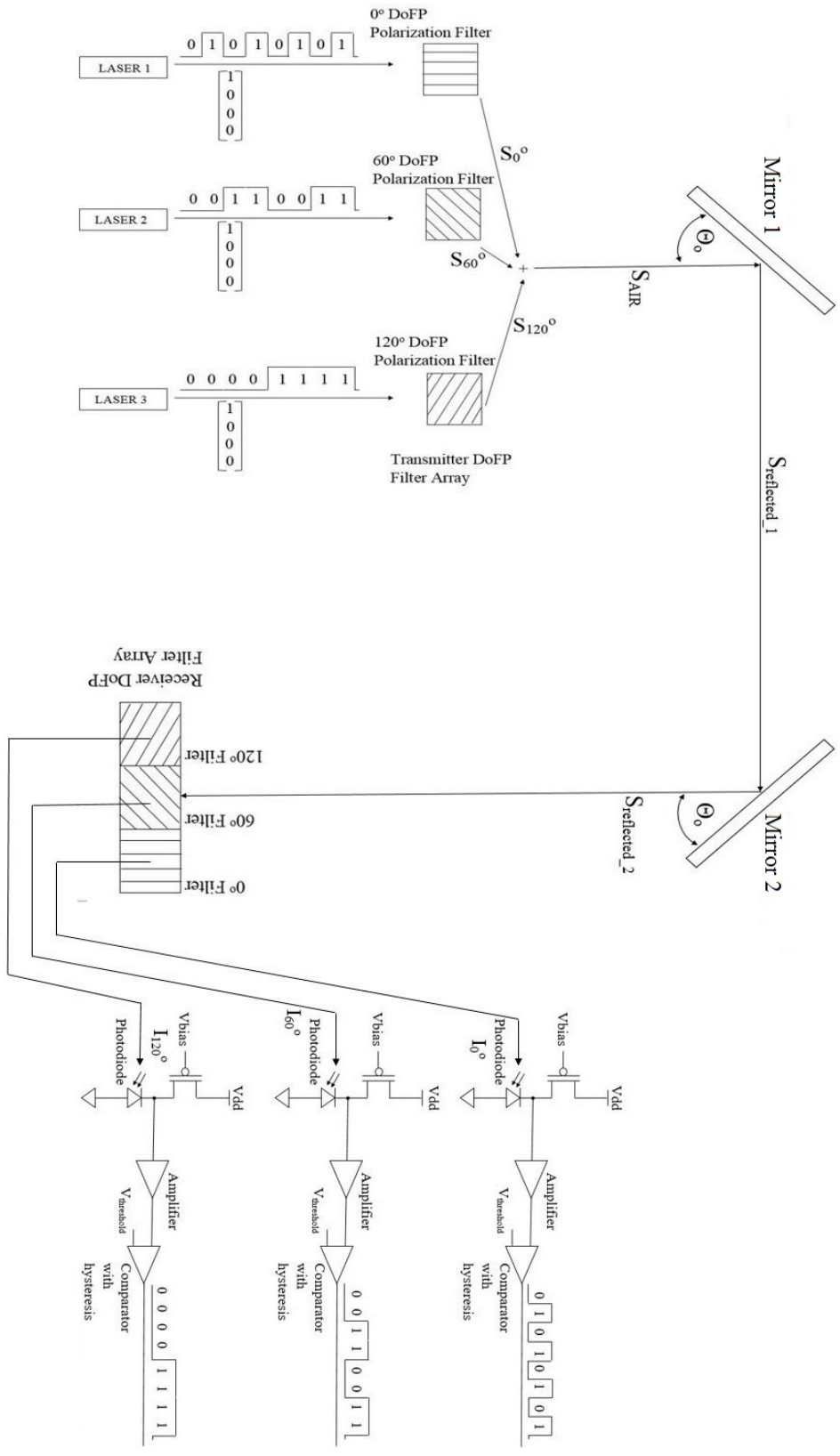

Figure 6.39: Three channel chip-to-chip system with mirrors.

0	1	0	1	0	1	0	1
0	0	1	1	0	0	1	1
0	0	0	0	1	1	1	1

$$\mathbf{S_{reflected\_1}} = \begin{bmatrix} 0 \\ 0 \\ 0 \\ 0 \end{bmatrix} \begin{bmatrix} 0.0683 \\ 0.064 \\ 0 \\ 0 \end{bmatrix} \begin{bmatrix} 0.341 \\ -0.308 \\ 0.1386 \\ 0.045 \end{bmatrix} \begin{bmatrix} 0.409 \\ -0.243 \\ 0.1386 \\ 0.045 \end{bmatrix} \begin{bmatrix} 0.341 \\ -0.308 \\ -0.139 \\ -0.045 \end{bmatrix} \begin{bmatrix} 0.409 \\ -0.243 \\ -0.139 \\ -0.045 \end{bmatrix} \begin{bmatrix} 0.6817 \\ -0.615 \\ 0 \\ 0 \end{bmatrix} \begin{bmatrix} 0.75 \\ -0.551 \\ 0 \\ 0 \end{bmatrix}$$

Figure 6.40: $S_{reflected\_1}$ for three channel chip-to-chip system.

that reflects off the second mirror is defined as $S_{reflected\_2}$ and it is calculated as

$$S_{reflected\_2} = M_R S_{reflected\_1} \tag{6.83}$$

The reflected signal off the second mirror $S_{reflected\_2}$ is presented for all eight possible binary combinations for the chip-to-chip three channel system in Figure 6.41.

0	1	0	1	0	1	0	1
0	0	1	1	0	0	1	1
0	0	0	0	1	1	1	1

$$\mathbf{S_{reflected\_2}} = \begin{bmatrix} 0 \\ 0 \\ 0 \\ 0 \end{bmatrix} \begin{bmatrix} 0.0213 \\ 0.0138 \\ 0 \\ 0 \end{bmatrix} \begin{bmatrix} 0.5667 \\ -0.558 \\ 0.08 \\ 0.058 \end{bmatrix} \begin{bmatrix} 0.5873 \\ -0.543 \\ 0.08 \\ 0.058 \end{bmatrix} \begin{bmatrix} 0.5667 \\ -0.558 \\ -0.08 \\ -0.058 \end{bmatrix} \begin{bmatrix} 0.5873 \\ -0.543 \\ -0.08 \\ -0.058 \end{bmatrix} \begin{bmatrix} 1.1327 \\ -1.115 \\ 0 \\ 0 \end{bmatrix} \begin{bmatrix} 1.1541 \\ -1.101 \\ 0 \\ 0 \end{bmatrix}$$

Figure 6.41: $S_{reflected\_2}$ for three channel chip-to-chip system.

This light signal $S_{reflected\_2}$ travels to the receiver chip and when it reaches the DoFP filter array the receiver three data channels for 0°, 60° and 120° polarized light are separated and

each channel photodiode input light signal can be calculated as

$$I_{0^\circ} = [1 \quad 0 \quad 0 \quad 0] M_{0^\circ} S_{\text{reflected\_2}} \tag{6.84}$$

$$I_{60^\circ} = [1 \quad 0 \quad 0 \quad 0] M_{60^\circ} S_{\text{reflected\_2}} \tag{6.85}$$

$$I_{120^\circ} = [1 \quad 0 \quad 0 \quad 0] M_{120^\circ} S_{\text{reflected\_2}} \tag{6.86}$$

We can now calculate all eight output values for each of the three channel which results in Table 6.24. The table shows all three receiver's channel 0°, 60° and 120° photodiode light inputs I_{0°, I_{60° and I_{120°.

Table 6.24: Outputs from three channel chip-to-chip system.

I_{120}	I_{60}	I_0	$Output_{120}$	$Output_{60}$	$Output_0$
0	0	0	0	0	0
0.003627	0.003627	0.008766	0	0	1
0.193532	0.227886	0.003623	0	1	0
0.19688	0.231234	0.012396	0	1	1
0.227886	0.193532	0.003623	1	0	0
0.231234	0.19688	0.012396	1	0	1
0.421139	0.421139	0.007254	1	1	0
0.424766	0.424766	0.016019	1	1	1

The 0° channel photodiode light input is compared inside the comparator with threshold value of 0.008 to yield binary value '0' or binary value '1' at its output.

At the same time, 60° and 120° channel photodiode light inputs are compared inside separate comparators with threshold values of 0.2 to yield binary value '0' or binary value '1' at their outputs.

6.3.3 Four Channel Chip-to-chip System

Figure 6.42 shows the four channel chip-to-chip system with mirrors.

To apply channel coding on the input transmitter side of the system, we apply different amplitudes for every channel's input laser on the transmitter chip. We apply 0.75 of the amplitude we used in all previous analysis examples for the 0° polarization angle data channel. For the 45° polarization angle channel we apply 0.8 of the same reference amplitude. For 90° polarization angle channel we apply the same reference amplitude when the light signal is ON and we apply 0.611 of the reference amplitude when the light signal is OFF. So in this case we never turn OFF light for that channel. Finally, for 135° polarization angle channel we apply 1.5 times the reference amplitude.

These four 0°, 45°, 90° and 135° polarized light signals are combined in air into light signal S_{AIR} and they travel from the transmitter chip to the first aluminum mirror.

$$S_{AIR} = b_0 S_{0^\circ} + b_{45} S_{45^\circ} + b_{90} S_{90^\circ} + b_{135} S_{135^\circ} \tag{6.87}$$

Also, S_{AIR} for all possible sixteen binary combinations of the four channels is shown in Figure 6.43.

The light beam S_{AIR} travels from the transmitter to the first aluminum mirror. It reaches the mirror with incident angle $\Theta_o = 45^\circ$ as shown in Figure 6.42. This light beam S_{AIR} reflects of the mirror by the same angle of 45°. This reflected light beam is defined as $S_{\mathrm{reflected\_1}}$ and is calculated as

$$S_{reflected\_1} = M_R S_{AIR} \tag{6.88}$$

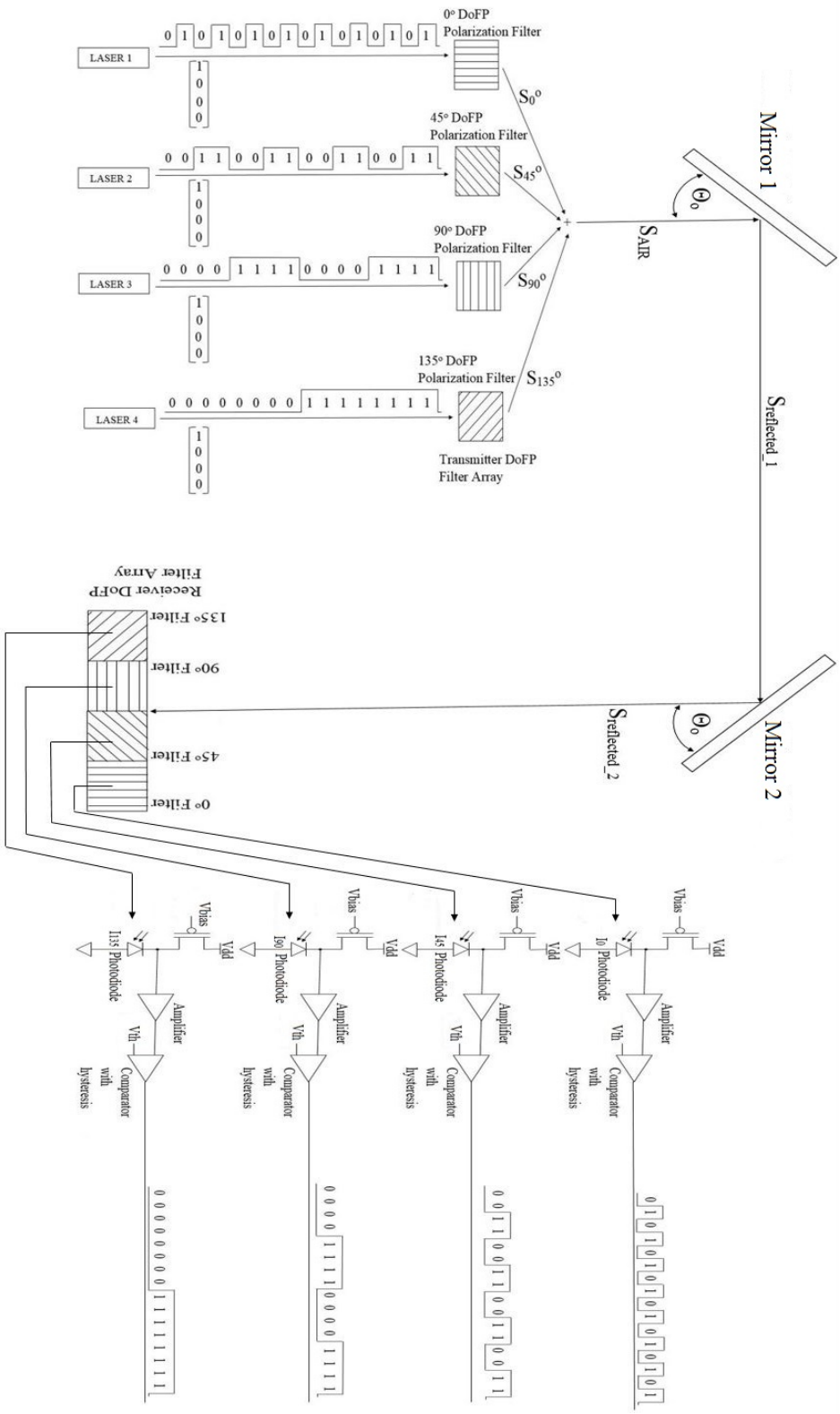

Figure 6.42: Four channel chip-to-chip system with mirrors.

0	1	0	1	0	1	0	1
0	0	1	1	0	0	1	1
0	0	0	0	1	1	1	1
0	0	0	0	0	0	0	0

$$S_{AIR} = \begin{bmatrix} 0.1528 \\ -0.1512 \\ 0 \\ 0 \end{bmatrix} \begin{bmatrix} 0.3403 \\ 0.0344 \\ 0 \\ 0 \end{bmatrix} \begin{bmatrix} 0.3528 \\ -0.1512 \\ 0.198 \\ 0 \end{bmatrix} \begin{bmatrix} 0.5403 \\ 0.0344 \\ 0.198 \\ 0 \end{bmatrix} \begin{bmatrix} 0.25 \\ -0.2475 \\ 0 \\ 0 \end{bmatrix} \begin{bmatrix} 0.4375 \\ -0.0619 \\ 0 \\ 0 \end{bmatrix} \begin{bmatrix} 0.45 \\ -0.2475 \\ 0.198 \\ 0 \end{bmatrix} \begin{bmatrix} 0.6375 \\ -0.0619 \\ 0.198 \\ 0 \end{bmatrix}$$

0	1	0	1	0	1	0	1
0	0	1	1	0	0	1	1
0	0	0	0	1	1	1	1
1	1	1	1	1	1	1	1

$$S_{AIR} = \begin{bmatrix} 0.5278 \\ -0.1512 \\ -0.3713 \\ 0 \end{bmatrix} \begin{bmatrix} 0.7153 \\ 0.0344 \\ -0.3713 \\ 0 \end{bmatrix} \begin{bmatrix} 0.7278 \\ -0.1512 \\ -0.1733 \\ 0 \end{bmatrix} \begin{bmatrix} 0.9153 \\ 0.0344 \\ -0.1733 \\ 0 \end{bmatrix} \begin{bmatrix} 0.625 \\ -0.2475 \\ -0.3713 \\ 0 \end{bmatrix} \begin{bmatrix} 0.8125 \\ -0.0619 \\ -0.3713 \\ 0 \end{bmatrix} \begin{bmatrix} 0.825 \\ -0.2475 \\ -0.1733 \\ 0 \end{bmatrix} \begin{bmatrix} 1.0125 \\ -0.0619 \\ -0.1733 \\ 0 \end{bmatrix}$$

Figure 6.43: S_{AIR} for four channel chip-to-chip system.

Recall that M_{R} is the Mueller matrix of the aluminum mirror and it is given by equation (2.79).

$S_{reflected\_1}$ for all sixteen binary combinations of the four channels system is shown in Figure 6.44.

The first mirror's reflected light signal $S_{reflected\_1}$ travels to the second aluminum mirror. The light signal $S_{reflected\_1}$ reaches the mirror with incident angle $\Theta_o = 45^\circ$ and it reflects of this mirror by the same angle of 45°. The light beam that reflects of the second mirror is defined as $S_{reflected\_2}$ and it is calculated using the following equation

$$S_{reflected\_2} = M_R S_{reflected\_1} \tag{6.89}$$

Again, M_{R} is the Mueller matrix of the aluminum mirror.

The reflected signal off of the second mirror $S_{reflected\_2}$ is shown in Figure 6.45.

The light signal $S_{reflected\_2}$ travels to the receiver chip and when it reaches DoFP filter array that is bonded on the surface of the receiver four data channels of 0°, 45°, 90° and 135° polarized light are separated as shown below

$$I_{0^\circ} = [1 \quad 0 \quad 0 \quad 0] M_{0^\circ} S_{\mathrm{reflected\_2}} \tag{6.90}$$

$$I_{45^\circ} = [1 \quad 0 \quad 0 \quad 0] M_{45^\circ} S_{\mathrm{reflected\_2}} \tag{6.91}$$

$$I_{90^\circ} = [1 \quad 0 \quad 0 \quad 0] M_{90^\circ} S_{\mathrm{reflected\_2}} \tag{6.92}$$

$$I_{135^\circ} = [1 \quad 0 \quad 0 \quad 0] M_{135^\circ} S_{\mathrm{reflected\_2}} \tag{6.93}$$

0	1	0	1	0	1	0	1
0	0	1	1	0	0	1	1
0	0	0	0	1	1	1	1
0	0	0	0	0	0	0	0

$$\mathbf{S_{reflected\_1}} = \begin{bmatrix} 0.2637 \\ -0.2633 \\ 0 \\ 0 \end{bmatrix} \begin{bmatrix} 0.315 \\ -0.2153 \\ 0 \\ 0 \end{bmatrix} \begin{bmatrix} 0.4637 \\ -0.4101 \\ 0.128 \\ 0.0416 \end{bmatrix} \begin{bmatrix} 0.515 \\ -0.3621 \\ 0.128 \\ 0.0416 \end{bmatrix} \begin{bmatrix} 0.4317 \\ -0.431 \\ 0 \\ 0 \end{bmatrix} \begin{bmatrix} 0.4829 \\ -0.383 \\ 0 \\ 0 \end{bmatrix} \begin{bmatrix} 0.6317 \\ -0.5778 \\ 0.128 \\ 0.0416 \end{bmatrix} \begin{bmatrix} 0.6829 \\ -0.5298 \\ 0.128 \\ 0.0416 \end{bmatrix}$$

0	1	0	1	0	1	0	1
0	0	1	1	0	0	1	1
0	0	0	0	1	1	1	1
1	1	1	1	1	1	1	1

$$\mathbf{S_{reflected\_1}} = \begin{bmatrix} 0.6387 \\ -0.5386 \\ -0.2399 \\ -0.078 \end{bmatrix} \begin{bmatrix} 0.69 \\ -0.4906 \\ -0.2399 \\ -0.078 \end{bmatrix} \begin{bmatrix} 0.8387 \\ -0.6854 \\ -0.112 \\ -0.0364 \end{bmatrix} \begin{bmatrix} 0.89 \\ -0.6374 \\ -0.112 \\ -0.0364 \end{bmatrix} \begin{bmatrix} 0.8067 \\ -0.7063 \\ -0.2399 \\ -0.078 \end{bmatrix} \begin{bmatrix} 0.8579 \\ -0.6583 \\ -0.2399 \\ -0.078 \end{bmatrix} \begin{bmatrix} 1.0067 \\ -0.8531 \\ -0.112 \\ -0.0364 \end{bmatrix} \begin{bmatrix} 1.0579 \\ -0.8051 \\ -0.112 \\ -0.0364 \end{bmatrix}$$

Figure 6.44: $S_{reflected\_1}$ for four channel chip-to-chip system.

0	1	0	1	0	1	0	1
0	0	1	1	0	0	1	1
0	0	0	0	1	1	1	1
0	0	0	0	0	0	0	0

$$\mathbf{S_{reflected\_2}} = \begin{bmatrix} 0.457 \\ -0.4569 \\ 0 \\ 0 \end{bmatrix} \begin{bmatrix} 0.4731 \\ -0.4466 \\ 0 \\ 0 \end{bmatrix} \begin{bmatrix} 0.7648 \\ -0.7505 \\ 0.074 \\ 0.0537 \end{bmatrix} \begin{bmatrix} 0.7808 \\ -0.7402 \\ 0.074 \\ 0.0537 \end{bmatrix} \begin{bmatrix} 0.748 \\ -0.7478 \\ 0 \\ 0 \end{bmatrix} \begin{bmatrix} 0.764 \\ -0.7375 \\ 0 \\ 0 \end{bmatrix} \begin{bmatrix} 1.0558 \\ -1.0414 \\ 0.074 \\ 0.0537 \end{bmatrix} \begin{bmatrix} 1.0718 \\ -1.0311 \\ 0.074 \\ 0.0537 \end{bmatrix}$$

0	1	0	1	0	1	0	1
0	0	1	1	0	0	1	1
0	0	0	0	1	1	1	1
1	1	1	1	1	1	1	1

$$\mathbf{S_{reflected\_2}} = \begin{bmatrix} 1.0341 \\ -1.0074 \\ -0.1387 \\ -0.1008 \end{bmatrix} \begin{bmatrix} 1.0501 \\ -0.9971 \\ -0.1387 \\ -0.1008 \end{bmatrix} \begin{bmatrix} 1.3418 \\ -1.301 \\ -0.0647 \\ -0.047 \end{bmatrix} \begin{bmatrix} 1.3578 \\ -1.2907 \\ -0.0647 \\ -0.047 \end{bmatrix} \begin{bmatrix} 1.3251 \\ -1.2983 \\ -0.1387 \\ -0.1008 \end{bmatrix} \begin{bmatrix} 1.3411 \\ -1.288 \\ -0.1387 \\ -0.1008 \end{bmatrix} \begin{bmatrix} 1.6328 \\ -1.5919 \\ -0.0647 \\ -0.047 \end{bmatrix} \begin{bmatrix} 1.6488 \\ -1.5816 \\ -0.0647 \\ -0.047 \end{bmatrix}$$

Figure 6.45: $S_{reflected\_2}$ for 4 channel chip-to-chip system.

If we calculate all sixteen values for each of four channels we will see that due to noise margin limitations there will be some errors in channels binary sequences. Light signals interfere between each other causing some error at each data channel.

In order to fix this issue we introduce simple channel coding routines on output to get correct binary sequences for all four channels. We apply different comparators with different thresholds for each channel. We also use multiple comparators with different thresholds for some channels. And we use multiplexers for some channels to obtain correct outputs all the time.

Receiver input light signals I_{0°, I_{45°, I_{90°, and I_{135° are shown in the Table 6.25. These light signals are inputs to the channel photodiodes.

Table 6.25: All 4 receiver channels' photodiode input light signals.

Input	0	1	2	3	4	5	6	7	8	9	10	11	12	13	14	15
I_{0°	0.001	0.008	0.005	0.012	0.002	0.008	0.006	0.013	0.009	0.016	0.013	0.02	0.01	0.016	0.014	0.021
I_{45°	0.114	0.118	0.21	0.214	0.187	0.191	0.282	0.286	0.224	0.228	0.319	0.323	0.297	0.301	0.392	0.396
I_{90°	0.227	0.229	0.377	0.378	0.372	0.374	0.522	0.523	0.508	0.509	0.657	0.659	0.653	0.654	0.802	0.803
I_{135°	0.114	0.118	0.173	0.177	0.187	0.191	0.246	0.25	0.293	0.297	0.351	0.355	0.366	0.37	0.424	0.428

The receiver output for the 135° polarization data channel is obtained by applying a comparator with threshold 0.26 on data points from Table 6.25, yielding Table 6.26.

Table 6.26: 135° polarization data receiver output signals.

Input	0	1	2	3	4	5	6	7	8	9	10	11	12	13	14	15
135°	0	0	0	0	0	0	0	0	1	1	1	1	1	1	1	1

The receiver output for the 0° polarization data channel is obtained by applying two comparators with thresholds of 0.007 and 0.015 on data from Table 6.25. This decoding scheme is shown in Figure 6.46. The outputs of the comparators are shown in Table 6.27.

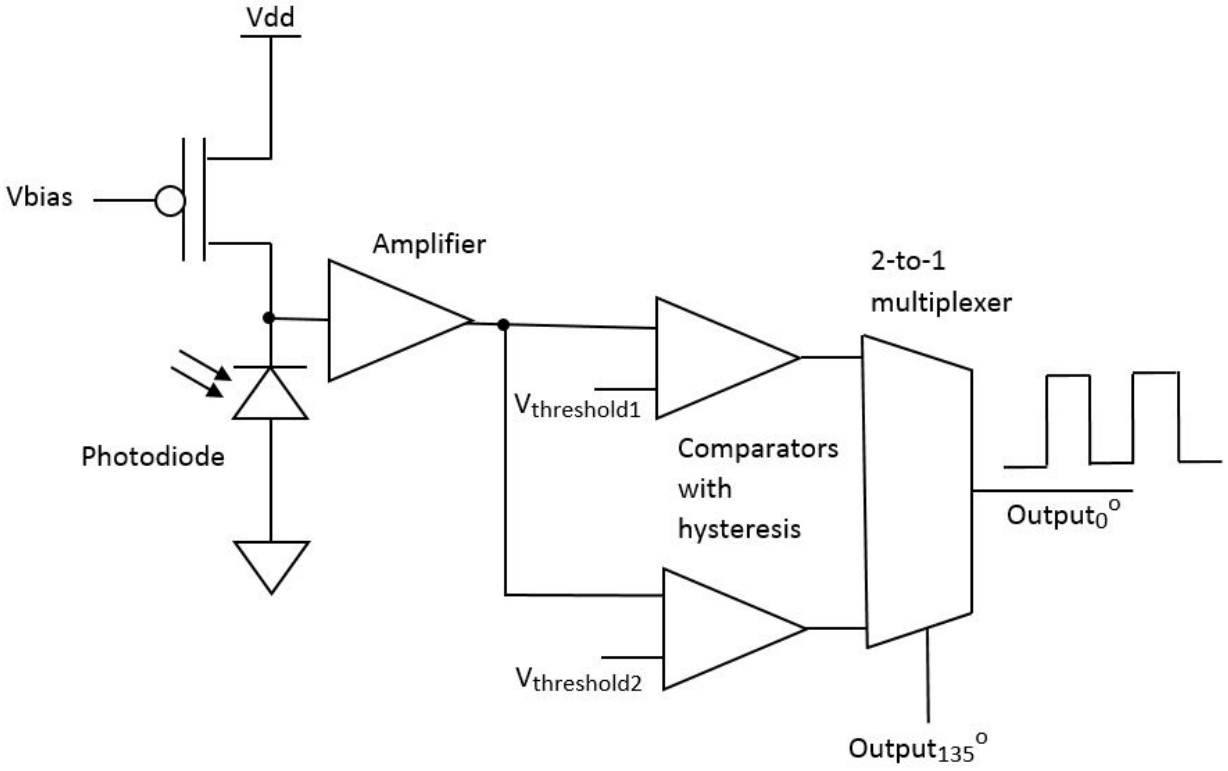

Figure 6.46: 0° data channel circuit with two comparators and 2-to-1 multiplexer.

Table 6.27: 0° polarization data receiver channel 2 comparators output signals.

Input	0	1	2	3	4	5	6	7	8	9	10	11	12	13	14	15
$I_{0^\circ} > 0.007$	0	1	0	1	0	1	0	1	1	1	1	1	1	1	1	1
$I_{0^\circ} > 0.015$	0	0	0	0	0	0	0	0	0	1	0	1	0	1	0	1

If the 135° output is equal to b'0', then I_{0° polarization signal with comparator threshold of 0.007 is the data channel output and if the 135° output is equal to b'1', then I_{0° polarization signal with comparator threshold of 0.015 is the data channel output. The final output is shown in Table 6.28.

The receiver output for the 45° polarization data channel is also obtained by applying two comparators, in this case with thresholds of 0.2 and 0.31, on data from Table 6.25. The outputs of the two comparators are given in Table 6.29.

Table 6.28: 0º polarization data receiver output signal.

Input	0	1	2	3	4	5	6	7	8	9	10	11	12	13	14	15
0° output	0	1	0	1	0	1	0	1	0	1	0	1	0	1	0	1

Table 6.29: 45º polarization data receiver channel 2 comparators' outputs.

Input	0	1	2	3	4	5	6	7	8	9	10	11	12	13	14	15
$I_{45^\circ} > 0.2$	0	0	1	1	0	0	1	1	1	1	1	1	1	1	1	1
$I_{45^\circ} > 0.31$	0	0	0	0	0	0	0	0	0	0	1	1	0	0	1	1

If the 135° output is equal to b'0', then I_{45° polarization data with comparator threshold of 0.2 is the data channel output. If the 135° output is equal to b'1', then I_{45° polarization data with comparator threshold of 0.31 is the data channel output. This is shown in Table 6.30.

Table 6.30: 45º polarization data receiver output signal.

Input	0	1	2	3	4	5	6	7	8	9	10	11	12	13	14	15
45° output	0	0	1	1	0	0	1	1	0	0	1	1	0	0	1	1

Finally, the receiver output for the 90º polarization data channel is obtained by applying three comparators with thresholds 0.24, 0.51, and 0.7 on data from Table 6.25 as is shown in Figure 6.47. The outputs from the three comparators are shown in Table 6.31.

The 3-to-1 multiplexer decision logic works as a function of I_{135° and I_{45°. If the 135° and 45° outputs are both equal to b'0' then the 0.24 threshold is used to determine the 90° output. If the 135° and 45° outputs are both equal to b'1' then the 0.7 threshold is used to determine the 90° output. If the 135° and 45° outputs are not equal to each other then the 0.51 threshold is used to determine the 90° output. The results of these choices are shown in Table 6.32.

Table 6.32 shows 90º polarization data channel output. This table shows that I_{90° or 90º polarization data channel output binary stream is b‘0000111100001111' as it is expected.

Table 6.31: 90° polarization data receiver 3 comparators' outputs.

Input	0	1	2	3	4	5	6	7	8	9	10	11	12	13	14	15
$I_{90^\circ} > 0.24$	0	0	1	1	1	1	1	1	1	1	1	1	1	1	1	1
$I_{90^\circ} > 0.51$	0	0	0	0	0	0	1	1	0	0	1	1	1	1	1	1
$I_{90^\circ} > 0.7$	0	0	0	0	0	0	0	0	0	0	0	0	0	0	1	1

Table 6.32: 90° polarization data receiver output signal.

Input	0	1	2	3	4	5	6	7	8	9	10	11	12	13	14	15
90° output	0	0	0	0	1	1	1	1	0	0	0	0	1	1	1	1

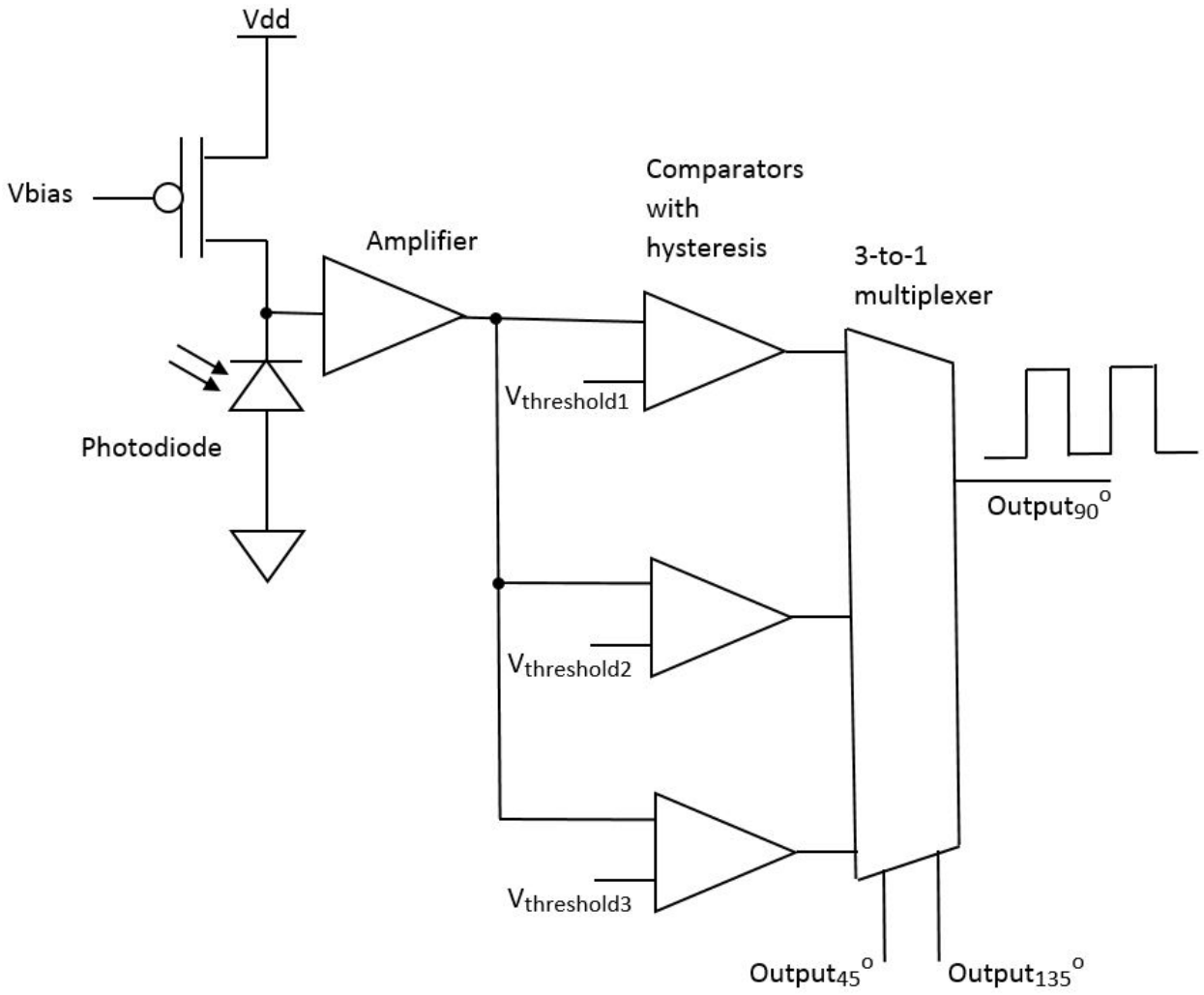

Figure 6.47: 90° data channel circuit with three comparators and 3-to-1 multiplexer.

Chapter 7

Analysis of Design Trade-offs

In this chapter, we will express the relationships between optical power, number of channels, and noise margins that are pertinent to the polarization division multiplexing communication system.

7.1 Noise Properties

The VLC PDM system noise properties can be separated into two distinct domains:

- Noise properties of the optical portions of the system
- Noise properties of electrical portions of the system

We will address each in turn below.

7.1.1 Noise Properties of Optical Subsystem

2, 3 or 4 channel VLC PDM systems have various optical characteristics that impact optical noise properties of the system. As the input transmitter's light beams are launched towards the receiver, they are characterized with the unpolarized Stokes vector $S_{\text{IN}} = [I_T \quad 0 \quad 0 \quad 0]^T$ where I_T represents light intensity of a transmitter. The light intensity I_T is the first parameter of the optical part of the system that impacts system noise properties.

Each unpolarized input light beam is filtered through the transmitter DoFP filter array and the light beams become polarized. Each filter from the array is defined by its Mueller matrix $M_{\Theta-transmitter}$. These Mueller matrices $M_{\Theta-transmitter}$ also impact system noise properties.

All polarized light beams are combined into one light beam and they travel from the transmitter's DoFP filter array to the receiver's DoFP filter array via some transmission media which for example can be air, fiber or waveguide. System noise properties are impacted by the number of channel n_{ch} in the system because polarized light channels are interfering between each other as they travel through the transmission media.

Also system noise properties are impacted by transmission media which is defined by Mueller matrix M_{FIBER} if system transmission media is fiber or matrix M_R if a mirror is used.

In addition, system noise properties are also impacted by the receiver's DoFP filter array. These filters separate every polarized light beam into receiver output data channels. Each filter from the array is defined by its Mueller matrix $M_{\Theta-receiver}$. Each receiver's channel light beam can be defined as I_Θ where Θ is a VLC PDM system data channel polarization angle. These light beams are then send to photodiode circuits and converted into electrical currents.

Therefore we can define that each receiver channel light beam I_Θ is a function of

- Input light intensity I_T
- Mueller matrix of transmitter DoFP filter $M_{\Theta-transmitter}$
- The system number of channel n_{ch}
- Media path m_p - Transmission media Mueller matrices for fiber, M_{FIBER}, and mirrors, M_R, when either is present
- Mueller matrix of receiver DoFP filter $M_{\Theta-receiver}$

Each receiver channel's input light beam I_Θ can be expressed as a function of these elements.

$$I_\Theta = f(I_T, M_{\Theta-transmitter}, n_{ch}, m_p, M_{\Theta-receiver}) \tag{7.1}$$

Various forms that this function can take have been illustrated in the previous chapters.

Each receiver channel's input light beam I_Θ has two distinct nominal values:

- $I_{\Theta-H}$ which represents binary value of b'1' and
- $I_{\Theta-L}$ which represents binary value of b'0'.

Manufacturing variations will, of course, alter these nominal values, as illustrated in Chapter 3 for the aluminum nanowire filter implementation.

However, as we have previously seen, the actual values received can vary not only based on the factors expressed above, but also on the values being transmitted by the other channels. In fact, for the three and four channel designs, it is this latter effect, inter-channel interference, that dominates.

Considering worst-case scenarios for the manufacturing variability and inter-channel interference, we can re-express the input light beam as a minimum value for a b'1' input, $I_{\Theta-H(MIN)}$, and a maximum value for a b'0' input, $I_{\Theta-L(MAX)}$.

7.1.2 Noise Properties of Electrical Subsystem

Figure 7.1 shows a general VLC PDM system receiver data channel. The receiver's data channel input light beam I_Θ reaches the channel's photodiode where it is converted into a current signal.

Then the current signal is converted into a voltage signal which is amplified before it reaches the comparator as is shown in Figure 7.1. The data channel voltage signal V_C can be defined as

$$V_C = G_{IE} G_{OI} I_\Theta \pm \epsilon_{out}. \tag{7.2}$$

In equation (7.2), G_{OI} specifies the gain of the photodiode that converts the input light signal I_Θ into current, G_{IE} specifies the gain of the transimpedance amplification that converts photodiode current into voltage, and ϵ_{out} represents the electrical noise in the channel reflected at the output.

Alternatively, one can express the electrical noise reflected at the input of the first-stage amplifier

$$V_C = G_{IE}(G_{OI} I_\Theta \pm \epsilon_{in}). \tag{7.3}$$

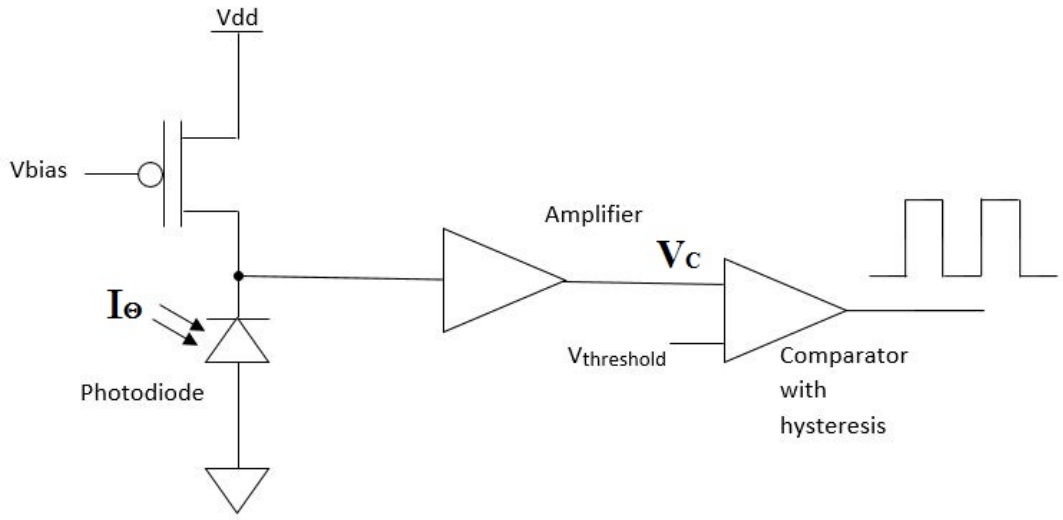

Figure 7.1: Receiver data channel.

Since we have access to empirical data for output-reflected noise (from Chapter 4), we will utilize equation (7.2) in what follows.

Since the optical interference can be characterized as static (i.e., it is not a function of time) and the electrical noise is dynamic, we will separate their contributions to the noise margins and describe the worst-case electrical inputs to the comparator as follows

$$V_{C-H(MIN)} = G_{IE}G_{OI}I_{\Theta-H(MIN)} - \epsilon_{out} \tag{7.4}$$

and

$$V_{C-L(MAX)} = G_{IE}G_{OI}I_{\Theta-L(MAX)} + \epsilon_{out}. \tag{7.5}$$

Figure 7.2 illustrates the entire voltage range for receiver data channel voltage V_C, including a threshold voltage for the comparator.

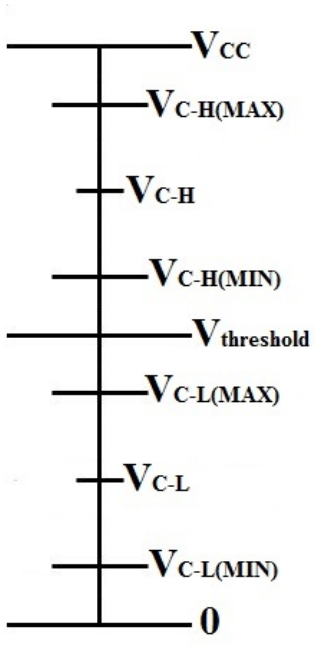

Figure 7.2: Receiver data channel comparator input voltage V_C range.

The high and low noise margins are defined as follows (illustrated in Figure 7.2).

- High noise margin is

$$V_{N-H} = V_{C-H(MIN)} - V_{threshold} \tag{7.6}$$

- Low noise margin is

$$V_{N-L} = V_{threshold} - V_{C-L(MAX)} \tag{7.7}$$

We next apply the above noise assessment on the 2 and 3 channel VLC PDM systems based on the linear CMOS sensor from Chapter 4 to provide quantitative values for the noise margins.

7.1.3 Noise Margin of Two Channel System

From Figure 4.10 mean and standard deviation voltage readings for 2 Channel (0° and 90°) system design are used to determine noise margins of a 2 channel VLC PDM system based on the linear CMOS sensor.

Table 7.1 shows outputs of both receivers' 0° and 90° data channels as function of comparator input voltage V_C mean values ($V_{C-H(MEAN)}$ and $V_{C-L(MEAN)}$) without any electrical noise considerations yet applied.

Table 7.1: Two channel system comparator voltages only with optical noise.

V_{C_90}	V_{C_0}	$Output_{90}$	$Output_0$
0	0	0	0
0.038	2.864	0	1
2.864	0.038	1	0
2.902	2.902	1	1

For 0° polarization angle for voltage 2.902V standard deviation is $\sigma_1 = 0.035$ V and for voltage 2.864V standard deviation is $\sigma_2 = 0.034$ V. Also for 90° polarization angle this value is $\sigma_3 = 0.003$ V. If we apply these three values on equations (7.4) and (7.5) we obtain the following values for

$$V_{C-H} = \begin{cases} V_{C-H(MAX)} = G_{IE}G_{OI}I_{\Theta-H(MAX)} + \epsilon_{out} = 2.902 + 6\sigma_1 = 2.902 + 0.21 = 3.112V \\ V_{C-H(MIN)} = G_{IE}G_{OI}I_{\Theta-H(MIN)} - \epsilon_{out} = 2.846 - 6\sigma_2 = 2.846 - 0.204 = 2.642V \end{cases} \tag{7.8}$$

$$V_{C-L} = \begin{cases} V_{C-L(MAX)} = G_{IE}G_{OI}I_{\Theta-L(MAX)} + \epsilon_{out} = 0.038 + 6\sigma_3 = 0.038 + 0.018 = 0.056V \\ V_{C-L(MIN)} = G_{IE}G_{OI}I_{\Theta-L(MIN)} - \epsilon_{out} = 0.038 - 6\sigma_3 = 0.038 - 0.018 = 0.02V \end{cases} \tag{7.9}$$

The worst case scenario for noise margins is $V_{C-H(MIN)} = 2.642$ V and $V_{C-L(MAX)} = 0.056$ V. If we apply a comparator threshold voltage half way between $V_{C-H(MIN)}$ and $V_{C-L(MAX)}$ we get

$$V_{threshold} = \frac{V_{C-H(MIN)} + V_{C-L(MAX)}}{2} = 1.349V \tag{7.10}$$

From defined $V_{C-H(MIN)}$, $V_{C-L(MAX)}$ and $V_{threshold}$ in worst case noise margins scenario we obtain Table 7.2 shown below.

Table 7.2: Two channel system with optical and electrical noise.

V_{C_90}	V_{C_0}	$Output_{90}$	$Output_0$
0	0	0	0
0.056	2.642	0	1
2.642	0.056	1	0
2.692	2.692	1	1

Using equations (7.6) and (7.7) we calculate

$$V_{N-H} = V_{C-H(MIN)} - V_{threshold} = 1.293\ V \tag{7.11}$$

$$V_{N-L} = V_{threshold} - V_{C-L(MAX)} = 1.293\ V. \tag{7.12}$$

Clearly, for the two channel system, the noise margins are sufficient for reliable operation.

7.1.4 Noise Margin of Three Channel System

We next perform the same noise analysis on 3 channel system design as we just performed on 2 channel system design. From Figure 4.10, the mean and standard deviation voltage readings for 3 channel (0^o, 60^o and 120^o) are used to determine noise margins of 3 channel VLC PDM system based on the linear low-noise CMOS sensor.

Table 7.3 shows outputs for three receiver's 0^o, 60^o and 120^o data channels outputs as function of comparator input voltage V_C mean values ($V_{C-H(MEAN)}$ and $V_{C-L(MEAN)}$) without standard deviation noise margins applied.

Table 7.3: Three channel VLC PDM system only with optical noise.

V_{C_120}	V_{C_60}	V_{C_0}	$Output_{120}$	$Output_{60}$	$Output_0$
0	0	0	0	0	0
0.802	0.724	2.846	0	0	1
0.724	2.846	0.724	0	1	0
1.526	3.5	3.5	0	1	1
2.846	0.724	0.802	1	0	0
3.5	1.448	3.5	1	0	1
3.5	3.5	1.526	1	1	0
3.5	3.5	3.5	1	1	1

Adding in the electrical noise, we get

$$V_{C-H} = \begin{cases} V_{C-H(MAX)} = G_{IE}G_{OI}I_{\Theta-H(MAX)} + \epsilon_{out} = 3.5 + 6\sigma_1 = 3.5 + 0.246 = 3.746\ V \\ V_{C-H(MIN)} = G_{IE}G_{OI}I_{\Theta-H(MIN)} - \epsilon_{out} = 2.846 - 6\sigma_2 = 2.846 - 0.204 = 2.642\ V \end{cases} \tag{7.13}$$

$$V_{C-L} = \begin{cases} V_{C-L(MAX)} = G_{IE}G_{OI}I_{\Theta-L(MAX)} + \epsilon_{out} = 1.526 + 6\sigma_3 = 1.526 + 0.120 = 1.646\ V \\ V_{C-L(MIN)} = G_{IE}G_{OI}I_{\Theta-L(MIN)} - \epsilon_{out} = 0.724 - 6\sigma_3 = 0.724 - 0.072 = 0.652\ V \end{cases} \tag{7.14}$$

The worst noise margins case scenario is if the system has $V_{C-H(MIN)}$ = 2.642 V and $V_{C-L(MAX)}$ = 1.646 V. If we apply a comparator threshold voltage half way between $V_{C-H(MIN)}$ and $V_{C-L(MAX)-120}$ we get

$$V_{threshold} = \frac{V_{C-H(MIN)} + V_{C-L(MAX)}}{2} = 2.144\ V \tag{7.15}$$

From defined $V_{C-H(MIN)}$, $V_{C-L(MAX)}$, and $V_{threshold}$ in the worst case scenario we obtain Table 7.4.

Using equations (7.6) and (7.7) we calculate

$$V_{N-H} = V_{C-H(MIN)} - V_{threshold} = 0.498\ V \tag{7.16}$$

$$V_{N-L} = V_{threshold} - V_{C-L(MAX)} = 0.498\ V. \tag{7.17}$$

Table 7.4: Three channel VLC PDM system with optical and electrical noise.

V_{C_120}	V_{C_60}	V_{C_0}	$Output_{120}$	$Output_{60}$	$Output_0$
0	0	0	0	0	0
0.88	0.796	2.642	0	0	1
0.796	2.642	0.796	0	1	0
1.646	3.254	3.254	0	1	1
2.642	0.796	0.88	1	0	0
3.254	1.562	3.254	1	0	1
3.254	3.254	1.646	1	1	0
3.254	3.254	3.254	1	1	1

While not as robust as the noise margins for the two channel system, these noise margins are also sufficient to enable the system to be quite reliable.

7.2 PAM4 Modulation of a Two Channel System

Noise analysis of two and three channel linear low-noise CMOS sensor based VLC PDM air systems showed that noise margins are good enough for that type of VLC PDM system. Four channel system needs channel coding on the transmitter and on the receiver's side as we show in Chapter 5 in order to properly function.

An alternative approach to increasing the data rate is alternative modulation, and in this section we explore the notion of using Pulse-Amplitude Modulation with 4 levels (PAM4) in conjunction with the two channel system. Figure 7.3 shows a VLD PDM receiver data channel based on PAM4. As we can see from Figure 7.3, we use four voltage levels in entire voltage range 0 to V_{CC} and three comparators with three distinct thresholds V_{TH-LOW}, $V_{TH-middle}$ and $V_{TH-HIGH}$ to get two bits of data per single channel.

We next apply a candidate PAM4 on the two channel VLC PDM air system. Four nominal voltage levels at the receiver are used in this design: 0.5, 1.5, 2.5 and 3.5 V. Also, the following comparator thresholds are used in this design: $V_{TH-LOW} = 1.0$ V, $V_{TH-middle} = 2.0$ V and $V_{TH-HIGH} = 3.0$ V.

Next we apply expected noise to these nominal signals to show that a two channel PAM4 air VLC PDM system has good noise margins.

If we apply equation (4.1) to all four voltage levels 0.5, 1.5, 2.5 and 3.5 V we obtain the following electrical noise for each voltage level:

- For 0.5 V voltage level, from equation (4.1) $\sigma = \pm 0.009$ and noise levels for this voltage level are $6\sigma = \pm 0.054$ which yields maximum value of 0.557 V.

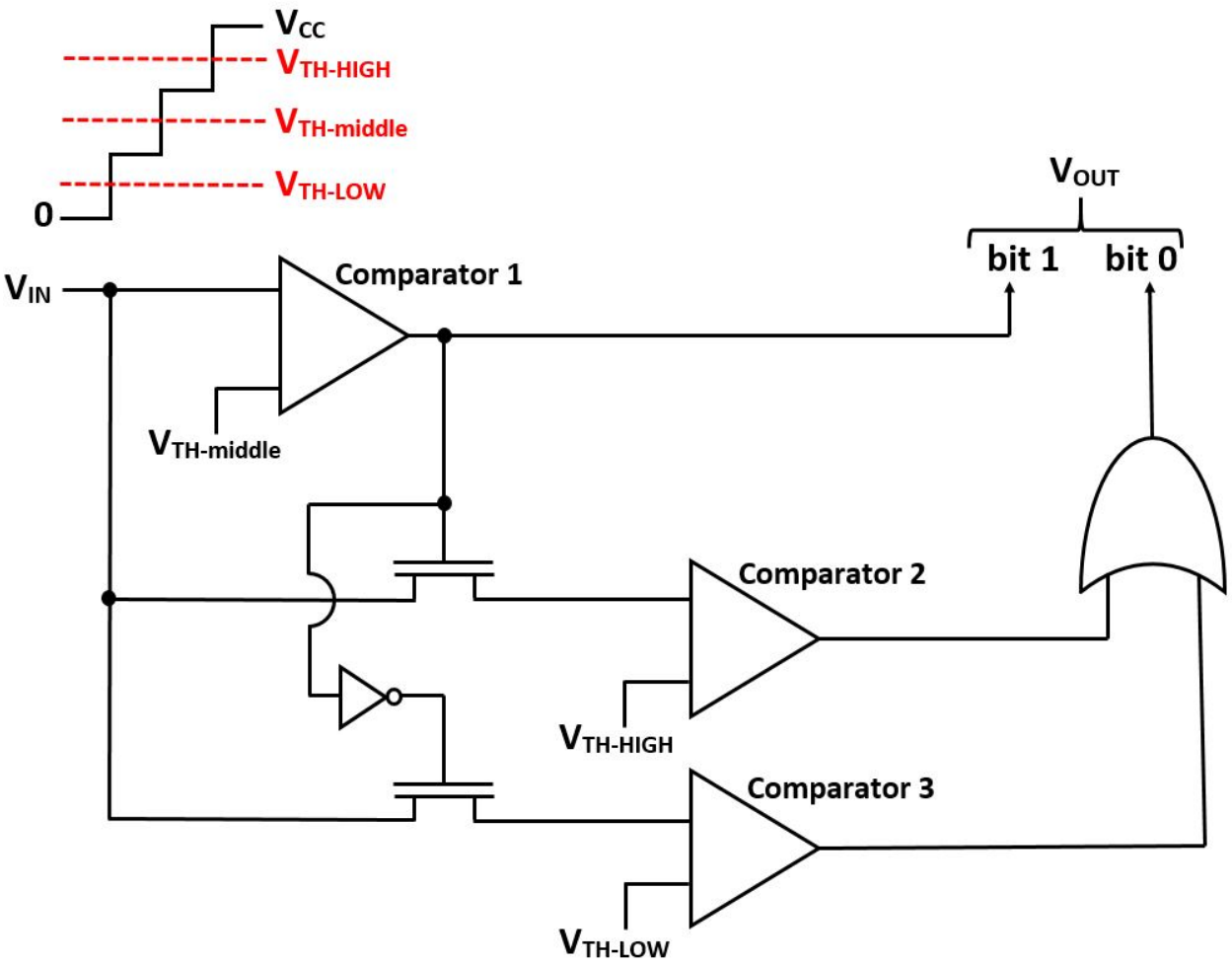

Figure 7.3: VLC PDM receiver data channel based on PAM4.

- For 1.5 V voltage level, from equation (4.1) $\sigma = \pm 0.02$ and noise levels for this voltage level are $6\sigma = \pm 0.12$ which yields minimum and maximum values of 1.383 V and 1.623 V.

- For 2.5 V voltage level, from equation (4.1) $\sigma = \pm 0.03$ and noise levels for this voltage level are $6\sigma = \pm 0.18$ which yields minimum and maximum values of 2.323 V and 2.683 V.

- For 3.5 V voltage level, from equation (4.1) $\sigma = \pm 0.041$ and noise levels for this voltage level are $6\sigma = \pm 0.246$ which yields minimum value of 3.257 V.

Also we need to add optical interference noise between 0° and 90° polarized light signals to all four voltage levels 0.5, 1, 2.5 and 3.5 V. Optical interference for each voltage level is:

- For 0.5 V voltage level, optical interference noise between 0° and 90° polarized light signals is 0.007 V.
- For 1 V voltage level, optical interference noise between 0° and 90° polarized light signals is 0.02 V.
- For 2.5 V voltage level, optical interference noise between 0° and 90° polarized light signals is 0.033 V.
- For 3.5 V voltage level optical interference noise between 0° and 90° polarized light signals is 0.047 V.

We apply the worst noise cases to each of the three channel thresholds $V_{TH-LOW} = 1.0$ V, $V_{TH-middle} = 2.0$ V and $V_{TH-HIGH} = 3.0$ V to determine the noise margins.

First, we test worst case noise for $V_{TH-LOW} = 1.0$ V and $V_{TH-HIGH} = 3.0$ V. Table 7.5 shows the worst case noise for thresholds V_{TH-LOW} and $V_{TH-HIGH}$.

For threshold $V_{TH-LOW} = 1.0$ V, we have $V_{C-H(MIN)} = 1.387$ V and $V_{C-L(MAX)} = 0.601$ V which yields:

$$V_{N-H} = 1.387 - V_{TH-LOW} = 0.387\ V \tag{7.18}$$

$$V_{N-L} = V_{TH-LOW} - 0.601 = 0.399\ V. \tag{7.19}$$

Table 7.5: Two channel PAM4 system worst case noise for V_{TH-LOW} and $V_{TH-HIGH}$.

V_{C_90}	V_{C_0}	$Output_{90}$		$Output_0$	
		bit 3	bit 2	bit 1	bit 0
0.561	0.561	0	0	0	0
0.574	1.387	0	0	0	1
0.587	2.687	0	0	1	0
0.601	3.261	0	0	1	1
1.387	0.574	0	1	0	0
1.4	1.4	0	1	0	1
1.413	2.7	0	1	1	0
1.427	3.274	0	1	1	1
2.687	0.587	1	0	0	1
2.7	1.413	1	0	1	0
2.713	2.713	1	0	1	0
2.727	3.287	1	0	1	1
3.261	0.601	1	1	0	0
3.274	1.427	1	1	0	1
3.287	2.727	1	1	1	0
3.301	3.301	1	1	1	1

For threshold $V_{TH-HIGH} = 3.0$ V, we have $V_{C-H(MIN)} = 3.261V$ and $V_{C-L(MAX)} = 2.727$ V which yields:

$$V_{N-H} = 3.261 - V_{TH-HIGH} = 0.261\ V \tag{7.20}$$

$$V_{N-L} = V_{TH-HIGH} - 2.727 = 0.273\ V. \tag{7.21}$$

Second worst case noise analysis is testing noise margins for $V_{TH-middle} = 2.0$ V. Table 7.6 shows the worst case noise for threshold $V_{TH-middle}$.

If we apply 6σ noise requirements for threshold $V_{TH-middle} = 2.0$ V, we have $V_{C-H(MIN)} = 2.327V$ and $V_{C-L(MAX)} = 1.667V$ which yields:

Table 7.6: Two channel PAM4 system worst case noise for $V_{TH-middle}$

V_{C_90}	V_{C_0}	$Output_{90}$		$Output_0$	
		bit 3	bit 2	bit 1	bit 0
0.561	0.561	0	0	0	0
0.574	1.627	0	0	0	1
0.587	2.687	0	0	1	0
0.601	3.261	0	0	1	1
1.627	0.574	0	1	0	0
1.64	1.64	0	1	0	1
1.653	2.687	0	1	1	0
1.667	3.274	0	1	1	1
2.327	0.587	1	0	0	1
2.34	1.653	1	0	1	0
2.353	2.687	1	0	1	0
2.367	3.287	1	0	1	1
3.261	0.601	1	1	0	0
3.274	1.667	1	1	0	1
3.287	2.687	1	1	1	0
3.301	3.301	1	1	1	1

$$V_{N-H} = 2.327 - V_{TH-middle} = 0.327\ V \tag{7.22}$$

$$V_{N-L} = V_{TH-middle} - 1.667 = 0.333\ V. \tag{7.23}$$

These noise margins are also completely compatible with a robust system.

The result is a monotonic decrease in noise margin as we move from a two channel system with binary modulation, to a three channel system with binary modulation, to a two channel system with PAM4 modulation (effectively four channels).

Chapter 8

Conclusions and Future Work

The research described in this dissertation is motivated by the desire to investigate and effectively utilize optics in high speed digital communications using polarization division multiplexing. In modern high speed digital communications, optics dominates in long distance communications where very large amounts of data are transferred between the cities, countries, across oceans, etc., using wavelength division multiplexing.

However, in short distance high speed digital communications, for example within the building, room, between servers, board-to-board, or chip-to-chip, electrical signals using copper connections are still predominantly used. A common reason why optics is not utilized as much for short distances and why electrical signaling copper communication links are still dominant is that wavelength division multiplexing is not practical to be introduced on short distances.

Placing wavelength division multiplexing on integrated circuits that are used in servers or computers inside offices and similar environments is not very practical because it would require a lot of resources on the integrated chips and it would be very costly.

On the other hand polarization division multiplexing, even if it has practical limitations with actual number of channels, can be very effectively used in digital communications links with short distances. Optical digital communications links on short distances that utilize polarization division multiplexing are compatible with standard CMOS processing, which is a significant cost benefit.

8.1 Contributions and Conclusions

In this research we developed several optical multi-channel digital communication systems based on polarization division multiplexing.

Source laser light signals are polarized using DoFP filter arrays that create multiple channels of high speed digital data each differentiated from the rest of channels by its angle of polarization. Polarized light signals are represented with Stokes vectors and DoFP filters are represented with their Mueller matrix. The process of polarization of light and creation of multiple channels of data is simulated in this research. DoFP filters are currently used in imaging applications as they are routinely bonded on integrated chips and used for image processing applications such are medical imaging.

In this research we use these DoFP filter arrays to show that they can be effectively used in high-speed optical communications. Also they are very cost effective and they do not take a lot of resources on the integrated chips.

Polarized light data channels are combined and they travel via air or a fiber optic cable until they reach the receiver. This light traveling through the air or through a fiber optic cable is also simulated in this research. When the combined polarized light data channels reach the

receiver they are separated by a DoFP filter array in the same way as they were polarized on the transmitter side.

This is also simulated in the research. The separated light channels are then converted by a photodiode into an electrical signal, amplified and processed through a comparator to recover the input digital data stream. This receiver circuitry is defined, designed and simulated using the Cadence 0.5 μm process software tools.

The analysis shows that two and three channel systems are viable (with positive noise margins); however, the four channel system is unable to uniquely decode all 16 possible inputs. We addressed this limitation by introducing simple channel coding techniques to the four channel system.

Channel coding on the input transmitter side means that we applied different amplitudes for different light source channels. On the output receiver side the channel coding means that we applied different thresholds on comparators for different channels and for some channels multiple comparators were used together with multiplexers which were controlled by other channels outputs to recover correct data streams.

In addition, an example of the system receiver was designed and fabricated using Cadence 0.5 μm process. Test showed that the receiver chip correctly operates with either an electrical or an optical input signal.

We explored the noise properties of the system though data collection that utilized two distinct CMOS imaging sensors. The first has a linear response, and the second has a logarithmic response. These data are used to calibrate the noise models used in each of our systems.

Finally, and end-to-end analysis of the systems illustrates the trade-offs between signal power, number of channels, and noise margins for a wide variety of candidate designs. Quantitative

results are presented for two and three channel systems using binary (on-off) modulation as well as a two channel system that exploits pulse amplitude modulation (PAM4) on each optical channel.

8.2 Future Work

Since we were not able to bond a DoFP filter array to the receiver chip and perform test, the priority future work is to perform that experiment. The availability of a chip with an installed filter array will enable us to demonstrate the entire system in the laboratory.

In the analysis of the fiber optic cable media, we used published data from a long (10 km) cable, yet our anticipated use case is considerably shorter (under 1 km). Future work will include the assessment of shorter fibers, and possibly the utilization of polarization preserving fiber.

Analysis and simulation of the system with more than four channels is another future experiment we will consider. Noise and power limitations are going to be investigated more in this experiment. More sophisticated channel coding techniques will be introduced in this simulation model.

In terms of the speed of the system, there are a lot of examples in the literature how to make lasers on chip for high-speed digital data communications. We know that DoFP filter arrays are not limiting factors for achieving a high-speed designs. Also high-speed photodiodes on a chip are also available in the literature.

We will need to replace amplifier circuit and comparator with hysteresis with TIA amplifier which is really suited for this type of high-speed digital data communications. There are a lot of TIA designs in the literature and we will have to investigate more what type of

TIA amplifier will be good for our application and then we will design and simulate it using Cadence software tools before we build a chip and test it out.

References

[1] Bryan Ackland, Behzad Razavi, and Larry West. "A Comparison of Electrical and Optical Clock Networks in Nanometer Technologies." In: *Proc. of IEEE Custom Integrated Circuits Conf.* 2005, pp. 779–782.

[2] Maruf Newaz Ahmed. "Transimpedance Amplifier (TIA) Design for 400 Gb/s Optical Fiber Communications." MA thesis. Blacksburg, Virginia, USA: Virginia Polytechnic Institute and State University, 2013.

[3] S. Banerjee and B. Streetman. *Solid State Electronic Devices*. 6th edition. Prentice Hall, 2006.

[4] B. Blanco-Filgueira, P. Lopez, and J.B. Roldan. "A Verilog-AMS photodiode model including lateral effects." In: *Microelectronic Journal* 43.12 (2012), pp. 980–984.

[5] B. Chen, Y. Wu, M. Han, and Q. Zhang. "A novel architecture of millimeter-wave full-duplex radio-over-fiber system with source-free BS based on polarization division multiplexing and wavelength division multiplexing." In: *Progress in Electromagnetics Research C* 80 (2018), pp. 103–110.

[6] Wei-Zen Chen, Ying-Lien Cheng, and Da-Shin Lin. "A 1.8-V 10-Gb/s Fully Integrated CMOS Optical Receiver Analog Front-End." In: *IEEE Journal of Solid-State Circuits* 40.6 (2005), pp. 1388–1396.

[7] Zhi-Yu Chen, Lian-Shan Yan, Yan Pan, Lin Jiang, An-Lin Yi, Wei Pan, and Bin Luo. "Use of polarization freedom beyond polarization-division multiplexing to support high-speed and spectral-efficient data transmission." In: *Light: Science & Applications* 6.2 (2017), e16207.

[8] Philippe Ciprut, B. Gisin, Nicolas Gisin, Rogerio Passy, J.P. Von der Weid, F. Prieto, and Christian W. Zimmer. "Second-Order Polarization Mode Dispersion: Impact on Analog and Digital Transmissions." In: *Journal of Lightwave Technology* 16.5 (1998), pp. 757–771.

[9] Tomas Cizmar and Kishan Dholakia. "Shaping the light transmission through a multimode optical fibre: complex transformation analysis and applications in biophotonics." In: *Optics Express* 19.20 (2011), pp. 18871–18884.

[10] Hui Dong, Ping Shum, Min Yan, JQ Zhou, GX Ning, YD Gong, and CQ Wu. "Measurement of Mueller matrix for an optical fiber system with birefringence and polarization-dependent loss or gain." In: *Optics Communications* 274.1 (2007), pp. 116–123.

[11] Xinyu Dou, Hongxi Yin, Hehe Yue, and Yu Jin. "Experimental demonstration of polarization-division multiplexing of chaotic laser secure communications." In: *Applied Optics* 54.14 (2015), pp. 4509–4513.

[12] René-Jean Essiambre, Gerhard Kramer, Peter J. Winzer, Gerard J. Foschini, and Bernhard Goebel. "Capacity Limits of Optical Fiber Networks." In: *Journal of Lightwave Technology* 28.4 (2010), pp. 662–701.

[13] Stephen G. Evangelides, Jr., Linn F. Mollenauer, James P. Gordon, and Neal S. Bergano. "Polarization Multiplexing with Solitons." In: *Journal of Lightwave Technology* 10.1 (1992), pp. 28–35.

[14] Jason E. Fritts and Roger D. Chamberlain. "Breaking the Memory Bottleneck with an Optical Data Path." In: *Proc. of 35th Annual Simulation Symposium*. Apr. 2002, pp. 352–362.

[15] Paul M. Furth, Yen-Chun Tsen, Vishnu B. Kulkarni, Thilak K.Poriyani, and House Raju. "On the Design of Low-Power CMOS Comparators with Programmable Hysteresis." In: *Proc. of Midwest Symp. on Circuits and Systems*. 2010.

[16] Missael Garcia, Tyler Davis, Steven Blair, Nan Cui, and Viktor Gruev. "Bioinspired polarization imager with high dynamic range." In: *Optica* 5.10 (2018), pp. 1240–1246.

[17] Missael Garcia, Christopher Edmiston, Radoslav Marinov, Alexander Vail, and Viktor Gruev. "Bio-inspired color-polarization imager for real-time in situ imaging." In: *Optica* 4.10 (2017), pp. 1263–1271.

[18] Jan-Willem Goossens, Mansoor I. Yousefi, Jaouen Hafermann, and Hartmut Haferman. "Polarization-Division Multiplexing Based on the Nonlinear Fourier Transform." In: *Optics Express* 25.22 (2017), pp. 26437–26452.

[19] *6.5µm, 4MP Scientific BSI CMOS Image Sensor*. GSENSE2020BSI. Rev. 0.2. GpixelINC. July 2017.

[20] Viktor Gruev, Rob Perkins, and Timothy York. "CCD Polarization Imaging Sensor with Aluminum Nanowire Optical Filters." In: *Optics Express* 18.18 (2010), pp. 19087–19094.

[21] G. Van Harten, F. Snik, and C.U. Keller. "Polarization properties of real aluminum mirrors, I. Influence of the aluminum oxide layer." In: *Publications of the Astronomical Society of the Pacific* 121.878 (2009), pp. 377–383.

[22] M.I. Hayee, M.C. Cardakli, A.B. Sahin, and A.E. Willner. "Doubling of bandwidth utilization using two orthogonal polarizations and power unbalancing in a polarization-division-multiplexing scheme." In: *IEEE Photonics Technology Letters* 13.8 (2001), pp. 881–883.

[23] Claude Herard and Alain Lacourt. "New multiplexing technique using polarization of light." In: *Applied Optics* 30.2 (1991), pp. 222–231.

[24] Peter De Heyn et al. "Fabrication-Tolerant Four-Channel Wavelength-Division-Multiplexing Filter Based on Collectively Tuned Si Microrings." In: *Journal of Lightwave Technology* 31.16 (2013), pp. 3085–3092.

[25] P.M. Hill, R. Olshansky, and W.K. Burns. "Optical polarization division multiplexing at 4 Gb/s." In: *IEEE Photonics Technology Letters* 4.5 (1992), pp. 500–502.

[26] Chin-Wei Hsu, Chien-Hung Yeh, and Chi-Wai Chow. "Using adaptive equalization and polarization-multiplexing technology for gigabit-per-second phosphor-LED wireless visible light communication." In: *Optics & Laser Technology* 104 (2018), pp. 206–209.

[27] Seok Hun Hyun. "Design of High-Speed CMOS Laser Driver Using a Standard CMOS Technology for Optical Data Transmission." PhD thesis. Atlanta, Georgia, USA: Georgia Institute of Technology, 2004.

[28] Lucas Illing and Matthew B. Kernel. "Shaping Current Waveforms for Direct Modulation of Semiconductor Lasers." In: *IEEE Journal of Quantum Electronics* 40.5 (2004), pp. 445–452.

[29] Hideki Ishio, Junichiro Minowa, and Kiyoshi Nosu. "Review and Status of Wavelength-Division-Multiplexing Technology and Its Application." In: *Journal of Lightwave Technology* 2.4 (1984), pp. 448–463.

[30] Darko Ivanovich, Roger D. Chamberlain, Amit Deliwala, and Viktor Gruev. *Chip-to-chip Optical Data Communications using Polarization Division Multiplexing*. Under review. 2019.

[31] Darko Ivanovich, Samuel B. Powell, Viktor Gruev, and Roger D. Chamberlain. "Polarization Division Multiplexing for Optical Data Communications." In: *Proc. of SPIE 10538, Optical Interconnects XVIII*. 2018, p. 105381D.

[32] Alexandra M. Kern. "CMOS Circuits for VCSEL-Based Optical IO." PhD thesis. Boston, Massachusetts, USA: Massachusetts Institute of Technology, 2004.

[33] J.M. Krijger, R. Snel, G. van Harten, J.H.H. Rietjens, and I. Aben. "Mirror contamination in space I: mirror modelling." In: *Publications of the Atmospheric Measurement Techniques* 7 (2014), pp. 3387–3398.

[34] Vishnu B. Kulkarni. "Low-Voltage CMOS Comparators with programmable hysteresis." MA thesis. Las Cruces, New Mexico, USA: New Mexico State University, 2005.

[35] Do-Hoon Kwon, Sung-Jin Kim, Se-Hoon Yang, and Sang-Kook Han. "Optimized pre-equalization for gigabit polarization division multiplexed visible light communication." In: *Optical Engineering* 54.7 (2015), p. 076101.

[36] S. Latif, S.E. Kocabas, L. Tang, C. Debaes, and D.A.B. Miller. "Low capacitance CMOS silicon photodetectors for optical clock injection." In: *Applied Physics A* 95.4 (2009), pp. 1129–1135.

[37] B. E. Lemoff, M. E. Ali, G. Panotopoulos, G. M. Flower, B. Madhavan, A. F. J. Levi, and D. W. Dolfi. "MAUI: Enabling fiber-to-the-processor with parallel multiwavelength optical interconnects." In: *Journal of Lightwave Technology* 22.9 (Sept. 2004), pp. 2043–2054.

[38] Anthony F. J. Levi. "Silicon Photonics Stumbles at the Last Meter." In: *IEEE Spectrum* (Sept. 2018), pp. 38–43.

[39] Chih-Fan Liao and Shen-Iuan Liu. "40 Gb/s Transimpedance-AGC Amplifier and CDR Circuit for Broadband Data Receivers in 90nm CMOS." In: *IEEE Journal of Solid-State Circuits* 43.3 (2008), pp. 642–655.

[40] Zhenghao Lu, Kiat Seng Yeo, Wei Meng Lim, Manh Anh Do, and Chirn Chye Boon. "Design of a CMOS Broadband Transimpedance Amplifier with Active Feedback." In: *IEEE Transactions on Very Large Scale Integration (VLSI) Systems* 18.3 (2010), pp. 461–472.

[41] Dietrich Marcuse, C. R. Menyuk, and P. K. A. Wai. "Application of the Manakov-PMD Equation to Studies of Signal Propagation in Optical Fibers with Randomly Varying Birefringence." In: *Journal of Lightwave Technology* 15.9 (1997), pp. 1735–1746.

[42] William H. McMaster. "Matrix Representation of Polarization." In: *Reviews of Modern Physics* 33.1 (1961), pp. 8–28.

[43] William H. McMaster. "Polarization and the Stokes Parameters." In: *American Journal of Physics* 22.6 (1954), pp. 351–362.

[44] Y. Miyamoto and H. Takenouchi. "Dense Space-division-multiplexing Optical Communications Technology for Petabit-per-second Class Transmission." In: *ResearchGate GmbH*. 2014.

[45] Maria Morant, Joaquin Pérez, and Roberto Llorente. "Polarization Division Multiplexing of OFDM Radio-over-Fiber Signals in Passive Optical Networks." In: *Advances in Optical Technologies* 2014 (2014), Article ID 269524.

[46] Samuel L.I. Olsson, Junho Cho, Sethumadhavan Chandrasekha, Xi Chen, Peter J. Winzer, and Sergejs Makovejs. "Probabilistically shaped PDM 4096-QAM transmission over up to 200 km of fiber using standard intradyne detection." In: *Optics Express* 26.4 (2018), pp. 4522–4530.

[47] Robert Perkins and Viktor Gruev. "Signal-to-noise analysis of Stokes parameters in division of focal plane polarimeters." In: *Optics Express* 18.25 (2010), pp. 25815–25824.

[48] Samuel B. Powell and Viktor Gruev. "Calibration methods for divison-of-focal-plane polarimeters." In: *Optics Express* 21.18 (2013), pp. 21039–21055.

[49] Robert Pownall, Charles Thangaraj, Guangwei Yuan, Phil Nikkel, Tom W. Chen, and Kevin L. Lear. "CMOS optoelectronic components for clock distribution." In: *Microelectronic Engineering* 87.10 (2010), pp. 1838–1845.

[50] Georg Rademacher et al. "Long-Haul Transmission Over Few-Mode Fibers With Space-Division Multiplexing." In: *Journal of Lightwave Technology* 36.6 (2018), pp. 1382–1388.

[51] V. Ramaswamy, R. Standley, D. Sze, and W.G. French. "Polarization effects in short length single mode fibers." In: *Bell Syst. Tech. Journal* 57.3 (1978), pp. 635–651.

[52] S.C. Rashleigh. "Origins and control of polarization effects in single-mode fibers." In: *Journal of Lightwave Technology* 1.2 (1983), pp. 312–331.

[53] S.C. Rashleigh, W.K. Burns, R.P. Moeller, and R. Ulrich. "Polarization holding in birefringent single-mode fibers." In: *Optics Letters* 7.1 (1982), pp. 40–42.

[54] Behzad Razavi. *Design of Analog CMOS Integrated Circuits*. 1st edition. McGraw-Hill Education, New York, NY, 2001.

[55] Behzad Razavi. "Prospects of CMOS Technology for High-Speed Optical Communication Circuits." In: *IEEE Journal of Solid-State Circuits* 37.9 (2002), pp. 1135–1145.

[56] D.J. Richardson, J.M. Fini, and L.E. Nelson. "Space-division multiplexing in optical fibers." In: *Nature Photonics* 7.5 (2013), pp. 354–362.

[57] Roland Ryf et al. "Space-division multiplexing over 10 km of three-mode fiber using coherent 6×6 MIMO processing." In: *Proc. of Optical Fiber Communication Conference/National Fiber Optic Engineers Conference*. 2011.

[58] Saman Saeedi and Azita Emami. "A 25Gb/s 170µW/Gb/s Optical Receiver in 28nm CMOS for Chip-to-Chip Optical Communication." In: *Proc. of IEEE Radio Frequency Integrated Circuits Symposium*. 2014, pp. 283–286.

[59] Luqman Safar and Muna Samir Zaki. "Design and simulation of Differential Transimpedance Amplifier (TIA) Based on 0.18µm CMOS Technology." In: *Al-Rafadain Engineering Journal* 21.4 (2013), pp. 121–130.

[60] *Stokes parameters*. `https://en.wikipedia.org/wiki/Stokes_parameters`. 2019.

[61] Claudio Talarico, Gaurav Agrawal, Janet Wang-Roveda, and Hani Lashgari. "Design Optimization of a Transimpedance Amplifier for a Fiber Optic Receiver." In: *Circuits, Systems, and Signal Processing* 34.9 (2015), pp. 2785–2800.

[62] Charles Thangaraj, Robert Pownall, Phil Nikkel, Guangwei Yuan, Kevin L. Lear, and Tom Chen. "Fully CMOS-Compatible On-Chip Optical Clock Distribution and Recovery." In: *IEEE Transactions on Very Large Scale Integration (VLSI) Systems* 18.10 (2010), pp. 1385–1389.

[63] Alex Turpin, Yurii Loiko, Todor K. Kalkandjiev, and Jordi Mompart. "Free-space optical polarization demultiplexing and multiplexing by means of conical refraction." In: *Optics Letters* 37.20 (2012), pp. 4197–4199.

[64] J Scott Tyo. "Optimum linear combination strategy for an N-channel polarization-sensitive imaging or vision system." In: *Journal of the Optical Society of America A* 15.2 (1998), pp. 359–366.

[65] Gregory D. VanWiggeren and Rajarshi Roy. "Transmission of linearly polarized light through a single-mode fiber with random fluctuations of birefringence." In: *Applied Optics* 38.18 (1999), pp. 3888–3892.

[66] P. K. A. Wai and C. R. Menyuk. "Polarization mode dispersion, decorrelation, and diffusion in optical fibers with randomly varying birefringence." In: *Journal of Lightwave Technology* 14.2 (1996), pp. 148–157.

[67] Yuanquan Wang, Chao Yang, Yiguang Wang, and Nan Chi. "Gigabit polarization division multiplexing in visible light communication." In: *Optics Letters* 39.7 (2014), pp. 1823–1826.

[68] Klaus Werner, Jun Sakaguchi, Benjamin J. Puttnam, Yoshinari Awaji, and Naoya Wada. "Optical Technologies for Space Division Multiplexing." In: *Proc. of IEEE 13th Workshop of Information Optics*. 1984.

[69] Wm A Wulf and Sally A McKee. "Hitting the memory wall: Implications of the obvious." In: *ACM SIGARCH Computer Architecture News* 23.1 (1995), pp. 20–24.

[70] Steve X. Yao, L.S. Yan, B. Zhang, A.E. Willner, and Junfeng Jiang. "All-optic scheme for automatic polarization division demultiplexing." In: *Optics Express* 15.12 (2007), pp. 7407–7414.

[71] Timothy York and Viktor Gruev. "Optical Characterization of a Polarization Imager." In: *Proc. of IEEE International Symposium of Circuits and Systems*. 2011, pp. 1576–1579.

[72] Bart Van Zeghbroeck. *Principles of Semiconductor Devices and Heterojunctions*. 1st edition. Prentice Hall, 2010.

[73] Wang Zinan and Xie Chongjin. "Automatic optical polarization demultiplexing for polarization division multiplexed signals." In: *Optics Express* 17.5 (2009), pp. 3183–3189.

Appendix A

Simulation Models

A.1 VerilogA model for 2 channel receiver DoFP filtering of polarized light

When combined 0° and 90° polarized light beams that respectively represent binary sequences b'0101' and b'0011' reach the receiver's DoFP filter array in air, there is filtering of the combined polarized light beam. Two independent light beams are results of this filtering.

These independent light beams represent binary sequences b'0101' and b'0011' and they are converted into electrical currents using photodiode circuits for each 0° and 90° data channels. This analysis is presented in Figure 3.13 in Chapter 3.

In order to simulate the visible light portion of the Cadence system we use a VerilogA model that is presented here. The VerilogA module name is

DoFP_Polarimeter_Mueller_Matrix_2_Channel_1

and this VerilogA model creates a hardware component with the same name that is used in Chapter 3 Cadence simulation of the 2 channel receiver system.

```
\\Module: DoFP_Polarimeter_Mueller_Matrix_2_Channel_1
`include "constants.vams"
`include "disciplines.vams"

module DoFP_Polarimeter_Mueller_Matrix_2_Channel_1(Light_Ch_In_1,
    Light_Ch_In_2, Light_Ch_Out_1, Light_Ch_Out_2, vss);

parameter real pi = 3.14159;
real theta1;
real theta2;
real T;
real D;

input Light_Ch_In_1, Light_Ch_In_2;
inout vss;
output Light_Ch_Out_1, Light_Ch_Out_2;

parameter delay =0, ttime=1p;
electrical Light_Ch_In_1, Light_Ch_In_2, Light_Ch_Out_1,
    Light_Ch_Out_2,vss;
real S0_0, S1_0, S2_0, S0_90, S1_90, S2_90, S0_IN, S1_IN, S2_IN, I0, I90;

    analog begin
```

```
        theta1 = 0;
        theta2 = pi/2;
        T = 0.5;
        D = 0.99;
        S0_0 = 1;
        S1_0 = 1;
        S2_0 = 0;
        S0_90 = 1;
        S1_90 = -1;
        S2_90 = 0;
        S0_IN = S0_0*V(Light_Ch_In_1)+S0_90*V(Light_Ch_In_2);
        S1_IN = S1_0*V(Light_Ch_In_1)+S1_90*V(Light_Ch_In_2);
        S2_IN = S2_0*V(Light_Ch_In_1)+S2_90*V(Light_Ch_In_2);
        I0 = 0.5*T*S0_IN + 0.5*T*D*S1_IN*cos(2*theta1)+
            0.5*T*D*S2_IN*sin(2*theta1);
        I90 = 0.5*T*S0_IN + 0.5*T*D*S1_IN*cos(2*theta2)+
            0.5*T*D*S2_IN*sin(2*theta2);
    V(Light_Ch_Out_1) <+ transition(I0, delay, ttime);
    V(Light_Ch_Out_2) <+ transition(I90, delay, ttime);
end
endmodule
```

A.2 VerilogA model for 3 channel receiver DoFP filtering of polarized light

When combined 0°, 60° and 120° polarized light beams that respectively represent binary sequences b'01010101', b'00110011' and b'00001111' reach the receiver's DoFP filter array in air, there is filtering of the combined polarized light beam. Three independent light beams are results of this filtering.

These independent light beams represent binary sequences b'01010101', b'00110011' and b'00001111' and they are converted into electrical currents using photodiode circuits for each of 0°, 60° and 120° data channels. This analysis is presented in Figure 3.15 in Chapter 3.

In order to simulate the visible light portion of the Cadence system we use a VerilogA model that is presented here. The VerilogA module name is

DoFP_Polarimeter_Mueller_Matrix_3_Channel_1

and this VerilogA model creates a hardware component with the same name that is used in Chapter3 Cadence simulation of the 3 channel receiver system.

```
\\Module: DoFP_Polarimeter_Mueller_Matrix_3_Channel_1
`include "constants.vams"
`include "disciplines.vams"

module DoFP_Polarimeter_Mueller_Matrix_3_Channel_1(Light_Ch_In_1,
    Light_Ch_In_2, Light_Ch_In_3, Light_Ch_Out_1, Light_Ch_Out_2,
    Light_Ch_Out_3, vss);
```

```
parameter real pi = 3.14159;
real theta1;
real theta2;
real theta3;
real T;
real D;

input Light_Ch_In_1, Light_Ch_In_2, Light_Ch_In_3;
inout vss;
output Light_Ch_Out_1, Light_Ch_Out_2, Light_Ch_Out_3;

parameter delay =0, ttime=1p;
electrical Light_Ch_In_1, Light_Ch_In_2, Light_Ch_In_3, Light_Ch_Out_1,
    Light_Ch_Out_2, Light_Ch_Out_3, vss;
real S0_0, S1_0, S2_0, S0_60, S1_60, S2_60, S0_120, S1_120, S2_120, S0_IN,
    S1_IN, S2_IN, I0, I60, I120;

    analog begin
        theta1 = 0;
        theta2 = pi/3;
        theta3 = 2*pi/3;
        T = 0.5;
        D = 0.99;
        S0_0 = 1;
        S1_0 = 1;
```

```
        S2_0 = 0;
        S0_60 = 1;
        S1_60 = -0.5;
        S2_60 = sqrt(3)/2;
        S0_120 = 1;
        S1_120 = -0.5;
        S2_120 = -sqrt(3)/2;
        S0_IN = S0_0*V(Light_Ch_In_1)+S0_60*V(Light_Ch_In_2)+
            S0\_120*V(Light_Ch_In_3);
        S1_IN = S1_0*V(Light_Ch_In_1)+S1_60*V(Light_Ch_In_2)+
            S1\_120*V(Light_Ch_In_3);
        S2_IN = S2_0*V(Light_Ch_In_1)+S2_60*V(Light_Ch_In_2)+
            S2\_120*V(Light_Ch_In_3);
        I0 = 0.5*T*S0_IN+0.5*T*D*S1_IN*cos(2*theta1)+0.5*T*D*S2_IN*sin(2*theta1);
        I60 = 0.5*T*S0_IN+0.5*T*D*S1_IN*cos(2*theta2)+0.5*T*D*S2_IN*sin(2*theta2);
        I120 = 0.5*T*S0_IN+0.5*T*D*S1_IN*cos(2*theta3)+0.5*T*D*S2_IN*sin(2*theta3);
    V(Light_Ch_Out_1) <+ transition(I0, delay, ttime);
    V(Light_Ch_Out_2) <+ transition(I60, delay, ttime);
    V(Light_Ch_Out_3) <+ transition(I120, delay, ttime);
end
endmodule
```

A.3 VerilogA model for 3 channel DoFP filtering of polarized light with errors

In Chapter 3 we also simulate Cadence model of 3 channel system with errors. VerilogA model for this simulation is named

DoFP_Polarimeter_Mueller_Matrix_3_Channel_1_w_errors

and it is shown here:

```
\\Module: DoFP_Polarimeter_Mueller_Matrix_3_Channel_1_w_errors
`include "constants.vams"
`include "disciplines.vams"

module DoFP_Polarimeter_Mueller_Matrix_3_Channel_1_w_errors(Light_Ch_In_1,
    Light_Ch_In_2, Light_Ch_In_3, Light_Ch_Out_1, Light_Ch_Out_2,
    Light_Ch_Out_3, vss);

parameter real pi = 3.14159;
real theta1;
real theta2;
real theta3;
real T;
real D;

input Light_Ch_In_1, Light_Ch_In_2, Light_Ch_In_3;
```

```
inout vss;
output Light_Ch_Out_1, Light_Ch_Out_2, Light_Ch_Out_3;

parameter delay =0, ttime=1p;
electrical Light_Ch_In_1, Light_Ch_In_2, Light_Ch_In_3, Light_Ch_Out_1,
    Light_Ch_Out_2, Light_Ch_Out_3, vss;
real S0_0, S1_0, S2_0, S0_60, S1_60, S2_60, S0_120, S1_120, S2_120, S0_IN,
    S1_IN, S2_IN, I0, I60, I120;

    analog begin
        theta1 = pi/36;
        theta2 = 11*pi/36;
        theta3 = 25*pi/36;
        T = 0.5;
        D = 0.99;
        S0_0 = 1;
        S1_0 = 1;
        S2_0 = 0;
        S0_60 = 1;
        S1_60 = -0.5;
        S2_60 = sqrt(3)/2;
        S0_120 = 1;
        S1_120 = -0.5;
        S2_120 = -sqrt(3)/2;
        S0_IN = S0_0*V(Light_Ch_In_1)+S0_60*V(Light_Ch_In_2)+
            S0_120*V(Light_Ch_In_3);
```

```
        S1_IN = S1_0*V(Light_Ch_In_1)+S1_60*V(Light_Ch_In_2)+
            S1_120*V(Light_Ch_In_3);
        S2_IN = S2_0*V(Light_Ch_In_1)+S2_60*V(Light_Ch_In_2)+
            S2_120*V(Light_Ch_In_3);
        I0 = 0.5*T*S0_IN+0.5*T*D*S1_IN*cos(2*theta1)+
            0.5*T*D*S2_IN*sin(2*theta1);
        I60 = 0.5*T*S0_IN+0.5*T*D*S1_IN*cos(2*theta2)+
            0.5*T*D*S2_IN*sin(2*theta2);
        I120 = 0.5*T*S0_IN+0.5*T*D*S1_IN*cos(2*theta3)+
            0.5*T*D*S2_IN*sin(2*theta3);
    V(Light_Ch_Out_1) <+ transition(I0, delay, ttime);
    V(Light_Ch_Out_2) <+ transition(I60, delay, ttime);
    V(Light_Ch_Out_3) <+ transition(I120, delay, ttime);
end
endmodule
```

A.4 VerilogA model for 4 channel receiver DoFP filtering of polarized light

When combined 0°, 45°, 90° and 135° polarized light beams that respectively represent binary sequences b'0101010101010101', b'0011001100110011', b'0000111100001111' and b'0000000011111111' reach the receiver's DoFP filter array in air, there is filtering of the combined polarized light beam. Four independent light beams are results of this filtering.

These independent light beams represent binary sequences b'0101010101010101', b'0011001100110011', b'0000111100001111' and b'0000000011111111' and they are converted into electrical currents

using photodiode circuits for each of 0°, 45°, 90° and 135° data channels. This analysis is presented in Figure 3.19 in Chapter 3.

In order to simulate the visible light portion of the Cadence system we use a VerilogA model that is presented here. The VerilogA module name is

DoFP_Polarimeter_Mueller_Matrix_4_Channel_1

and this VerilogA model creates a hardware component with the same name that is used in Chapter 3 Cadence simulation of the 4 channel receiver system.

```
\\Module: DoFP_Polarimeter_Mueller_Matrix_4_Channel_1
`include "constants.vams"
`include "disciplines.vams"

module DoFP_Polarimeter_Mueller_Matrix_4_Channel_1(Light_Ch_In_1,
    Light_Ch_In_2, Light_Ch_In_3, Light_Ch_In_4, Light_Ch_Out_1,
    Light_Ch_Out_2, Light_Ch_Out_3, Light_Ch_Out_4, vss);

parameter real pi = 3.14159;
real theta1;
real theta2;
real theta3;
real theta4;
real T;
real D;

input Light_Ch_In_1, Light_Ch_In_2, Light_Ch_In_3, Light_Ch_In_4;
```

```
inout vss;
output Light_Ch_Out_1, Light_Ch_Out_2, Light_Ch_Out_3, Light_Ch_Out_4;

parameter delay =0, ttime=1p;
electrical Light_Ch_In_1, Light_Ch_In_2, Light_Ch_In_3, Light_Ch_In_4,
    Light_Ch_Out_1, Light_Ch_Out_2, Light_Ch_Out_3, Light_Ch_Out_4, vss;
real S0_0, S1_0, S2_0, S0_45, S1_45, S2_45, S0_90, S1_90, S2_90, S0_135,
    S1_135, S2_135, S0_IN, S1_IN, S2_IN, I0, I45, I90, I135;

    analog begin
        theta1 = 0;
        theta2 = pi/4;
        theta3 = pi/2;
        theta4 = 3*pi/4;
        T = 0.5;
        D = 0.99;
        S0_0 = 1;
        S1_0 = 1;
        S2_0 = 0;
        S0_45 = 1;
        S1_45 = 0;
        S2_45 = 1;
        S0_90 = 1;
        S1_90 = -1;
        S2_90 = 0;
        S0_135 = 1;
```

```
        S1_135 = 0;
        S2_135 = - 1;
        S0_IN = S0_0*V(Light_Ch_In_1)+S0_45*V(Light_Ch_In_2)+
            S0_90*V(Light_Ch_In_3)+S0_135*V(Light_Ch_In_4);
        S1_IN = S1_0*V(Light_Ch_In_1)+S1_45*V(Light_Ch_In_2)+
            S1\_90*V(Light_Ch_In_3)+S1_135*V(Light_Ch_In_4);
        S2_IN = S2_0*V(Light_Ch_In_1)+S2_45*V(Light_Ch_In_2)+
            S2\_90*V(Light_Ch_In_3)+S2_135*V(Light_Ch_In_4);
        I0 = 0.5*T*S0_IN + 0.5*T*D*S1_IN*cos(2*theta1)+
            0.5*T*D*S2_IN*sin(2*theta1);
        I45 = 0.5*T*S0_IN + 0.5*T*D*S1_IN*cos(2*theta2)+
            0.5*T*D*S2_IN*sin(2*theta2);
        I90 = 0.5*T*S0_IN + 0.5*T*D*S1_IN*cos(2*theta3)+
            0.5*T*D*S2_IN*sin(2*theta3);
        I135 = 0.5*T*S0_IN + 0.5*T*D*S1_IN*cos(2*theta4)+
            0.5*T*D*S2_IN*sin(2*theta4);
    V(Light_Ch_Out_1) <+ transition(I0, delay, ttime);
    V(Light_Ch_Out_2) <+ transition(I45, delay, ttime);
    V(Light_Ch_Out_3) <+ transition(I90, delay, ttime);
    V(Light_Ch_Out_4) <+ transition(I135, delay, ttime);
end
endmodule
```

A.5 VerilogA model of photodiode

Photodiode model for each receiver channel is defined in Chapter 3. For Cadence system design VerilogA model was designed and then Photodiode hardware symbol is defined and it is used in all Cadence systems simulation model. VerilogA model of Photodiode is defined as

PhotodiodeDesign

and it is shown here:

```
\\Module: PhotodiodeDesign
`include "constants.vams"
`include "disciplines.vams"

module PhotodiodeDesign(Anode,Cathode,Light);
    inout Anode, Cathode, Light;
    electrical Anode, Cathode, Light;

        //Semicondutor parameters
        //-----------------------------------------------------------------

        //Acceptor concetration (p-side junction)
        parameter real Na=1.0e17;
        //Acceptor concetration (n-side junction)
        parameter real Nd=1.0e15;
        //Intrinsic electron and hole concetration for Si at room temperature
        parameter real ni=1.5e10;
```

```
//Carrier Recombination Lifetime (p-side junction)
parameter real tau_n=1.0e-7;
//Carrier Recombination Lifetime (n-side junction)
parameter real tau_p=1.0e-5;
//Hole Mobility (p-side junction)
parameter real u_p_p=200;
//Electron Mobility (p-side junction)
parameter real u_n_p=700;
//Hole Mobility (n-side junction)
parameter real u_p_n=450;
//Electron Mobility (n-side junction)
parameter real u_n_n=1300;

//Necessary parameters
//-----------------------------------------------------------------

//Temperature
parameter real T=300.0;
//Relative dielectric coefficient of silicon
parameter real er=11.8;
//Dielectric constant of Vacuum
parameter real eo=8.854187817e-14;
//Boltzmann Constant
parameter real k=1.3806488e-23;
//Basic e- charge
parameter real q=1.60217657e-19;
```

```
//Area of Si pn junction
parameter real A=1.0e-4;
//Absorbtion coeff. of Si
parameter real alpha=500;
//Red Light
parameter real Eph=1.8;

//Variables
//-----------------------------------------------------------------

//Thermal Voltage
real Vt;
//Optical Source Power
real Popt;
//Optical Generation Rate
real g_op;
//Diffusion coefficient on P-side of Si
real Dp;
//Diffusion coefficient on N-side of Si
real Dn;
//Diffusion length for holes
real Lp;
//Diffusion length for electrons
real Ln;
//Minority concetration of electrons in P-side of Si
real pn;
```

```
        //Minority concetration of protons in N-side of Si
        real np;
        //Contact potential
        real Vo;
        //Depletion
        region width
        real W;
        //Photogenerated current
        real Ioptical;
        //Dark current
        real Idark;

branch (Anode,Cathode) b1;

analog begin
            //Optical Source Power
            Popt=V(Light);
            //Thermal Voltage
            Vt=k*T/q;
            //Optical Generation Rate
            g_op=(Popt*alpha)/(Eph*q);
            //Diffusion coefficient on N-side of Si
            Dp=Vt*u_p_n;
            //Diffusion coefficient on P-side of Si
            Dn=Vt*u_n_p;
            //Diffusion length for holes
```

```
            Lp=sqrt(Dp*tau_p);
            //Diffusion length for electrons
            Ln=sqrt(Dn*tau_n);
            //Minority concetration of electrons in P-side of Si
            pn=(ni*ni)/Nd;
            //Minority concetration of protons in N-side of Si
            np=(ni*ni)/Na;
            //Contact potential
            Vo=Vt*ln((Na*Nd)/(ni*ni));
            //Depletion region width
            W=sqrt((Vo+V(b1))*(1.0/Nd+1.0/Na)*(2*eo*er)/q);
            //Photogenerated current
            Ioptical=q*A*g_op*(Lp+Ln+W);
            //Forward biased current
            Idark=q*A*(Dp*pn/Lp+Dn*np/Ln)*exp((V(b1)/Vt)-1);

//Photodiode current
I(b1)<+ Idark;
I(b1)<+ -Ioptical;
end
endmodule
```

A.6 VerilogA model of the full air 2 channel optical part of the system

Figure 6.17 in Chapter 6 uses the following VerilogA model for the optical part of the system:

DoFP_Polarimeter_Tx_Air_Rx_2_Ch_Full_System.

This VerilogA model defines transmitter's laser input light beams that represent binary sequences b'0101' and b'0011' that are polarized by 0° and 90° DoFP filters.

After polarization filtering by the transmitter DoFP filter array two light beams are combined and they travel through air until they reach receiver's 0° and 90° DoFP filter array where they are separated to two light beams that still represent binary sequences b'0101' and b'0011' and then they are sent to two receiver's electrical signal channels to decode the binary sequences.

VerilogA model DoFP_Polarimeter_Tx_Air_Rx_2_Ch_Full_System is shown here:

```
\\Module: DoFP_Polarimeter_Tx_Air_Rx_2_Ch_Full_System
`include "constants.vams"
`include "disciplines.vams"

module DoFP_Polarimeter_Tx_Air_Rx_2_Ch_Full_System(Light_Ch_In_1, Light_Ch_In_2,
    Light_Ch_Out_1, Light_Ch_Out_2, vss);

parameter real pi = 3.14159;
real theta1;
real theta2;
```

```
real T;
real D;

input Light_Ch_In_1, Light_Ch_In_2;
inout vss;
output Light_Ch_Out_1, Light_Ch_Out_2;

parameter delay =0, ttime=1p;
electrical Light_Ch_In_1, Light_Ch_In_2, Light_Ch_Out_1, Light_Ch_Out_2,vss;
real S0_0, S1_0, S2_0, S0_90, S1_90, S2_90, S0_trans_media, S1_trans_media,
    S2_trans_media, I0, I90;

    analog begin
       theta1 = 0;
   theta2 = pi/2;
        T = 0.5;
        D = 0.99;
        S0_0 = 0.5*T;
        S1_0 = 0.5*T*D*cos(2*theta1);
        S2_0 = 0.5*T*D*sin(2*theta1);
        S0_90 = 0.5*T;
        S1_90 = 0.5*T*D*cos(2*theta2);
        S2_90 = 0.5*T*D*sin(2*theta2);
        S0_trans_media = S0_0*V(Light_Ch_In_1)+S0_90*V(Light_Ch_In_2);
        S1_trans_media = S1_0*V(Light_Ch_In_1)+S1_90*V(Light_Ch_In_2);
        S2_trans_media = S2_0*V(Light_Ch_In_1)+S2_90*V(Light_Ch_In_2);
```

```
        I0 = 0.5*T*S0_trans_media + 0.5*T*D*S1_trans_media*cos(2*theta1)
            +0.5*T*D*S2_trans_media*sin(2*theta1);
        I90 = 0.5*T*S0_trans_media + 0.5*T*D*S1_trans_media*cos(2*theta2)
            +0.5*T*D*S2_trans_media*sin(2*theta2);
    V(Light_Ch_Out_1) <+ transition(I0, delay, ttime);
    V(Light_Ch_Out_2) <+ transition(I90, delay, ttime);
end
endmodule
```

A.7 VerilogA model of the full air 3 channel optical part of the system

Figure 6.20 in Chapter 6 uses the following VerilogA model for the optical part of the system:

DoFP_Polarimeter_Tx_Air_Rx_3_Ch_Full_System.

This VerilogA model defines transmitter's laser input light beams that represent binary sequences b'01010101', b'00110011' and b'00001111' that are polarized by 0°, 60° and 120° DoFP filters.

After polarization filtering by the transmitter DoFP filter array three light beams are combined and they travel through air until they reach receiver's 0°, 60° and 120° DoFP filter array where they are separated to two light beams that still represent binary sequences b'01010101', b'00110011' and b'00001111' and then they are sent to three receiver's electrical signal channels to decode the binary sequences.

VerilogA model DoFP_Polarimeter_Tx_Air_Rx_3_Ch_Full_System is shown here:

```
\\Module: DoFP_Polarimeter_Tx_Air_Rx_3_Ch_Full_System

`include "constants.vams"
`include "disciplines.vams"

module DoFP_Polarimeter_Tx_Air_Rx_3_Ch_Full_System(Light_Ch_In_1, Light_Ch_In_2,
    Light_Ch_In_3, Light_Ch_Out_1, Light_Ch_Out_2, Light_Ch_Out_3, vss);

parameter real pi = 3.14159;
real theta1;
real theta2;
real theta3;
real T;
real D;

input Light_Ch_In_1, Light_Ch_In_2, Light_Ch_In_3;
inout vss;
output Light_Ch_Out_1, Light_Ch_Out_2, Light_Ch_Out_3;

parameter delay =0, ttime=1p;
electrical Light_Ch_In_1, Light_Ch_In_2, Light_Ch_In_3, Light_Ch_Out_1,
    Light_Ch_Out_2, Light_Ch_Out_3, vss;
real S0_0, S1_0, S2_0, S0_60, S1_60, S2_60, S0_120, S1_120, S2_120, S0_trans_media,
    S1_trans_media, S2_trans_media, I0, I60, I120;

    analog begin
```

```
theta1 = 0;

theta2 = pi/3;

theta3 = 2*pi/3;

T = 0.5;

D = 0.99;

S0_0 = 0.5*T;

S1_0 = 0.5*T*D*cos(2*theta1);

S2_0 = 0.5*T*D*sin(2*theta1);

S0_60 = 0.5*T;

S1_60 = 0.5*T*D*cos(2*theta2);

S2_60 = 0.5*T*D*sin(2*theta2);

S0_120 = 0.5*T;

S1_120 = 0.5*T*D*cos(2*theta3);

S2_120 = 0.5*T*D*sin(2*theta3);

S0_trans_media = S0_0*V(Light_Ch_In_1)+S0_60*V(Light_Ch_In_2)
    +S0_120*V(Light_Ch_In_3);

S1_trans_media = S1_0*V(Light_Ch_In_1)+S1_60*V(Light_Ch_In_2)
    +S1_120*V(Light_Ch_In_3);

S2_trans_media = S2_0*V(Light_Ch_In_1)+S2_60*V(Light_Ch_In_2)
    +S2_120*V(Light_Ch_In_3);

I0 = 0.5*T*S0_trans_media+0.5*T*D*S1_trans_media*cos(2*theta1)
    +0.5*T*D*S2_trans_media*sin(2*theta1);

I60 = 0.5*T*S0_trans_media+0.5*T*D*S1_trans_media*cos(2*theta2)
    +0.5*T*D*S2_trans_media*sin(2*theta2);

I120 = 0.5*T*S0_trans_media+0.5*T*D*S1_trans_media*cos(2*theta3)
    +0.5*T*D*S2_trans_media*sin(2*theta3);
```

```
    V(Light_Ch_Out_1) <+ transition(I0, delay, ttime);
    V(Light_Ch_Out_2) <+ transition(I60, delay, ttime);
    V(Light_Ch_Out_3) <+ transition(I120, delay, ttime);
end
endmodule
```

A.8 VerilogA model of the full air 4 channel optical part of the system

Figure 6.23 in Chapter 6 uses the following VerilogA model for the optical part of the system:

DoFP_Polarimeter_Tx_Air_Rx_4_Ch_Full_System.

This VerilogA model defines transmitter's laser input light beams that represent binary sequences b'0101010101010101', b'0011001100110011', b'0000111100001111' and b'0000000011111111' that are polarized by 0º, 45º, 90º and 135º DoFP filters.

After polarization filtering by the transmitter DoFP filter array four light beams are combined and they travel through air until they reach receiver's 0º, 45º, 90º and 135º DoFP filter array where they are separated to four light beams that still represent binary sequences b'0101010101010101', b'0011001100110011', b'0000111100001111' and b'0000000011111111' and then they are send to four receiver's electrical signal channels to output the binary sequences.

VerilogA model DoFP_Polarimeter_Tx_Air_Rx_4_Ch_Full_System is shown here:

```
\\Module: DoFP_Polarimeter_Tx_Air_Rx_4_Ch_Full_System
```

```
`include "constants.vams"
`include "disciplines.vams"

module DoFP_Polarimeter_Tx_Air_Rx_4_Ch_Full_System(Light_Ch_In_1,
    Light_Ch_In_2, Light_Ch_In_3, Light_Ch_In_4, Light_Ch_Out_1,
    Light_Ch_Out_2, Light_Ch_Out_3, Light_Ch_Out_4, vss);

parameter real pi = 3.14159;
real theta1;
real theta2;
real theta3;
real theta4;
real T;
real D;

input Light_Ch_In_1, Light_Ch_In_2, Light_Ch_In_3, Light_Ch_In_4;
inout vss;
output Light_Ch_Out_1, Light_Ch_Out_2, Light_Ch_Out_3, Light_Ch_Out_4;

parameter delay =0, ttime=1p;

electrical Light_Ch_In_1, Light_Ch_In_2, Light_Ch_In_3, Light_Ch_In_4,
    Light_Ch_Out_1, Light_Ch_Out_2, Light_Ch_Out_3, Light_Ch_Out_4, vss;

real S0_0, S1_0, S2_0, S0_45, S1_45, S2_45, S0_90, S1_90, S2_90,
    S0_135, S1_135, S2_135, S0_trans_media, S1_trans_media,
```

```
S2_trans_media, I0, I45, I90, I135;


analog begin
    theta1 = 0;
    theta2 = pi/4;
    theta3 = pi/2;
    theta4 = 3*pi/4;
    T = 0.5;
    D = 0.99;
    S0_0 = 0.5*T;
    S1_0 = 0.5*T*D*cos(2*theta1);
    S2_0 = 0.5*T*D*sin(2*theta1);
    S0_45 = 0.5*T;
    S1_45 = 0.5*T*D*cos(2*theta2);
    S2_45 = 0.5*T*D*sin(2*theta2);
    S0_90 = 0.5*T;
    S1_90 = 0.5*T*D*cos(2*theta3);
    S2_90 = 0.5*T*D*sin(2*theta3);
    S0_135 = 0.5*T;
    S1_135 = 0.5*T*D*cos(2*theta4);
    S2_135 = 0.5*T*D*sin(2*theta4);
    S0_trans_media = S0_0*V(Light_Ch_In_1)+S0_45*V(Light_Ch_In_2)
        +S0_90*V(Light_Ch_In_3)+S0_135*V(Light_Ch_In_4);
    S1_trans_media = S1_0*V(Light_Ch_In_1)+S1_45*V(Light_Ch_In_2)
        +S1_90*V(Light_Ch_In_3)+S1_135*V(Light_Ch_In_4);
    S2_trans_media = S2_0*V(Light_Ch_In_1)+S2_45*V(Light_Ch_In_2)
```

```
            +S2_90*V(Light_Ch_In_3)+S2_135*V(Light_Ch_In_4);
        I0 = 0.5*T*S0_trans_media + 0.5*T*D*S1_trans_media*cos(2*theta1)
            + 0.5*T*D*S2_trans_media*sin(2*theta1);
        I45 = 0.5*T*S0_trans_media + 0.5*T*D*S1_trans_media*cos(2*theta2)
            + 0.5*T*D*S2_trans_media*sin(2*theta2);
        I90 = 0.5*T*S0_trans_media + 0.5*T*D*S1_trans_media*cos(2*theta3)
            + 0.5*T*D*S2_trans_media*sin(2*theta3);
        I135 = 0.5*T*S0_trans_media + 0.5*T*D*S1_trans_media*cos(2*theta4)
            + 0.5*T*D*S2_trans_media*sin(2*theta4);
    V(Light_Ch_Out_1) <+ transition(I0, delay, ttime);
    V(Light_Ch_Out_2) <+ transition(I45, delay, ttime);
    V(Light_Ch_Out_3) <+ transition(I90, delay, ttime);
    V(Light_Ch_Out_4) <+ transition(I135, delay, ttime);
end
endmodule
```